Universidade de Aveiro Departamento de Química
2014

CATARINA MAIA SECO SEIÇA NEVES

TRATAMENTO DE EFLUENTES AQUOSOS CONTAMINADOS COM LÍQUIDOS IÓNICOS

TREATMENT OF AQUEOUS EFFLUENTS CONTAMINATED WITH IONIC LIQUIDS

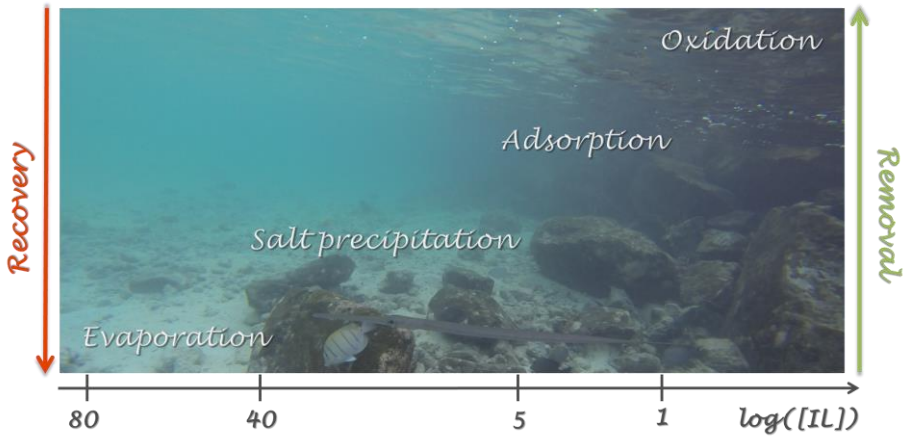

Universidade de Aveiro Departamento de Química
2014

CATARINA MAIA SECO SEIÇA NEVES

TRATAMENTO DE EFLUENTES AQUOSOS CONTAMINADOS COM LÍQUIDOS IÓNICOS

TREATMENT OF AQUEOUS EFFLUENTS CONTAMINATED WITH IONIC LIQUIDS

Tese apresentada à Universidade de Aveiro para cumprimento dos requisitos necessários à obtenção do grau de Doutor em Química, realizada sob a orientação científica do Professor Doutor João Manuel da Costa e Araújo Pereira Coutinho, Professor Catedrático do Departamento de Química da Universidade de Aveiro, e coorientação da Doutora Mara Guadalupe Freire Martins, Investigadora Coordenadora no Departamento de Química, CICECO, da Universidade de Aveiro

Apoio financeiro do POCTI no âmbito do III Quadro Comunitário de Apoio. Cofinanciamento do POPH/FSE.

O doutorando agradece o apoio financeiro da FCT no âmbito do III Quadro Comunitário de Apoio (SFRH / BD / 70641 / 2010).

Dedico este trabalho aos que me ajudaram a chegar aqui

o júri

Presidente

Prof. Doutor José Carlos da Silva Neves
professor catedrático do Departamento de Eletrónica, Telecomunicações e Informática da Universidade de Aveiro

Prof. Doutor Artur Manuel Soares da Silva
professor catedrático do Departamento de Química da Universidade de Aveiro

Prof. Doutor João Manuel da Costa e Araújo Pereira Coutinho
professor catedrático do Departamento de Química da Universidade de Aveiro

Prof. Doutor Luís Manuel das Neves Belchior Faia dos Santos
professor associado do Departamento de Química e Bioquímica da Faculdade de Ciências da Universidade do Porto

Prof. Doutor José Palomar Herrero
professor associado da Sección de Ingeniería Química do Departamento de Química Física Aplicada da Universidad Autónoma de Madrid

Prof. Doutor Eduardo Jorge Morilla Filipe
professor auxiliar do Departamento de Engenharia Química e Biológica do Instituto Superior Técnico da Universidade de Lisboa

Prof. Doutor Jorge Fernando Brandão Pereira
professor assistente doutor da Faculdade de Ciências Farmacêuticas da Universidade Estadual Paulista

Doutor Pedro Jorge Marques Carvalho
estagiário de pós-doutoramento do Departamento de Química da Universidade de Aveiro

agradecimentos

Começo por agradecer aos meus orientadores, Prof. João Coutinho e Mara. Obrigada por todo o incentivo e apoio nesta etapa da minha vida. Agradeço todo o conhecimento que me transmitiram e todas as oportunidades "fora de portas" que me proporcionaram, que não só me fizeram crescer profissionalmente mas também pessoalmente. Muito obrigada pelo "Pathminho" trilhado ao longo destes últimos quatro anos.

O meu muito obrigado também ao Prof. Artur por todo o tempo que dispensou para ver e rever espectros, para me tirar todas as dúvidas, o que me permitiu adquirir todo o conhecimento que tenho principalmente sobre RMN.

Agradezco también al Prof. Palomar el acogimiento que me dio en Madrid (ciudad por la cual me enamore) y en su grupo de investigación. Agradezco a todos los compañeros que tuve, en particular a Jesús, Maca y Carmén. Muchas gracias por todo!

Thank you to Prof. Rogers for the opportunity to work with. A special thank to the people that helped me in such different country and culture. A special thank to Luis for all the patience to wait and give the "caronas" back home, to Patrick and Kate that helped since the first moment I arrived, to Courtney, Andrea and Javad for all the good moments shared.

Ao grupo Path, agradeço todos os colegas e amigos que fiz, desde os "JurassicPath" aos "MiniPath", sem esquecer a passagem de todos os "TouristPath". Agradeço a todos a contribuição pessoal e profissional que me deram. De forma especial agradeço ao Pedro, Mariana, Marta, Mónia e Tânia, por serem os amigos do dia a dia, nas travessuras e desafios que diariamente temos que superar. À "Fluffy Hair" mais "fófinha" e ao Jorge "bad mood" agradeço especialmente pelos três meses de companheirismo, união e diversão das sextas-feiras à noite no Alabama. Sem vocês a estadia em terras do "Uncle Sam" teria sido impossível. Agradeço também aos alunos que "orientei", Carlos, Raquel, Sofia, Leila e Michael, que me ajudaram bastante no trabalho que foi desenvolvido ao longo destes anos.

Aos meus amigos de "toda a vida" agradeço o estarem presentes para todo o apoio. Por todos os momentos que partilhamos, por todas as datas que celebramos, por todas as lágrimas que vertemos. Muito obrigada a vocês pelo carinho e amizade!

À minha família agradeço tudo. Não só aqueles que são desde que nasci, mas também aqueles que adquiri ao longo do meu percurso. Um especial muito obrigada à minha mãe, lutadora de todos os dias.

palavras-chave Líquidos iónicos, água, tratamento de água, sistemas aquosos bifásicos, recuperação, adsorção, carvão ativado

Resumo

Devido às suas propriedades ímpares, nos últimos anos, os líquidos iónicos têm sido propostos como solventes alternativos aos solventes orgânicos voláteis e nefastos para o meio ambiente. Uma vez que os líquidos iónicos não são voláteis, e na maioria das vezes são líquidos a temperaturas próximas da temperatura ambiente, os processos industriais em que estes foram incluídos apresentaram melhorias significativas. Apesar desta classe de solventes não contribuir para a poluição atmosférica, uma vez que apresentam pressões de vapor negligenciáveis, os líquidos iónicos podem, no entanto, contaminar o meio ambiente através de descargas sobre os efluentes aquosos. Neste sentido, os principais objetivos deste trabalho consistem no estudo das solubilidades mútuas entre diversos líquidos iónicos e água, de forma a depreender sob o seu impacto ambiental, e na proposta de métodos eficientes para remover, e sempre que possível, recuperar os líquidos iónicos de meios aquosos.

O equilíbrio líquido-líquido dos sistemas constituídos por líquidos iónicos e água foi determinado no intervalo de temperaturas entre (288.15 e 318.15) K. No entanto, para os líquidos iónicos com temperaturas de fusão superiores à temperatura ambiente, este intervalo foi mais estreito. Através dos resultados obtidos das solubilidades mútuas (valores de saturação), foi possível alcançar uma melhor perceção dos efeitos estruturais dos líquidos iónicos sob o equilíbrio de fases, nomeadamente a família, isomerismo, simetria e comprimento da cadeia alquílica do catião, e a natureza do anião. Os dados experimentais foram também suportados pelo modelo COSMO-RS (COnductor-like Screening MOdel for Real Solvents), e em alguns sistemas também foi aplicada simulação molecular dinâmica de forma a obter informação sobre os mesmos ao nível molecular.

Por outro lado, foram estudados dois métodos diferentes de forma a remover e recuperar os líquidos iónicos de soluções aquosas: um com base em sistemas aquosos bifásicos, onde foi possível a recuperação quase completa de líquidos iónicos hidrofílicos (que são aqueles que a temperaturas próximas da ambiente são completamente miscíveis com água), pela adição de agentes de *salting-out* fortes ($Al_2(SO_4)_3$ ou $AlK(SO_4)_2$); e outro focado na adsorção de líquidos iónicos a carvão ativado. O primeiro método, além de permitir a remoção dos líquidos iónicos de soluções aquosas, permite também a recuperação do mesmo e a reutilização dos restantes componentes do sistema. No entanto, no estudo da adsorção, apenas foi alcançada a etapa de remoção do líquido iónico. Contudo, foi possível compreender os efeitos estruturais do líquido iónico aquando do processo de adsorção, e também conseguir uma melhoria na adsorção de líquidos iónicos hidrofílicos pela adição de um sal inorgânico. Ainda assim, é necessário estudar com mais enfoque o processo de recuperação que permita, por sua vez, a reutilização do líquido iónico visando o desenvolvimento de processos sustentáveis.

keywords Ionic liquids, solubility, water, water treatment, aqueous biphasic systems, recovery, adsorption, activated carbon

Abstract

Ionic liquids are a class of solvents that, due to their unique properties, have been proposed in the past few years as alternatives to some hazardous volatile organic compounds. They are already used by industry, where it was possible to improve different processes by the incorporation of this kind of non-volatile and often liquid solvents. However, even if ionic liquids cannot contribute to air pollution, due to their negligible vapour pressures, they can be dispersed thorough aquatic streams thus contaminating the environment. Therefore, the main goals of this work are to study the mutual solubilities between water and different ionic liquids in order to infer on their environmental impact, and to propose effective methods to remove and, whenever possible, recover ionic liquids from aqueous media.

The liquid-liquid phase behaviour of different ionic liquids and water was evaluated in the temperature range between (288.15 and 318.15) K. For higher melting temperature ionic liquids a narrower temperature range was studied. The gathered data allowed a deep understanding on the structural effects of the ionic liquid, namely the cation core, isomerism, symmetry, cation alkyl chain length and the anion nature through their mutual solubilities (saturation values) with water. The experimental data were also supported by the COnductor-like Screening MOdel for Real Solvents (COSMO-RS), and for some more specific systems, molecular dynamics simulations were also employed for a better comprehension of these systems at a molecular level.

On the other hand, in order to remove and recover ionic liquids from aqueous solutions, two different methods were studied: one based on aqueous biphasic systems, that allowed an almost complete recovery of hydrophilic ionic liquids (those completely miscible with water at temperatures close to room temperature) by the addition of strong salting-out agents ($Al_2(SO_4)_3$ or $AlK(SO_4)_2$); and the other based on the adsorption of several ionic liquids onto commercial activated carbon. The first approach, in addition to allowing the removal of ionic liquids from aqueous solutions, also makes possible to recover the ionic liquid and to recycle the remaining solution. In the adsorption process, only the removal of the ionic liquid from aqueous solutions was attempted. Nevertheless, a broad understanding of the structural effects of the ionic liquid on the adsorption process was attained, and a final improvement on the adsorption of hydrophilic ionic liquids by the addition of an inorganic salt (Na_2SO_4) was also achieved. Yet, the development of a recovery process that allows the reuse of the ionic liquid is still required for the development of sustainable processes.

Contents

List of Figures

List of Tables

Nomenclature

Abbreviations

ABS	Aqueous Biphasic Systems
AC	Activated Carbon
AC-MkU	AC supplied by Merck
AG1	Agricultural soil
AMP	Adenosine MonoPhosphate
ATR	Attenuated Total Reflection
BET	Brunauer–Emmett–Teller theory
BP_TZVP	Basis Parameterization_Triple-ζ Valence Polarized
CL	Clayey soil
COSMO-RS	COnductor-like Screening MOdel for Real Solvents
DABCO	1,4-Diazabicyclo[2.2.2]octane
DSC	Differential Scanning Calorimetry
EC50	Half maximal Effective Concentration
EEV	Effective Excluded Volume
eNRTL	electrolyte Non-Random Two Liquids
EoS	Equations of State
ESI	Electrospray Ionization
EtOH	Ethanol
FCM	Functional Carbonaceous Material
FTIR	Fourier Transform InfraRed
GC	Gas Chromatography
GCMs	Group-Contribution Methods
HM	Hydrothermal Mineralization
HPLC	High Performance Liquid Chromatography
IC50	Half maximal Inhibition Concentration
ICP-OES	Inductively Coupled Plasma-Optical Emission
ILs	Ionic Liquids
IUPAC	International Union of Pure and Applied Chemistry
KF	Karl Fischer
LLE	Liquid-Liquid Equilibrium
MD	Molecular Dynamics
Morph	Morpholinium
MS	Mass Spectrometry
NMR	Nuclear Magnetic Resonance

NRTL	Non-Random Two Liquids
OECD	Organization for Economic Cooperation and Development
PD	Photocatalytic Degradation
PE	Peaty soil
PID	Proportional-Integral-Derivative controller
PL	Pond Large
PS	Pond Small
RDFs	Radial Distribution Functions
Rpm	Revolutions per minute
SLE	Solid-Liquid Equilibrium
SOM	Sediment Organic Matter
TGA	Thermal Gravimetric Analysis
TLLs	Tie-Line Lengths
TLs	Tie-Lines
TOC	Total Organic Content
UCST	Upper Critical Solution Temperature
UNIQUAC	UNIversal QUAsi-Chemical
USEPA	United States Environmental Protection Agency
UV	UltraViolet
UV-Vis	UltraViolet-Visible
VLE	Vapour-Liquid Equilibrium
VOCs	Volatile Organic Compounds

Chemical Formulas

$C_4H_4O_6^{2-}$	Tartrate anion
$C_6H_5O_7^{3-}$	Citrate anion
Ca^{2+}	Calcium cation
$CH_3CO_2^-$	Acetate anion
CH_3CO_2H	Acetic acid
Cl^-	Chloride anion
CO	Carbon monoxide
CO_2	Carbon dioxide
CO_3^{2-}	Carbonate anion
Cs^+	Cesium cation
Fe^{3+}	Iron(III) cation
H_2O	Water
H_2O_2	Hydrogen peroxide
$H_2PO_4^-$	Dihydrogen phosphate anion
HCO_3^-	Hydrogen carbonate anion
HPO_4^{2-}	Hydrogen phosphate anion
HSO_4^-	Hydrogen sulphate anion

Mg^{2+}	Magnesium(II) cation
Na^{+}	Sodium cation
Ni^{2+}	Nickel(II) cation
NO_x	Nitrogen oxides
OH^{-}	Hydroxide anion
PO_4^{3-}	Phosphate anion
SO_3^{2-}	Sulphite anion
SO_4^{2-}	Sulphate anion
SO_x	Sulfur oxides
Sr^{2+}	Strontium cation
TiO_2	Titanium oxide

Salts

$Al_2(SO_4)_3$	Aluminium sulphate
$AlK(SO_4)_2$	Aluminium potassium sulphate
$Ca(OH)_2$	Calcium hydroxide
K_2CO_3	Potassium carbonate
K_2HPO_4	Potassium hydrogen phosphate
K_3PO_4	Potassium phosphate
KCl	Potassium chloride
KOH	Potassium hydroxide
$[N_{4444}][PF_6]$	Tetrabutylammonium hexafluorophosphate
Na_2CO_3	Sodium carbonate
Na_2SO_4	Sodium sulphate
Na_3PO_4	Sodium phosphate
NaCl	Sodium chloride
NaH_2PO_4	Sodium di-hydrogen phosphate
$(NH_4)_2SO_4$	Ammonium sulphate
$[P_{4444}][PF_6]$	Tetrabutylphosphonium hexafluorophosphate

Ionic Liquid Cations

$[aC_1im]^{+}$	1-Allyl-3-methylimidazolium
$[C_{10}C_1im]^{+}$	1-Decyl-3-methylimidazolium
$[C_{11}OC_1\text{-}3\text{-}OHpy]^{+}$	3-Hydroxy-1-undecanoxymethylpyridinium
$[C_{12}C_1im]^{+}$	1-Dodecyl-3-methylimidazolium
$[C_{14}C_1im]^{+}$	1-Methyl-3-tetradecylimidazolium
$[C_{16}C_1C_1im]^{+}$	1-Hexadecyl-2,3-dimethylimidazolium
$[C_{16}C_1im]^{+}$	1-Hexadecyl-3-methylimidazolium
$[C_1C_1im]^{+}$	1,3-Dimethylimidazolium
$[C_1im]^{+}$	1-Methylimidazolium
$[C_2C_1im]^{+}$	1-Ethyl-3-methylimidazolium
$[C_2C_2im]^{+}$	1,3-Diethylimidazolium
$[C_2C_3im]^{+}$	1-Ethyl-3-propylimidazolium
$[C_2im]^{+}$	1-Ethylimidazolium

$[C_2im]^+$	Ethylimidazolium
$[(C_2OCOC_1)C_1im]^+$	1-(2-Ethoxy-2-oxoethyl)-3-methylimidazolium
$[C_2py]^+$	1-Ethylpyridinium
$[C_3\text{-}3\text{-}C_1py]^+$	3-Methyl-1-propylpyridinium
$[C_3C_1im]^+$	1-Methyl-3-propylimidazolium
$[C_3C_1pip]^+$	1-Methyl-1-propylpiperidinium
$[C_3C_1pyr]^+$	1-Methyl-1-propylpyrrolidinium
$[C_3C_3im]^+$	1,3-Dipropylimidazolium
$[C_4\text{-}3\text{-}C_1py]^+$	1-Butyl-3-methylpyridinium
$[C_4\text{-}4\text{-}C_1py]^+$	1-Butyl-4-methylpyridinium
$[C_4C_1C_1im]^+$	1-Butyl-2,3-dimethylimidazolium
$[C_4C_1im]^+$	1-Butyl-3-methylimidazolium
$[C_4C_1pyr]^+$	1-Butyl-1-methylpyrrolidinium
$[C_4C_2im]^+$	1-Butyl-3-ethylimidazoilium
$[C_4C_4im]^+$	1,3-Dibutylimidazolium
$[C_4py]^+$	1-Butylpyridinium
$[C_5C_1im]^+$	1-Methyl-3-pentylimidazolium
$[C_5C_5im]^+$	1,3-Dipentylimidazolium
$[C_6\text{-}4\text{-}N(CH_3)_2py]^+$	1-Hexyl-4-(dimethylamino)pyridinium
$[C_6C_1im]^+$	1-Hexyl-3-methylimidazolium
$[C_6C_2im]^+$	1-Ethyl-3-hexylimidazolium
$[C_6py]^+$	1-Hexylpyridinium
$[C_7C_1im]^+$	1-Heptyl-3-methylimidazolium
$[(C_7COOH)C_1im]^+$	1-(6-Carboxyhexyl)-3-methylimidazolium
$[(C_7H_7)C_1im]^+$	1-Benzyl-3-methylimidazolium
$[C_8\text{-}3\text{-}C_1py]^+$	3-Methyl-1-octylpyridinium
$[C_8C_1im]^+$	1-Methyl-3-octylimidazolium
$[C_8C_2im]^+$	1-Ethyl-3-octylimidazolium
$[C_8py]^+$	1-Octylpyridinium
$[im]^+$	Imidazolium
$[OHC_2C_1im]^+$	1-Hydroxyethyl-3-methylimidazolium
$[OHC_8C_1im]^+$	1-(8-Hydroxyoctyl)-3-methylimidazolium
$[P_{4441}]^+$	Tributylmethylphosphonium
$[P_{4444}]^+$	Tetrabutylphosphonium
$[P_{i(444)1}]$	Tri(isobutyl)methylphosphonium
$[P_{66614}]^+$	Trihexyl(tetradecyl)phosphonium

Ionic Liquid Anions

$[B(CN)_4]^-$	Tetracyanoborate
$[BF_4]^-$	Tetrafluoroborate
Br^-	Bromide
$[C(CN)_3]^-$	Tricyanomethane
$[C_2H_5SO_4]^-$	Ethylsulphate

$[C_8H_{17}SO_4]^-$	Octylsulphate
$[CF_3CO_2]^-$	Trifluoroacetate
$[CF_3SO_3]^-$	Trifluoromethanesulfonate, triflate
$[CH_3CO_2]^-$	Acetate
$[CH_3SO_3]^-$	Methanesulfonate
$[CH_3SO_4]^-$	Methylsulphate
Cl^-	Chloride
$[Deca]^-$	Decanoate
$[FAP]^-$	Tris(pentafluoroethyl)trifluorophosphate
$[HSO_4]^-$	Hydrogensulphate
I^-	Iodide
$[N(CN)_2]^-$	Dicyanamide
$[NTf_2]^-$	Bis(trifluoromethylsulfonyl)imide
$[PF_6]^-$	Hexafluorophosphate
$[Phosph]^-$	Bis(2,4,4-trimethylpentyl)phosphinate
$[Sac]^-$	Saccharinate
$[Tos]^-$	Tosylate

Symbols

$\%R$	Percentage recovery efficiency
C	Concentration of adsorbate in the fluid phase
D	Distribution coefficients
E	Energy interaction
K	Partition coefficient
K_d	Apparent distribution coefficients
m	Mass
Mw	Molecular weight
N	Avogadro constant
p	Pressure
P	Partition coefficient
ϕ	Objective function
Q	Concentration of adsorbate in the solid phase
R	Ideal gas constant
R^2	Correlation coefficient
S	Selectivity
T	Temperature
V	Volume
wt%	Weight fraction percentage
x	Mole fraction

Z	Lattice coordination number of the liquid
α	Non-randomness parameter
α	Ratio between the mass of the IL-rich phase and the total mass of the mixture
α_p	Isobaric thermal expansion coefficient
ΔG	Variation of Gibbs free energy
ΔH	Variation of enthalpy
ΔS	Variation of entropy
η	Viscosity
K	Conductivity
ρ	Density
σ	Standard deviation
τ	Interaction parameter

Subscripts

AC	Activated Carbon
aq	Aqueous
Caf	Caffeine
E	Equilibrium
EtOH	Ethanol
exp	Experimental
i-j	Binary molecular pair
IL	Ionic Liquid
M	Molarity
M	Mixture
mesop	Mesopore
microp	Micropore
mod	Calculated values by NRTL
nic	Nicotine
ow	Oil-water
P	Pressure
sol	Solution
svt	Solvation
V	Volume
W	Water
W	Weight

Superscripts

0	Standard
Aq	Aqueous
IL	Ionic Liquid

Chapter 1 – General Introduction

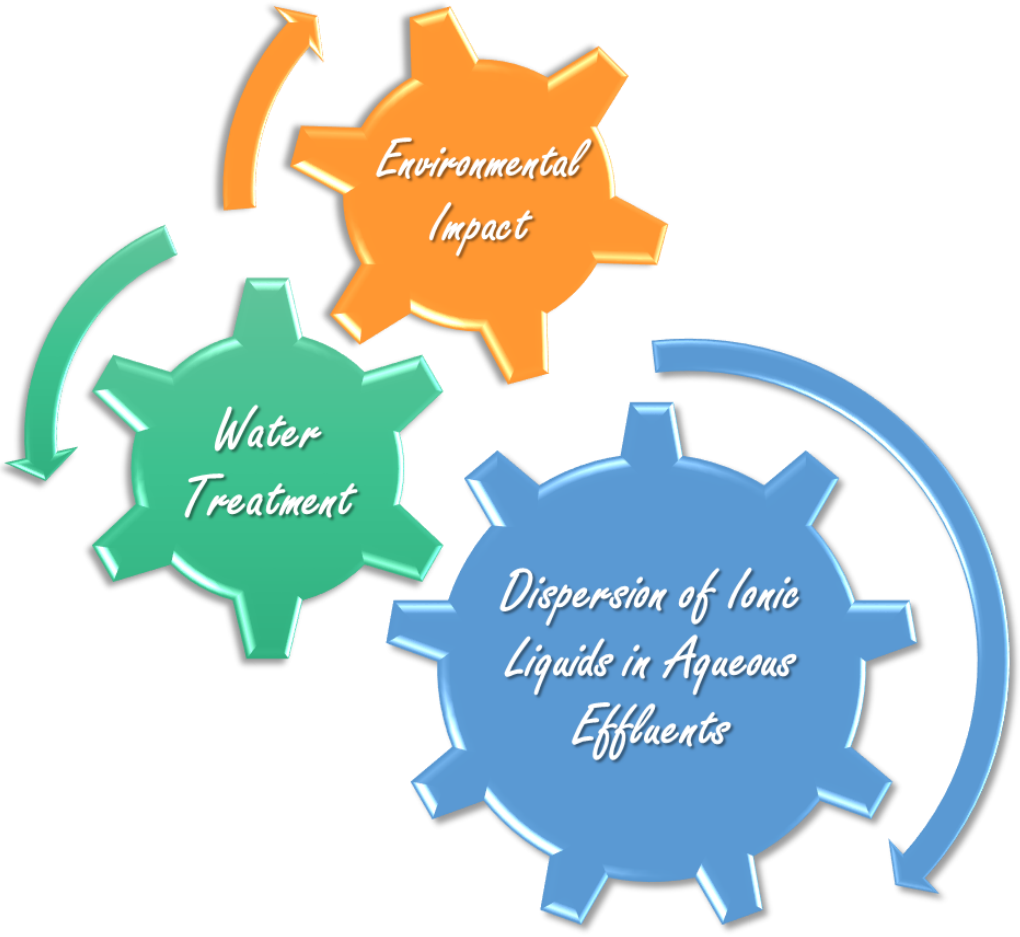

1.1. General context

The potential use of ionic liquids (ILs) as novel solvents or fluids for a diverse range of applications has become increasingly evident.[1,2] Ionic liquids belong to the molten salts group and are usually formed by large organic cations and smaller organic or inorganic anions, allowing them to remain liquid at temperatures below 100 °C. Since ionic liquids are constituted by ionic species, they present particular properties not common in molecular solvents, such as negligible vapour pressures, general non flammability, high thermal and chemical stabilities, among others. Moreover, the possibility of controlling their properties by the adequate manipulation of the cation and/or the anion allows the design of these solvents to present selective solubilities for particular fluid mixtures.[3] This tailoring ability makes of ionic liquids excellent alternative solvents for the most diverse extraction purposes, and coupled with their negligible vapour pressures, contributed for their classification as potential "green solvents" of industrial interest.[4] The intrinsic non-volatile nature of ionic liquids provides an opportunity to reduce, or even completely eliminate, hazardous and toxic emissions to the atmosphere. Nevertheless, although ionic liquids cannot contribute to air pollution, some of them (even those considered hydrophobic) present a non-negligible solubility in water,[5–7] thus leading to aquatic environmental concerns. Indeed, for hydrophobic ionic liquids, their solubilities in water, at 298.15 K, range between 1.62×10^{-5} and 2.904×10^{-3} in mole fraction, that when converted to weight fraction values range from 0.0501 to 3.359 for $[C_2C_1im][FAP]$ and $[C_2C_1im][B(CN)_4]$, respectively.[8,9] Hence, an imperative study regarding their risks to the aquatic environment, by the determination of their solubility saturation values in water, is of crucial importance before their factual industrial applications. Finally, the development of novel processes for their removal and recovery is a mandatory issue when envisaging their large-scale applications.

MUTUAL SOLUBILITIES WITH WATER

Although a large range of ionic liquids is completely miscible with water at temperatures close to room temperature (hydrophilic ionic liquids), there are others that present

limited solubility in water (hydrophobic ionic liquids), and accurate analytical methods are currently employed for their quantification in aqueous systems. Indeed, in the past few years, a wide range of results for the mutual solubilities of water and hydrophobic ionic liquids systems have been reported.[5–8,10–17] These studies comprised[5–8,10–17] imidazolium-, pyridinium-, pyrrolidinium- and piperidinium-based cations combined with bis(trifluoromethylsulfonyl)imide ($[NTf_2]^-$), hexafluorophosphate ($[PF_6]^-$), tetrafluoroborate ($[BF_4]^-$), tricyanomethane ($[C(CN)_3]^-$), tetracyanoborate ($[B(CN)_4]^-$) and tris(pentafluoroethyl)trifluorophosphate ($[FAP]^-$) anions. In these works it was possible to evaluate the effects of the increase of the alkyl side chain length,[5–7,10,12,15,17] isomerism,[6,10,14–16] the cation family,[6,7,11,13,17] and the anion identity[6,8,11,12,17] on their liquid-liquid phase diagrams with water. From these studies it was possible to state that besides the hydrophobicity of all ionic liquids studied, they present a considerable solubility in water, which can in fact contaminate the aqueous effluents. In general, the temperature decrease or an increase in the cation alkyl chain length leads to a decrease on their mutual solubilities with water.[5–7,10,12,15,17] The inclusion of a third methyl group replacing the most acidic hydrogen at the imidazolium cation showed to have different impacts in both phases, which was addressed by the relative influence of the hydrogen bonding capacity in these.[6,14] The hydrophobicity of the anions increases in the order $[BF_4]^- < [C(CN)_3]^- < [B(CN)_4]^- < [PF_6]^- < [NTf_2]^- < [FAP]^-$.[6,8,11,12,17] The hydrophobicity of the cations increases in the rank imidazolium < pyridinium ≤ pyrrolidinium < piperidinium in the IL-rich phase,[6,11,17] while at the water rich-phase, the solubility of ionic liquids increases in the order: piperidinium- < pyridinium- < pyrrolidinium- < imidazolium-based ionic liquids.[6,7,11,13,17] Concerning the isomeric effects, the presence of distinct ionic liquid isomers has shown to lead to different trends on the mutual solubilities between ionic liquids and water.[10,14,16]

1.1.1 Ionic liquids environmental impact

ADSORPTION TO SOILS

Gorman-Lewis and co-workers[18] were the pioneer research group that investigated the adsorption of ionic liquids onto several environmentally relevant surfaces. The authors[18]

studied the adsorption of [C_4C_1im]Cl to Gram-positive soil bacterial species (*Bacillus subtilis*), gibbsite, quartz and Na-montmorillonite. The experiments were conducted aiming at evaluating the effect of the pH of the solution, solid:IL ratio, equilibration time and ionic strength. The authors[18] found that the ionic liquid is stable in aqueous solution only in the pH range from 6 to 10, and that the adsorption of the ionic liquid was only effective in the Na-montmorillonite surface, while this adsorption was highly dependent on the ionic strength. The distribution coefficients (K_d) for the adsorption of the ionic liquid to the Na-montmorillonite were also calculated.[18] The distribution coefficients values changed with the ionic strength of the solution: K_d = 1735 ± 269 L·kg^{-1} for an ionic strength of 10^{-4} M, and K_d = 1133 ± 291 L·kg^{-1} for 10^{-1} M. In summary, the gathered results[18] indicate that [C_4C_1im]Cl does not adsorb to silica or alumina surfaces or to Gram-positive bacteria *B. subtilis*, allowing the ionic liquid to travel without restraint in groundwater systems in which these types of surfaces are predominant.

Later, Stepnowski[19] analysed the adsorption of some tetrafluoroborate-based ionic liquids (combined with [(C_3-C_6)C_1im]- and [C_4C_2im]-based cations) to different soils (agricultural soil (AG1), clayey soil (CL), and peaty soil (PE)) and with a marine sediment (SE) taken from the Baltic Sea. The author[19] found that the adsorption onto the soil and sediment increases with the ionic liquid lipophilicity. On the other hand, the desorption process decreases with the cation alkyl chain length increase.[19] In addition, all ionic liquids showed an effective, and practically irreversible, adsorption, and revealed a strong affinity to the marine sediment.[19]

In 2007, Stepnowski et al.[20] studied the adsorption of several ionic liquids based on imidazolium and pyridinium cations, making use of chloride as the counter anion, into fluvial agricultural soil, clay agricultural soil and forest soil, all from the northern region of Poland; and a sample from the industrialized and highly polluted area around the Gdańsk oil refinery. The results obtained show that at low concentrations of ionic liquid, the [C_6C_1im]Cl adsorbs faster than [C_4C_1im]Cl, indicating a clear dependence on the cation alkyl chain length.[19] However, at higher concentrations, the cation alkyl chain length does not seem to be responsible for the sorption strength of the ionic liquid.[19]

Beaulieu et al.[21] studied different ionic liquids, based on the alkylmethylimidazolium cation with halide-based anions (Cl^- and Br^-), in four types of aquatic sediments. The sediments used were collected from the littoral zone of a small pond (Juday Creek, South Bend, IN) and sieved while wet into two size fractions: Pond Large (PL) and Pond Small (PS); another sample was collected from the profoundly zone of a small eutrophic lake (St. Joseph lake, Notre Dame, IN); and finally, the last sediment tested was sand purchased at a local hardware store. At an initial concentration of 0.5 mM of ionic liquid none of the tested ionic liquids sorbed to sand. On the contrary, the PL sediment sorbed 75-90%, the PS sediment sorbed 75-92%, and the Lake sediment sorbed 40-73% of ionic liquid.[21] Moreover, the authors[21] found that the Sediment Organic Matter (SOM) is directly related with the adsorption capacity and that the PL sediment adsorbs more strongly the ionic liquids than the remaining sediments. The authors[21] concluded that the cation exchange is not dominant in the adsorption phenomenon, since at the highest concentration of PL, this sediment absorbed seven times more ionic liquid than could be accounted by cation exchange. In addition, they found that the adsorption to the lake sediment is independent of the alkyl chain length, showing that the hydrophobic interactions are not the most relevant forces ruling the adsorption mechanism.[21] These results are in good agreement with those reported by Stepnowski et al.[20]

Markiewicz et al.[22] studied the adsorption of $[C_8C_1im]Cl$ into a forest soil with a pH of 3.5 and 1.23% of organic carbon content. The adsorption of this ionic liquid to the soil was poor, mainly due to the low pH, that allows a protonation of the soil with silica and aluminium oxides that occupy the negatively charged sites, not leaving empty sites for the adsorption of the cation; and due to the low concentration of organic matter of the soil, that did not allow its hydrophobic interactions with the cation and mainly responsible for the adsorption mechanism.[22]

An additionally adsorption study was conducted by Matzke et al.[23] with $[C_4C_1im][BF_4]$, $[C_8C_1im][BF_4]$ and $[C_4C_1im][NTf_2]$ into soils with organic matter and different clay minerals (kaolinite or smectite). The addition of the two clay minerals to soil samples induced different behaviours: with smectite the adsorption of all ionic liquids increases (the

highest value being observed for [C_8C_1im][BF_4]), while with kaolinite the adsorption phenomena is less pronounced.[23] Again, [C_8C_1im][BF_4] was the ionic liquid most adsorbed into the soil with organic matter, but not as higher as with smectite.[23] Taking into account the desorption process, the results obtained[23] are in agreement with those published by Stepnowski[19] where no (or minimal) desorption of the ionic liquids from the soil was observed. The authors suggested, and in line with other authors,[20–22] that the dominant adsorption mechanism is the interaction of the ionic liquid cation with the negatively charged sites of clay minerals.[23]

Studzinska et al.[24] studied five soils with different compositions (differing mostly in the organic carbon content, ranging from 0.1% to 44.8%) and three ionic liquids ([C_2C_1im]Cl, [C_4C_1im]Cl and [C_6C_1im]Cl). The results obtained indicate that chloride anions are not sorbed in any of the used soils. Nevertheless, all ionic liquid cations were sorbed to all soils, although with higher sorption values in the cases of soils with higher organic carbon content and with the most hydrophobic cations. Although the results are in line with those of other authors[25,26] the authors[24] interpreted them at the light of the importance of the hydrophobic interactions (mainly van der Waals forces) between the sorbent and the soil sediment.

All the results presented[18–24] show that the sorption mechanisms of ionic liquids vary with the soil type and its composition. Nevertheless, the range of ionic liquids studied is very limited since essentially only imidazolium-based fluids were studied combined with halides and $[BF_4]^-$anions. However, it should be remarked that the degradation of $[BF_4]^-$ in aqueous environments was not taken into account by the authors.[27] The limited results available show that it is still required additional work for ionic liquids containing different cations and anions to draw a full picture of the adsorption mechanisms of ionic liquids into soils, and to get a better understanding of the ionic liquids fate after their release into aqueous environments.

BIODEGRADATION

Biodegradation assays are generally carried out according to the OECD (Organization for Economic Cooperation and Development) Guidelines for Testing of Chemicals: a series of guidelines with the aim of assessing the effects of chemicals on workers and on the environment.[28] Based on these guidelines, nowadays the tests approved are: Die-Away test (OECD 301 A),[28] closed bottle test (301 D),[29] CO_2 headspace test (ISO 14593),[30,31] OECD 309 – aerobic mineralization in surface water[32] and ASTM 5988 – standard method for determining aerobic biodegradation in soil of plastic materials or residual plastic materials after composting.[33] If a specific compound reaches a biodegradation level higher than 60% in a 28-day period, then it will be referred as ''readily biodegradable'', which is defined as "an arbitrary classification of chemicals which have passed certain specified screening tests for ultimate biodegradability; the conditions in these tests are so stringent – relatively low density of non-acclimatized bacteria, relatively short duration, absence of other compounds – that such chemicals will rapidly and completely biodegrade in aquatic environments under aerobic conditions".[34]

Despite the exponential increase of research regarding ionic liquids in the last decade, only in 2002, Gathergood and Scammells[35] discussed, for the first time, the biodegradability of ionic liquids. In order to improve the biodegradability of ionic liquids, and with the knowledge gathered from the biodegradation of typical surfactants,[36,37] they modified the alkyl chain in $[C_4C_1im]$-based ionic liquids incorporating an ester group.[35] They used a modified Saturm test (ISO 9439) to study two ionic liquids: $[(C_2OCOC_1)C_1im][BF_4]$ and $[(C_2OCOC_1)C_1im]Br$.[35] As a result, the authors[35] concluded that $[(C_2OCOC_1)C_1im][BF_4]$ is at the border line to pass the level of biodegradability while $[(C_2OCOC_1)C_1im]Br$ degrades slower (CO_2 evolution of 59% and 48%, respectively, after a 20-day period). In another work,[34] imidazolium-based ionic liquids incorporating esters and amide groups were tested using a Closed Bottle Test. This study showed that ionic liquids with the amide group in the cation alkyl chain present very low biodegradability, while those with ester moieties present an improved biodegradability.[34] This biodegradability enhancement is due to the ester moiety that allows an enzymatic hydrolysis step which initiates the degradation pathway to other products.[34] In addition,

they found that the alkyl chain length increase slightly enhances the biodegradability of the ionic liquid.[34] Later, the same group of researchers[38] found that the octylsulphate anion improves the biodegradability of ionic liquids, when compared with other anions. Yet, the ionic liquid $[C_4C_1im][C_8H_{17}SO_4]$ was not "readily biodegradable". Finally, the combination of an imidazolium-based cation with an alkyl side chain incorporating an ester group, and with the octylsulphate as the counter ion, has leaded to the first known biodegradable ionic liquid.[39]

Kumar et al.[40] studied the fate of $[C_4C_1im][BF_4]$ in contact with soil-microorganisms, and waste-water-microorganisms such as *Pseudomonas putida* and *Escherichia coli*. They concluded that the cation suffers degradation by the action of all the microorganisms tested, although by different pathways.[40] The breakdown products were identified by GC-MS (Gas Chromatography-Mass Spectrometry) after solid phase extraction.[40] In addition, the authors found that only the biotic biodegradation in the same conditions took place, since no abiotic degradation was observed.[40]

Stasiewicz et al.[41] studied the biodegradation of several ionic liquids, based on the 1-alkoxymethyl-3-hydroxypyridinium cation combined with the chloride, acesulfamate and saccharinate anions, and using the Closed Bottle test. From all the ionic liquids tested, only the $[C_{11}OC_1$-3-OHpy][Sac] showed to be readily biodegradable.[41] However, after the period of the test, the biodegradation of the remaining ionic liquids showed an improvement.[41]

Stolte et al.[42] studied the biodegradation of several ionic liquids with two different inocula: a commercially available freeze-dried micro-organism mixture used for the determination of sewage water qualities[43] (that proved to be not suitable for the evaluation of biodegradability of compounds accordingly to the OECD guidelines), and an activated sludge from a wastewater treatment plant. The ionic liquids explored comprise mono- and di-substituted imidazolium, and mono-, di- and tri-substituted pyridinium-based cations with halides as counter anions.[42] On the primary biodegradation test (with conditions very similar to the ready biodegradability test according to OECD guideline 301 D) only few ionic liquids showed total biodegradation after 17 days ($[OHC_8C_1im]Br$ and

[(C_7COOH)C_1im]Br), 24 days ([C_8C_1im]Cl and [C_8py]Cl) and 31 days ([C_8-3-C_1py]Cl and [C_6-4-N(CH_3)$_2$py]Cl).[42] These results revealed the low biodegradability of the imidazolium- and pyridinium-based ionic liquids with short alkyl side chain lengths. The biodegradability did not improve either for imidazolium-based ionic liquids with short alkyl chain lengths functionalized with ether, nitrile or hydroxyl groups.[42] The products of the [C_8C_1im]-based ionic liquids biodegradation after 24 days were studied by HPLC-MS (High Performance Liquid Chromatography-Mass Spectrometry).[42] The transformation proposed starts with the oxidation of the terminal methyl group catalysed by mono-oxygenases. The alcohol formed is subsequently oxidized by dehydrogenases *via* aldehydes to carboxylic acids. The resulting carboxylic acids can undergo β-oxidation and the two released carbon fragments can enter the tricarboxylic acid cycle as acetylCo-A.[42] In addition, other products with non-terminal hydroxyl groups were detected with identical masses but different retention times.[42] An experimental process based on denitrifying conditions, in order to remove efficiently imidazolium- and pyridinium-based ionic liquids from the environment, was also presented by Neuman et al.,[44] and proved not to be the solution to the treatment of contaminated wastewater streams with ionic liquids.

Esquivel-Viveros et al.[45] studied the biodegradability of the [C_4C_1im][PF_6] as a carbon source in a culture media of *Fusarium* fungus at various concentrations of ionic liquid. The *Fusarium* fungus showed no inhibition in the presence of ionic liquid. Indeed, a linear radial growth rate was observed with the ionic liquid increasing concentration.[45] The same ionic liquid was tested using a membrane-aerated biofilm reactor, and the biodegradability was addressed by UV (Ultraviolet) spectroscopy.[45] The concentration of the ionic liquid decreased 80% after 28 days of incubation at 30 °C.[45] In 2010, Zhang et al.[46] reported the complete biodegradation of [C_2py][BF_4] and [C_2py][CH_3CO_2] in an axenic culture with the *Corynebacterium* bacteria. The same process did not work with the [C_4C_1im][BF_4] ionic liquid and may be related with the impact of the $[BF_4]^-$ degradation products through the microorganisms.[46]

The biodegradability of phosphonium-based ionic liquids were poorly studied and only two works were published hitherto.[47,48] Wells and Coombe[48] studied, for the first time,

phosphonium-based ionic liquids with linear alkyl chains at the cation (ethyltri(butyl)phosphonium diethylphosphate and trihexyl(tetradecyl)phosphonium chloride) and found that these ionic liquids do not show biodegradability, since they are toxic to the microorganisms responsible for the biodegradation. Atefi et al.[47] studied ionic liquids based on the tricyclohexylphosphine and on the tri-*n*-hexylphosphine with various ester side chains, and anions such as halides (Cl^-, Br^- and I^-), bis(trifluorosulfonyl)imide and octylsulphate. The biodegradability study was carried out with the CO_2 headspace test and showed no biodegradation of the ionic liquids studied.[47] These results reinforce the results of Wells and Coombe.[48]

The biodegradation of ammonium-based ionic liquids was studied by Yu et al.[49] In this work, several cholinium-based ionic liquids with naphtalenic acid derivatives-based anions were studied.[49] These ionic liquids were submitted to the closed bottle test revealing that the biodegradation was higher than 60% for most of the ionic liquids studied. Those that failed the test have an anion based on polycyclic residues (2-naphthoxyacetate and anthracene-9-carboxylate), and that have been demonstrated by Boethling et al.[50] to increase the resistance to biological breakdown. These ionic liquids were shown to be degraded by activated sludge in wastewater treatment plants by Grabinska-Sota and Dmuchowski.[51]

Pretti et al.[52] reported the biodegradation of *N*-alkyl-*N*-methylmorpholonium and *N*-alkyl substituted 1,4-diazabicyclo[2.2.2]octane based ionic liquids as a function of the alkyl chain length. The CO_2 headspace test was used for that purpose, and the results showed that the ionic liquids studied display a low biodegradation ability, not reaching the necessary percentage to be considered "readily biodegradable" (> 60%).[52]

TOXICITY OF IONIC LIQUIDS

Ranke et al.[53] published a review on the impact of several ionic liquids on enzymatic inhibition. Later, Arning et al.[54] found that the inhibitory effects on the acetylcholinesterase enzyme are due to the cationic nature of the ionic liquids, because of their delocalized aromatic system, lipophilicity of the alkyl side chains and the positively

charged nitrogen atom. They found that the morpholinium and phosphonium cations inhibit less the enzyme than quinolinium-, imidazolium- or pyridinium-based cations.[54] The incorporation of a hydroxyl, ether or nitrile group decreased the inhibitory effect.[54] On the other hand, the increasing of the alkyl chain decreases the activity of the enzyme.[54] Concerning the ionic liquid anion effect, several ionic fluids were studied, such as those containing inorganic, organic and complex borate anions. From all the studied anions, only fluoride or fluoride containing anions have shown some inhibitory effects.[54] This behaviour is explained by their limited interactions with the active centre of the enzyme.[55] In addition, Stasiewicz et al.[41] studied the inhibition activity of the same enzyme with a new class of ionic liquids: 1-alkoxymethyl-3-hydroxypyridinium with saccharinate, acesulfamate and chloride anions. Their results showed that these ionic liquids do not significantly affect the enzyme activity.[41] This low inhibition is due to the presence of the hydroxyl group that prevents the interaction between the ammonium cation and the anionic active site of the enzyme.[41] Skladanowsk et al.[56] studied the inhibitory effect of $[C_4C_1im]^+$-based ionic liquids combined with $[PF_6]^-$, $[BF_4]^-$, $[Tos]^-$ and Cl^- anions in an AMP (Adenosine MonoPhosphate) deaminase as a potential molecular method in risk assessment. They found a major inhibition of the enzyme with ionic liquids presenting fluorine-based anions ($[PF_6]^-$ and $[BF_4]^-$).[41] The authors[41] also concluded that the inhibition of the enzyme is dependent on the concentration of the ionic liquid. In another research work, carried out by Yu et al.,[57] the effects of acute exposure of intraperitoneal injection of aqueous $[C_8C_1im]Br$ on the antioxidant enzymes and lipid peroxidation of treated mouse liver were investigated. As major findings, the exposure of the treated mouse to ionic liquids aqueous solutions led to hepatotoxic harmful effects.[57]

In 2005, Garcia et al.[38] studied the acute toxicity of several ionic liquids, namely 1-[C_4, C_6 or C_8]-3-methylimidazolium-based cations with Br^-, Cl^-, $[PF_6]^-$ and $[BF_4]^-$ anions. To assess the aquatic toxicity, tests on freshwater crustacea (*Daphnia magna*) and on saltwater bacteria (*Photobacterium phosphoreum*) were carried out. The results showed that the concentration able to immobilise 50% of the crustacea population (IC_{50}) was one order of magnitude less than the effective concentration resulting in a 50% reduction of light produced by the bacteria (EC_{50}). This indicates that *Daphnia magna* is more sensitive to

these ionic liquids than the bacteria.[38] Also in the same research work,[38] the authors compared the toxicity of ionic liquids with common organic solvents. Ionic liquids are more toxic in both bioassays than the organic solvents evaluated (methanol, ethanol, isopropanol, acetonitrile, acetone, chloroform and dichloromethane). In addition, due to the similarity of long aliphatic tails, ionic liquids and typical surfactants were also compared.[38] The authors[38] found that the ionic liquids are more toxic to the crustacean and bacteria than similar cationic surfactants. It is well known that the toxicity of chemicals against aquatic species is caused by the ability of the molecules to disrupt the biological membranes, which are essentially non-polar interfaces. Thus, hydrophobic molecules or long aliphatic moieties have a greater ability to accumulate at this interface. They also found that the increasing of the cation side alkyl chain also enhances the toxicity of the ionic liquids.[38]

In order to have ionic liquids with lower toxicity, Nockemann et al.[58] synthesized cholinium-based ionic liquids with saccharinate and acesulfamate anions. Besides their low toxicity, they are easily prepared and cheaper than imidazolium- or pyridinium-based compounds. They are fully soluble in polar organic solvents, such as ethanol, dimethylsulfoxide, acetonitrile, acetone and dimethylformamide, and immiscible in less polar solvents (toluene, hexane, dichloromethane, chloroform, ethylacetate, diethylether and dioxane). This type of ionic liquids has low toxicity, since cholinium chloride (a precursor for synthesis of the ionic liquids studied in this work) is an animal feed additive (vitamin B4) and the anions used are artificial sweeteners. For the ecotoxicological tests, the authors[58] used a bioassay with the freshwater crustacean *Daphnia magna*. As expected, these ionic liquids showed to be, at least, two orders of magnitude less toxic than other imidazolium- or pyridinium-based ionic liquids widely used.[58]

The cytotoxicity of 1-alkoxymethyl-3-hydroxypyridinium-based ionic liquids with chloride, acesulphamate and saccharinate as anions were studied by Stasiewicz et al.[41] The cytotoxicity assay was conducted with the IPC-81 rat promyelocytic leukaemia cell line.[41] The chloride-based ionic liquids revealed to be more toxic to cells than those containing the acesulphamate and saccharinate anions.[41]

Microtox® essays were carried out by Pretti et al.[52] to test the toxicity of some morpholinium (Morph) and *N*-alkyl substituted 1,4-diazabicyclo[2.2.2]octane (DABCO) ionic liquids. The authors[52] observed that the EC_{50} values for both cation-based ionic liquids, with the same alkyl chain length, and with bromide as a counterion, were similar. They also concluded that increasing the cation alkyl side chain length, the EC_{50} values decrease.[52] With a comparable alkyl chain length, DABCO- and Morph-based ionic liquids are less toxic than imidazolium- or pyridinium-based salts.[52]

Ventura et al.[59] studied the toxicity of $[C_3C_1im][NTf_2]$ into five aquatic species at different trophic levels: freshwater algal growth inhibition (*Pseudokirchneriella subcapitata* and *Chlorella vulgaris*), freshwater cladocerans' immobilization and chronic traits (*Daphnia magna* and *Daphnia longispina*) and luminescent marine bacteria (*Vibrio fischeri*). The Microtox® essays (with *V. fischeri* bacteria) showed that this ionic liquid has a moderate toxicity, and in comparison with conventional organic solvents, this ionic liquid presents a lower toxicity.[59] Considering the algae tests, *P. subcapitata* seemed to be more tolerant to the ionic liquid than *C. vulgaris*.[59] Testing other organic solvents with the same algae, the ionic liquid toxicity is lower than xylenes.[59] The acute and chronic tests with *D. magna* and *D. longispina* demonstrated that the former species is more tolerant to higher ionic liquid concentrations than the latter one.[59] Later, the same group of researchers enlarged the knowledge of the ionic liquids toxicity by studying their structural effects, namely their cation aromaticity and alkyl substitutions, as well as the anion nature.[60] In this work, the toxicological data were analysed for different species: *V. fisheri*, *P. subcapitata* and *D. magna*. The authors[60] concluded that even if, in general, the toxicity increases with the hydrophobicity of the ionic liquid, the different response of these ionic liquids to the distinct toxicity tests shows that they could be divided into two different groups (aromatic and non-aromatic ionic liquids), and both their solubility and toxicity can be minimized by a correct manipulation of their aromaticity character.[60] Considering only the Microtox tests with the *V. fisheri* bacteria, it was possible to evaluate the toxicity of different ionic liquid cation families, *viz.* phosphonium, imidazolium and guanidinium.[61] Unlike imidazolium- and phosphonium-based ionic liquids, the authors found that the increasing of the alkyl chain length in guanidinium-based ionic liquids don't increase the toxicity of

these ionic liquids.[61] In fact, they also found that the incorporation of ester or ether groups in the alkyl chain of guanidinium and imidazolium ionic liquids decreases their toxicity, and the phosphonium-based compounds are the most toxic from the ionic liquids studied.[61] Considering the same toxicity test, the toxicity of cholinium-based ionic liquids was also evaluated and found to be higher than what was expected (higher than some common organic solvents), since the cholinium chloride is a complex B vitamin and widely used in food industry.[62] Therefore, the influence of the anion on the ionic liquid toxicity proved to be of utmost importance and cannot be discarded.[62] In addition, another class of ionic liquids were prepared based on mandelic acid, and their toxicity was evaluated using different bacterial and algae toxicity tests.[63] These ionic liquids consist on imidazolium and pyridinium cations with substituent groups derived from mandelic acid combined with chloride and bromide anions, and presented low toxicity to all freshwater green algae, and to Gram-positive (*Bacillus subtilis*) and Gram-negative (*Escherichia coli*, *Pseudomona fluoroscens*, *Pseudomona putida* (CP1), and *Pseudomona putida* (KT 2440)) bacteria strains studied.[63]

Despite all the ionic liquid toxicity studies made over the years, the majority still relays on the investigation of imidazolium-based fluids.[64] Furthermore, it seems that the research in this field is randomly done, and a conclusive analysis of the ionic liquids toxicity it's hard to find (majorly due to the large number of cations and anions combinations in ionic liquids).[64] Therefore, legislation demands and standardised tests should be mandatory before any industrial application of novel ionic liquids.[64]

1.1.2 Water treatments

AQUEOUS BIPHASIC SYSTEMS

Aqueous biphasic systems (ABS) are formed when two mutually incompatible, though both miscible with water (at least in a large extent), polymer/polymer, polymer/salt, or salt/salt combinations are mixed in water. Above a given concentration of those components, the spontaneous phase separation takes place.[65] Aiming at removing ionic liquids from aqueous effluents, studies promoting the separation of ionic liquids from

aqueous solutions through the creation of ABS, by salts addition, were carried out by several authors.[66–73]

Gutowski et al.[71] were the first to suggest that a hydrophilic ionic liquid ($[C_4C_1im]Cl$) could undergo phase separation in aqueous solution by the addition of an inorganic salt (K_3PO_4). In 2007, Zafarani-Moattar and Hamzehzadeh[74] studied the capability of $[C_4C_1im]Br$ to form ABS with aqueous solutions of K_2HPO_4 and K_3PO_4. From the gathered results, it was possible to conclude that the high-charge density K_3PO_4 had the largest potential to induce the IL-rich phase separation.[74] Moreover, the authors calculated the effective excluded volume (EEV) and found that an increase in this value is reflected in the ternary phase diagram, corresponding to an increase in the area representing the biphasic region. Pei et al.[75] studied the aqueous liquid-liquid equilibrium of some imidazolium-based ionic liquids ($[C_4C_1im]Cl$, $[C_6C_1im]Cl$, $[C_4C_1im]Br$, $[C_6C_1im]Br$, $[C_8C_1im]Br$ and $[C_{10}C_1im]Br$) with several inorganic salts (KOH, K_2HPO_4, K_2CO_3, K_3PO_4). Ionic liquids with longer alkyl chains, while combined with Br^-, can more easily form ABS.[75] In addition, the ability of the salts to promote the phase separation follows the order: $K_3PO_4 > K_2HPO_4 \approx K_2CO_3 > KOH$.[75] This trend could be explained on the basis of the Hofmeister[76] series. The salting-out inducing ions, PO_4^{3-}, HPO_4^{2-}, CO_3^{2-}, and OH^- have the ability to promote ABS. This implies that anions with a higher valence are better salting-out agents since they can form more hydrated complexes with water molecules, and thus decrease the amount of water available to hydrate the ionic liquids. The authors[75] also studied the effect of temperature on the ABS formation, which showed to have no significant influence on the temperature range evaluated.[75] Bridges et al.[77] studied the ABS formation with a large variety of salts, such as K_3PO_4, K_2HPO_4, K_2CO_3, KOH, and $(NH_4)_2SO_4$ and several ionic liquids, namely $[C_4C_1im]Cl$, $[C_4C_1C_1im]Cl$, $[C_4py]Cl$, $[N_{4444}]Cl$, and $[P_{4444}]Cl$. The authors[75] confirmed that the ability for ABS formation follows the rank: $K_3PO_4 > K_2HPO_4 > K_2CO_3 >> KOH$, while the facility of ionic liquids to undergo through phase separation follows the trend: $[P_{4444}]Cl > [N_{4444}]Cl >> [C_4py]Cl >> [C_4C_1C_1im]Cl \approx [C_4C_1im]Cl$.[77] In more extended works,[67–69] the ability of several ionic liquids towards their aqueous phase separation with K_3PO_4 was studied. With that aim diverse ionic liquids were studied by the combination of a large range of cations ($[C_1C_1im]^+$, $[C_2C_1im]^+$, $[C_4C_1im]^+$, $[C_6C_1im]^+$, $[(C_7H_7)C_1im]^+$, $[aC_1im]^+$,

$[OHC_2C_1im]^+$, $[im]^+$, $[C_1im]^+$, $[C_2im]^+$)[68] and various anions (Cl^-, Br^-, $[CH_3CO_2]^-$, $[HSO_4]^-$, $[CH_3SO_4]^-$, $[C_2H_5SO_4]^-$, $[CH_3SO_3]^-$, $[CF_3SO_3]^-$, $[CF_3CO_2]^-$ and $[N(CN)_2]^-$).[67] Taking into account the cation influence, the increase of the alkyl chain length (for mono- or di-substituted ionic liquids) increases the phase separation ability, whereas the insertion of a double bond, a benzyl group, or a hydroxyl group leads to a decrease on the ABS promotion capability. Furthermore, an unusual behaviour of the mono- and unsubstituted ionic liquids was observed.[68] For the same concentration of K_3PO_4, two monophasic and one biphasic regions were observed, and thus these system can be moved between the various phase regimes by simple variation of the ionic liquid concentration.[68] Concerning the anion effect, the ability of $[C_2C_1im]$ and $[C_4C_1im]$-based cations to form ABS follows the trend: $[C_2C_1im][CF_3SO_3]$ > $[C_2C_1im][C_2H_5SO_4]$ > $[C_2C_1im][CH_3SO_4]$ > $[C_2C_1im]Br$ > $[C_2C_1im]Cl$ ≈ $[C_2C_1im][CH_3CO_2]$ > $[C_2C_1im][CH_3SO_3]$ and $[C_4C_1im][CF_3SO_3]$ > $[C_4C_1im][N(CN)_2]$ > $[C_4C_1im][HSO_4]$ > $[C_4C_1im][CF_3SO_3]$ > $[C_4C_1im]Br$ > $[C_4C_1im]Cl$ ≈ $[C_4C_1im][CH_3CO_2]$ ≈ $[C_4C_1im][CH_3SO_3]$.[67] In this work it was observed that the facility of imidazolium-based ionic liquids to undergo aqueous phase separation closely follows the decrease on hydrogen bond accepting strength of the anions composing the ionic liquid.[67] In another work,[69] the salt K_3PO_4 was evaluated to promote ABS of phosphonium-based ionic liquids, such as tri(isobutyl)methylphosphonium tosylate ($[P_{i(444)1}][Tos]$), tributyl(methyl)phosphonium methylsulphate ($[P_{4441}][CH_3SO_4]$) and tetrabutylphosphonium bromide ($[P_{4444}]Br$). These phosphonium-based ionic liquids showed to be more easily extracted from the water phase than imidazolium-based ionic liquids with similar anions.[67] Taking into consideration the ability of different salts to promote the phase separation, a research work focused in ternary diagrams composed of sodium-, chloride- and acetate-based salts, water and a common ionic liquid ($[C_4C_1im][CF_3SO_3]$) was recently published.[73] The authors[73] explored the salt cation and anion ability to induce the liquid-liquid demixing and found that for sodium-based salts the following order was found: PO_4^{3-} > $C_6H_5O_7^{3-}$ > HPO_4^{2-} ≈ CO_3^{2-} > SO_4^{2-} ≈ SO_3^{2-} > $C_4H_4O_6^{2-}$ >> $H_2PO_4^-$ > OH^- > $CH_3CO_2^-$ ≈ HSO_4^- ≈ HCO_3^- > Cl^-. On the other hand, for chloride based-salts the cation rank follows the rank: Mg^{2+} ≈ Ni^{2+} ≈ Sr^{2+} > Ca^{2+} >> Na^+ > K^+

> Cs^+.[73] These trends show that the ion charge plays a dominant role in the ABS formation while closely following the Hofmeister series.[76]

Although many IL-based ABS have been reported in the last years,[65] only few works attempted them as a method to remove ionic liquids from aqueous solutions. Wu et al.[78,79] reported the recovery of different ionic liquids from aqueous solutions with different carbohydrates. With sucrose they could recover 65% of [aC_1im]Br and 63% of [aC_1im]Cl.[79] On the other hand, with the ionic liquid [C_4C_1im][BF_4] and changing the sugar the following recoveries were obtained (still not satisfactory): 74% for sucrose, 72% for xylose, 64% for fructose and 61% for glucose.[78] Deng et al.[80] presented the recovery of [aC_1im]Cl with three different salts: K_3PO_4, K_2HPO_4, and K_2CO_3. The authors[80] found that, at the same concentration of salts, the recovery efficiency follows the order K_3PO_4 > K_2HPO_4 > K_2CO_3. A 96.80% recovery of ionic liquid was attained by the addition of 46.48% of K_2HPO_4.[80] On the other hand, Li et al.[81] studied the effect of some sodium-based salts with [C_4C_1im][BF_4]. The salts used were Na_3PO_4, Na_2CO_3, Na_2SO_4, NaH_2PO_4, and NaCl, and they found that with a mass fraction of 16.94% of Na_2CO_3 a recovery efficiency of 98.77% was reached. Despite the good results obtained, the use of [C_4C_1im][BF_4] should embody higher precautions, since, as well known, this ionic liquid suffers hydrolysis in contact with water.[27]

PHYSICO-CHEMICAL TREATMENTS

Another type of approach commonly used, when envisaging the treatment of aqueous solutions containing ionic liquids, consists on their physico-chemical degradation. This type of treatment addresses mostly the oxidative, thermal and photocatalytic degradation.

In 2004, Awad et al.[82] reported a work on the thermal stability of several alkylimidazolium ionic liquids combined with $[PF_6]^-$, $[BF_4]^-$, $[NTf_2]^-$, Cl^- and Br^-, and the same salts intercalated into montmorillonite silicate. Using thermogravimetric analyses it was demonstrated that the thermal stability of these ionic liquids increases with their adsorption into montmorillonite silicate. Still, this enhanced stability was only observed

for the halide-based anions, while for $[PF_6]^-$ and $[BF_4]^-$ anions the improvement was minimal. In addition, the thermal stability of the ionic liquid incorporated with the mentioned silicate decreases by increasing the ionic liquid alkyl chain length, and with the atmospheric oxygen content.[82] Using thermogravimetric assays coupled with Fourier Transform Infrared Spectroscopy (TGA–FTIR), it was possible to identify the degradation products of $[C_{16}C_1C_1im][BF_4]$ and this salt intercalated with montmorillonite silicate.[82] The major products found were the same for both compounds, and are water, CO_2 and hydrocarbons.[82] The authors further found that the anion plays a fundamental role on the thermal stability of the pure ionic liquids that follows the trend: $Br^- \approx Cl^- < [BF_4]^- < [NTf_2]^- < [PF_6]^-$.[82]

Stepnowski and Zaleska[83] studied the photodegradation of imidazolium-based ionic liquids using three methods: UV, UV/H_2O_2 and UV/TiO_2. The most effective method to degrade ionic liquids was found to be the UV/H_2O_2. From all the ionic liquids studied the most stable was the $[C_2C_2im]$-based ionic liquid; yet, concerning the remaining ionic liquids, those with longer alkyl side chain lengths, like $[C_8C_1im]^+$, were found to be the most stable. Thus, the size of the cation side alkyl chain seems to be responsible for the ionic liquid stability, and from the ionic liquids investigated, $[C_8C_2im]^+$ and $[C_6C_2im]^+$ must be the most stable.

Berthon et al.[84] studied the photodegradation of $[C_4C_1im][PF_6]$ and $[C_4C_1im][NTf_2]$ under gamma radiolysis (^{137}Cs) in an argon atmosphere and air. The argon atmosphere was used to prevent the absorption of water and oxygen by the ionic liquid. The radiolysis under the argon atmosphere revealed to not influence some ionic liquids properties, such as density, surface tension and refractive index. On the other hand, properties such as viscosity and conductivity are directly affected with the irradiation of 30% of TBP-dodecane.[84] The viscosity increase could be related to the hydrogen bonding between the radiolysis products and protons of the imidazolium ring, while the decreasing on conductivity is totally related with the increasing of viscosity under gamma radiation.[84] With NMR (Nuclear Magnetic Resonance) and ESI–MS (Electrospray Ionization–Mass

Spectrometry) data, minimal concentrations of the products of degradation were detected. The same conclusions were achieved under the air atmosphere.[84]

Li and co-workers[85] investigated the degradation of 1,3-dialkylimidazolium ionic liquids in an H_2O_2/CH_3CO_2H aqueous solution assisted by ultrasonic chemical radiation. They found that, after 12 h and at 50 °C, the diverse 1,3-alkylimidazolium ionic liquids degraded 93%, while after 72 h, the degradation reached a value closer to 99%.[85] By GC–MS results, it was concluded that the first attack is to the hydrogens of the imidazolium ring.[85] With this type of oxidation, this work shows that the anion nature and the alkyl side chain length do not affect the degradation process.[85] Finally, a mechanism for the degradation was proposed and the products obtained were identified.[85] The vulnerable sites of the C-N bonds and the kinetic inertness of N-C-N moiety in these ionic liquids and derivatives were particularly important for the radical assisted oxidative cleavages.[85] The stable products of degradation are acetoxyacetic acid and biurea, after selective cleavages on the C-N bond that led to the ring opening.[85]

In 2008, Siedlecka et al.[86] reported the degradation of $[C_4C_1im]Cl$ in water using a Fenton-like system. This system consists in a solution of hydrogen peroxide (H_2O_2) and an iron catalyst (Fe^{3+}) that is used to oxidize contaminants. This is a simple and effective method that decomposes almost all the ionic liquid content in aqueous solution in 90 min. As reported before,[85] the primary step of the degradation is the attack to one of the hydrogens present at the imidazolium ring.

Siedlecka et al.[87] further studied the generated fragments resulting from the photocatalytic degradation with a Fenton-like system (with 100 mM of H_2O_2). In general, the intermediates of the ionic liquid degradation change over the reaction time.[87] Furthermore, 10 min after the beginning of the decomposition, the first intermediates were molecules functionalized with carbonyl substituents in the imidazolium ring.[87] After 10 min, the $[C_4C_1im]^+$ imidazole derivatives dominate the products of degradation while, after 20 min, the major products result from the opening of the imidazole ring.[87]

Itakura et al.[88] studied the photocatalytic degradation (PD) of the organic cation of the ionic liquids $[C_2C_1im]Br$, $[C_2C_1im][PF_6]$ and $[C_4C_1im][BF_4]$, and removed the inorganic anions by a simple hydrothermal mineralization (HM) with $Ca(OH)_2$.[89,90] PD tests with $[C_2C_1im]Br$ confirmed that the cation is decomposed into ethylamine, that further decomposes into CO_2 (the anion Br^- is not toxic, so its treatment was not addressed). To apply an adequate treatment to $[C_2C_1im][PF_6]$, it was found that only a combined treatment of HM, to remove the anion, followed by a PD, to decompose the cation, could remove both decomposed products as precipitation products and CO_2, respectively. The same result was obtained with $[C_4C_1im][BF_4]$, showing that there is almost no difference in PD treatment for $[C_2C_1im]^+$ and $[C_4C_1im]^+$.[88]

Siedlecka and Stepnowski[91] studied the degradation of some alkylmethylimidazolium (C_4, C_6 and C_8) and 3-methyl-*N*-butylpyridinium chloride ionic liquids with different concentrations of hydrogen peroxide in a Fenton-like system. The results showed a total degradation of the $[C_4C_1im]Cl$ after 60 min with the concentration of 400 mM of H_2O_2.[91] This result was proven by ^1H NMR spectra, where the ring showed a total degradation and also demonstrated that the first stage of the degradation (30 min) occurs through a non-specific attack of the radical $OH^\bullet$, with no changes in the ring or alkyl chain.[91] In general, the degradation was improved with increasing concentrations of H_2O_2 and longer aliphatic moieties showed more resistance to the degradation. These conclusions are valid for imidazolium-based cations; yet, pyridinium-based ionic liquids showed better degradation to the lowest concentration of H_2O_2 (100 mM). In addition, the change of the cation from imidazolium to pyridinium also reduces the ionic liquid degradation capability.[91]

ADSORPTION ONTO ACTIVATED CARBON

In 2001, Anthony et al.[92] were the first to purpose the removal of ionic liquids from aqueous solutions by adsorption onto activated carbon (AC). In particular, the capability of AC to adsorb $[C_4C_1im][PF_6]$[92] or toluene[93,94] was compared. The authors concluded that around 50 times less AC is required to remove toluene from water than $[C_4C_1im][PF_6]$.[92] Since AC is generally more efficient for removing small and nonpolar compounds such as

toluene, rather than polar or ionic species like ionic liquids, this was indeed an expected result. However, even if it was possible to remove this ionic liquid from aqueous solution, its recovery wasn't successful.[92]

Later, Palomar et al.[95] studied the effect of the ionic liquid structure on the adsorption onto AC. Taking into consideration the cation, increasing the cation alkyl chain length was found to rises the adsorption capacity.[95] In addition, the capacity of the AC to adsorb ionic liquids is highly influenced by the nature of the anion, following the hydrophobicity order: $[NTf_2]^-$ > $[PF_6]^-$ > $[CF_3SO_3]^-$ > $[BF_4]^-$ > $[CF_3CO_2]^-$ > Cl^-.[95] The effect of temperature on the adsorption capacity was also studied, and an increase in the temperature decreases the adsorption capacity of AC to adsorb $[C_8C_1im][PF_6]$. Particularly of high importance, the addition of acetone was suggested as a process to recover the ionic liquid from AC. Even if the capacity of the AC was maintained,[95] there are still some reservations considering the degradation of the ionic liquid due to the contact with acetone.[96,97] Nevertheless, this was the first[95] and only attempt up to now regarding the investigation of the ionic liquid recovery after its adsorption onto AC. Finally, the influence of different treatments on AC was explored. It was found that by increasing the oxygenated groups in the AC surface reduces the adsorption capacity for the most hydrophobic ionic liquids, whereas for the most hydrophilic ionic liquids, the increase of oxygenated groups in the AC surface improves the adsorption of ionic liquids, particularly those with more basic anions (like Cl^- and $[CH_3SO_3]^-$).[95] In the same line of thought, it should be highlighted that the same group published additional works.[98–100] The authors found that the kinetics of the ionic liquid adsorption is much more slower than that of phenol (as a reference solute).[98] The effect of temperature, AC particle size, stirring velocity (that showed to have a marginal influence), and the initial concentration of the ionic liquid were also evaluated.[98] Considering the particle size, the adsorption rate of $[C_8C_1im][PF_6]$ clearly increases when decreasing the AC particle size, whereas the equilibrium capacity remains almost constant.[98] Increasing the initial concentration of ionic liquid leads to a higher driving force which further gives rise to a faster adsorption, while the plateau of the kinetic curves is reached at a nearly similar contact time, and therefore a significantly higher amount of ionic liquid is adsorbed onto the AC at equilibrium. Finally, higher

temperatures have the advantage of a faster adsorption. However, for longer contact times, a higher capacity of adsorption is attained at lower temperatures.[98] A proper selection of the AC type, namely high surface area, high content of accessible pores narrower than 8 nm, and low concentration of oxygen surface groups on the carbon surface, leads to an improved removal of hydrophobic ionic liquids from water.[99]

Recently, Qi et al.[101,102] modified the surface of a carbonaceous material in order to improve the adsorption of hydrophilic ionic liquids. First, they loaded functional carbonaceous material (FCM) with carboxylic groups by hydrothermal carbonization of cellulose in the presence of acrylic acid.[102] The resultant material has a low surface area and exhibits an adsorption capacity comparable to that of commercial AC. Therefore, the high adsorption capacity for ionic liquids can be attributed to the high content of polar oxygenated groups.[102] The authors[101] further prepared a carbonaceous material with a higher number of oxygenated groups, but with higher surface area. This modified carbonaceous material presented an adsorption capacity, for a representative number of hydrophilic ionic liquids, up to three times higher than that of commercial AC.[101]

1.2. Scope and objectives

As mentioned above, ionic liquids present a wide variety of interesting properties that allow them to be good alternative solvents for a large plethora of applications.[2] In this context, Chapter 2 represents a proof of concept on the improvements afforded by ionic liquids in two separation processes. Here, the ability of IL-based ABS to completely extract alkaloids (like caffeine and nicotine) in one single-step procedure from artificial human urine samples was demonstrated envisaging the development of cost-effective procedures for doping control. The second process demonstrated the enhanced capability of ionic liquids to separate ethanol-water mixtures by a liquid-liquid extraction – an energetically less expensive approach when compared to distillation where the ethanol-water azeotrope is the major drawback. However, even if these solvents cannot contribute to air pollution, in both approaches they are in contact with water and can be further dispersed into aquatic streams,[5–7] thus leading to environmental problems.

Hence, their relative toxicity[52,59,60,63,103–107] and poor biodegradability[44,52,103,108–110] represent two of their major concerns. In this context, the treatment of wastewater streams is imperative. Most of these treatments consist on oxidative[86,87,91], thermal[82] and photocatalytic[19,84,85,88–90] degradations. Nevertheless, these kind of treatments don't allow the recovery of the ionic liquid since they are removed by degradation reactions, although the products of these reactions are usually less toxic.[82,88]

Taking into consideration the panorama here described, one of the principal aims of this work is to evaluate the impact of ionic liquids in aquatic streams by the determination of their solubility in water (saturation values), and to propose efficient, low-cost, and greener processes to remove and/or recover ionic liquids from wastewater streams. To this end, the mutual solubilities between different hydrophobic ionic liquids and water were experimentally measured and are reported in Chapter 3. The different structures of the ionic liquids used allowed a deep understanding of the amount of dispersion of these solvents. It was evaluated the anion nature, the cation family, and the alkyl chain length, isomerism and symmetry of the cation through their liquid-liquid phase diagrams with water. To complement the experimental data measured, the thermodynamic functions of solution were additionally determined. The solubility data were also used to evaluate the ability of COSMO-RS to predict the phase diagrams aiming at avoiding further extensive experimental measurements. Finally, molecular dynamics simulations were also attempted in order to achieve a better understanding of the liquid-liquid systems behaviour at a molecular level.

Envisaging the removal and recovery of ionic liquids from aqueous streams, in Chapter 4, ABS composed of aluminium-based salts, commonly used in water treatment processes, were employed in order to address the ionic liquids recovery efficiency. Taking into consideration previous works,[78–81] here, and beyond the improved recovery obtained for all the ionic liquids investigated, a simple process to recover the ionic liquid and to recycle the remaining salt solution is also proposed. This approach proved to be valuable for the removal of large amounts of hydrophilic ionic liquids from aqueous solutions.

Another approach that has been studied in the past few years,[92,95,98,99,101,102] for the removal of ionic liquids from aqueous environments, consists on the ionic liquids adsorption onto activated carbon. In this line of research, the activated carbon was here tested as a way to remove several ionic liquids from aqueous solutions. By several structural combinations it was possible to get a broad knowledge on the influence of the ionic liquid chemical structure through its adsorption onto AC. In particular, the effects of the anion nature, cation family, alkyl side chain length, symmetry and number of alkyl substitutions at the cation are presented in Chapter 5. Since hydrophobic ionic liquids can be more easily adsorbed than hydrophilic ones,[95,98,99] in the same chapter, the investigation regarding the addition of an inorganic salt aiming the improvement of the ionic liquids adsorption is also presented. In order to complement the experimental data, the COSMO-RS was also used for a more comprehensive study on the role of the cationic and anionic structures in the adsorption process.

Chapter 2 – Ionic-Liquid-based Processes

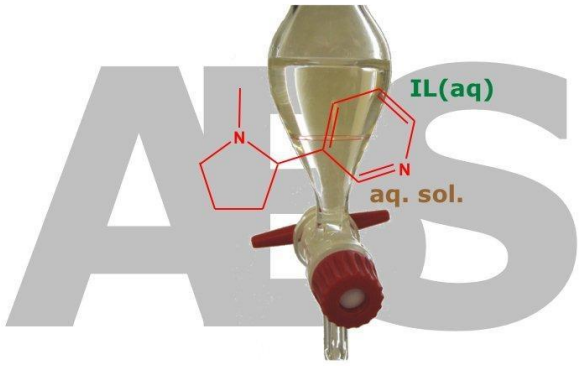

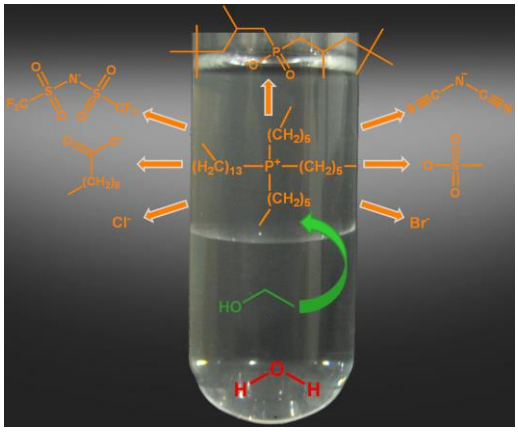

2.1. High-performance extraction of alkaloids using aqueous two-phase systems with ionic liquids

Mara G. Freire, Catarina M. S. S. Neves, Isabel M. Marrucho, José N. Canongia Lopes, Luís Paulo N. Rebelo and João A. P. Coutinho, Green Chemistry 12 (2010) 1715-1718, DOI: 10.1039/c0gc00179a.

The use of doping agents by athletes to improve athletic performance is a major concern in endurance sports. The International Olympic Committee listed caffeine and nicotine, two easily obtainable alkaloids – see Figure 2.1 – as stimulant, ergogenic and restricted drugs.[111–113]

Figure 2.1. Molecular structures of caffeine (a) and nicotine (b).

Although not prohibited by the World Anti-Doping Agency, their use is limited to specific levels. For instance, in the case of caffeine, threshold urinary levels of 12 $\mu g \cdot mL^{-1}$ have been established by several sports federations.[111–113] Levels above such threshold are viewed as achieved through a deliberate attempt at doping by the athlete. Drugs and/or metabolites in human fluid samples are usually identified by mass spectrometry.[114,115] Although most analyses are qualitative, in some cases, quantitative determinations are required (*e.g.* caffeine, ephedrine and opium alkaloids). Quantitative determinations are regularly accomplished by chromatographic and spectroscopic methods, which inherently require the pre-treatment of samples by the application of extraction methods (mainly to increase the metabolites and drug concentration from the original sample); later, if appropriate, hydrolysis and/or derivatization steps are performed.[114,115] There is already

evidence that, for instance, the direct quantification of opium alkaloids, testosterone and epitestosterone in IL-rich phases using High Performance Liquid Chromatography (HPLC) is possible, and no interferences of the ionic liquid were found.[116,117]

Aqueous two-phase systems or aqueous biphasic systems (ABS) are composed of two immiscible phases, both of which are water-rich phases. ABS constitute a "greener" and potentially more efficient pre-treatment solution in liquid-liquid extractions. ABS were first introduced[118] in the eighties and have since been applied for separation, fractionation, and molecular characterization of biological macromolecules. In the past few years, ABS have been intensely explored for the recovery of metal ions, radiochemicals, dyes, drug molecules, small organic species and inorganic particles.[119–121]

Recently, Rogers and co-workers[71] have demonstrated the ability of ionic liquids (ILs) to induce ABS in the presence of inorganic salts. Attempts to extract (bio)molecules and/or drugs using such IL-based ABS are rare: merely short chain alcohols,[71] phenol,[122] bovine serum albumine,[123,124] testosterone,[116] epitestosterone,[116] penicillin G,[125] opium alkaloids,[117] L-tryptophan,[67–69] and antibiotics[126] have been investigated as partitioning solutes. Efforts to extract alkaloids such as caffeine, nicotine and opium alkaloids using IL-based ABS may be highly relevant as a new approach in liquid-liquid extraction trials. The remarkably strong ability of IL-based ABS to extract (completely) caffeine and nicotine in a single-step procedure is here reported for the first time. Therefore, there is potential both for achieving highly concentrated samples of alkaloids for further quantitative analysis and for engineering strategies to obtain alkaloid-free matrixes. It is here shown that due to the very high concentration effect attained by using IL-based ABS on alkaloid-containing solutions, human fluid samples can *e.g.* be effortlessly checked for their alkaloid content. In addition, the required quantities of ionic liquid can be reduced to very low levels.

Most previous studies[116,117,122–125] have focused on just one ionic liquid (usually $[C_4C_1im]Cl$ or $[C_nC_1im]Br$ with n = 4, 6 and 8) and on the influence of several inorganic salts in phase diagrams (where the ion's influence follows the well-known Hofmeister series[66,127,128]). However, the efficiency of IL-based ABS extractions should also be planned taking into

account the correct choice of the anion and/or cation that compose the ionic liquid. Therefore, in this work, the focus is testing the marked ability of distinct ionic liquids as constituents of the extraction media – both in aqueous phases and more complex matrixes, such as human urine-type samples – and on the influence of ionic liquid/inorganic salt concentrations. To this end, the partition coefficients, *K*, of two main alkaloids – caffeine and nicotine – between an aqueous IL-rich phase and an aqueous K_3PO_4-rich phase were measured. The partition coefficients of caffeine (K_{caf}) or nicotine (K_{nic}) are defined as the ratio between the concentrations of the alkaloids in the IL- and K_3PO_4-rich phases. Details regarding equilibration time and experimental procedures, as well as the mapping of ternary phase behaviour, can be found elsewhere.[67,68,129,130] Rather than attempting to provide the partition coefficients of both alkaloids, this work is focused in providing a comprehensive emphasis on the improved ability of ionic liquids as extraction media.

The influence of both ionic liquid cation and anion in extracting caffeine and nicotine while maintaining the same inorganic salt (K_3PO_4) for ABS formation, as well the composition in the ternary phase diagrams, have been evaluated. Here, several ionic liquids, that are reported in Table 2.1 and their structures depicted in Figure 2.2, have been used to assess the impact of their chemical nature.

Table 2.1. ILs used and respective acronym, supplier and structure correspondence.

IL		Supplier	Structure
Name	Acronym		
1-ethyl-3-methylimidazolium methylsulphate	$[C_2C_1im][CH_3SO_4]$	Iolitec	(i)
1-ethyl-3-methylimidazolium ethylsulphate	$[C_2C_1im][C_2H_5SO_4]$	Iolitec	(ii)
1-ethyl-3-methylimidazolium acetate	$[C_2C_1im][CH_3CO_2]$	Iolitec	(iii)
1-ethyl-3-methylimidazolium trifluoromethanesulfonate (triflate)	$[C_2C_1im][CF_3SO_3]$	Iolitec	(iv)
1-ethyl-3-methylimidazolium chloride	$[C_2C_1im]Cl$	Iolitec	(v)
1-butyl-3-methylimidazolium chloride	$[C_4C_1im]Cl$	Iolitec	(vi)
1-butyl-3-methylimidazolium bromide	$[C_4C_1im]Br$	Iolitec	(vii)
1-butyl-3-methylimidazolium methylsulfonate	$[C_4C_1im][CH_3SO_3]$	Iolitec	(viii)
1-butyl-3-methylimidazolium trifluoromethanesulfonate (triflate)	$[C_4C_1im][CF_3SO_3]$	Iolitec	(ix)
1-butyl-3- methylimidazolium trifluoroacetate	$[C_4C_1im][CF_3CO_2]$	Solchemar	(x)
1-butyl-2,3-dimethylimidazolium chloride	$[C_4C_1C_1im]Cl$	Iolitec	(xi)
1-hydroxyethyl-3-methylimidazolium chloride	$[OHC_2C_1im]Cl$	Iolitec	(xii)
1-benzyl-3-methylimidazolium chloride	$[(C_7H_7)C_1im]Cl$	Iolitec	(xiii)
1-allyl-3-methylimidazolium chloride	$[aC_1im]Cl$	Iolitec	(xiv)
1-hexyl-3-methylimidazolium chloride	$[C_6C_1im]Cl$	Iolitec	(xv)
1-heptyl-3-methylimidazolium chloride	$[C_7C_1im]Cl$	Iolitec	(xvi)
1-methyl-3-octylimidazolium chloride	$[C_8C_1im]Cl$	Iolitec	(xvii)
1-decyl-3-methylimidazolium chloride	$[C_{10}C_1im]Cl$	Iolitec	(xviii)
1-dodecyl-3-methylimidazolium chloride	$[C_{12}C_1im]Cl$	Iolitec	(xix)

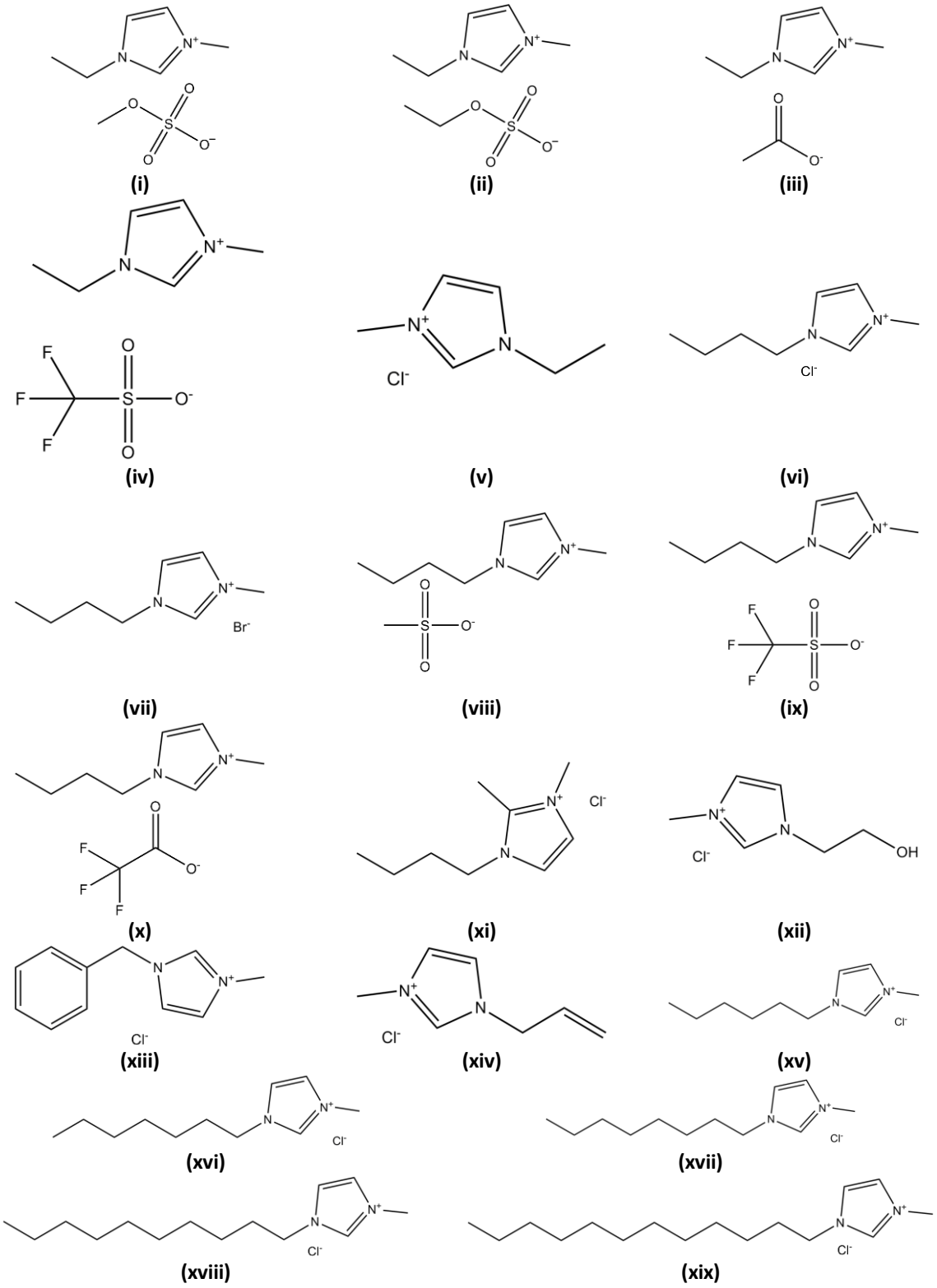

Figure 2.2. Chemical structures of the ILs used.

The quantification of the alkaloids in both phases was carried out by UV spectroscopy. Initial concentrations of caffeine and nicotine for phase distribution at the water ternary

composition were, respectively, 2.6 × 10^{-2} mol·dm^{-3} and 2.5 × 10^{-2} mol·dm^{-3}. Possible interferences of the inorganic salt, ionic liquid or urea with the analytical method were taken into account and blank control samples were used whenever necessary. The partition coefficients and respective standard deviations are the result of at least three independent determinations. The partition coefficients of caffeine and nicotine in the ABS containing [$C_nC_1$im]Cl, [$C_4C_1C_1$im]Cl, [aC_1im]Cl, [OHC_2C_1im]Cl, [$(C_7H_7)C_1$im]Cl and [$C_nC_1$im][CF_3SO_3], at 298 K and at atmospheric pressure, are depicted in Figure 2.3. The partition coefficients at the same temperature for [C_2C_1im]- and [C_4C_1im]-based ionic liquids containing distinct anions are presented in Figure 2.4.

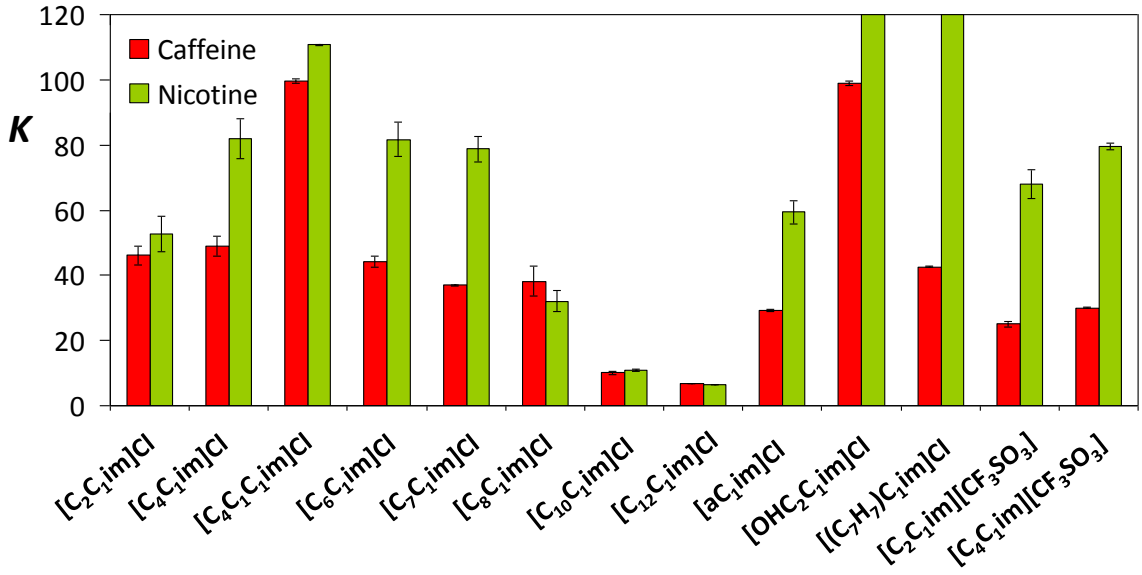

Figure 2.3. Partition coefficients, *K*, of caffeine and nicotine in different ILs/K_3PO_4 ABS at 298 K. All ABS are based on chloride or triflate ILs and contain 25 wt% of IL and 15 wt% of K_3PO_4, except the case of [OHC_2C_1im]Cl in which its concentration is 40 wt%.

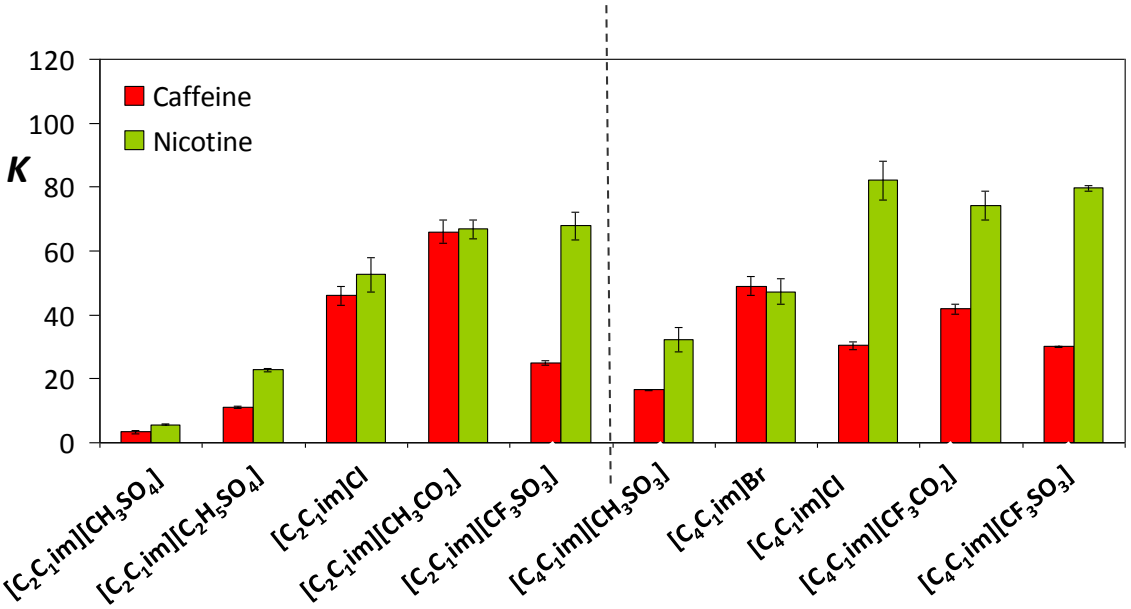

Figure 2.4. Partition coefficients, *K*, of caffeine and nicotine in different ILs/K_3PO_4 ABS at 298 K. All ABS are based on 1-ethyl-3-methylimidazolium (left) or 1-butyl-3-methylimidazolium (right) ILs and contain 25 wt% of IL and 15 wt% of K_3PO_4. The different anions were ordered according to a Hofmeister-like series.[67]

The efficiency of the extractions, reported in detail in Appendix, show that complete extraction (no detection of alkaloid in the K_3PO_4-rich phase) of each alkaloid is attained at a partition coefficient greater than *circa* 120.

It should be remarked that in previous works[67–69] it has been demonstrated that the addition of solutes at infinite dilution to the ternary ABS does not have a significant impact on the tie-lines and tie-line lengths (tie-lines and tie-line lengths are presented in Tables S2.1 and S2.2 in Appendix).

From the results depicted in Figures 2.3 and 2.4, it is clear that nicotine presents higher partition coefficients compared to caffeine in basically all the studied IL-based systems. This feature mirrors that of the affinity for organic-rich phases, *i.e.*, similar behaviour is displayed in octanol-water partition coefficients (K_{ow}), where reported K_{ow} values[131] for caffeine and nicotine are, respectively, 0.85 and 14.79. Although both compounds are water soluble, nicotine's methyl-pyrrolidine ring accounts for its less-polar character and its concomitant affinity for organic phases. On the contrary, the caffeine purine ring, with two attached oxygen atoms, contributes to the compound's polarity, and thus, to a lower affinity for organic fluids. However, one should note that these (K_{ow}) values are many

times smaller than the *K* values reported here. Part of the difference may be attributed to the fact that ABS include a K_3PO_4-rich aqueous phase where the salting-out effect of the inorganic salt promotes the extraction of the alkaloids to the other (IL-rich) phase. Nevertheless, the presence of the ionic liquid also plays an important role in the process, as can be seen in Figures 2.3 and 2.4, with *K* values ranging from 3 to complete extraction.

In general terms, the influence of the ionic liquid on the complete extraction of the alkaloids depends much more on the nature of the cations than that of the anions. The results seem to indicate that extractions are driven by different factors including: *i*) hydrogen-bond interactions between the non-bonding electron pairs present in the oxygen and nitrogen atoms of the alkaloids; *ii*) acidic hydrogen atoms present in the cations of the ionic liquid; *iii*) π···π interactions between the aromatic part of the solutes and the imidazolium cation; and *iv*) dispersive-type interactions between alkyl groups of the alkaloids and the alkyl side chains of the imidazolium-based ions. Examples of such factors at work can be noticed in systems like $[(C_7H_7)C_1im]Cl$ (enhanced aromatic interactions) or $[OHC_2C_1im]Cl$ (enhanced hydrogen-bonding capabilities) that have performed especially well. The effect of the length of the alkyl side chain can be seen in the imidazolium-based ionic liquid series (left of Figure 2.3), with the *K* values achieving a maximum at $[C_4C_1C_1im]Cl$, followed by a decrease to $[C_{12}C_1im]Cl$. This can be rationalized in terms of the competition between the need to accommodate the non-polar parts of the alkaloid solutes and the progressive dilution of the ionic part of the ionic liquid as one progresses along the family.[132]

Concerning the influence of the ionic liquid anion, there seems to be a close relation to the ionic liquid salting-in/-out behaviour. From a molecular point of view, salting-in/-out effects can be understood as a delicate balance between the interactions of the two salts (ionic liquid and K_3PO_4) and the solvent (water). Previously[18] it was demonstrated the relationship between the ionic liquid anion hydrogen-bonding accepting ability and the ionic liquid ABS formation capability and the ionic liquid anions have been ranked according to their salting-in/-out inducing capacity (Hofmeister-like series). Generally, and as shown in Figure 2.4, salting-in inducing anions such as $[CF_3SO_3]^-$ are more efficient at

extracting solutes from a second liquid phase than salting-out inducing anions, such as $[CH_3SO_3]^-$, $[CH_3SO_4]^-$ and $[C_2H_5SO_4]^-$.

Figures 2.3 and 2.4 present the results for a fixed ternary system composition (ionic liquid at 25 wt% and K_3PO_4 at 15 wt%). Yet we have extended the study of the ionic liquids' extraction ability through a range of ionic liquid concentrations. Figure 2.5, illustrate the effect of increasing the ionic liquid mass fraction in the partition coefficients of caffeine and nicotine.

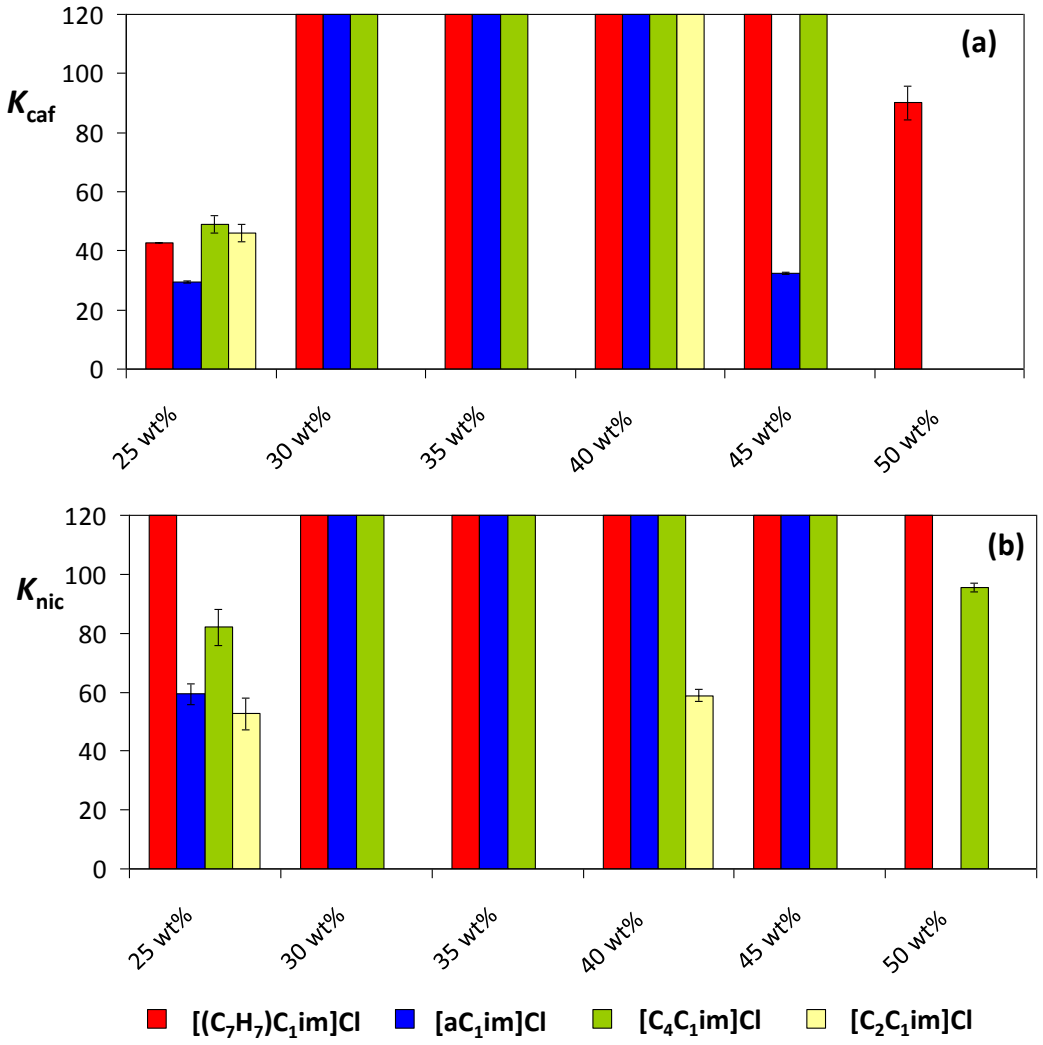

Figure 2.5. Partition coefficients of (a) caffeine and (b) nicotine in different ILs/K_3PO_4 ABS at 298 K, with K_3PO_4 at 15 wt% and different wt% of IL.

The results show that an increase of 5 wt% of ionic liquid in the overall system leads to the complete extraction of both alkaloids. In this sequence, the ionic liquid $[OHC_2C_1im]Cl$ was also studied at 40 wt% with 15 wt% of K_3PO_4, and also showed complete extraction of nicotine and a high extraction efficiency for caffeine. The results indicate that there seems to be an optimum value for the ionic liquid concentration above which the partition coefficients start to decrease. From a molecular perspective, this maximum of partition coefficients is probably related to salting-out effects of the ionic liquid over the solute. At high concentrations of ionic liquids, competition begins between the inorganic salt ions and the ionic liquid ions to salt-out such solutes. At specific concentrations, ionic liquid ions start to salt-out caffeine and nicotine to the aqueous K_3PO_4-rich phase. Curiously, the trend observed (the concentration at which each ionic liquid starts to promote salting-out) intrinsically follows the cation sequence previously observed[68] in respect to their salting-in/-out ability.

In the case of the system containing $[(C_7H_7)C_1im]Cl$, the mass fraction of K_3PO_4 was further adjusted from 15 wt% to 30 wt% in order to evaluate the inorganic salt's impact on the partitioning coefficients of nicotine and caffeine. All the results (not shown graphically but given in Appendix) led to the complete extraction of the alkaloids. This behaviour corroborates the previous results, and no maximum in the partition coefficients was found – the inorganic salt is a much stronger salting-out agent than the ionic liquid is. For economical purposes, the ionic liquid can be maintained at 25 wt% while increasing the inorganic salt concentration aiming at completely extracting both alkaloids from aqueous phases.

After the fine-tuning of ionic liquids and respective mass fraction compositions, the direct extraction of alkaloids from a synthetic biological sample – artificial human urine (with a composition described in Appendix) – was further evaluated. Quantitative extraction of caffeine and nicotine into the IL-rich phase from complex matrixes of artificial human urine is displayed in Figure 2.6. Partition coefficients obtained when employing simple aqueous phases, as previously shown, are also included for comparison.

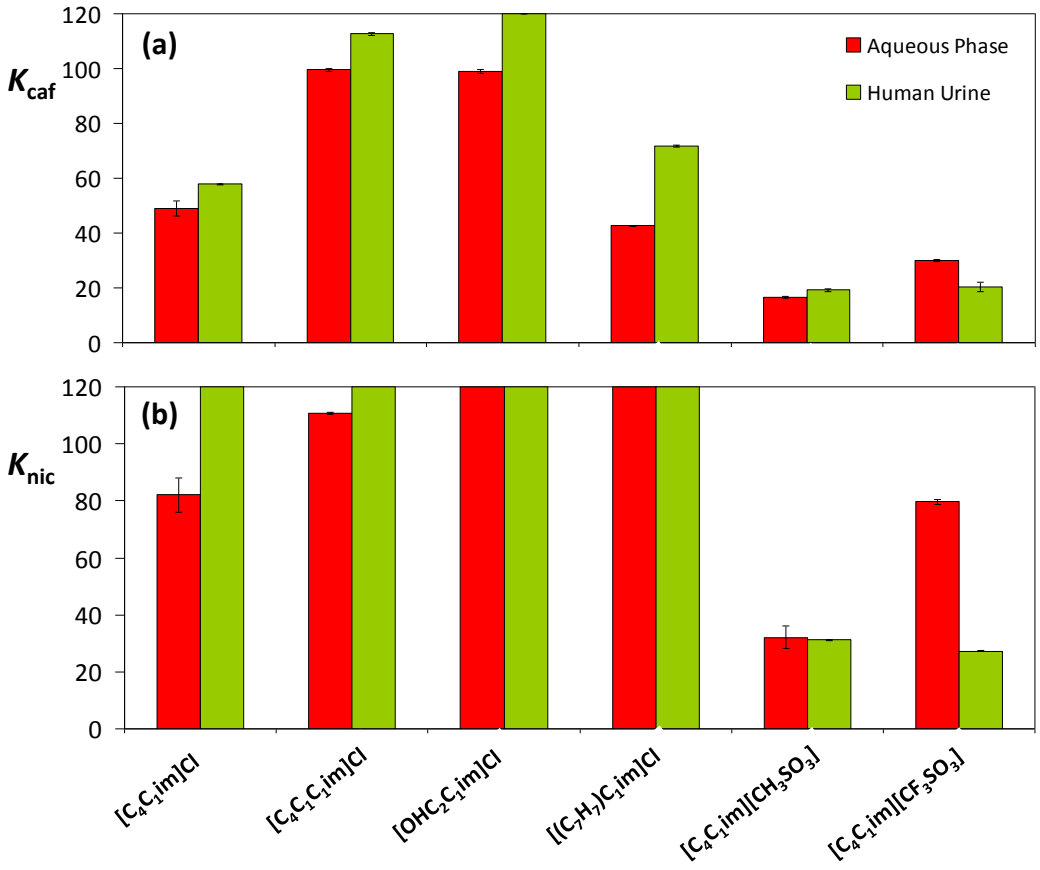

Figure 2.6. Partition coefficients of (a) caffeine and (b) nicotine in different ABS at 298 K. All ABS contain 25 wt% of IL and 15 wt% of K_3PO_4, except the case of $[OHC_2C_1im]Cl$ in which its concentration is 40 wt%.

Aiming at isolating the ionic liquid cation and anion contributions, ionic liquids based on several combinations were used to perform the extraction experiments with artificial human urine samples. The results show that with human urine samples the extractions performances of both alkaloids are significantly improved. The presence of a more complex matrix, which now includes NaCl and urea, favours the alkaloids partitioning for the IL-rich phase. Indeed, there are particular examples showing complete extraction of both alkaloids which were not previously observed with simpler aqueous phases. The main exception is the system containing the $[C_4C_1im][CF_3SO_3]$ ionic liquid, where a decrease in *K* was observed for the two partitioning solutes (nicotine and caffeine). It must be stressed out that in this case the IL-rich phase is much more concentrated in ionic liquid, as compared with the other studied ABS (see tie-lines in Tables S2.1 and S2.2 in Appendix). This fact – the relative water depletion in the IL-rich phase – may explain

the anomalous trend between the aqueous solutions with and without urea. The poorer hydration of solutes and ions at the IL-rich phase with $[C_4C_1im][CF_3SO_3]$ involves, for its turn, a higher competition between water-ion, water-urea and water-alkaloid interactions.

We have shown that complete extractions of archetypal alkaloids using IL-based Aqueous Biphasic Systems have been successfully accomplished, and, thus, new methodologies to be used for analytical purposes are immediately envisaged. The method also opens new views for the separation and concentration of other bioactive drugs. Compared to conventional liquid-liquid or solid-liquid extractions, this new approach avoids the use of volatile organic solvents, replacing them with relatively small amounts of (recyclable) ionic liquid solvents in a second aqueous phase.

2.2. Separation of ethanol-water mixtures by liquid-liquid extraction using phosphonium-based ionic liquids

Catarina M.S.S. Neves, José F.O. Granjo, Mara G. Freire, Al Robertson, Nuno M. C. Oliveira and João A. P. Coutinho, Green Chemistry 13 (2011) 1517-1526, DOI: 10.1039/C1GC15079K.

2.2.1. Abstract

Bioalcohols are produced from biomass by fermentation, and distillation is commonly used to separate the alcohol from the aqueous phase. This is, however, a high energy consumption process, and alternative approaches to this separation are being pursued. In this work, the use of phosphonium-based ionic liquids for the extraction of ethanol from fermentation broths is investigated. Ternary phase diagrams, necessary for the design and to implement an alternative liquid-liquid extraction process for the alcohol recovery, were determined for seven ionic liquids. The modelling of the equilibrium data was performed using the COSMO-RS and NRTL models; the first aiming at screening other ionic liquids not experimentally studied, and the latter aiming at designing a separation

process. The gathered data indicate that phosphonium-based ionic liquids are the best yet reported to perform water-ethanol separations. Based on the most promising phase diagrams, an analysis of the alcohol and ionic liquid recovery steps was carried out and a liquid-liquid extraction stage coupled to an extractive fermentation, where the ionic liquid is continuously recycled to the fermentator and the ethanol concentration is carried out by pervaporation, is here proposed as an alternative to distillation.

2.2.2. Introduction

The continuous depletion of oil reservoirs, the increasing oil extraction costs, the emergence of new economies where oil demand is rising exponentially, and the unstable politic situation coupled to the occurrence of natural disasters in oil producing areas, are forcing governments to redefine their energetic strategies to maintain a sustainable social development. Significant environmental concerns result from an incessant consumption of petroleum-based fuels. The combustion of fossil fuels leads to emissions of greenhouse gases and other pollutants, such as NO_x, SO_x, CO and organic volatile compounds. Consequently, a strong effort is currently being directed towards the development of sustainable alternatives to fossil fuels.

Bioethanol is being actively studied as an alternative for transportation fuels, used either as an additive to gasoline or as a standalone fuel. It can be produced from a variety of renewable staples and, hopefully, in the near future from a variety of lignocellulosic raw materials – that are widely available and do not compete with the production of food crops. It allows a cleaner combustion, reducing the emission of hazardous gases to atmosphere, and may have an important contribution to reduce CO_2 emissions and fossil fuels dependency.[133]

Bioethanol is produced by the fermentation of carbohydrates. One of the main issues associated with its production is the purification from fermentation broths. If ethanol is produced from pentoses, alcohol concentrations are usually below 5 wt%.[134] Though in general this separation is technically not very challenging for ethanol concentrations in the 5-15% range,[134] since it can be achieved through common distillation, it nevertheless

entails high energy consumptions. According to Vane,[135] the energy required to separate ethanol from water by distillation typically amounts to 10% of the energetic content of the recovered ethanol. This value increases exponentially for ethanol concentrations below 10% wt. For instance, with an ethanol solution of 6 wt% that energy cost corresponds to 17%, while for a 2 wt% alcohol mixture this value reaches 50 % of the energetic content of ethanol in the mixture.[135] Hence, a significant amount of energy is expended in the first concentration step, the so called beer column, for the purification of ethanol through a typical distillation. On the other hand, at the opposite concentration extreme, distillation is only effective up to approximately 85 wt% of ethanol. Above this turnover composition, the recovery of ethanol becomes more difficult to accomplish (due to the decrease of the volatility towards the azeotropic point), requiring the use of complementary approaches to attain anhydrous ethanol.[134,135]

In addition to the above limitations, when the manufacture of ethanol from lignocellulosic sources is considered, important differences in the production scales can be dictated by the availability of the raw materials, and new opportunities for energy and mass integration appear in the context of the additional processing steps that compose a typical biorefinery. These new features can make the classical solutions for ethanol purification less attractive in this novel context, requiring thus a systematic evaluation of alternative separation technologies.[134,136]

Arlt and co-workers[137,138] were the first to propose the use of ionic liquids (ILs) as potential solvents in extractive distillation to separate water-ethanol mixtures. The authors studied imidazolium-based ionic liquids, with chloride and tetrafluoborate anions, and concluded that these ionic solvents are improved entrainers, capable of breaking the water-ethanol azeotrope.[138] Therein after, a number of academic studies followed this work questing for ionic liquids able to effectively break the azeotropic mixture.[139–142]

Another approach, less energy intensive, used for the separation of ethanol-water mixtures is liquid-liquid extraction, especially when coupled with the use of extractive fermentations.[134,135] Boudreau and Hill[143] reported that liquid-liquid extraction could reduce the energy consumption on the ethanol-water separation by *circa* 40% when

compared with the distillation technique. Fadeev and Meagher[144] reported the pioneer work on the use of ionic liquids for the separation of alcohol-water mixtures by liquid-liquid extraction. The authors suggested the use of hexafluorophosphate-based ionic liquids. In addition, Swatloski et al.[145] presented ternary phase diagrams for ethanol + water + ionic liquids systems, while Najdanovic-Visak et al.[146,147] further explored these systems through the evaluation of the alcohol effect in the water-IL phase behaviour. Yet, both $[BF_4]^-$ and $[PF_6]^-$ anions are not water stable under particular conditions,[27] and following studies with ionic liquids based on water stable anions were later reported by Najdanovic-Visak et al..[148] However, the type 3 phase diagrams obtained, with all the pairs of compounds exhibiting only partial miscibility, are not favourable for a selective extraction of ethanol from aqueous-rich phases. Recently, Chapeaux et al.[149] reported the ternary phase diagrams for 1-hexyl-3-methylimidazolium bis(trifluoromethylsulfonyl)imide (the IUPAC standard ionic liquid), water and two alcohols: ethanol and 1-butanol. The authors concluded that although both systems could be used for the separation of alcohol-water mixtures, the ethanol selective separation was not very favourable.

Most studies comprising ionic liquids have been focused in imidazolium-based compounds. Phosphonium-based ionic liquids, despite their advantages (less expensive and thermally more stable than the equivalent imidazolium-based counterparts, availability on a multi-ton scale,[150] and already been used in industrial processes[2]) have received little attention. As a result, phosphonium-based ionic liquids are particularly interesting candidates for liquid-liquid extraction purposes. Moreover, unlike most ionic liquids, they are less dense than water, facilitating the use of conventional units designed for systems that require the aqueous phase decantation. Regarding the few works considering phosphonium-based ionic liquids, Domańska and co-workers[151–154] have been studying their phase equilibria with alcohols and hydrocarbons. There are also some works reporting their thermophysical properties,[155,156] their phase equilibria with water,[156,157] have shown that they are better than imidazolium-based ionic liquids at dissolving carbon dioxide,[158–160] their potential use in the extraction of diamondoids from natural gas[161] and their application in aqueous two phase systems aiming at purifying

value-added biomolecules.[69] Still, until this work and from the best of our knowledge, phosphonium-based ionic liquids have not been previously studied for the selective separation of ethanol-water mixtures.

Aiming at developing efficient liquid-liquid extraction techniques for the selective separation of ethanol-water mixtures a large range of phosphonium-based ionic liquids was here investigated. Experimental measurements of liquid-liquid equilibrium (LLE) tie-lines for ternary systems (water + ethanol + ionic liquid) were carried out for each of the ionic liquids at 298 K. Moreover, the resulting experimental data were modelled using the NRTL free energy model. The experimental results were also compared with predictions obtained from the COSMO-RS application. Due to its predictive capability, the COSMO-RS model was also used to evaluate the LLE of additional $[P_{66614}]$-based ionic liquids with different anions (for which experimental data are currently not available), aiming at screening tailored ionic liquids with improved features towards the extraction of ethanol.

2.2.3. Experimental procedure

2.2.3.1. Materials

The ternary systems ionic liquid + water + ethanol were determined for seven phosphonium-based ionic liquids, namely, trihexyl(tetradecyl)phosphonium chloride, $[P_{66614}]Cl$ (mass fraction purity ≈ 93-95%); trihexyl(tetradecyl)phosphonium bromide, $[P_{66614}]Br$ (mass fraction purity ≈ 96-98%); trihexyl(tetradecyl)phosphonium bis(trifluoromethylsulfonyl)imide, $[P_{66614}][NTf_2]$ (mass fraction purity > 98%); trihexyl(tetradecyl)phosphonium bis(2,4,4-trimethylpentyl) phosphinate $[P_{66614}]$[Phosph] (mass fraction purity ≈ 93%); trihexyl(tetradecyl)phosphonium decanoate, $[P_{66614}]$[Deca] (mass fraction purity ≈ 97%); trihexyl(tetradecyl)phosphonium dicyanimide, $[P_{66614}][N(CN)_2]$ (mass fraction purity ≈ 97%) and trihexyl(tetradecyl)phosphonium methanesulfonate $[P_{66614}][CH_3SO_3]$ (mass fraction purity ≈ 98-99%). The ionic liquids molecular structures are shown in Figure 2.7. All ionic liquids were kindly provided by Cytec Industries Inc., and the mass fraction purities described correspond to the acquired commercial products. The chloride mass fraction content is $< 10^{-3}$ for all samples.

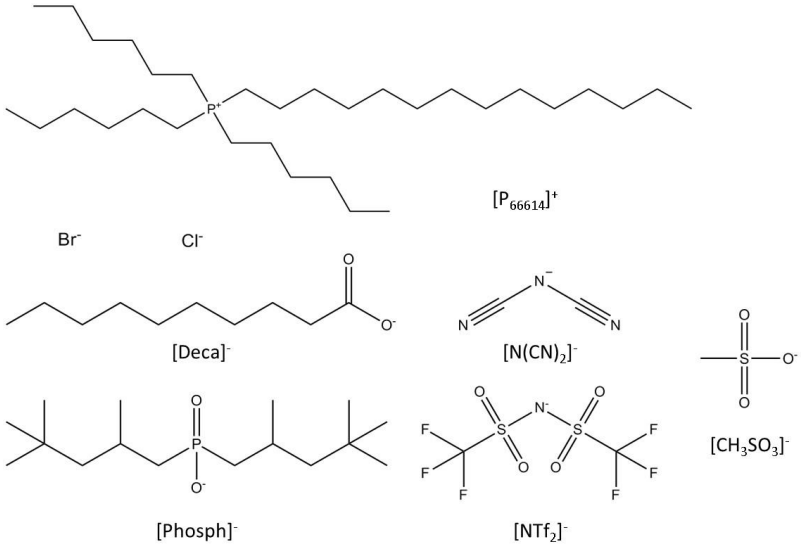

Figure 2.7. Chemical structures of the common IL cation ($[P_{66614}]^+$) combined with the different anions studied in this work.

Given the low purity of most ionic liquids they were further purified by a repetitive washing procedure with ultrapure water and further dried under vacuum (10^{-3} Pa), at a moderate temperature (80 ºC), and for at least 48 h. After this process, the purity of all ionic liquids was evaluated by ^{31}P, ^{1}H, ^{13}C and ^{19}F NMR spectra displaying purity mass fractions of > 99%. After the drying procedure, the water content in all samples was less than 5×10^{-4} in mass fraction as measured by Karl-Fischer titration. The ethanol used (EtOH, 2.6×10^{-4} of water in mass fraction) was > 99.8% pure from Riedel de Haën. The water used was double distilled, passed through a reverse osmosis system, and further treated with a Milli-Q plus 185 water purification apparatus.

2.2.3.2. Methods

To determine the tie-lines reported in this work, individual samples at various compositions of the three components (ionic liquid, water and EtOH) within the two phase region were prepared by weight, vigorously stirred, and allowed to reach the equilibrium by phase separation for 12 h at 298 K. After this period and to ensure the complete separation of both phases, all samples were centrifuged at 3000 rpm for 20 min. A sample of ≈ 0.1 g was taken from both phases with a glass syringe and injected directly into a Metrohm 831 Karl Fischer (KF) coulometer to determine the water content in each phase. In order to quantify the ionic liquid, a sample of ≈ (0.1 to 0.5) g of each

phase was collected, weighted and further dried under moderated vacuum in a glass flask designed for the purpose to remove the water and EtOH. After this process, the ionic liquid content was determined by weight. The mass of EtOH in both phases was determined as the difference between the sample total mass and the mass of water and ionic liquid. For each sample and for each phase, at least three individual measurements were performed, with an average uncertainty within 0.2 wt%. All the mass fraction quantifications were performed gravimetrically within ± 10^{-4} g.

The COSMO-RS calculations were performed at the BP/TZVP level (Turbomole,[162,163] DFT/COSMO calculation with the BP functional and TZVP[164] basis set using the optimized geometries at the same level of theory) with the parameter file BP_TZVP_C2.1_0110. The calculations were made for a multicomponent mixture where the cation and anion were treated as isolated species at equimolar conditions.

2.2.4. Results and discussion

The chemical structures of the phosphonium-based ionic liquids studied in this work are depicted in Figure 2.7. The tie-lines measured for the seven ternary systems considered are displayed in the ternary phase diagrams presented in Figure 2.8, along with the modelling results obtained both by COSMO-RS and NRTL. The phase equilibrium compositions and a simultaneous comparison between all the experimental results obtained are presented in Table S2.4 in Appendix. The consistency of the tie-lines was checked using the Othmer-Tobias correlation,[165] and the correlation for each system is also provided in Figure S2.8 in Appendix.

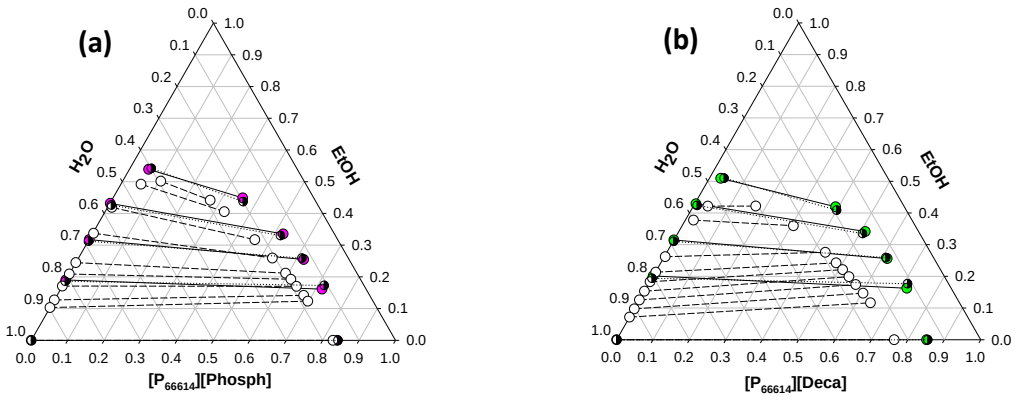

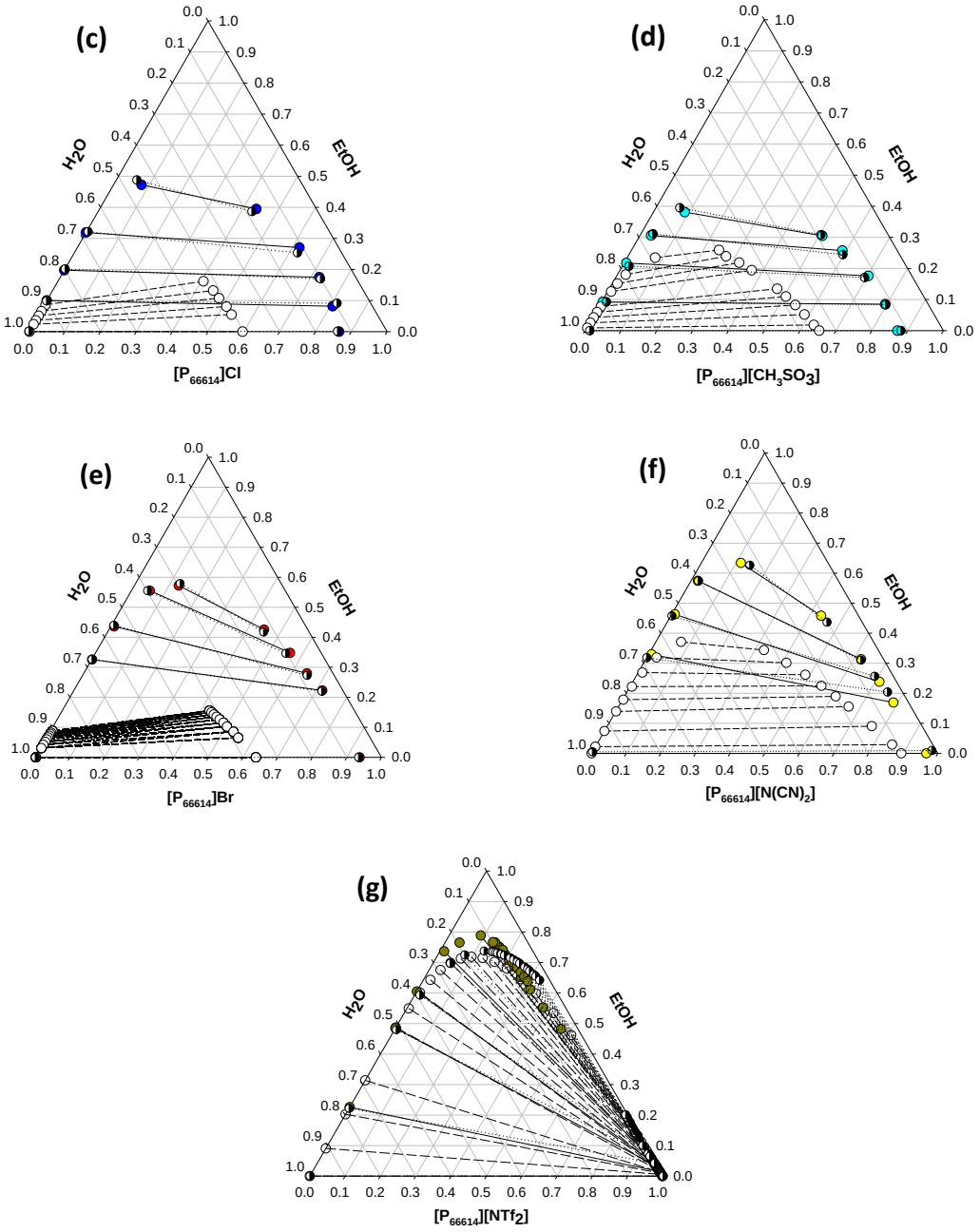

Figure 2.8. Ternary phase diagrams for the system IL + EtOH + H_2O at 298.15 K (mass fraction units): (a) [P_{66614}][Phosph]; (b) [P_{66614}][Deca]; (c) [P_{66614}]Cl; (d) [P_{66614}][CH_3SO_3]; (e) [P_{66614}]Cl; (f) [P_{66614}][$N(CN)_2$]; (g) [P_{66614}][NTf_2]. The full symbols and the solid lines represent the experimental data, the semi-filled symbols and the dotted lines represent the prediction by the NRTL model, and the empty symbols and the dashed lines represent the prediction by COSMO-RS.

All the phosphonium-based ionic liquids investigated are fully soluble in ethanol while presenting limited solubility in water (below 10^{-5} in a mole fraction basis). The water solubility in ionic liquids is more significant and ranges from 2.2 wt% for [P_{66614}][NTf_2] to 16 wt% for [P_{66614}][Phosph]. The water solubility increase in ionic liquids follows the anion

trend $[NTf_2]^-$ < $[N(CN)_2]^-$ < Br^- < Cl^- ≈ $[CH_3SO_3]^-$ < $[Deca]^-$ < $[Phosph]^-$. The water solubility results obtained are in good agreement with those previously reported.[156,157] The critical points for each system, estimated by applying the Sherwood method,[166] are reported in Table S2.4 in Appendix.

All of the ternary systems studied exhibit type 1 liquid-liquid phase diagrams, where partial miscibility is only observed in the IL-water binary system, presenting thus large biphasic regions. The two phase region envelope decreases with the water solubility trend presented above. In fact, the $[NTf_2]$-based system presents the largest two phase region observed in this work. As a result, the water solubility values in all ionic liquids (binary systems results) can be used as an initial guide to identify promising ionic liquids for ethanol extraction. This criterion is important since due to the non-volatile nature of ionic liquids, it is possible to obtain ethanol-rich phases by liquid-liquid extraction, followed by evaporation of the volatile components in the extract and recycle of the ionic liquid. Using this approach, ionic liquids with a larger two phase region tend to originate extract evaporates with higher ethanol concentrations, and are therefore preferable, from a selectivity viewpoint.

The two phase regions of phosphonium-based systems are in general larger than those previously observed for imidazolium-based ionic liquids with the same anion.[149] The maximum ethanol concentration that can be reached by each system was estimated from the ternary phase diagrams by identifying the point in the IL-rich phase that by removal of the ionic liquid would produce a mixture with the highest concentration in ethanol. These ethanol concentrations are reported in Table 2.2. The ethanol concentrations range from 65 wt% with $[P_{66614}][CH_3SO_3]$ to *circa* 90 wt% using $[P_{66614}][NTf_2]$. These values compare with a maximum reported by Chapeaux et al.[149] of approximately 65 wt% with $[C_6C_1im][NTf_2]$ (1-hexyl-3-methylimidazolium bis(trifluoromethylsulfonyl)imide). As a result, phosphonium-based ionic liquids combined with appropriate anions can be viewed as potential improved candidates for the extraction of ethanol from fermentation broths. Additional characteristics of phosphonium-based ionic liquids, such as lower toxicity compared to imidazolium-based media, are also discussed below.

Table 2.2. Ethanol distribution coefficients and selectivities for each system at the composition of 20 wt% of ethanol, calculated by the correlation of *D* and *S* along the ethanol content, and maximum ethanol concentration obtainable by complete evaporation from the IL-rich phase (all values reported in mass basis).

System	*D*	*S*	Maximum EtOH extraction (%)
$[P_{66614}][Phosph]$	0.83	5.1	72
$[P_{66614}][Deca]$	0.82	4.9	70
$[P_{66614}]Cl$	0.88	6.6	72
$[P_{66614}][CH_3SO_3]$	0.82	4.6	65
$[P_{66614}]Br$	0.70	8.4	78
$[P_{66614}][N(CN)_2]$	0.51	6.8	82
$[P_{66614}][NTf_2]$	0.31	2.0	87
$[P_{66614}][B(CN)_4]$	-	-	91[a]
$[P_{66614}][C(CN)_3]$	-	-	80[a]

[a]Predicted by COSMO-RS.

Table 2.2 also presents the ethanol distribution coefficients (*D*) and selectivities (*S*) between the two phases: IL-rich phase (IL) and aqueous-rich phase (aq). The distribution coefficients are defined as

$$D = w_{EtOH}^{IL} \Big/ w_{EtOH}^{aq} \tag{2.1}$$

where w_{EtOH} represents the mass fraction of ethanol at each phase, while *D* expresses the relative capacity of the ionic liquid to remove ethanol from aqueous mixtures. The selectivity of each system for ethanol was determined using eq 2.2

$$S = \frac{w_{EtOH}^{IL} / w_{W}^{IL}}{w_{EtOH}^{aq} / w_{W}^{aq}} \tag{2.2}$$

where the subscripts "EtOH" and "W" designate ethanol and water, respectively. *S* indicates the ability of each IL to selectively remove ethanol.

The determined ethanol distribution coefficients and selectivities can be used to compare the performances of the current ionic liquids with alternative solvents previously studied for the ethanol recovery through liquid-liquid extraction.[143–149,167] In Table 2.2 for a 20

wt% of ethanol composition, the distribution coefficients range from 0.3 to 0.9, while the ethanol selectivities vary between 2 and 8. These values correspond to reasonable values in the range of known alternative solvents, given that *D* is reported in a mass fraction basis. The exception to this pattern appears to be the [NTf_2]-based ionic liquid, that presents both low selectivities and distribution coefficients for a 20 wt% of ethanol solution. Nevertheless, it should be reminded that this ionic liquid displays improved selectivity for low concentrations of ethanol (see Table S2.4 in Appendix). For comparison, under approximately similar conditions the [C_6C_1im][NTf_2] system studied by Chapeaux et al.[149] presented values of D = 0.15 and S = 11, which translate into better selectivity but a lower solvent capacity for ethanol. Considering the maximum ethanol concentrations reported in Table 2.2, while for the systems studied liquid-liquid extraction cannot be directly used to break the ethanol-water azeotrope, the possibility of using this approach in concentrating ethanol from dilute aqueous solutions will be analysed below, in the context of reducing the energy costs required in the ethanol purification process.

COSMO-RS

The COSMO-RS model (COnductor-like Screening MOdel for Real Solvents) allows the prediction of the fluids phase equilibria using unimolecular quantum calculations coupled to statistical thermodynamic approaches.[168–172] Previous studies applied COSMO-RS for predicting the LLE of binary systems of ionic liquids and the most diverse molecular solvents, namely alcohols, hydrocarbons, ethers, ketones and water.[5,6,157,173–179] Nevertheless, few publications have considered the application of COSMO-RS (or related modified versions) to ternary systems containing ionic liquids.[180–182] Gibbs free energy models such as non-random two liquids (NRTL), or universal quasi-chemical (UNIQUAC), group-contribution methods (GCMs) and equations of state (EoS) require experimental data to estimate the model intrinsic parameters. Alternatively, COSMO-RS is a purely predictive model, and therefore can be highly valuable in the investigation of systems involving ionic liquids where experimental data are not yet available. Considering the large number of possible ionic liquids, including their combination with molecular

solvents, the availability of predictive methods appears as extremely convenient since they can be used as screening tools to select ionic liquids for specific applications.

The ternary phase diagrams measured were used to evaluate the performance of the COSMO-RS model in the prediction of the LLE of these systems. In agreement with results previously reported[157] with the bromide and chloride anions, COSMO-RS is unable to provide enhanced quantitative descriptions of the phase diagrams. However, for the remaining systems, a reasonable prediction of the binodal curves is achieved, as shown in Figures 2.9a, b, f and g, where the predicted phase diagrams for the ionic liquids with phosphinate, decanoate, $[N(CN)_2]^-$ and $[NTf_2]^-$ are compared with the experimental data. Nevertheless, it should be pointed out that in most systems the predictions by COSMO-RS for the compositions of each component at both co-existing phases is still far from the experimental data. As previously observed,[175,176,183,184] COSMO-RS can provide a good description of the LLE data when the compounds are poorly miscible. Since the COSMO-RS calculations consider that the interactions are made on the conductor interface surrounding the molecules (thus treated as isolated species), stronger interactions responsible for larger mutual solubilities are not adequately taken into account by COSMO-RS. Given the large biphasic regions presented by these systems, and on the qualitative trends predicted by COSMO-RS, it seems that COSMO-RS can be used to investigate the suitability of other non-fluorinated anions for the ethanol-water separation. While much less precise than the experimental measurements on providing the phase diagrams, COSMO-RS allows the screening of ionic liquids not currently available, and that can be further synthesized and used in experimental approaches.

The COSMO-RS was used to study the ternary phase diagrams of a series of $[P_{66614}]$-based ionic liquids combined with different anions, such as methyl sulphate ($[CH_3SO_4]^-$), ethyl sulphate ($[C_2H_5SO_4]^-$), tosylate ($[Tos]^-$), tetracyanoborate ($[B(CN)_4]^-$) and tricyanomethane ($[C(CN)_3]^-$). While the predicted ternary phase diagrams for most of these ionic liquids were not satisfactory with respect to the objective of this work, systems with tetracyanoborate ($[B(CN)_4]^-$) and tricyanomethane ($[C(CN)_3]^-$) seem promising in the selective extraction of ethanol, and further experimental measurements on these systems

are immediately envisaged. Figure 2.9 presents the predicted ternary phase diagrams for the $[P_{66614}][B(CN)_4]$ and $[P_{66614}][C(CN)_3]$ ionic liquids. Table 2.2 also lists the estimated maximum ethanol concentrations that can be obtained by complete evaporation of the extract phases resulting from these systems. Thus, although not yet experimentally available, the cyano-based ionic liquids appear as potential solvents regarding the ethanol extraction from aqueous phases.

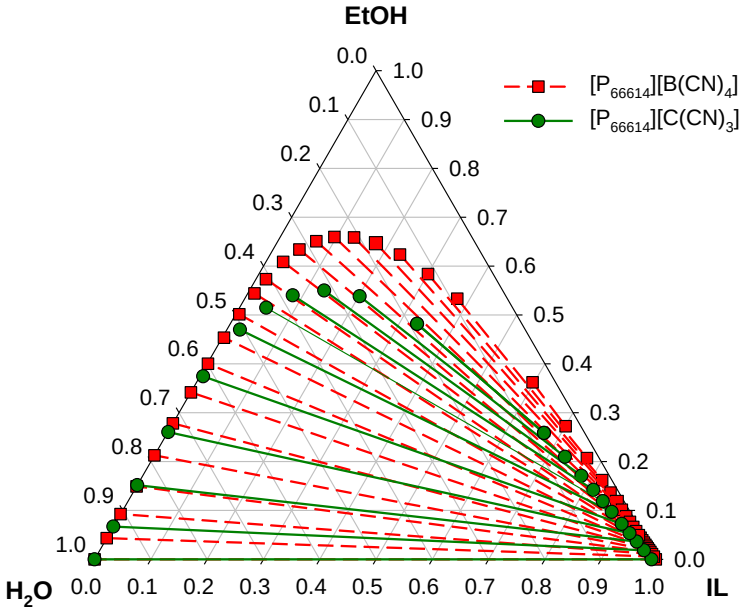

Figure 2.9. Prediction of the ternary systems $[P_{66614}][B(CN)_4]$ + EtOH + H_2O and $[P_{66614}][C(CN)_3]$ + EtOH + H_2O at 298.15 K (mass fraction units) by COSMO-RS.

NRTL MODELLING

The NRTL model[185] has been successfully used over a wide range of vapour-liquid equilibrium (VLE) and LLE systems to describe the non-ideality in the liquid phase. It is based on the local composition concept to express the effect of the intermolecular forces (short-range) in the non-randomness of the mixtures. One of the main advantages of NRTL is that multicomponent LLE and VLE can be predicted using only binary interaction parameters, which can be estimated from experimental data. For each binary molecular pair *i-j*, the model has three parameters – two interaction parameters τ_{ij} and τ_{ji} and the non-randomness parameter α_{ij} (α_{ij} = α_{ji}). Parameters τ_{ij} are related to the Gibbs free energy of interaction between a species *i* around a central specie *j* (Δg_{ij}) in a hypothetical

cell in the liquid. The parameter α_{ij} is related with the lattice structure of the liquid and it is proportional to 2/Z, where Z is the lattice coordination number of the liquid (this varies commonly from 8 to 12; 10 is usually considered).

Although the NRTL model was not developed to describe the behaviour of solutions containing electrolyte species, it has found successful applications in ternary water + alcohol + ionic liquid LLE systems.[149,186–189] This can be related with the fact that in ionic liquids the ion charge is usually disperse and the long-range electrostatic forces are weak compared with the short-range intermolecular forces (so that they can be neglected), and thus allowing the applicability of the NRTL model.

The use of the NRTL model to correlate the LLE data should be seen as a first choice of a simple theoretical model that could provide a reasonably precise description of the equilibrium conditions, while being of practical value for design calculations. This also provides a comparison of the accuracies obtained with simpler equilibrium models, used in data regression, and the predictions of more complex models, such as COSMO-RS.

Different approaches have been considered for the parameter estimation problem with the NRTL model to obtain the best set of parameters that describe the LLE data available.[188,190] In the present work, this task was formulated as the solution of a nonlinear programming problem, using the weighted norm of the differences between the experimental mass fractions and the values predicted by the model as the objective function, and as described by eq 2.3:[190]

$$\min_{z} \ \phi = \sum_{i}^{n_t} \sum_{j}^{n_c} \sum_{k}^{2} \omega_{ijk} e_{ijk}(\tau)^2 \qquad (2.3)$$

Here $e_{ijk}(\tau) = w_{ijk}^{\exp} - w_{ijk}^{\mathrm{mod}}(\tau)$, where the superscripts *exp* and *mod* correspond to the experimental and calculated mass fraction values, respectively. The summations in this equation are taken over all tie-lines (*i*), components (*j*) and phases (*k*), and ω_{ijk} is a weight factor associated with each error term. Using the isothermal data available for each system, the objective function ϕ was minimized by simultaneous determination of all unknowns (composition variables and model parameters, here collectively denoted by *z*),

subject to constraints of iso-activity, the NRTL activity coefficient model, sum of mass and molar fraction restrictions, and magnitude bounds for the model parameters τ_{ij}. Mass fractions were used in the data regression, due to the large differences in molecular weights between the ionic liquids and the molecular components. More details about the NRTL parameter estimation are presented in Appendix.

Since the experimental data available were registered at only one temperature, the α_{ij} parameters in the model were considered constant, and equal to recommended values for each pair of components in the mixture. Values of α_{13} = 0.2 and α_{23} = 0.3 were used as suggested by Song and Chen.[61] The parameters τ_{12}, τ_{21} and α_{12}, referring to the water-ethanol binary pair, were retrieved from existing data in Song and Chen[61], and are given by α_{12} = 0.3031, τ_{12} = 670.4/T and τ_{21} = -55.2/T. The weights ω_{ijk} were considered to be unitary for all data points available. Table 2.3 summarizes the values obtained for the optimized parameters of the NRTL model.

From the ternary phase diagrams displayed in Figure 2.8, it is possible to observe that the NRTL model is able to provide a close fit of the experimental data. Results for the absolute deviation between experimental data and correlated results, for each tie-line and each system, are presented in Table S2.5 in Appendix. The average of absolute deviations between experimental data and the NRTL correlated results is presented in Table 2.3.

Table 2.3. NRTL binary interaction parameters and average absolute deviations between the experimental mass fraction compositions and NRTL correlation results, for each system at 298 K.

IL	NRTL binary interaction parameters				Average Absolute Deviation ($\lvert w_{exp} - w_{NRTL} \rvert$)		
	τ_{13}	τ_{31}	τ_{23}	τ_{32}	w_{IL}	w_{EtOH}	w_{H2O}
$[P_{66614}][Phosph]$	25.25	-1.450	6.064	-3.917	0.004	0.006	0.005
$[P_{66614}][Deca]$	23.82	-1.169	5.487	-3.559	0.005	0.006	0.005
$[P_{66614}]Cl$	11.14	-2.555	5.230	-3.181	0.006	0.007	0.008
$[P_{66614}][CH_3SO_3]$	11.09	-3. 487	5.998	-3.318	0.009	0.006	0.006
$[P_{66614}]Br$	21.09	6.265	4.688	-2.760	0.003	0.003	0.005
$[P_{66614}][N(CN)_2]$	14.82	1.313	4.865	-2.873	0.016	0.012	0.010
$[P_{66614}][NTf_2]$	11.36	4.674	4.798	-1.520	0.024	0.023	0.002

The main exception was observed with the [NTf_2]-based system, where the NRTL model shows more difficulties in providing an exact representation of the binodal curve, giving the localization of the critical point in the right branch at a relatively low concentration of ethanol. To achieve these results with the [NTf_2]-based system, additional experimental measurements of the composition of the water phase along the saturation line were required, since the values of the parameters displayed a high sensitivity to the data available in this region. The experimental saturation line was completed using the cloud point titration method, and the respective data points are also presented in Figure 2.8g.

The relative precision of the NRTL model description of the experimental data is comparable to the quality of the regressions for other ionic liquids provided by different authors using the NRTL, eNRTL and UNIQUAC models.[149,191,192] For this reason, no alternative models were tested with the present experimental data.

APPLICATION IN THE ETHANOL PURIFICATION

As mentioned above, the ternary phase diagrams here studied have a large biphasic region, and present different distribution coefficients from other ionic liquids previously studied.[149] These observations raise the question on how these features can be used to build alternative ethanol purification schemes with reduced energy requirements relative to the classical distillation approach. Since only LLE data of these systems were determined, and just at one temperature, the process alternatives here considered are focused on the potential use of these ionic liquids as solvents for liquid-liquid extraction.

The medium ethanol concentration range is the region where higher liquid-liquid selectivities were observed towards this species. However, the use of this solution presupposes the existence of additional units for the initial ethanol concentration from the fermentation broth. Also, this is the region where distillation is more effective and strongly competes with alternative technologies, due to the larger relative volatility of ethanol. Furthermore, there are significant limitations to the direct use of liquid-liquid extraction in the high concentration region, since the biphasic envelope is much more

limited in this concentration range. Hence, the use of liquid-liquid extraction is perhaps most effective in the low concentration regime.

The direct application of liquid-liquid extraction to the fermentation broth is restricted by the comparatively low selectivities (in the order of 5-6) observed in this region. This means that a large number of stages (coupled with large mass flow rates of ionic liquid) would be necessary to concentrate ethanol and to achieve a residue with a small concentration of this component. However, given the relatively large distribution coefficients registered here, a more favourable solution would be to use a single liquid-liquid extraction stage coupled to an extractive fermentation, where the IL is recycled continuously to the fermentator, as sketched in Figure 2.10.

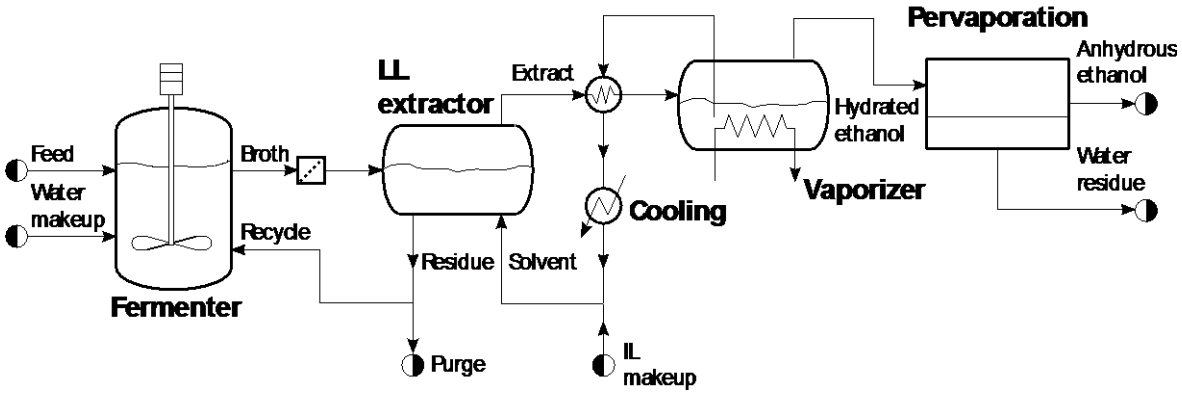

Figure 2.10. Block diagram for ethanol purification based on liquid-liquid extraction and pervaporation.

This process configuration, while very distinct from the conventional batch fermentation typically used to achieve very high feed conversion, has already been investigated in detail with classical solvents.[193] One important advantage of this configuration is that it allows the recycling of the residue current back to the fermentator with a relatively high concentration of ethanol, where it can absorbs more ethanol before being reprocessed. The liquid-liquid extract has relatively poor water content, and therefore can be evaporated to originate a binary mixture with a significant ethanol concentration. If done under slight vacuum, this evaporation can use residual heat that might be available in the process at low temperature levels, having therefore the potential to reduce the energy

costs of the purification stage. Additional energy savings can also be contemplated by coupling various similar effects, operating at distinct pressures.

The proposed solution was tested with the ternary diagram containing the $[N(CN)_2]$-based ionic liquid for a 2 wt% of ethanol feed, using an equal mass of solvent. It is possible to conclude that the concentration of ethanol in the two phases is very similar, with an approximate total mass equi-distribution between the extract and residue currents. However, the mass concentration of water in the extract is much smaller than that in the residue. Due to this trend, complete evaporation of the extract leads to a mixture with approximately 65 wt% in ethanol. While smaller than the maximum ethanol extraction reported for this system (approximately 82%) this value is remarkable, since it is reachable with a single extraction step of a diluted solution, followed by evaporation of the extract. A further purification of this current towards anhydrous ethanol can be achieved through application of a similar procedure (requiring in this case a much smaller solvent flow rate), in order to approach the maximum ethanol extraction possible by liquid-liquid extraction. For this purpose, the values presented in Table 2.2 become important to differentiate the behaviour between the various studied ionic liquids.

As alternatives to the application of additional liquid-liquid extraction stages (given the previous considerations), available options include the use of conventional distillation up to the azeotrope followed by ethanol dehydration, or the use of pervaporation. In this last case, common specifications of anhydrous ethanol (99.5 wt%) are reachable for feeds with ethanol compositions in the range of 60-65 wt%, through the use of two consecutive pervaporation stages with hydrophilic membranes, and typical selectivities of S = 10 – 12, using processing schemes similar to the one described by Roza and Maus.[194] This configuration would therefore allow the production of anhydrous ethanol from extractive fermentation, while completely avoiding the use of distillation in the purification phase. While potentially interesting, a comparison of the performance of this alternative with the more classical distillation-based approaches requires a detailed evaluation of many aspects, not only related to the separation phase, but also relative to the reactor configuration and the interaction between these two processing phases, such as, the

inhibition effects of the ionic liquids and other metabolites present in the recycle stream, their path in the separation process and the consequent modifications in the simple scheme represented in Figure 2.10 required to address them.

An additional paramount practical aspect of the use of ionic liquids is their relative toxicity towards microorganisms. Unfortunately, toxicity data for phosphonium-based ionic liquids are rather scarce in the literature. Yet, it was possible to retrieve the EC_{50} values for the enzymatic activity from the UFT/Merck ionic liquids biological effects database,[195] for the ionic liquids studied in this work. Nevertheless, it should be remarked that enzyme assays may not be prime determinants for the microorganisms involved in fermentation processes. Most ionic liquids affect cell membranes primarily and any enzyme effects would only be applicable for ionic liquids that can cross such a membrane. The EC_{50} values are reported in Figure 2.11 and are compared with various imidazolium-based counterparts, and also previously proposed for the water-ethanol separation process.[149] Values above 1000 µmol·L^{-1} indicate a low inhibition potential. Accordingly to these results, the phosphonium-based ionic liquids present a lower inhibition potential when compared with imidazolium-based solvents. With the exception of [P_{66614}][FAP], [P_{66614}]Br and [P_{66614}][CH_3SO_3], phosphonium ionic liquids present low inhibition capacity. Therefore, in addition to the advantages previously discussed, the phosphonium-based ionic liquids here proposed are also more favourable, concerning their toxicity, when compared with other ionic liquids previously studied.

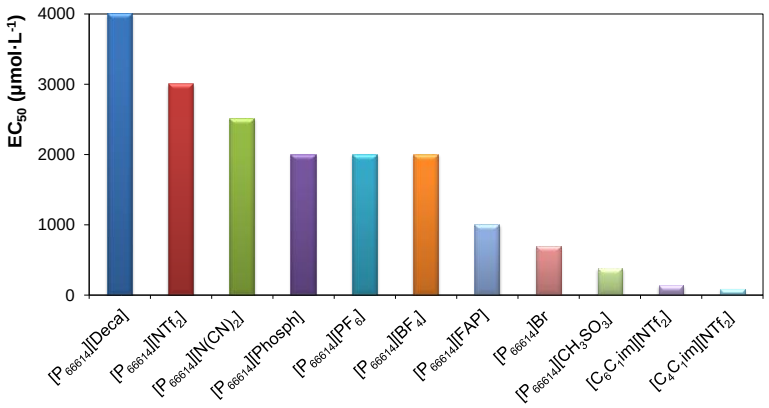

Figure 2.11. EC_{50} values for enzymatic activity in several ILs.[195]

2.2.5. Conclusions

Phosphonium-based ionic liquids were evaluated in this work for potential use as solvents in the extraction of ethanol from fermentation broths. Ternary phase diagrams for seven distinct ionic liquids, water and ethanol at 298 K were experimentally determined and presented. Predictions from the COSMO-RS model were evaluated against the experimental data and were mainly used to screen other ionic liquids not experimentally studied. These simulations suggest that the $[P_{66614}][C(CN)_3]$ and $[P_{66614}][B(CN)_4]$ ionic liquids are also potential alternatives for this purpose. A conceptual analysis of the alcohol recovery steps was carried out. As an alternative to classical distillation, a liquid-liquid extraction stage coupled to an extractive fermentation was proposed, where the ionic liquid is continuously recycled to the fermentator and the ethanol concentration is carried out by pervaporation, aiming at reducing the energy costs involved in the purification of ethanol.

Chapter 3 – Mutual Solubilities of Ionic Liquids and Water

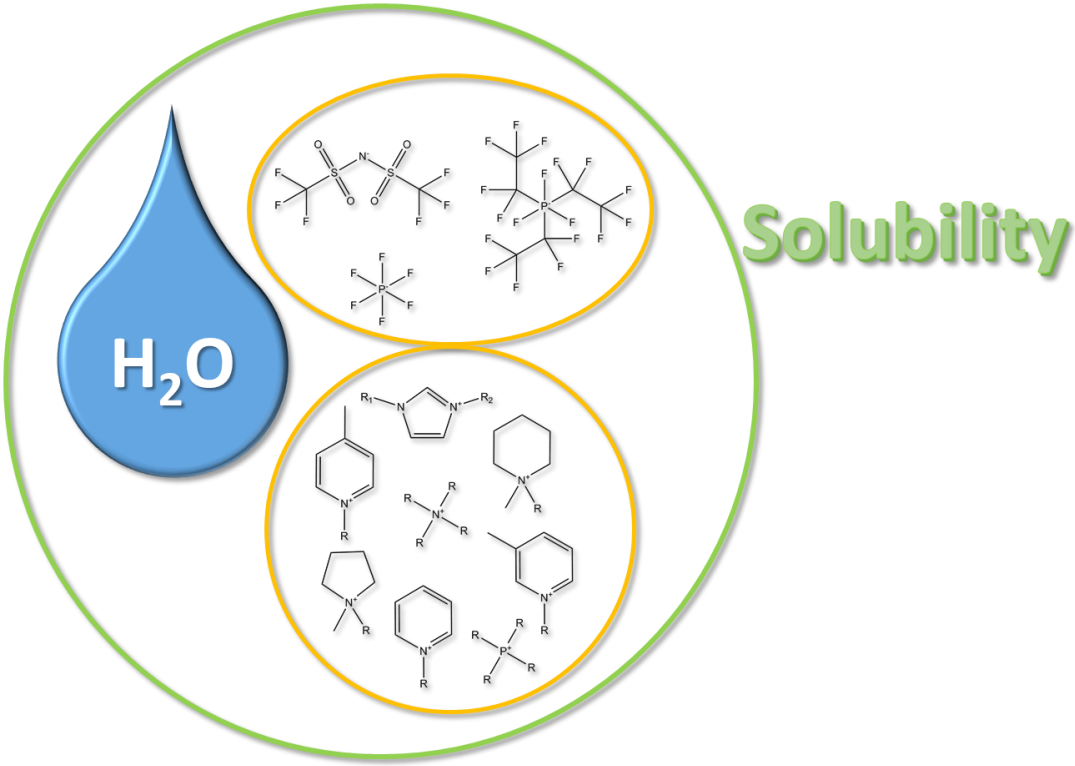

3.1. Introduction

A special feature of ionic liquids (ILs) is that their physical and chemical properties, such as density, viscosity, mutual solubilities with water, as well as their toxicity can be easily tuned by an appropriate selection of their constituting ions.[2,65] For example, the solubility of water in 1-butyl-3-methylimidazolium ([C_4C_1im]-based-ILs) can be significantly decreased by changing the anion from tetrafluoroborate, $[BF_4]^-$, to bis(trifluoromethylsulfonyl)imide, $[NTf_2]^-$. In contrast, changing the alkyl chain from [C_4C_1im][NTf_2] to 1-hexyl-3-methylimidazolium bis(trifluoromethylsulfonyl)imide, [C_6C_1im][NTf_2], has a much more limited effect although also leading to a decrease in the mutual solubilities with water.[5] However, in what concerns the toxicity, the change in the anion has a much smaller impact than the increase in the cation alkyl chain length.[196] These trends suggest that both the cation or the anion of the ionic liquid can be molecularly-engineered for specific physico-chemical properties to meet the requirement of a specific application.[6] For a deeper understanding on the design ability of ionic liquids, the effect of the anion nature,[6] isomerisation or *quasi* isomerisation,[10] and the position and size of the alkyl side chain and its symmetry have been addressed.[10]

The use of hydrophobic ionic liquids, considered here as those not completely miscible with water at temperatures close to room temperature, has shown promising results as media for the recovery of value-added organic compounds from aqueous solutions.[192,197–199] They may also play an important role in the separation of (bio)alcohols from fermentation broths.[145,148,149,167,192] To design separation processes involving ionic liquids at an industrial scale, there are, at least, two key factors to be considered. First, it is necessary to know a wide range of thermophysical properties, thermodynamic data, and solid-liquid (SLE), liquid-liquid (LLE), and vapour-liquid equilibrium (VLE). Thermophysical properties along with the equilibrium data are also important to get a better understanding on the physicochemical behaviour of ionic liquids and to develop related thermodynamic models.[200–203] Second, when ionic liquids are applied as media for extraction processes from aqueous solutions, they will be in contact with water. Even the

most hydrophobic ionic liquids present noticeable solubility in water[5] that must be taken into account due to the fact that most of these ionic liquids are non-biodegradable. Instead, they accumulate in the aquatic ecosystems with potential harmful effects for microorganisms and humans.[105,106] Therefore, in the development of ionic liquids as alternative industrial solvents, the optimisation of technical properties should run in parallel with the minimisation of potential hazards.

In order to evaluate the influence of the ionic liquid structure on their toxicity behaviour, an extensive range of ionic liquids has been studied.[52,59–61,103,104,204–211] Furthermore, several approaches were attempted aiming at understanding the relationship between the ionic liquids toxicity and other properties, such as hydrophobic nature,[212] membrane water partitioning,[213] and lipophilicity.[55,213] In a recent publication, using a large number of ionic liquids, it has been shown a close relationship between the ionic liquids toxicity and their solubility in water.[60] The results clearly indicate that the less soluble non-aromatic ionic liquids also present a lower toxicity when comparing with aromatic ionic liquids with higher solubility in water.[60] In addition, it was also demonstrated that the distribution of the cation alkyl chains by the two nitrogen atoms in symmetric cations does not seem to have an impact on the toxicity.[60] Nevertheless, a difference in the central atom between the ammonium and phosphonium families does have an impact.[214]

Based on the concepts expressed above, the work reported on this chapter was carried out to investigate the mutual solubilities of water and a wide range of ionic liquids. In addition, the experimental solubility data were also compared with predictive results from the COnductor like Screening MOdel for Real Solvents (COSMO-RS).[42,43] Aiming at gather a deeper understanding of the underlying mechanism of the ionic liquid and/or water solvation phenomena, for some systems, molecular dynamics simulations (MD) have also been performed.

3.2. Experimental procedure

3.2.1. Materials

The study of the water-IL mutual solubilities was carried out for the ionic liquids or salts (depending on their melting temperatures) described in Table 3.1.

Table 3.1. Salts or ILs used and respective acronym, mass fraction purity, supplier, method used to confirm the purity and structure correspondence.

IL/salt		Purity (%)	Supplier	NMR spectra	Structure
Name	Acronym				
1-ethyl-3- methylimidazolium hexafluorophosphate	$[C_2C_1im][PF_6]$	99	Iolitec	^{1}H, ^{13}C, ^{19}F, ^{31}P	(i)
1-methyl-3-propylimidazolium hexafluorophosphate	$[C_3C_1im][PF_6]$	99	Iolitec	^{1}H, ^{13}C, ^{19}F, ^{31}P	(ii)
3-methyl-1-propylpyridinium hexafluorophosphate	$[C_3\text{-}3\text{-}C_1py][PF_6]$	99	Iolitec	^{1}H, ^{13}C, ^{19}F, ^{31}P	(iii)
1-methyl-1-propylpyrrolidinium hexafluorophosphate	$[C_3C_1pyr][PF_6]$	99	Iolitec	^{1}H, ^{13}C, ^{19}F, ^{31}P	(iv)
1-methyl-1-propylpiperidinium hexafluorophosphate	$[C_3C_1pip][PF_6]$	99	Iolitec	^{1}H, ^{13}C, ^{19}F, ^{31}P	(v)
Tetrabutylammonium hexafluorophosphate	$[N_{4444}][PF_6]$	99	Apollo Scientific	^{1}H, ^{13}C, ^{19}F, ^{31}P	(vi)
Tetrabutylphosphonium hexafluorophosphate	$[P_{4444}][PF_6]$	99	Fluka	^{1}H, ^{13}C, ^{19}F, ^{31}P	(vii)
1-ethyl-3-methylimidazolium tris(pentafluoroethyl)trifluorophosphate	$[C_2C_1im][FAP]$	98	Merck	^{1}H, ^{13}C, ^{19}F, ^{31}P	(viii)
1-butylpyridinium bis(trifluoromethylsulfonyl)imide	$[C_4py][NTf2]$	99	Iolitec	^{1}H, ^{13}C, ^{19}F	(ix)
1-hexylpyridinium bis(trifluoromethylsulfonyl)imide	$[C_6py][NTf_2]$	99	Iolitec	^{1}H, ^{13}C, ^{19}F	(x)
1-octylpyridinium bis(trifluoromethylsulfonyl)imide	$[C_8py][NTf_2]$	99	Iolitec	^{1}H, ^{13}C, ^{19}F	(xi)
1-butyl-3-methylpyridinium bis(trifluoromethylsulfonyl)imide	$[C_4\text{-}3\text{-}C_1py][NTf_2]$	> 99	Iolitec	^{1}H, ^{13}C, ^{19}F	(xii)
1-butyl-4-methylpyridinium bis(trifluoromethylsulfonyl)imide	$[C_4\text{-}4\text{-}C_1py][NTf_2]$	> 99	Iolitec	^{1}H, ^{13}C, ^{19}F	(xiii)
1,3-dimethylimidazolium bis(trifluoromethylsulfonyl)imide	$[C_1C_1im][NTf_2]$	> 99	Iolitec	^{1}H, ^{13}C, ^{19}F	(xiv)
1,3-diethylimidazolium bis(trifluoromethylsulfonyl)imide	$[C_2C_2im][NTf_2]$	> 99	Iolitec	^{1}H, ^{13}C, ^{19}F	(xv)

1,3-dipropylimidazolium bis(trifluoromethylsulfonyl)imide	$[C_3C_3im][NTf_2]$	> 99	Iolitec	^1H, ^{13}C, ^{19}F	(xvi)
1,3-dibutylimidazolium bis(trifluoromethylsulfonyl)imide	$[C_4C_4im][NTf_2]$	> 99	Iolitec	^1H, ^{13}C, ^{19}F	(xvii)
1,3-dipentylimidazolium bis(trifluoromethylsulfonyl)imide	$[C_5C_5im][NTf_2]$	> 99	Iolitec	^1H, ^{13}C, ^{19}F	(xviii)
1-methylimidazolium bis(trifluoromethylsulfonyl)imide	$[C_1im][NTf_2]$	> 99	Iolitec	^1H, ^{13}C, ^{19}F	(xxv)
1-ethylimidazolium bis(trifluoromethylsulfonyl)imide	$[C_2im][NTf_2]$	> 99	Iolitec	^1H, ^{13}C, ^{19}F	(xxvi)
1-ethyl-3-propylimidazolium bis(trifluoromethylsulfonyl)imide	$[C_2C_3im][NTf_2]$	> 99	Iolitec	^1H, ^{13}C, ^{19}F	(xxvii)
1-butyl-2,3-dimethylimidazolium bis(trifluoromethylsulfonyl)imide	$[C_4C_1C_1im][NTf_2]$	> 99	Iolitec	^1H, ^{13}C, ^{19}F	(xxviii)

Most salts described in Table 3.1 present melting temperatures near or below 373 K, so they are commonly referred as ionic liquids. The main exception in this group are $[P_{4444}][PF_6]$ and $[N_{4444}][PF_6]$ that present melting temperatures higher than 373 K, as it will be shown later by DSC results. The structure of the different ILs/salts here studied are presented in Figure 3.1.

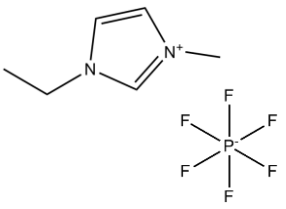

(i)

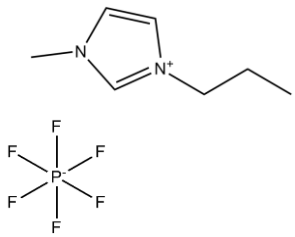

(ii)

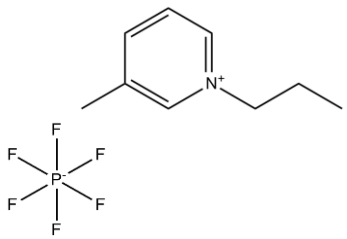

(iii)

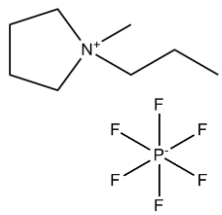

(iv)

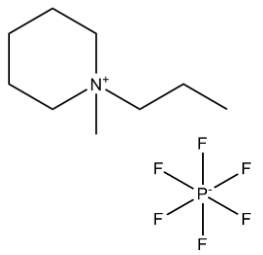

(v)

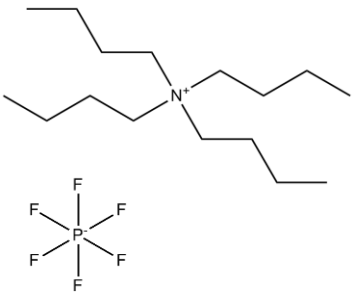

(vi)

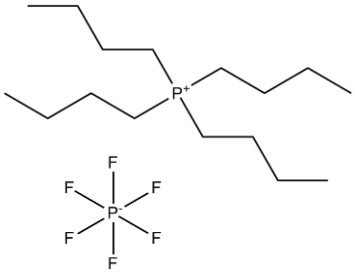

(vii)

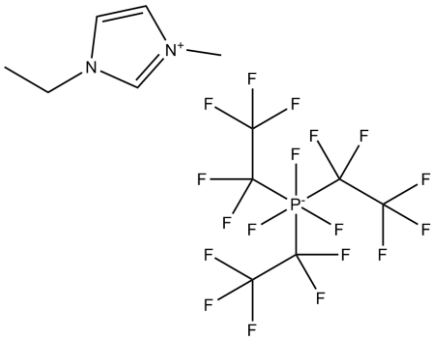

(viii)

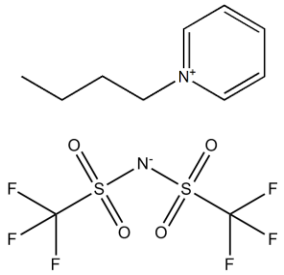

(ix)

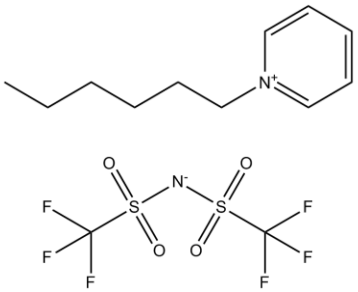

(x)

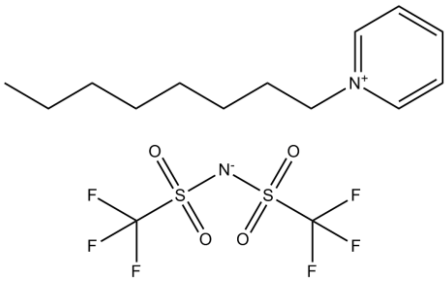

(xi)

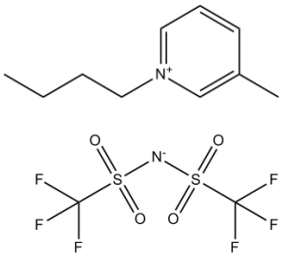

(xii)

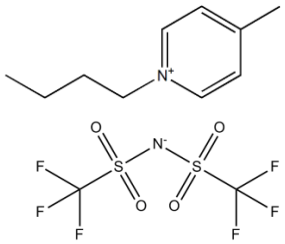

(xiii)

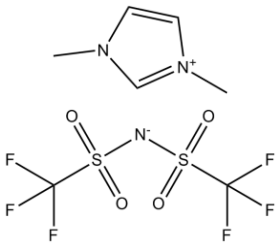

(xiv)

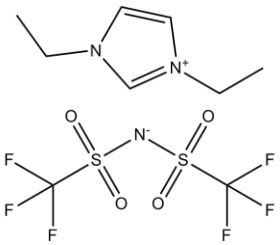

(xv)

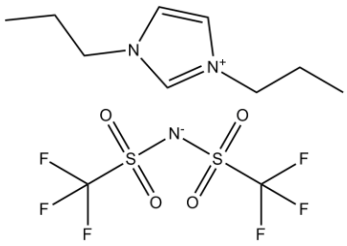

(xvi)

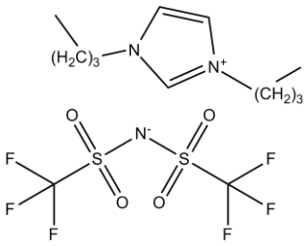

(xvii)

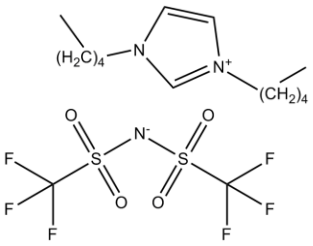

(xviii)

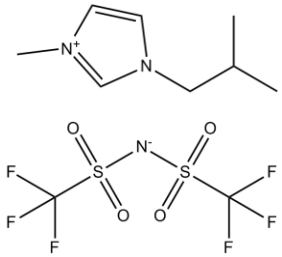

(xix)

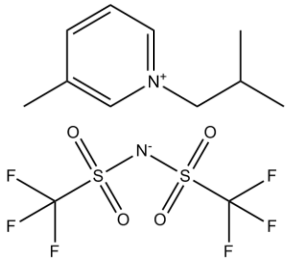

(xx)

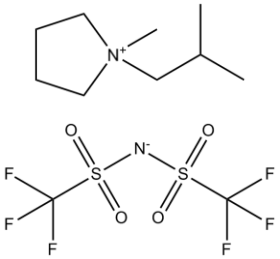

(xxi)

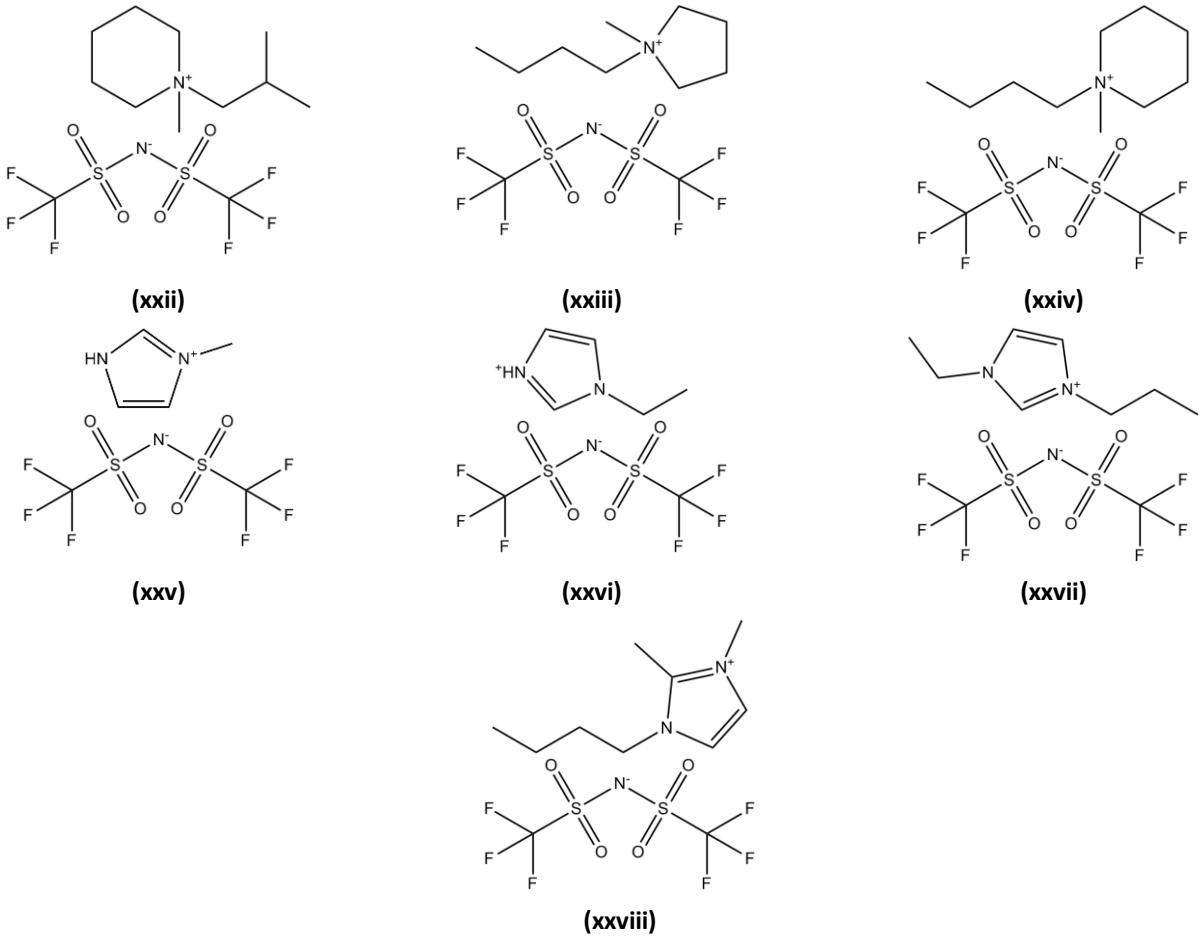

Figure 3.1. Chemical structures of the ILs/salts investigated in this work.

All salts were purified (to reduce their content in water and other volatile components), by drying individual samples at *circa* 353 K for at least 48 h, and under constant stirring and moderate vacuum conditions (≈ 0.1 Pa). After this procedure, NMR analyses confirmed the purity of the ionic liquid samples, and all presented purity higher than 99%.

Double-distilled water (passed by a reverse osmosis system and further treated with a MilliQ plus 185 water purification apparatus) was used in the preparation of all (ionic liquid + water) binary mixtures. Purity analyses revealed resistivity values of 18.2 MΩ·cm and a TOC (Total Organic Content) smaller than 5 $\mu g \cdot dm^{-3}$. The analyte used for the coulometric Karl-Fischer (KF) titration was Hydranal® – Coulomat AG from Riedel-de Haën.

3.2.2. Methods

DIFFERENTIAL SCANNING CALORIMETRY MEASUREMENTS

In this work not all ionic liquids used are liquid at room temperature. Therefore, the melting temperatures of some of them were determined by Differential Scanning Calorimetry (DSC).

The phase transition temperatures and enthalpies of all aliphatic [PF_6]-based salts were determined using a Q200 DSC from TA Instruments. Samples of about 5 mg were tightly sealed in hermetic aluminium pans. The temperature range for the different salts was between (183.15 and 423.15) K for [C_3C_1pip][PF_6], (183.15 and 423.15) K for [C_3C_1pyr][PF_6], (183.15 and 548.15) K for [N_{4444}][PF_6] and (183.15 and 523.15) K for [P_{4444}][PF_6]. The analytical procedure included a cooling ramp down to 183.15 K and a heating ramp up to the maximum temperature (salt dependent) at a rate of 0.167 $K \cdot s^{-1}$. In the case of [C_3C_1pip][PF_6] the results were obtained with a heating rate of 0.0167 $K \cdot s^{-1}$. The underlying reason for this difference is the appearance of an extra solid-solid phase transition at this slow heating rate. All salts were submitted to three cycles of cooling and heating. A constant nitrogen flow of 0.833 $cm^3 \cdot s^{-1}$ was supplied to the DSC cell in order to avoid condensation of water at the lower temperatures. At least 2 independent runs were performed for each salt.

Concerning the aromatic [PF_6]-based ionic liquids, the respective melting temperature was determined using a DSC PerkinElmer equipment. The sample was also tightly sealed in an aluminium pan and the temperature scans were of 0.167 $K \cdot s^{-1}$. This procedure was carried out in the temperature range between (273.15 and 373.15) K.

MUTUAL SOLUBILITIES MEASUREMENTS

The mutual solubilities measurements between water and ILs/salts were carried out at temperatures from (288.15 to 318.15) K and at atmospheric pressure. The main exception was for the systems with the [C_2C_1im][PF_6] and [C_2C_1im][FAP] where the temperature range was between (288.15 and 363.15) K. The saturation of both phases was

accomplished by mixing water and the respective ionic liquid in excess (approximately 10 cm^3 of each). The two macroscopic separated phases were initially vigorously agitated and allowed to reach the equilibrium for at least 48 h. After this period all mole fraction solubilities, in both rich phases, have shown to be constant, and thus the equilibrium conditions were attained for all ionic liquids. Due to the high melting temperatures of $[C_2C_1im][PF_6]$, the solubility of water in this ionic liquid was only measured in its liquid state — in the temperature range from (333.15 to 363.15) K — and a different procedure was carried out. Prior to this work, Wong et al.[215] have observed the formation of white solid flakes, indicative of the ionic liquid anion degradation when the mixture was placed at high temperatures for more than 48 h. For that reason, in this work, the liquid-liquid phase behaviour of the binary system $[C_2C_1im][PF_6]$ + H_2O at temperatures above 333.15 K was determined after 2 h of equilibration. This period of time proved to be enough for the two liquid phases to remain stable and clear throughout the measurement period and from (333.15 to 363.15) K. The temperature was maintained within ± 0.01 K using a PID temperature controller driven by a calibrated Pt100 (class 1/10) and by inserting the glass vials containing the two phases at equilibrium in an aluminium block, which in turn is placed inside of an isolated air bath. The temperature sensor is inserted directly in the aluminium block embracing the glass vials. A plain scheme of this apparatus is depicted in Figure 3.2. Further details about the equilibration conditions and equipment can be found elsewhere.[5–7,66,157]

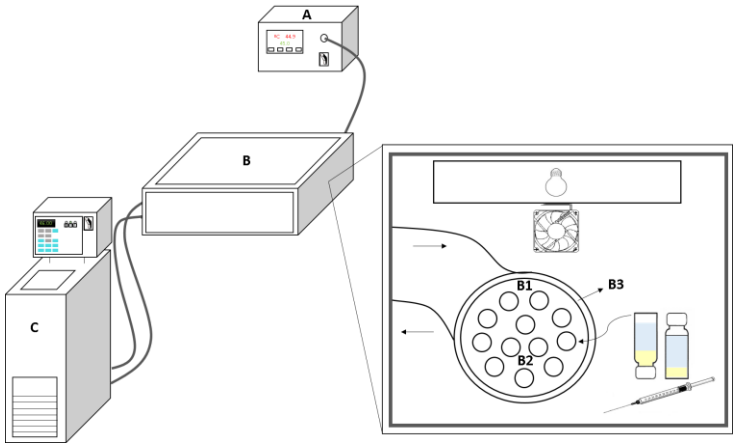

Figure 3.2. Scheme of the apparatus used for the mutual solubility measurements. (A), PID temperature controller; (B), Isolated air bath; (B1) Aluminium block; (B2), Pt100 (class 1/10) temperature sensor; (B3), Thermostatic fluid; (C), Refrigerated bath, Julabo F25-HD.

The water solubility in the IL-rich phase, whenever it is in the liquid state, was determined by Karl Fischer (KF) titration using a Metrohm 831 KF coulometric titrator, while the solubility of the ionic liquid/salt in the aqueous-rich phase was accomplished by UV spectroscopy with a SHIMADZU UV-1700 Pharma-Spec Spectrometer (for the aromatic-based ionic liquids) or with a Mettler Toledo S47 SevenMulti™ dual meter pH / conductivity, coupled with an InLab®741 Conductivity Probe as electrode (for the aliphatic ones). The calibration of the conductivity meter was carried out with two solutions of KCl with concentrations of 0.1 M and 0.01 M. Corresponding calibration curves were performed for each ionic liquid/salt and in an adequate concentration range. At least three calibration curves for each ionic liquid/salt were determined to confirm that no gravimetric errors occurred during the stock solutions preparation. Both phases were sampled from the equilibrium glass vials using glass syringes maintained dry and at the same temperature of the measurements, avoiding thus phase split or water absorption by temperature variations. All samples were quantified gravimetrically with an uncertainty in the order of ± 10^{-5} g. The mutual solubilities data are the result of an average of at least five independent measurements, *i.e.*, five equilibrated samples.

VISCOSITY AND DENSITY MEASUREMENTS

Measurements of viscosity and density were performed using an automated SVM 3000 Anton Paar rotational Stabinger viscometer-densimeter. For the solid ionic liquids at room temperature, viscosities and densities were only determined above the respective melting temperature. The SVM 3000 Anton Paar rotational Stabinger viscometer-densimeter uses Peltier elements for fast and efficient thermostatization. Further details regarding the operation system can be found elsewhere.[216] The uncertainty in temperature is within ± 0.02 K. The relative uncertainty in the dynamic viscosity is ± 0.35% whereas the absolute uncertainty in density is ± 5 × 10^{-4} g·cm^{-3}.

3.3. Theoretical approaches

THERMODYNAMIC FUNCTIONS OF SOLUTION

In order to describe the experimental mutual solubilities obtained two correlations were employed.[217] The correlations are particularly useful both to obtain the saturation values at non-working temperatures and to determine the thermodynamic functions of solution. The solubility of water in the IL-rich phase was described by,

$$\ln x_w = A + \frac{B}{T/K} \tag{3.1}$$

where x_w is the mole fraction solubility of water in the IL-rich phase, T is the absolute temperature and A and B are fitting parameters. It should be pointed out that eq 3.1 assumes that the molar enthalpy of solution in water, within the working temperature range, is temperature independent (B is constant).

On the other hand, the solubility of each ionic liquid in water was correlated by eq 3.2,

$$\ln x_{IL} = C + \frac{D}{T/K} + E \ln(T/K) \tag{3.2}$$

where x_{IL} is the mole fraction solubility of an ionic liquid as a function of temperature T, and C, D and E are the fitting parameters.

Since the solubility of water in all the studied ionic liquids is well above of what could be considered infinite dilution, the associated molar thermodynamic functions of solution cannot be determined.

At the equilibrium state the chemical potentials of the ionic liquid at the aqueous-rich and at the IL-rich phases have to be equivalent, while the electroneutrality of both phases must be obeyed. Quite the opposite of what was observed for the IL-rich phase, the solubility of ionic liquids in the aqueous-rich phase can be considered at infinite dilution, and thus no main solute-solute interactions and/or ion-pairing occur.[218] Therefore, the standard thermodynamic functions of solution, such as standard molar enthalpy ($\Delta_{sol}H_m^0$),

molar Gibbs energy ($\Delta_{sol}G_m^0$) and molar entropy ($\Delta_{sol}S_m^0$) were determined only for the ionic liquids solvation in water (water-rich phase). These thermodynamic functions can be calculated accordingly to eqs 3.3 to 3.5.[219]

$$\Delta_{sol}G_m^0 = -RT\ln(x_{IL})_p \tag{3.3}$$

$$\frac{\Delta_{sol}H_m^0}{RT^2} = \left(\frac{\partial \ln x_{IL}}{\partial T}\right)_p \tag{3.4}$$

$$\Delta_{sol}S_m^o = R\left(\frac{\partial \ln x_{IL}}{\partial \ln T}\right)_p \tag{3.5}$$

where x_{IL} is the mole fraction solubility of the solute (ionic liquid), R is the ideal gas constant, T is the temperature (K) and the subscript p indicates that the process takes place under constant pressure. The subscript m refers to the molar quantity.

Furthermore, when dealing with liquid-liquid equilibrium, the standard molar properties of solvation can be estimated using the following equations:[5]

$$\Delta_{sol}H_m^0 = \Delta_{svt}H_m^0 + \Delta_l^g H_m^0 \tag{3.6}$$

$$\Delta_{svt}G_m^0 = \Delta_{sol}G_m^0 + RT\ln\left(\frac{p(s2,T)}{p^0}\right) \tag{3.7}$$

$$\Delta_{svt}S_m^0 = \frac{\Delta_{svt}H_m^0 - \Delta_{svt}G_m^0}{T} \tag{3.8}$$

where $p(s2,T)$ is the vapour pressure of the solute at the temperature T and p^0 is the standard pressure of 10^5 Pa.

The standard molar enthalpy of solution, $\Delta_{sol}H_m^0$, is a sum of the standard molar enthalpy of solvation, $\Delta_{svt}H_m^0$, that reflects the solute-solvent interaction, and the standard molar enthalpy of vaporization of the solute to form an ideal gas, $\Delta_l^g H_m^0$. The standard molar Gibbs energy of solvation, $\Delta_{svt}G_m^0$, can be then derived using the hypothetical reference state for the solute, which considers the solute in the gas phase and at the standard pressure.

DENSITY GROUP CONTRIBUTION METHOD

In order to estimate the density data for pure ionic liquids, an extension of the Ye and Shereeve group contribution method previously proposed by Gardas and Coutinho[220] was used as described by eq 3.9,

$$\rho = \frac{Mw}{NV(a + bT + cp)} \tag{3.9}$$

where ρ is the density in kg·m^{-3}, Mw is the ionic liquid molecular weight in kg·mol^{-1}, N is the Avogadro constant, V is the ionic liquid volume in m^3, T is the temperature in K, and p is the pressure in MPa. The coefficients a, b and c, with values of 0.8005 ± 0.0002, (6.652 ± 0.007) × 10^{-4} K^{-1} and (-5.919 ± 0.024) × 10^{-4} MPa^{-1}, respectively, were proposed in a previous work.[216]

ISOBARIC THERMAL EXPANSION COEFFICIENT

The isobaric thermal expansion coefficients (α_p) associated to each ionic liquid were calculated using eq 3.10,

$$\alpha_p = -\frac{1}{\rho}\left(\frac{\partial \rho}{\partial T}\right)_p = -\left(\frac{\partial \ln \rho}{\partial T}\right)_p \tag{3.10}$$

where ρ is the density in kg·m^{-3}, T is the temperature in K and p is the pressure in MPa.

VISCOSITY GROUP CONTRIBUTION METHOD

The experimental viscosity data here measured were correlated using the Vogel-Tammann-Fulcher model described in eq 3.11,

$$\ln \eta = A_\eta + \frac{B_\eta}{(T - T_{0\eta})} \tag{3.11}$$

where η is viscosity in Pa·s, T is temperature in K, and A_η, B_η and $T_{0\eta}$ are adjustable parameters.

The prediction of viscosities for the studied ionic liquids was also carried out based on the group contribution method proposed by Gardas and Coutinho[221] which makes use of the

Vogel-Tammann-Fulcher model described in eq 3.11. A_η and B_η are obtained by a group contribution method accordingly to,

$$A_\eta = \sum_{i=1}^{k} n_i a_{i,\eta} \tag{3.12}$$

$$B_\eta = \sum_{i=1}^{k} n_i b_{i,\eta} \tag{3.13}$$

where n_i is the number of groups of type *i* and *k* is the total number of different groups in the molecule.

COSMO-RS

The COnductor-like Screening MOdel for Real Solvents (COSMO-RS) is based on quantum chemical calculations and can be used to predict the thermodynamic properties of fluid mixtures. COSMO-RS is a novel and efficient method for the *a priori* prediction of thermophysical data and has been developed in 1994. More details about COSMO-RS are described in the literature.[171,222] Previously, COSMO-RS was used to predict the equilibrium behaviour of ionic liquids and water and already confirmed its capability as a predictive tool.[5,6]

The standard procedure of COSMO-RS calculations employed here consisted essentially in two steps: *i*) the continuum solvation COSMO calculations of electronic density and molecular geometry that were performed with the TURBOMOLE program package on the density functional theory level, utilizing the BP functional B88-P86 with a triple-ζ valence polarized basis set (TZVP) and the resolution of identity standard (RI) approximation; *ii*) the estimation of the phase diagrams of binary mixtures of ionic liquids and water performed with the COSMOtherm program using different parameter files taking in consideration the different versions here used.

For the systems containing the ionic liquids $[C_3C_1im][PF_6]$, $[C_3\text{-}3\text{-}C_1py][PF_6]$, $[C_3C_1im][NTf_2]$ and $[C_3\text{-}3\text{-}C_1py][NTf_2]$, the COSMO-RS calculations were performed at the BP/TZVP level (Turbomole,[162,163] DFT/COSMO calculation with the BP functional and TZVP[164] basis set

using the optimized geometries at the same level of theory) with the parameter files BP_TZVP_C2.1_0110 and BP_TZVP_C2.1_0105.

On the other hand, for the salts $[C_3C_1pyr][PF_6]$, $[C_3C_1pip][PF_6]$, $[N_{4444}][PF_6]$ and $[P_{4444}][PF_6]$ and the ionic liquids $[C_1C_1im][NTf_2]$, $[C_2C_2im][NTf_2]$, $[C_3C_3im][NTf_2]$, $[C_4C_4im][NTf_2]$ and $[C_5C_5im][NTf_2]$, the TURBOMOLE 6.1 program package[223] was used. The solubility calculation of the several salts/ionic liquids mutual solubilities with water was performed with the COSMOthermX_2.1 program using the parameter file BP_TZVP_C21_0111 (COSMOlogic GmbH & Co KG, Leverkusen, Germany).[224]

In all systems, the calculations were made for a ternary mixture and the ionic liquids were always treated as isolated ions at the quantum chemical level. It has been shown before that the best predictions of the experimental data were obtained with the lowest energy conformations or with the global minimum for both cation and anion.[176] Thus, here, the lowest energy conformations of all the species involved were used in the COSMO-RS calculations.

MOLECULAR DYNAMICS SIMULATION

Molecular dynamics (MD) simulations were performed on condensed-phase water/IL mixtures using the DL_POLY program version 2.17.[225] The ionic liquids studied in the MD simulations with that version of the program included $[C_4py][NTf_2]$, and its three methyl-substituted derivatives (*ortho*, *meta*, and *para*): 1-butyl-2-methylpyridinium bis(trifluoromethylsulfonyl) imide, $[C_4\text{-}2\text{-}C_1py][NTf_2]$, $[C_4\text{-}3\text{-}C_1py][NTf_2]$, and $[C_4\text{-}4\text{-}C_1py][NTf_2]$. These were modelled using an extended version of the CL&P force field.[218] The $[NTf_2]^-$ anion and $[C_npy]^+$ cations had been previously described in the second and third parts of a sequence of articles concerning the application of the CL&P force field to different ionic liquid ions and their homologous series.[226,227] The methyl-substituted $[C_4\text{-}n\text{-}C_1py]^+$ cations were parameterized in the present work taking into account supplementary *ab initio* calculations at the RHF/6-31G(d) (geometry optimization) and MP2/cc-pVTZ(-f) (electron density calculation) levels using the Gaussian 03 package[228] that yielded new atomic point charges for these cations. All other parameters (bond, angle, dihedral angle,

and van der Waals parameters) were taken either from the CL&P[218,229] or the OPLS-aa[230–232] force fields. Water molecules were modelled using the SPC model.[233] System sizes were chosen to contain about 10 000 atoms, and so, the numbers of cations, anions, and water molecules varied according to the composition of the mixtures. Since these ionic liquids are only partially soluble in water, and most simulations were to be performed under single-phase conditions, two distinct sets of mixtures were considered: $[C_4py]^+$, $[C_4$-n-$C_1py]^+$, and $[NTf_2]^-$ ions at very high dilution in water (1 cation, 1, 3, 10, or 20 ion pairs in 3000 water molecules) and water molecules dissolved in the ionic liquid solvent up to concentrations below the water solubility limit in the ionic liquids (5, 10, 30, and 40 water molecules in 250 ion pairs). All MD simulation runs were started from low-density configurations, with all ions and water molecules placed at random in period cubic boxes. These were then equilibrated for a period of 0.8-1.0 ns to attain liquid-like densities and structures at 300 K and 1 bar. Temperature and pressure were maintained using Nosé-Hoover thermostats and Hoover barostats. Production runs then took 0.6 ns with an explicit cut-off distance of 16 Å for nonbonded interactions, and long-range corrections were applied for repulsive-dispersive interactions. Electrostatic energies were calculated using the Ewald summation method with k-values set to 5 and α = 0.185 Å. The structural quantities pertinent to the interpretation of the experimental solubility results were assessed through the calculation of pair radial distribution functions for selected pairs of atoms.

The MD of condensed phases of the other different pure ionic liquids here studied ($[C_2C_1im][FAP]$ and $[C_2C_1im][PF_6]$) and their aqueous mixtures were carried out using a more recent DLPOLY package.[234] Water and all ionic liquids were modelled using, respectively, the SPC model[233] and a previously described all atom force field (CL&P),[226,235,236] which is based on the OPLS-AA framework,[230] but was to a large extent developed specifically to encompass entire ionic liquid families.

For the pure $[C_2C_1im][PF_6]$ and $[C_2C_1im][FAP]$ ionic liquids, the runs also started from low-density configurations composed of 200 ion pairs. For the mixtures, again, the runs started from low-density initial configurations composed either of 1 ion pair and 600

water molecules (water-rich mixtures) or 200 ionic liquid ion pairs and 20 water molecules (IL-rich mixtures). For $[C_2C_1im][PF_6]$ simulations with 11 water molecules and 200 ion pairs in order to compare ($[C_2C_1im][FAP]$ + water and $[C_2C_1im][PF_6]$ + water) mixtures, where the water molecules occupy approximately the same volume fraction, were also performed.

The boxes were equilibrated under isothermal–isobaric ensemble conditions for 1 ns at 318 K and 1 atm using the Nosé−Hoover thermostat and isotropic barostat with time constants of 0.5 and 2 ps, respectively. Several consecutive simulation runs of 1 ns were used to produce equilibrated systems — at least four runs in the case of water-rich mixtures and at least eight runs in the case of IL-rich mixtures or neat ionic liquids — and to obtain the trajectories used to acquire the pertinent structural data. Electrostatic interactions were treated using the Ewald summation method considering six reciprocal-space vectors, and repulsive−dispersive interactions were explicitly calculated below a cut-off distance of 1.6 nm (long-range corrections were applied assuming the system has an uniform density beyond that cut-off radius). Details concerning this type of simulation can be found elsewhere.[226,235,236]

3.4. Thermophysical properties and water saturation of $[PF_6]$-based ionic liquids

Catarina M. S. S. Neves, Marta L. S. Batista, Ana Filipa M. Cláudio, Luís M. N. B. F. Santos, Isabel M. Marrucho, Mara G. Freire and João A. P. Coutinho, Journal of Chemical & Engineering Data 55 (2010) 5065-5073, DOI: 10.1021/je100638g

3.4.1. Abstract

In this work, mutual solubilities of two $[PF_6]$-based ionic liquids with water and their thermophysical properties, namely melting properties of pure ionic liquids, and densities and viscosities of both pure and water-saturated ionic liquids, were determined. The selected ionic liquids comprise 1-methyl-3-propylimidazolium and 1-methyl-3-

propylpyridinium cations combined with the anion hexafluorophosphate. Mutual solubilities with water were measured in the temperature range from (288.15 to 318.15) K. From the experimental solubility data dependence on temperature, the molar thermodynamic functions of solution, such as Gibbs energy, enthalpy and entropy of the ionic liquids in water were further derived. In addition, a prediction study based on the COSMO-RS methodology was carried out. For both pure ionic liquids and water-equilibrated samples, densities and viscosities were determined in the temperature interval between (303.15 and 373.15) K. The isobaric thermal expansion coefficients for pure and water-saturated ionic liquids were calculated based on the density dependence on temperature.

3.4.2. Results and discussion

MELTING TEMPERATURE

The melting temperatures of the dried ionic liquids, solid at room temperature, were determined by DSC. Only one phase transition was observed in the temperature range evaluated. The melting temperatures, enthalpies and entropies changes at the corresponding melting temperatures, for the crystal to isotropic liquid phase transitions, are respectively 311.6 K, 16.7 $kJ \cdot mol^{-1}$ and 53.6 $J \cdot K^{-1} \cdot mol^{-1}$ for $[C_3\text{-}3\text{-}C_1py][PF_6]$ (water mole fraction of 0.0038) and 311.2 K, 15.0 $kJ \cdot mol^{-1}$ and 48.2 $J \cdot K^{-1} \cdot mol^{-1}$ for $[C_3C_1im][PF_6]$ (water mole fraction of 0.0012). The correspondent thermograms are presented in Figures S3.1 and S3.2 in Appendix. The melting temperature of $[C_3C_1im][PF_6]$ obtained in this work is in close agreement with that previously shown in literature (313.15 K).[237] The melting temperatures of the ionic liquids saturated with water are substantially lower than those of the pure ionic liquids, allowing therefore the measurements of $[C_3C_1im][PF_6]$ to be carried out in the entire temperature range, while for $[C_3\text{-}3\text{-}C_1py][PF_6]$ only for temperatures above 308.15 K the thermophysical properties were evaluated.

MUTUAL SOLUBILITIES MEASUREMENTS

The measured solubility data and the respective standard deviations are presented in Table S3.2 in Appendix and depicted in Figure 3.3. For the studied ionic liquids, the

mutual solubilities increase with temperature displaying an upper critical solution temperature behaviour. The mole fraction solubility of ionic liquids in water is in the order ≈ 10^{-3} but the water solubility in ionic liquids is typically in the order ≈ 10^{-1}, indicating that they are highly "hygroscopic", and as previously shown for other hydrophobic ionic liquids.[5,6,238] Thus, while the water-rich phase can be considered as an almost pure phase with the ionic liquid at infinite dilution, the IL-rich phase presents a significant water content.

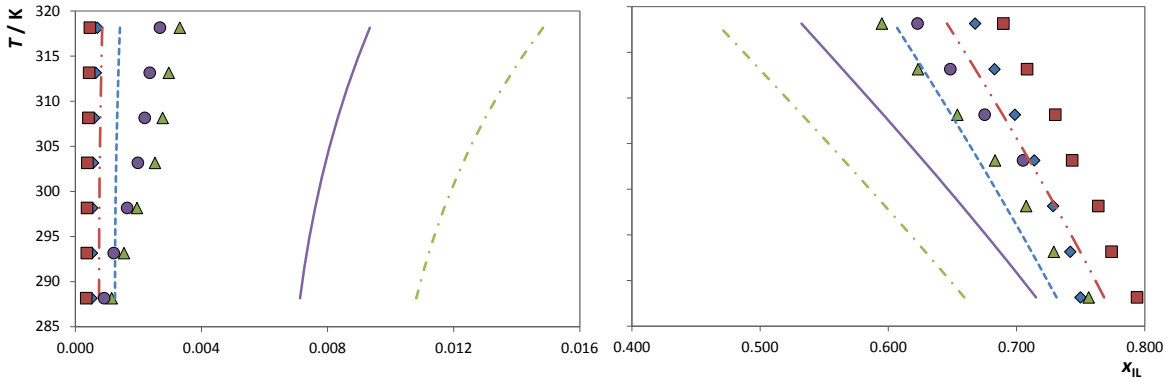

Figure 3.3. Liquid-liquid phase diagram for water and ILs: ◆, ---, [C_3C_1im][NTf_2];[5] ■, – · · –, [C_3-3-C_1py][NTf_2];[6] ▲, – · –, [C_3C_1im][PF_6]; ●, —, [C_3-3-C_1py][PF_6]. The single symbols and the lines represent, respectively, the experimental data and COSMO-RS prediction results (parameter file BP_TZVP_C2.1_0110).

Concerning the ionic liquids cation influence, it is possible to observe that the hydrophobicity increases from imidazolium- to pyridinium-based ionic liquids, as shown in Figure 3.3. Comparing with literature data[5,6,238] for other ionic liquids with common cations, the ionic liquid anion hydrophobicity increases from $[PF_6]^-$ to $[NTf_2]^-$. Evaluating the influence of both ionic liquids cation and anion on the liquid-liquid equilibria with water, it is clear that the major role is played by the ionic liquid anion, as previously observed.[6]

The correlation constants obtained from the fittings using eqs 3.1 and 3.2 are presented in Table S3.3 in Appendix. For the IL-rich phase, the proposed correlation shows a relative maximum average deviation from the experimental mole fraction data of 1%. Since the solubility of water in all the studied ionic liquids is well above of what could be considered infinite dilution, the associated molar thermodynamic functions of solution cannot be determined. For the water-rich phase, and because the melting points of both ionic

liquids are above 298.15 K, the parameters were calculated in a smaller temperature range from (303.15 to 318.15) K, in order to avoid the disparities occurring between solid-liquid and liquid-liquid equilibria. The proposed correlation presents a relative maximum deviation from experimental mole fraction data in the order of 1%.

The standard molar enthalpy, Gibbs energy and entropy of solution were calculated using eqs 3.3 to 3.5 and are reported in Table 3.1.

Table 3.2. Standard thermodynamic molar properties of solution of ILs in water at 298.15 K.

IL	$(\Delta_{sol}H^0_m \pm \sigma^a)$ / kJ·mol^{-1}	$(\Delta_{sol}G^0_m \pm \sigma^a)$ / kJ·mol^{-1}	$(\Delta_{sol}S^0_m \pm \sigma^a)$ / J·K^{-1}·mol^{-1}
$[C_3C_1im][PF_6]$	9.3 ± 1.5	15.460 ± 0.014	-20.7 ± 5.1
$[C_3\text{-}3\text{-}C_1py][PF_6]$	9.1 ± 1.5	15.888 ± 0.043	-22.7 ± 5.2
$[C_3C_1im][NTf_2]$[5]	5.9 ± 1.5	18.652 ± 0.001	-42.6 ± 5.0
$[C_3\text{-}3\text{-}C_1py][NTf_2]$[6]	6.5 ± 1.5	19.555 ± 0.016	-43.9 ± 5.1

[a]Standard deviation

The molar enthalpies of solution of the studied ionic liquids in water, at 298.15 K, show that the solubilisation of ionic liquids in water is an endothermic process, which is almost independent of the cation nature. Major differences in the enthalpies of solution are observed only for the anion identity (when compared with literature data[5,6]). This behaviour is in agreement with the fact discussed above where the solvation of the anion is the main issue controlling the solubility of the ionic liquid in water. The molar entropies of solution are shown to be negative and with a slight dependence on the cation family, falling within the associated standard deviations. Even so, there are significant differences in the molar entropies of solution when changing the anion while maintaining the cation.[5,6] More hydrophilic anions are responsible for larger entropic change effects suggesting that the ionic liquids dissolution in water is controlled by the anion solvation in the IL-rich phase. The higher (less negative) the entropic change, the higher the solubility of the ionic liquids in water, as can be seen by comparing, for instance, the solubilities for $[C_3C_1im][NTf_2]$[5] and $[C_3C_1im][PF_6]$. $[C_3C_1im][PF_6]$ is a highly solvated ionic liquid in the IL-rich phase, leading to higher (less negative) entropic variations when in equilibrium with the aqueous-rich phase.

Aiming at predicting the ionic liquids-water LLE, COSMO-RS[168–172] was here evaluated. The results obtained with COSMO-RS are displayed in Figure 3.3 and show an acceptable qualitative agreement with the experimental data. The cation core hydrophobic character increase from $[C_3C_1im]^+$ to $[C_3\text{-}3\text{-}C_1py]^+$ observed experimentally was also verified by the COSMO-RS predictions. Moreover, the anion influence trough the phase behaviour of ionic liquids and water is also well qualitatively predicted. In a previous work,[6] using an older version of COSMO-RS (parameter file BP_TZVP_C2.1_0105), some deviations from experimental data were reported, especially regarding the ionic liquid anion influence in the liquid-liquid equilibrium. Using the new version of COSMO-RS (parameter file BP_TZVP_C2.1_0110), the prediction of the anion influence is fully consistent with the experimental data, where the anion $[PF_6]^-$ presents a smaller liquid-liquid envelope with water when compared to ionic liquids containing the anion $[NTf_2]^-$. The comparison of both versions of COSMO-RS is depicted in Figure 3.4.

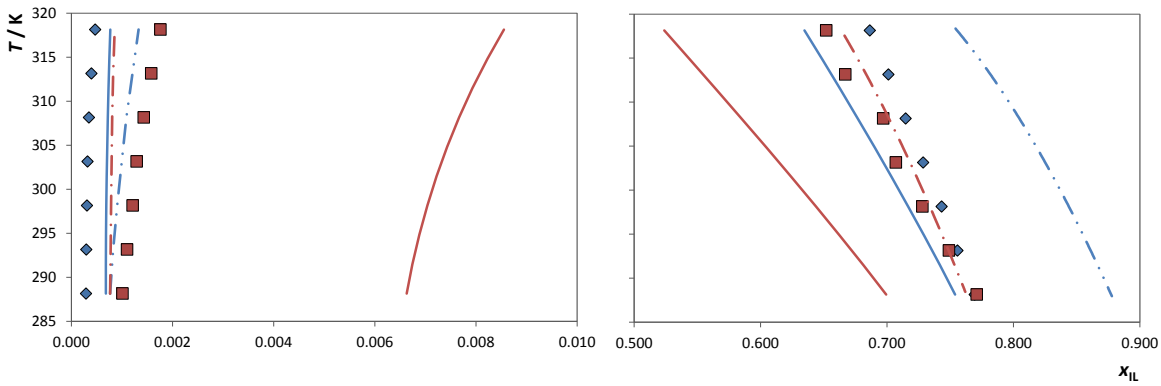

Figure 3.4. Comparison of COSMO-RS versions for the liquid-liquid phase diagrams of water and ILs: ◆, – · · –, —, $[C_4C_1im][NTf_2]$;[5] ■, – · –, —, $[C_4C_1im][PF_6]$.[6] The single symbols, the lines with dots and the full lines represent, respectively, the experimental data, the COSMO-RS older version (parameter file BP_TZVP_C2.1_0105) and the COSMO-RS new version (parameter file BP_TZVP_C2.1_0110) predictions.

Although improvements in the IL-water phase behaviour were observed for the most recent version of COSMO-RS, it should be pointed out that the relative deviations to the experimental values have increased. Nevertheless, the prediction of the correct trend on the influence of ionic liquids cations and anions in the liquid-liquid phase behaviour using the new version of COSMO-RS is of main importance when the goal is a screening of ionic liquids before experimental measurements. In spite of the quantitative deviations of the COSMO-RS predictions, this method shows to be a useful tool in predicting binary systems

behaviour, allowing thus an improved choice of the cation and anion composing the ionic liquid aiming at designing ionic liquids for specific purposes.

An alternative approach to the estimation of the mutual solubilities of ionic liquids and water is the use of a QSPR correlation.[7] Using this correlation, the predicted values for the solubilities of ionic liquids in water at 303.15 K are 2.48×10^{-3} and 1.29×10^{-3} for $[C_3C_1im][PF_6]$ and $[C_3\text{-}3C_1py][PF_6]$, respectively, while the solubilities of water in the ionic liquids at the same temperature are 0.31 and 0.29 (both in mole fraction units). These values, when compared with the experimental data, have maximum deviations of 2.5% and 5.5% for the solubility of the ionic liquids in water and water in ionic liquids, respectively.

DENSITY

The novel experimental density data for both dried and water-saturated ionic liquids are presented in Table S3.4 in Appendix and depicted in Figure 3.5. Due to the melting temperatures of both dried ionic liquids, densities and viscosities of these "pure" ionic liquids were only measured at temperatures above 318.15 K. For the water-saturated ionic liquids, the presence of an eutectic point allowed the measurements to be carried out in the temperature range between (303.15 to 363.15) K. Figure 3.5 also depicts the density results obtained in this work together with some literature values.[239,240]

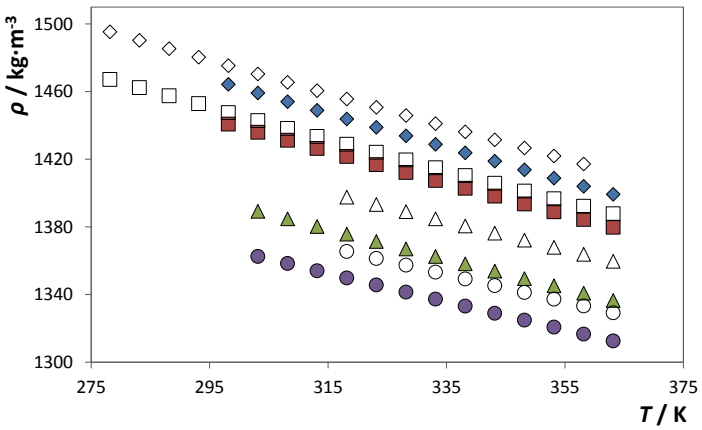

Figure 3.5. Experimental density as a function of temperature and at 0.1 MPa for the dried ILs (empty symbols) and water-saturated ILs (full symbols): ◇, ◆, $[C_3C_1im][NTf_2]$;[241] □, ■, $[C_3\text{-}3\text{-}C_1py][NTf_2]$;[240] △, ▲, $[C_3C_1im][PF_6]$; ○, ●, $[C_3\text{-}3\text{-}C_1py][PF_6]$.

For both anions, $[PF_6]^-$ and $[NTf_2]^-$, the density values decrease from imidazolium- to pyridinium-based ionic liquids. The molar volumes for a series of ionic liquids with a common anion seem to increase with the effective cation size from imidazolium- to pyridinium-based ionic liquids. Indeed, this tendency is in close agreement with the results previously presented,[242] where the molar volumes follow the rank: imidazolium- < pyrrolidinium- < pyridinium- < piperidinium-based ionic liquids. For a given cation, $[C_3C_1im]^+$ or $[C_3\text{-}3\text{-}C_1py]^+$, the ionic liquid density decreases from $[NTf_2]^-$ to $[PF_6]^-$ anions. Therefore, the ionic liquids molar volumes also increase with the effective anion size.

Figure 3.5 also presents the results for the water-saturated samples. The presence of water in ionic liquids is shown to decrease their density and has a major impact in ionic liquids that have higher water contents at saturation conditions. However, the trends of the water-saturated ionic liquids are identical to those observed for the dry ionic liquids. At 318.15 K, the density relative deviations of the water-saturated samples with respect to the pure ionic liquids were in the order of 1.6% and 1.1% for $[C_3C_1im][PF_6]$ and $[C_3mpy][PF_6]$, respectively. These relative deviations, which seem to be temperature independent (note that the water content in both ionic liquids was maintained constant in the entire temperature interval), can be considerable negligible for most of their application purposes.

In order to estimate the density data for pure ionic liquids, eq 3.9 was employed while the required ionic volumes are reported in Table 3.2.

Table 3.3. Ionic volumes, *V*, determined with the Gardas and Coutinho group contribution model.[220]

Species	*V* / Å^3
Cations	
1,3-dimethylimidazolium	154 [220]
1,3-dimethylpyridinium	174
Anions	
Hexafluorophosphate	107 [220]
Additional groups	
$-CH_2$	28 [220]

To obtain the volume parameter for the cation group 1,3-dimethylpyridinium, not previously available, 132 experimental density values taken from literature (ionic liquids with a similar cation but different anions) were used.[240,243–246] Figure 3.6 presents a comparison between the predicted density values based on the group contribution method and the experimental data obtained in this work.

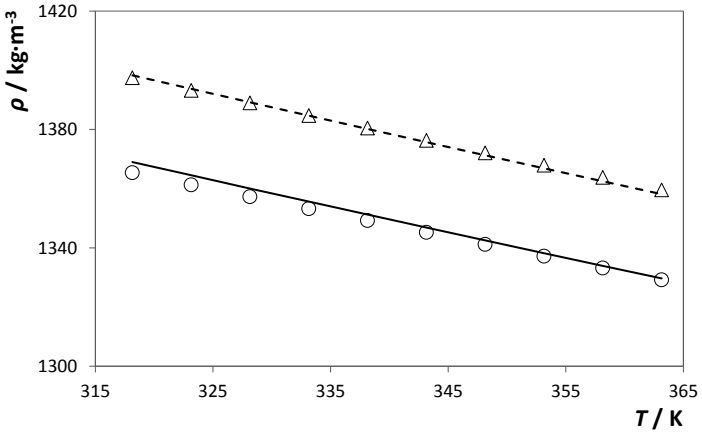

Figure 3.6. Experimental density as a function of temperature, and at 0.1 MPa, for the dried ILs (symbols) and respective prediction with the Gardas and Coutinho group contribution method[45] (lines): △ , ---, $[C_3C_1im][PF_6]$; ○, —, $[C_3\text{-}3\text{-}C_1py][PF_6]$.

The predicted values are in excellent agreement with the experimental data, presenting maximum relative deviations of 0.05% and 0.14% for $[C_3C_1im][PF_6]$ and $[C_3\text{-}3\text{-}C_1py][PF_6]$, respectively. This method shows to be highly valuable in the prediction of density data for new ionic liquids where no experimental data is yet available. The complete temperature dependence between the predicted values and those obtained experimentally is depicted in Figure S3.4 in Appendix.

In Table 3.4 are presented the values of isobaric thermal expansion coefficients (α_p) associated to each ionic liquid here studied that were calculated using eq 3.10 and obtained from the linear relationship between $\ln\rho$ and T using the experimental data gathered in this work.

Table 3.4. Thermal expansion coefficients, α_p, for both pure and water-saturated ILs at 318.15 K and 0.1 MPa.

	10^4 ($\alpha_p \pm \sigma^a$) / K^{-1}			
	$[C_3C_1im][PF_6]$	$[C_3\text{-}3\text{-}C_1py][PF_6]$	$[C_3C_1im][PF_6]$	$[C_3\text{-}3\text{-}C_1py][PF_6]$
T / K	Pure		x_w = (0.306 ± 0.004[a])	x_w = (0.249 ± 0.006[a])
318.15	6.023 ± 0.004	5.886 ± 0.004	6.381 ± 0.005	6.174 ± 0.003

[a]Standard deviation

The thermal expansion coefficients were determined at a temperature of 318.15 K due the high melting temperatures of the ionic liquids under study. For $[C_3C_1im][PF_6]$ and $[C_3\text{-}3\text{-}C_1py][PF_6]$ the values are (6.02 and 5.89) × 10^{-4} K^{-1} for the dried samples and (6.38 and 6.17) × 10^{-4} K^{-1} for the water-saturated samples. The α_p of both ionic liquids are in close agreement with literature values for related ionic liquids.[240,247] For both dried and water-saturated, and at a constant temperature, imidazolium-based ionic liquids present higher thermal expansion than their pyridinium-based counterparts. Furthermore, the presence of water increases the values of the isobaric thermal expansion coefficients (α_p).

VISCOSITY

The novel viscosity data were determined in the temperature range from (318.15 to 363.15) K for the dried ionic liquids and from (303.15 to 363.15) K for the water-saturated samples. Experimental results are presented in Table S3.5 and in Figure 3.7. Also in Figure 3.7, some literature data[239,240] are presented for evaluation purposes and to assist the discussion.

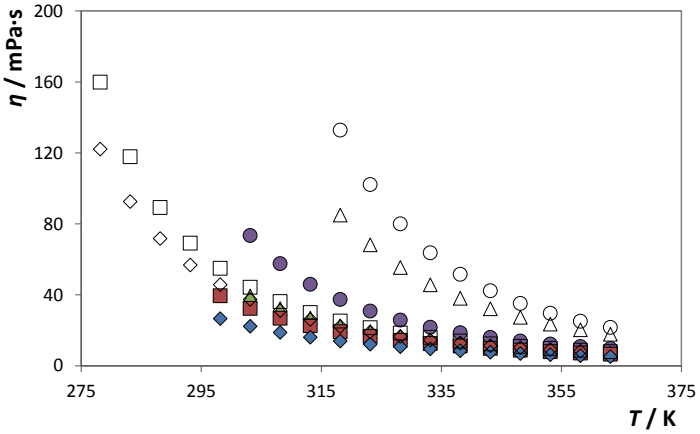

Figure 3.7. Experimental viscosity as a function of temperature, and at 0.1 MPa, for the dried ILs (empty symbols) and water-saturated ILs (full symbols): ◇, ◆, [C_3C_1im][NTf_2];[239] □, ■, [C_3-3-C_1py][NTf_2];[240] △, ▲, [C_3C_1im][PF_6]; ○, ●, [C_3-3-C_1py][PF_6].

The viscosity describes the internal resistance of a fluid to a shear stress and, as well-known, ionic liquids present higher viscosities than common volatile organic compounds. Nevertheless, the ionic liquids high viscosities are also a direct consequence of their high molecular weights. Since viscosity is mainly dependent on intermolecular interactions (H-bonding, dispersive and Coulombic interactions), an increase in temperature will substantially decrease the intensity of H-bonding interactions, and therefore the viscosity largely decreases. While densities decrease from imidazolium- to pyridinium-based ionic liquids, the viscosities decrease from pyridinium- to imidazolium-based ionic liquids. This is in agreement with the results of Crosthwaite et al.[248] that showed that pyridinium-based salts are generally more viscous than the equivalent imidazolium salts. In addition, for a common cation, $[C_3C_1im]^+$, the viscosities decrease for ionic liquids based on $[PF_6]^-$ to $[NTf_2]^-$. From the inspection of Figure 3.7, the ionic liquids viscosities seem to be more dependent on the anion than on the ionic liquid cation nature.

As for density values, the presence of water in ionic liquids decreases their viscosity and has a major impact in those which are less hydrophobic. Relative deviations of the water-saturated samples to the pure ionic liquids, at 318.15 K, were 73% and 72% for [C_3C_1im][PF_6] and [C_3-3-C_1py][PF_6], respectively. The influence of the water content in the viscosity is much more pronounced than in density. However, as temperature increases, the effect of water becomes less important because of the weakening of the H-bonding interactions between ionic liquids and water.

In Table 3.5 are presented the parameters A_η, B_η and $T_{0\eta}$ determined from the correlation of the experimental data for both dried and water-saturated ionic liquids gathered in this work, using the model described in eq 3.11.

Table 3.5. Correlation Parameters A_η and B_η obtained from the Vogel-Tammann-Fulcher correlation[221] applied to experimental data for dried and water-saturated ILs.

IL	A_η		B_η / K		$T_{0\eta}$ / K	
	Dried	Saturated	Dried	Saturated	Dried	Saturated
$[C_3C_1im][PF_6]$	-9.363	-9.426	1055.34	982.29	165.06	143.98
$[C_3\text{-}3\text{-}C_1py][PF_6]$	-10.009	-10.021	1220.37	1174.10		

Figure 3.8 displays the experimental data and respective comparison with the proposed correlation. The average relative deviations between the correlated values and experimental data are 0.20% for $[C_3C_1im][PF_6]$ and 0.70% for $[C_3\text{-}3\text{-}C_1py][PF_6]$ for pure ionic liquids, and 0.72% for $[C_3C_1im][PF_6]$ and 1.24% for $[C_3\text{-}3\text{-}C_1py][PF_6]$ for water-saturated ionic liquids. The Vogel-Tammann-Fulcher method provides a good description of the viscosity dependence on temperature for both ionic liquids and for both pure and water-saturated samples.

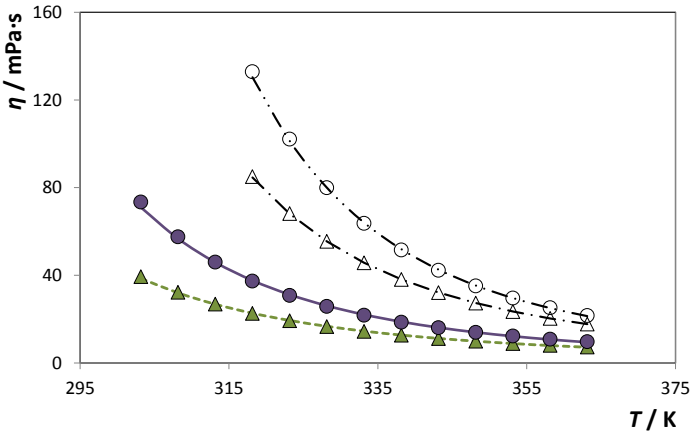

Figure 3.8. Experimental viscosity as a function of temperature, and at 0.1 MPa, for the dried ILs (empty symbols), water-saturated ILs (full symbols) and respective correlations using the Vogel-Tammann-Fulcher[221] method (lines): △, – · –, ---, $[C_3C_1im][PF_6]$; ○, – · · –, —, $[C_3\text{-}3\text{-}C_1py][PF_6]$.

The prediction of viscosities for the studied ionic liquids was also carried out based on the group contribution method proposed by Gardas and Coutinho[221] which makes use of the Vogel-Tammann-Fulcher model described in eq 3.11. Parameters $a_{i\eta}$ and $b_{i\eta}$ are provided

in Table 3.6 for the studied ionic liquids. Some of these values were previously estimated and were taken from literature.[221]

Table 3.6. Group Contribution Parameters $a_{i,\eta}$ and $b_{i,\eta}$ for the group contribution method proposed by Gardas and Coutinho[221] based on the Vogel-Tammann-Fulcher correlation.

Species	$a_{i,\eta}$	$b_{i,\eta}$ / K
Cations		
1,3-dimethylimidazolium	-7.271 [221]	510.51 [221]
1,3-dimethylpyridinium	-7.581	605.98
Anions		
Hexafluorophosphate	-1.834 [221]	433.14 [221]
Additional groups		
$-CH_2$	-7.528×10^{-2} [221]	40.92 [221]

A new group (cation 1,3-dimethylpyridinium) is here proposed. This new group was obtained by the correlation of the experimental viscosity values gathered in this work together with experimental data reported in literature.[240,243–246,248] For dried samples, the $T_{0\eta}$ of 165.06 K previously proposed was used.[221] The average of the absolute relative deviations between the predictions and the experimental data are 6.7% and 13.9% for pure ionic liquids $[C_3C_1im][PF_6]$ and $[C_3\text{-}3\text{-}C_1py][PF_6]$, respectively. The relative deviations between the experimental data and those predicted for the entire temperature interval are shown in Figure S3.5 Appendix. In Table 3.7 a comparison between predicted (using eqs 3.11 to 3.13) and correlated (applying only eq 3.11 to the experimental data) parameters A_η and B_η is presented.

Table 3.7. Comparison between the correlated and predicted parameters A_η and B_η from the Vogel-Tammann-Fulcher correlation applied to the experimental data and from the Group Contribution Method proposed by Gardas and Coutinho.[221]

IL	A_η		B_η / K	
	Predicted	Correlated	Predicted	Correlated
$[C_3C_1im][PF_6]$	-9.256	-9.363	1025.49	1055.34
$[C_3CF_1py][PF_6]$	-9.566	-10.009	1120.96	1220.37

3.5. Mutual solubility of water and structural/positional isomers of N-alkylpyridinium-based ionic liquids

Mara G. Freire, Catarina M. S. S. Neves, Karina Shimizu, Carlos E. S. Bernardes, Isabel M. Marrucho, João A. P. Coutinho, José N. Canongia Lopes and Luís Paulo N. Rebelo, Journal of Physical Chemistry B 114 (2010) 15925-15934, DOI: 10.1021/jp1093788

3.5.1. Abstract

In spite of many previous important contributions to the characterization of the liquid-liquid phase behaviour of ionic liquids plus water systems, a gap still exists as far as the isomers (of ionic liquids) effect is concerned. Therefore, in this work, a comprehensive study of the liquid-liquid equilibria between water and isomeric pyridinium-based ionic liquids has been performed. Atmospheric pressure mutual solubilities between water and pyridinium-based ionic liquids combined with the common anion bis(trifluoromethylsulfonyl)imide were experimentally determined between (288.15 and 318.15) K. The main goal of this work is to study the isomeric effects on the pyridinium-based cation, namely the structural and positional isomerism, as well as the alkyl side chain length. The influence of both structural and positional isomerism on the liquid-liquid behaviour in ionic liquids-containing systems, is an unexplored field and is here assessed for the first time. Moreover, from the experimental solubility data, several infinite dilution molar thermodynamic functions of solution, namely the Gibbs energy, the enthalpy and the entropy, were estimated and discussed. In addition, aiming at gathering a broader picture of the underlying thermodynamic solvation phenomenon, molecular dynamics simulations were also carried out for the same experimental systems.

3.5.2. Results and discussion

MUTUAL SOLUBILITIES MEASUREMENTS

Liquid-liquid phase diagrams of the pyridinium-based ionic liquids plus water systems were determined in the 288.15-318.15 K temperature range at atmospheric pressure. The

results are displayed in Table S3.6 in Appendix, along with their standard deviations. Due to the large differences in the molecular weight between the solute and the solvent it is worth to consider both mole and weight fraction solubilities (see Tables S3.6 and S3.7 in Appendix).

Mutual solubilities between water and $[C_4\text{-}3\text{-}C_1py][NTf_2]$ or $[C_6py][NTf_2]$ at (297 ± 1) K were previously published by Chapeaux et al..[249] For the IL-rich phase, our results deviate positively from literature[249] by 5.91% and 0.81% for $[C_4\text{-}3\text{-}C_1py][NTf_2]$ and $[C_6py][NTf_2]$, respectively. Nevertheless, for the water-rich phase, and although the results are of the same order of magnitude, the relative deviations of our results in respect to those published by Chapeaux et al.[249] are 6.38% and 75.36% for $[C_4\text{-}3\text{-}C_1py][NTf_2]$ and $[C_6py][NTf_2]$, respectively. Note that our mole fraction results are always greater than those presented in literature.[249] We believe that the major deviations result from the time employed in the equilibration for both phases separation. Chapeaux et al.[249] performed their experiments by mixing both phases during 12 h followed by 12 h of rest (for equilibrium conditions attainment). Nevertheless, we found the measurements of the ionic liquids $[C_6py][NTf_2]$ and $[C_8py][NTf_2]$ particularly difficult, and only after 48 h the equilibrium was attained, while for the remaining ionic liquids, 24 h of equilibration was required. A general example for the time-dependent saturation conditions is presented in Appendix, Figure S3.12.

The liquid-liquid phase diagrams of all the ionic liquids studied along with that previously investigated,[6] $[C_3\text{-}3\text{-}C_1py][NTf_2]$, are depicted in Figure 3.9. For each set of points, homogeneous mixtures of the ionic liquid and water are found above the curves, while, below them, macroscopic phase splitting occurs. The studied ionic liquids and water binary systems present thus a common upper critical solution temperature (UCST) behaviour,[146,250] asymmetrically centred in the low-concentration region of ionic liquid. It is observed that while the mole fraction solubility of the ionic liquids in water is of the order of 10^{-5} to 10^{-4}, the solubility of water in the ionic liquids is much higher, in the 10^{-1} magnitude. Hence, in spite of the extreme hydrophobic nature of these ionic liquids (mainly due to the anion contribution), it is here shown that they are highly hygroscopic.

Nevertheless, it should be mentioned that due to the large differences in the molecular weight between water and ionic liquids, when those values are converted to mass fraction compositions, the solubility of water in the IL-rich phase is only one order of magnitude superior to the solubility of the ionic liquid in the water-rich phase (*cf.* Table S3.7 in Appendix).

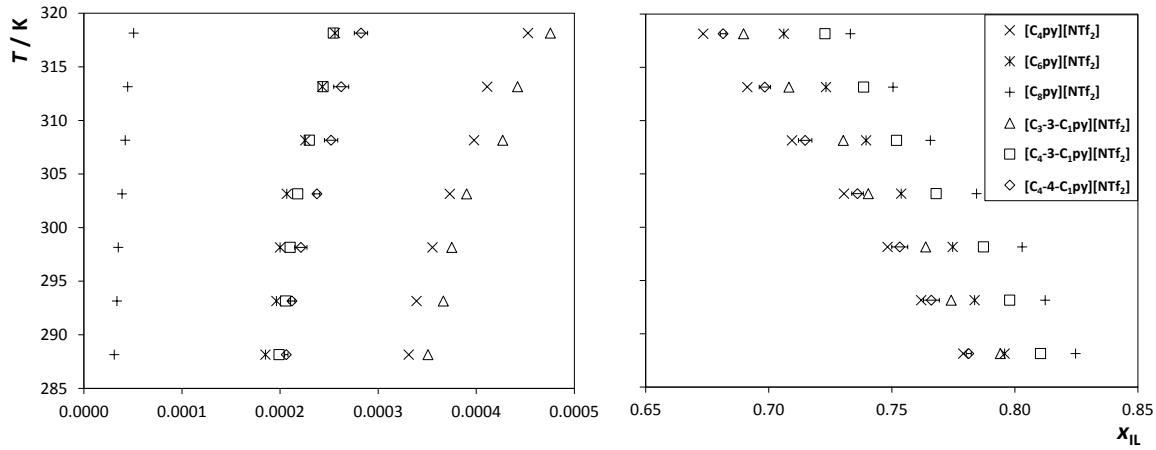

Figure 3.9. Temperature phase behaviour for the several studied ILs and water (left: water-rich phase; right: IL-rich phase). Standards deviations associated to the experimental measurements are presented for [C_4-4-C_1py][NTf_2] as an example. Literature data[6]: triangle; all other points represent our data.

It is well-known that the chemical and physical behaviour of mixtures incorporating ionic liquids are drastically affected by the ionic liquid anion.[6] Although in a milder fashion, it is here shown that the structure of the cation also influences the liquid-liquid phase behaviour of IL-water binary systems and can be used to fine-tune the phase diagrams. For instance, differences of one order of magnitude are observed in the water-rich phase for the solubilities of [C_4py][NTf_2] and [C_8py][NTf_2]. The mutual miscibility of ionic liquids and water decreases with the increase in the alkyl side chain length. The surface of an ionic liquid is usually composed of hydrophobic and hydrophilic moieties, including local charges. The number of carbon atoms in the alkyl chain is one of the main factors determining the hydrophobic nature of the studied ionic liquids, and thus, assuming that there is no micelle formation or similar types of segregation (or at least, likewise has been found for [$C_{10}C_1$im][NTf_2][251] we are working at saturation concentrations which are below the critical micelle concentration), the hydrophobic hydration of the ionic liquid alkyl chain controls their solubility in aqueous solution. As a matter of fact, that tendency

occurs both for the mono-substituted and di-substituted ionic liquids. Nevertheless, the main goal of this work is to provide a better understanding of the structural and positional isomeric effects, and, to this end, two main pairs are compared: [C_4py][NTf_2] and [C_3-3-C_1py][NTf_2],[6] and [C_4-3-C_1py][NTf_2] and [C_4-4-C_1py][NTf_2]. From Figure 3.9, it is clear that at the water-rich phase slight deviations exist among isomers. The solubility of [C_4py][NTf_2] in water is lower than that of the structural analogue [C_3-3-C_1py][NTf_2]. On the other hand, the solubility of [C_4-3-C_1py][NTf_2] and [C_4-4-C_1py][NTf_2] are indeed similar, although the *para* substituted ionic liquid presents a higher affinity for water. However, it is quite interesting to observe that the features of both structural and positional isomers are rather different at the IL-rich phase. Curiously, a switch in positions is observed between [C_4py][NTf_2] and [C_3-3-C_1py][NTf_2] at the IL-rich phase. The solubility of water in [C_4py][NTf_2] is higher than the solubility of water in [C_3-3-C_1py][NTf_2]. Additionally, now a significant deviation is clearly observed in respect to the two positional isomers, [C_4-3-C_1py][NTf_2] and [C_4-4-C_1py][NTf_2]. The solubility of water in [C_4-4-C_1py][NTf_2] ranges between that observed for [C_4py][NTf_2] and [C_3-3-C_1py][NTf_2]. Although larger alkyl chains are present in [C_4-4-C_1py][NTf_2], the *para* substitution contributes for an enormous increment of the affinity of water to the ionic liquid. Besides the ionic liquid molecular structure, the possibility of the ionic liquid to hydrogen-bond with water is playing a dominant role. The alkyl simultaneously substitutions in the positions C1-C4 at the pyridinium cation lead to an enhanced distribution of charge, or to a high charge density at the ionic liquid cation, when compared to the C1-C3 substitutions, favouring thus hydrogen-bonding between the cations and water molecules. Moreover, the packing of water in ionic liquids is fairly more efficient in the ionic liquid with the *para* substitutions due to a less significant steric hindrance caused by the two alkyl groups.

The correlation constants obtained from the fitting of the experimental data using eqs 3.1 and 3.2, in both rich phases, are presented in Table 3.8. The proposed correlations show a maximum relative deviation from experimental data of 2.34% and 2.36%, for the IL-rich (x_w) and water-rich (x_{IL}) phases, respectively. The higher relative deviations have been observed for the systems composed of [C_6py][NTf_2] or [C_8py][NTf_2] and water.

Table 3.8. Parameters and respective standard deviations, and R-squared correlations from the fitting of the experimental data to eqs 3.1 and 3.2.

IL	*A*	-*B*/K	R^2	-*C*	*D*/K	*E*	R^2
$[C_4py][NTf_2]$	2.66 ± 0.07	1203 ± 20	0.9930	236 ± 64	9501 ± 2896	34 ± 10	0.9962
$[C_6py][NTf_2]$	2.33 ± 0.13	1132 ± 40	0.9969	254 ± 93	10215 ± 4189	37 ± 14	0.9930
$[C_8py][NTf_2]$	2.79 ± 0.15	1311 ± 44	0.9972	219 ± 102	8155 ± 4597	32 ± 15	0.9960
$[C_3\text{-}3\text{-}C_1py][NTf_2]$[6]	2.69 ± 0.14	1228 ± 45	0.9969	222 ± 77	8354 ± 3499	32 ± 12	0.9965
$[C_4\text{-}3\text{-}C_1py][NTf_2]$	2.44 ± 0.10	1184 ± 31	0.9983	196 ± 39	7807 ± 1774	28 ± 16	0.9978
$[C_4\text{-}4\text{-}C_1py][NTf_2]$	2.52 ± 0.08	1166 ± 25	0.9988	167 ± 60	6315 ± 2734	24 ± 9	0.9968

Aiming at exploring the molecular solvation mechanisms involved, the molar thermodynamic functions of solution are particularly valuable. Although such properties are extremely important for molecular-based interpretations, meticulous studies on the liquid-liquid equilibria as a function of temperature are scarce.[5–7,11,66,146,157,250,252] Moreover, only molar properties of the IL-saturated solution in water can effectively be explored since only in this case one is dealing with conditions near or at infinite dilution. This is essential to assure that no solute-solute interactions (electrostatic contribution) and/or ion-pairing exist. Standard molar thermodynamic functions of the ionic liquid solutions, such as the standard molar enthalpy ($\Delta_{sol}H^o$), molar Gibbs energy ($\Delta_{sol}G^o$), and molar entropy ($\Delta_{sol}S^o$) are given in Table 3.9 along with their respective standard deviations. Further details regarding their calculation can be found elsewhere.[5,6] Figure 3.10 plots solubility data as a function of $\Delta_{sol}G^o$ and shows the internal consistency of the results.

Table 3.9. Standard molar thermodynamic functions of solution of ILs in water at 298.15 K, and respective standard deviations. Units of energies in $kJ\cdot mol^{-1}$ and of entropy in $J\cdot K^{-1}\cdot mol^{-1}$.

IL	$\Delta_{sol}H^o$	$\Delta_{sol}G^o$	$-\Delta_{sol}S^o$
$[C_4py][NTf_2]$	6.5 ± 1.5	19.69 ± 0.03	44.2 ± 5.1
$[C_6py][NTf_2]$	6.9 ± 1.5	21.11 ± 0.01	47.7 ± 5.1
$[C_8py][NTf_2]$	10.9 ± 1.5	25.43 ± 0.02	48.8 ± 5.1
$[C_3\text{-}3\text{-}C_1py][NTf_2]$[6]	6.5 ± 1.5	19.56 ± 0.02	43.9 ± 5.1
$[C_4\text{-}3\text{-}C_1py][NTf_2]$	5.3 ± 1.5	20.99 ± 0.05	52.7 ± 5.2
$[C_4\text{-}4\text{-}C_1py][NTf_2]$	7.2 ± 1.5	20.86 ± 0.07	45.7 ± 5.3

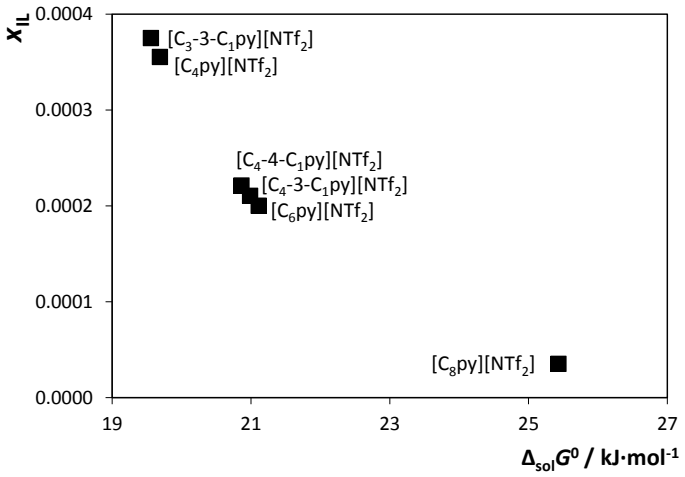

Figure 3.10. Mole fraction solubility of IL at the aqueous-rich phase, at 298.15 K, as a function of the respective standard molar Gibbs energy of solution.

The positive values for the enthalpies of solution indicate that the solubilisation of ionic liquids in water is indeed an endothermic process, thus leading to an UCST-type of phase diagram (phase splitting as temperature decreases).[253,254] It was previously shown that the enthalpies of solution of ionic liquids in water are not significantly dependent on the cation side alkyl chain length.[5] This feature was demonstrated with imidazolium-[5,6] and pyrrolidinium-based[66] ionic liquids, combined either with hexafluorophosphate[6] or bis(trifluoromethylsulfonyl)imide[5] anions. Enthalpies of solution are primarily defined by the ionic liquid anion.[6] Nevertheless, all previously studied ionic liquids[5–7,11,66,157] presented two or three alkyl chains substitutions at the cation, and for the di-substituted cations presented here, the same analogy is verified (after taking into account the associated standard deviations). Yet, for the mono-substituted ionic liquids studied, a significant increment on the enthalpy of solution is observed for $[C_8py][NTf_2]$. Nonetheless, such increment on the enthalpy of solution for $[C_8py][NTf_2]$ seems to result from a higher Gibbs energy of solution. The Gibbs energy of solution reflects the energy required for the formation of a cavity (in water – in this study) capable of accommodating the ionic liquid ions – the ions solvation by water molecules. The energy required for cavity creation will certainly increase with the cation alkyl chain, but it is here shown that the Gibbs energy of solution of $[C_8py][NTf_2]$ increases twice compared to the observed increment between $[C_4py][NTf_2]$ and $[C_6py][NTf_2]$. It was also previously shown[5,6] that the entropies of solution increase approximately -5 $J \cdot K^{-1} \cdot mol^{-1}$ *per* methylene addition at the

ionic liquid cation, a tendency that was shown to be independent both of the cation and anion nature. Although such increment on the entropy of solution is confirmed with the di-substituted ionic liquids with the alkyl chains at C1 and C3, [C_3-3-C_1py][NTf_2] and [C_4-3-C_1py][NTf_2], that trend is not observed for the mono-substituted cations. For the [$C_n$py][NTf_2] series, the increment *per* methylene addition (≈ -1 $J \cdot K^{-1} \cdot mol^{-1}$) is well below that observed for the remaining ionic liquids. Taking into account that the entropic contribution controls the ionic liquid solvation in water, such smaller increments induce the small differences verified in the ionic liquid mole fraction solubilities by the addition of consecutive -CH_2 groups. Indeed, as shown in Figure 3.9, the solubilities of ionic liquids in water are less dependent on the alkyl side chain length for the [$C_n$py][NTf_2] sequence. From these results a conclusion can be drawn: the increase on the alkyl side chain length in di-substituted cations affects much more the entropy of solution than the corresponding increase in mono-substituted cations. In addition, when changing the methyl group from the position C3 to C4, [C_4-4-C_1py][NTf_2], a slight decrease on the entropies of solution occurs when compared with the positional isomer [C_4-3-C_1py][NTf_2]. Again, such decrease on the entropies of solvation reflects a decrease on the ionic liquid solubility in water.

In summary, the enthalpies of solution for the ionic liquids dissolution in water do not significantly depend of the cation alkyl side chain length in di-substituted cations, while a slight dependence is verified for the mono-substituted cations. In addition, the decrease of the ionic liquids solubility in water is driven by the decrease on the entropies of solution. Moreover, structural and positional isomers undergo through a different liquid-liquid phase behaviour as a result of a delicate balance between energetic and entropic contributions.

The effect of the molar volume on the solubility of these ionic liquids in water, and water in the ionic liquids has been investigated. The molar volumes of all studied ionic liquids were determined based on density data taken from literature.[240] The dependence of the ionic liquid solubility in the water-rich phase, and that of the water solubility in the IL-rich phase, with the ionic liquids molar volumes is shown in Figure 3.11.

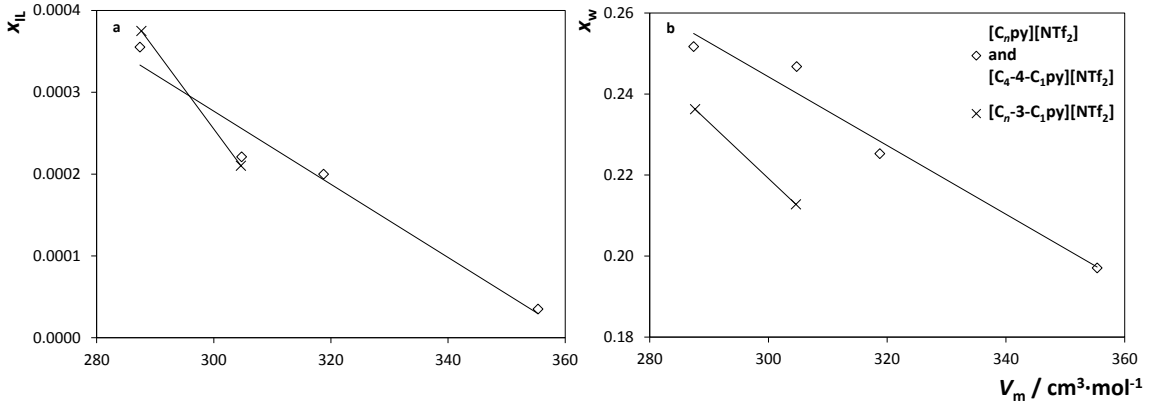

Figure 3.11. Mutual solubilities in the IL/water mixtures as a function of the IL molar volume. All data at 298.15 K and expressed as mole fraction of solute; (a) IL solubility, x_{IL}, in the water-rich phase; (b) water solubility, x_w, in the IL-rich phase.

In Figure 3.11a two main trends are present: one corresponding to the mono-substituted ionic liquids and the other corresponding to the di-substituted ionic liquids. These results indicate that the ionic liquids solvation in water (in structurally-analogue ionic liquids) certainly results, to a large extent, from entropic contributions ($-T\Delta_{sol}S^o > \Delta_{sol}H^o$). In addition, the two separate trends corroborate the distinction on entropic changes between mono-substituted and di-substituted ionic liquids (it is different to occupy the same volume at the end of an alkyl chain or at one of the positions of the pyridinium ring). These differences on the ionic liquids solvation mechanism with the number of alkyl substitutions present in the ionic liquid cation further depend on energetic contributions, which account for the different slopes of the two trends. It should be remarked that this simple approach describes quite well the experimental solubility results at the water-rich phase because it captures the key factor (entropy and its volume dependence) that rule the solvation mechanism between similar ionic liquids.

On the other hand, for the IL-rich phase (Figure 3.11b) two different trends are observed, one for the mono-substituted ionic liquids and the *para*-substituted cation and a different trend for the meta-substituted cations. Thus, the solubility of water in ionic liquids and its solvation mechanism, though still partially conditioned by entropic factors, are mainly ruled by enthalpic contributions. These will be highlighted by the results of the MD simulations discussed in the following section.

MOLECULAR DYNAMICS SIMULATION

The mutual solubility between an ionic liquid and water is largely determined by the nature of the anions that compose the ionic fluid. Thus, one can generally speak of halogen-based ionic liquids as more "hydrophilic" than hexafluorophophate-based ones, or bis(trfluoromethylsulfonyl)imide ($[NTf_2]^-$)-based ionic liquids as "hydrophobic". Simulation studies have confirmed this scenario by showing that, from a molecular point of view, most of the interactions in IL-water mixtures occur between the water molecules and the anions.[255]

By choosing a single anion ($[NTf_2]^-$), herein we force a situation in which the cation effect on the mutual solubility of the two components of the mixtures emerges in full, either directly *via* different cation-water interactions, or indirectly *via* different anion-water interactions due to changes in the polar network caused by dissimilar interactions between the common anion and the different cations. However, water-anion radial distribution functions in the ionic liquid-rich side of the several ionic liquid solutions under discussion (Figure 3.12) show that in this case the interactions between water and the anions are practically constant and independent of the nature of the cation. Thus, the relative solubilities of the different ionic liquids and water will be shaped mainly by the water-cation interactions, namely between the oxygen atom of water, OW, and the most positively charged parts of the cations – the hydrogen atoms of the aromatic ring.

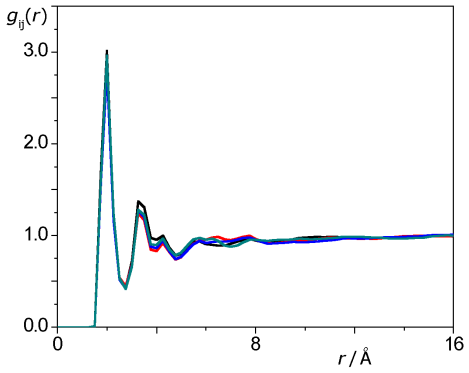

Figure 3.12. Anion-water radial distribution functions between the oxygen atom of water, OW, and those of $[NTf_2]^-$, OBT. All systems are composed of 40 water molecules diluted in 242 IL ion pairs (black line): $[C_4py][NTf_2]$ solution; (red): $[C_4\text{-}2\text{-}C_1py][NTf_2]$; (blue), $[C_4\text{-}3\text{-}C_1py][NTf_2]$; (cyan): $[C_4\text{-}4\text{-}C_1py][NTf_2]$.

Ab initio calculations of isolated $[C_4py]^+$ and $[C_4$-*n*-$C_1py]^+$ cations yielded point-charge distributions – from the application of the CHelpG algorithm to electron densities obtained at the MP2/cc-pVTZ(-f) level – showing that methyl substitution of the pyridinium ring at the C2 (*n* = 2, *ortho*), C3 (*n* = 3, *meta*) or C4 (*n* = 4, *para*) positions strongly affects the charge distribution in the ring, *cf.* Figure 3.13. Due to the typical resonance effects of a six-member aromatic ring, the C2 and C4 carbons of a non-substituted *N*-alkylpyridinium cation will receive most of the positive charge of the nitrogen atom (Figure 3.13a). When methyl substitution takes place at one of the C2, C3 or C4 positions the inductive effect of the methyl group causes the increase of the positive charge at that position and the reduction of the charges at the two positions adjacent to the substitution (Figure 3.13(b-d)). In terms of the interaction between the aromatic hydrogen atoms of the pyridinium ring and the oxygen atoms of water, the substitution effect can be summarized in the following rule-of-thumb: the more positive the charge of a given aromatic carbon, the more intense the interaction at that position between the cation and water.

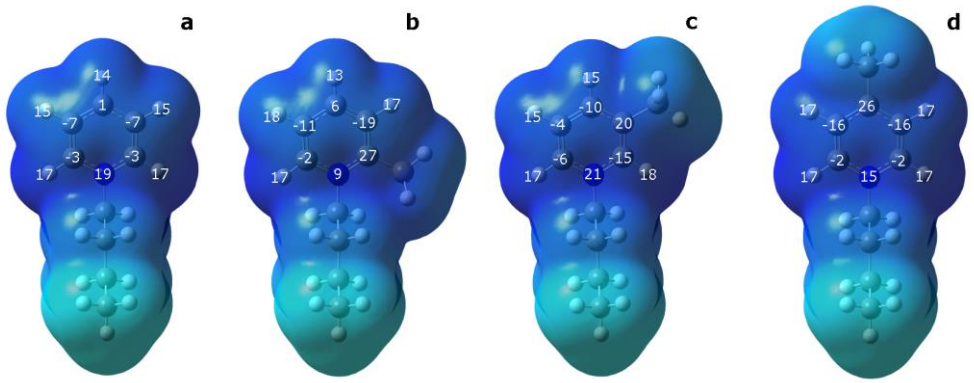

Figure 3.13. Electrostatic potential mapped onto an electron density isosurface (*ab initio* MP2/cc-pVTZ(-f)) and estimated atomic point charges (ChelpG method) on (a) N-butylpyridinium, (b) *N*-butyl-2-methylpyridinium, (c) *N*-butyl-3-methylpyridinium and (d) *N*-butyl-4-methylpyridinium cations. The values superimposed on selected atoms represent the corresponding atomic point-charge densities expressed in percentage of atomic charge units (a.c.u. %). The colour code represents all gradations from low positive charge densities (cyan) to high positive charge densities (dark blue). Some atomic point charges of the aromatic carbon atoms are negative**.**

It must be stressed at this point that in spite of having the most positive charge of the pyridinium ring, the carbon atom where the methyl substitution takes place loses its ability to interact with water due to the loss of its aromatic hydrogen atom. Additionally it

is expected that some stereochemical hindrance and charge induction effects should occur at the positions adjacent to the substitution. This state of affairs could in principle be studied using *ab initio* calculations between isolated cations and water molecules, however it is more practical to model the condensed phase using MD and perform the corresponding structural analysis by representation of the pair radial distribution functions (RDFs) of the atoms involved in the solvent-solute interactions.

Several RDFs, corresponding to the correlations between the oxygen atom of water (OW) and the aromatic carbon atoms at C3 and C4 of different pyridinium cations in IL-rich solutions, are presented in Figure 3.14a (OW-C3) and Figure 3.14b (OW-C4). When the methyl substitution occurs at C2, C3 or C4, all RDFs show, as expected, a shift to longer distances of the peak corresponding to the OW-C*N* (*N* = 2, 3 or 4) correlation at that position (depletion of oxygen, destruction of a possible hydrogen bond), and also a decrease in intensity of the peaks of the positions adjacent to the substituted carbon atom (no shift but decrease in intensity).

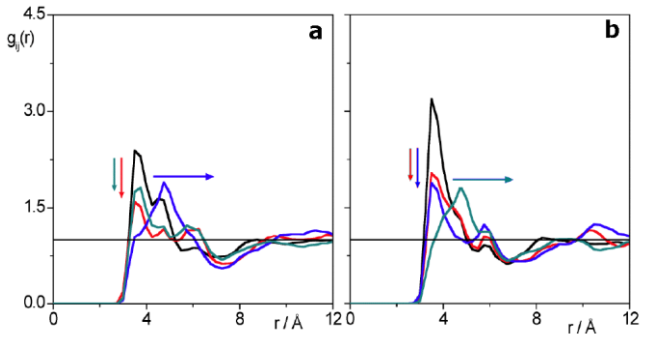

Figure 3.14. Site-site radial distribution functions of water diluted in [C_4py][NTf_2] (black), [C_4-2-C_1py][NTf_2] (blue), [C_4-3-C_1py][NTf_2] (red), and [C_4-4-C_1py][NTf_2] (cyan). Panel (a) C3-OW sites; (b) C4-OW sites. The arrows indicate either the elimination of the aromatic hydrogen - OW interaction at the substituted position (right shift) or the hindrance of that interaction at the adjacent positions (down shifts).

Figure 3.15 shows the combination of the two effects caused by the methylation of a given position of the pyridinium ring – charge changes and position blockage acting simultaneously. Each panel of the figure depicts RDFs corresponding to the correlations between the oxygen atom of water (OW) and the aromatic hydrogen atoms (H*N*) of unmethylated and methylated pyridinium cations contained in IL-rich solutions. Each set of RDFs is also accompanied by a schematic figure that shows the charge distribution and

position blockage in each type of pyridinium ring. Both representations – the schematic figures are based on charge distributions and induction effects calculated *ab initio*, the RDFs are calculated from the MD simulation data – not only convey self-consistent information but can also help explain the observed solubility trends in the IL-rich solutions.

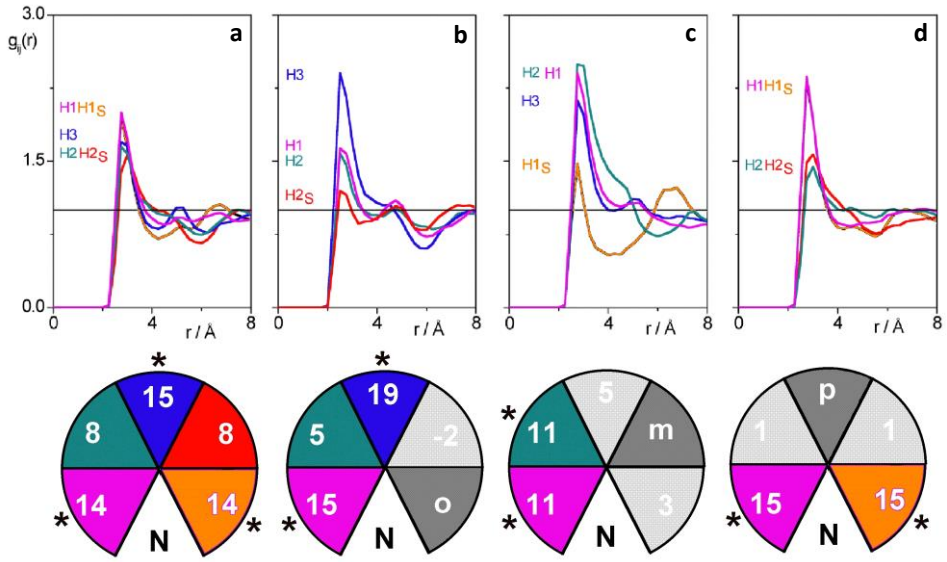

Figure 3.15. Top panels: Site-site radial distribution functions of water diluted in $[C_4py][NTf_2]$ (a), $[C_4\text{-}2\text{-}C_1py][NTf_2]$ (b), $[C_4\text{-}3\text{-}C_1py][NTf_2]$ (c), and $[C_4\text{-}4\text{-}C_1py][NTf_2]$ (d). H*N*-OW (*N* = 1, 1S, 2, 2S or 3) interactions are labelled and ordered directly in the graphs. Bottom panels: schematic representation of the pyridinium ring highlighting the positions (*) that perform stronger interactions with water. The numbers represent the atomic point charges (a.c.u. %) attributed to each sector of the ring; "o", "m" and "p" represent the methylated 2 (*ortho*), 3 (*meta*) and 4 (*para*) positions, respectively. Dark grey positions are not capable of interactions with OW due to methyl substitution; the corresponding adjacent positions (in light grey) are hindered.

The solubility of water in $[C_4py][NTf_2]$ is mainly due to the interactions between OW and the aromatic hydrogens at the *ortho* and *para* positions that are attached to the C2 and C4 carbon atoms, *cf.* Figure 3.15a. When methylation occurs at the *para* position, as in the case of the $[C_4\text{-}4\text{-}C_1py][NTf_2]$ ionic liquid, the solubility of water only decreases marginally because the two *ortho* hydrogens are not affected by the *para* substitution and, in fact, are able to compensate the loss of the hydrogen at the *para* position, *cf.* the charge changes at the *ortho* positions in Figure 3.15a and 3.15d. On the other hand, methylation in the *meta* position (leading to $[C_4\text{-}3\text{-}C_1py]$ $[NTf_2]$), hinders the interactions at the adjacent *para* and *ortho* positions, leaving just one available "strong" *ortho*

hydrogen to interact with water, *cf.* Figure 3.15c. The solubility of water in the ionic liquid is strongly decreased in this case.

Therefore, the solubility of water in $[C_n py][NTf_2]$, $[C_n\text{-}3\text{-}C_1py][NTf_2]$ and $[C_4\text{-}4\text{-}C_1py][NTf_2]$ ionic liquids can be understood at a molecular level taking into account different pieces of information gathered using *ab initio* or MD techniques providing an explanation for the observations reported in Figure 3.11b.

As mentioned before, the solubility of the ionic liquids in the water-rich media is controlled by entropic factors: water has to accommodate ions that have a rather large organic part, which implies the usual hydrophobic effect. The larger the organic part of a given ionic liquid ion, the larger such effect, which means that cations with longer alkyl side chains will have lower solubilities in water. It is also obvious that methyl substitution in the alkyl side chain is not the same as methyl substitution in the pyridinium ring: the former substitution increases the non-polar part of the cation, the latter does not; instead, it affects the way water molecules solvate the polar head of the cation. This explains the different trends found in Figure 3.11a. MD simulations performed in water-rich solutions have indeed demonstrated that the water molecules are able to solvate both the anion (mainly through hydrogen bonds between the oxygen atoms of the $[NTf_2]^-$ anion and the hydrogen atoms of water) and the pyridinium ring of the cation (*via* the interactions described in the previous paragraphs). The simulations have also shown that when the amount of ion pairs is larger than one (in simulations with 3000 water molecules), the ionic liquid ions tend to aggregate, confirming their strong tendency to form a second phase.

While the solubility of similar ionic liquids in water in entropically driven, as discussed above, the solvation process of water in the IL-rich solutions is of a completely different nature. In spite of their label of “hydrophobic” ionic liquids, $[NTf_2]^-$-based ionic liquids are in fact hygroscopic – they are able to incorporate in their midst quite a substantial amount of water molecules (especially if we tally them in terms of mole fraction). From the molecular and structural points of view the picture is quite simple: ionic liquids are nano-segregated fluids with a polar network permeated by non-polar domains. The

former regions have quite high-charge (positive and negative) densities and interact mainly through electrostatic forces. Water is "solvated" in these regions of the ionic liquid, and the amount of water tolerated depends mainly on the ability of the ionic fluid to incorporate it near its polar network without disrupting it. Ionic liquids with larger non-polar domains will exhibit polar networks that are already "overstretched" and are thus unable to solvate large amounts of water. That is the reason why, even when expressed in mole fraction, the solubility of water in $[C_n py][NTf_2]$ decreases as *n* increases. The ability of water to interact with the ions (or parts of them that are included in the polar network) is also important (in fact it is the ability to interact with the anion that matters most). It was concluded (Figure 3.11b) that the solubility of water in $[C_4\text{-}4\text{-}C_1py][NTf_2]$ is almost the same as that of $[C_4py][NTf_2]$. It does not matter that $[C_4\text{-}4\text{-}C_1py][NTf_2]$ is bulkier than $[C_4py][NTf_2]$: only the fact that water is able to interact in a similar way with the two cations is relevant. On the other hand, in ionic liquids of the type $[C_n\text{-}3\text{-}C_1py][NTf_2]$ the water-cation interactions are weaker and the resulting water solubility is smaller.

3.6. Solubility of non-aromatic hexafluorophosphate-based salts and ionic liquids in water determined by electrical conductivity

Catarina M. S. S. Neves, Ana R. Rodrigues, Kiki A. Kurnia, José M. S. S. Esperança, Mara G. Freire and João A. P. Coutinho, Fluid Phase Equilibria 358 (2013) 50-55, DOI: 10.1016/j.fluid.2013.07.061

3.6.1. Abstract

The knowledge of the salts solubility in water is of major interest for process design and optimization and for environmental monitoring. The water solubility of non-aromatic salts or ionic liquids requires the use of specific and expensive analytical equipment. In this work the use of electrical conductivity for the quantification of the solubility of sparingly soluble salts in water is proposed. Novel data for the water solubility of 1-methyl-1-propylpyrrolidinium hexafluorophosphate, 1-methyl-1-propylpiperidinium

hexafluorophosphate, tetrabutylammonium hexafluorophosphate, and tetrabutylphosphonium hexafluorophosphate, in the temperature range from (288.15 to 318.15) K, are reported. Using the gathered results, along with literature data, a correlation between the aqueous solubility of $[PF_6]$-based salts with their molar volume is proposed. The COSMO-RS predictive model was also used to estimate the solid-liquid equilibrium of the investigated systems. Since all the compounds are solid at room temperature, they were further characterized by differential scanning calorimetry, and the temperatures of solid-solid and solid-liquid phase transitions, as well as the respective enthalpies of phase transition, are presented.

3.6.2. Results and discussion

PHASE TRANSITIONS AND MELTING TEMPERATURES

The phase transitions of the $[PF_6]$-based salts, all solid at room temperature, were determined by DSC measurements. Besides the solid-liquid phase transitions, all these compounds also present solid-solid phase transitions. $[P_{4444}][PF_6]$ shows only one solid-solid phase transition, while the other three compounds present two solid-solid phase transitions in the temperature range evaluated. The phase transition temperatures and respective enthalpy changes are reported in Table 3.10. Since at least 2 independent runs were carried out for each salt, all the results are provided as an average with respective expanded uncertainty.

Table 3.10. Melting and solid phase transitions of the $[PF_6]$-based salts studied in this work obtained at 0.1 MPa.

Salt	1st Transition		2nd Transition		Melting Temperature	
	$T \pm 2u(T)^a$ / K	$\Delta H \pm 2u(\Delta H)^a$ / (kJ·mol^{-1})	$T \pm 2u(T)^a$ / K	$\Delta H \pm 2u(\Delta H)^a$ / (kJ·mol^{-1})	$T \pm 2u(T)^a$ / K	$\Delta H \pm 2u(\Delta H)^a$ / (kJ·mol^{-1})
$[N_{4444}][PF_6]$	303.95 ± 0.04	2.10 ± 0.08	360.70 ± 0.30	2.06 ± 1.16	524.3 ± 0.4	16.41 ± 0.26
$[P_{4444}][PF_6]$	265.37 ± 0.04	1.81 ± 0.04	-	-	498.6 ± 0.1	14.67 ± 0.04
$[C_3C_1pip][PF_6]$	310.60 ± 0.32	7.89 ± 0.18	350.96 ± 0.02	2.78 ± 0.02	368.2 ± 0.1	5.15 ± 0.04
$[C_3C_1pyr][PF_6]$	348.58 ± 0.64	2.76 ± 0.08	360.88 ± 0.84	2.30 ± 0.08	383.6 ± 0.7	3.66 ± 0.14

[a]Expanded uncertainty at the 0.95 confidence level, $2u(T)$ and $2u(\Delta H)$, evaluated from the standard deviation and applying a coverage factor $k = 2$.

The melting temperatures of the quaternary ammonium- and phosphonium-based salts are 524.33 K and 498.60 K, respectively. These salts are far from the definition of ionic liquids since their melting temperatures are well above 373 K. On the other hand, the melting temperatures of piperidinium- and pyrrolidinium-based salts are 368.23 K and 383.56 K, respectively. Thus, the piperidinium- and pyrrolidinium-based salts can be considered within the definition of ionic liquids, although the melting temperature of the pyrrolidinium-based salt that is slightly above 373 K.

VALIDATION OF THE SOLUBILITY MEASUREMENTS

In order to validate the equipment and methodology here proposed, the solubility of 1-butyl-3-methylimidazolium hexafluorophosphate, $[C_4C_1im][PF_6]$, in water was also measured by electrical conductivity and the respective results were compared with previous literature data determined by a different technique (UV-Vis spectroscopy).[6] The average relative deviation between the results obtained by electrical conductivity and UV-Vis spectroscopy at 2 different temperatures is 2.99%. Given the very low solubility of $[C_4C_1im][PF_6]$ in water (mole fraction in the range of 10^{-3}), the results here obtained are in acceptable agreement with those previously reported.[6] In fact, the deviations only occur at the third significant figure that is within the associated uncertainty of the UV-Vis quantification.[6] Moreover, higher deviations are currently observed amongst different authors.[6,256] Thus, the technique here proposed reveals to be an alternative and simple method to quantify the solubility of sparingly soluble salts in aqueous solutions.

It should be remarked that under more severe conditions of pH and temperature, the $[PF_6]^-$ anion is not stable and hydrolyses when in contact with aqueous media.[27] In this work this inherent degradation of the fluorinated anion was taken into consideration. At the temperatures and pH ranges here used we can guarantee that no degradation of the anion occurs.

SOLUBILITY OF HEXAFLUOROPHOSPHATE-BASED SALTS IN WATER

The solubility of the $[PF_6]$-based salts combined with the cations $[C_3C_1pip]^+$, $[C_3C_1pyr]^+$, $[N_{4444}]^+$ and $[P_{4444}]^+$ in water were determined in the temperature range from (288.15 to

318.15) K. In this temperature range all the salts are solid and the results correspond to solid-liquid equilibrium data. The experimental solubilities of each salt, expressed in mole fraction, are presented in Table S3.8, in Appendix, and depicted in Figure 3.16.

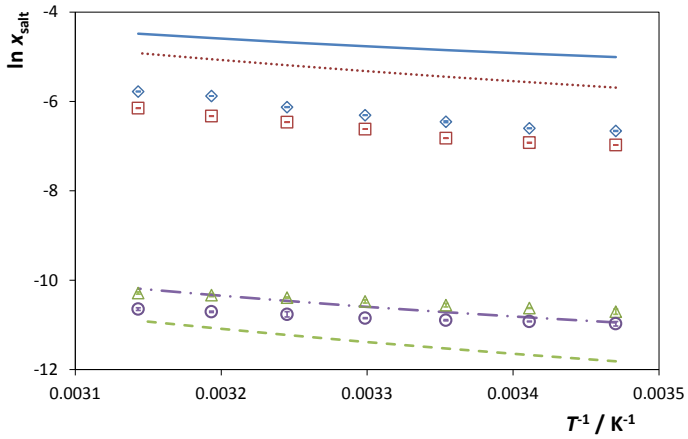

Figure 3.16. Mole fraction solubility of the [PF_6]-based salts in water as function of temperature: (◇, —) [C_3C_1pyr][PF_6], (□, ···) [C_3C_1pip][PF_6], (△, - - -) [N_{4444}][PF_6] and (○, — · —) [P_{4444}][PF_6]. The symbols and the lines represent, respectively, the experimental data and the COSMO-RS predicted results.

For all systems there is an increase in the salt solubility in water with an increase in temperature. Regarding the cation influence, the solubility of the hexafluorophosphate-based salts decrease in the following order: pyrrolidinium > piperidinium >>> ammonium > phosphonium. The two last [PF_6]-based salts show a very low solubility in water and in the order of 10^{-5} (mole fraction), while the salts comprising the piperidinium and pyrrolidinium cations present a solubility in water in the order of 10^{-4} (mole fraction).

Comparing with literature data concerning the solubility of other salts in water with the same anion,[11] and at a fixed temperature of 288.15 K, the solubility of the [PF_6]-based salts decreases in the rank: pyrrolidinium > imidazolium > piperidinium ≈ pyridinium >>> ammonium > phosphonium. On the other hand, at the temperature of 318.15 K this sequence changes and follows the order: imidazolium > pyrrolidinium > pyridinium > piperidinium >>> ammonium > phosphonium. This change behaviour is due to the fact that the [C_3C_1im][PF_6] or [C_3-3-C_1py][PF_6] and water correspond to liquid-liquid equilibrium systems while [C_3C_1pyr][PF_6] or [C_3C_1pip][PF_6] and water are solid-liquid systems, and that the solubilities of the former display a higher temperature dependency.

COSMO-RS

Aiming at predicting the solubility of the studied [PF_6]-based salts in water, the COSMO-RS model[168–172] was here evaluated. The solubility was predicted by taking into account the enthalpy of fusion and the additional enthalpies of phase transition of the respective salts. The predicted solubility values are given in Table S3.9 in Appendix. The predicted solubility values from COSMO-RS are closer to experimental data when the total enthalpy of fusion and enthalpies of phase transition is used, as depicted in Figure 3.16. Moreover, the pattern regarding the solubility dependence with temperature is also well described.

One advantage of COSMO-RS is that it provides the charge distribution of the specific polarity on the molecular surface that can be described by σ-profile histogram. Figure 3.17 presents the sigma profiles of the studied cations and the common anion.

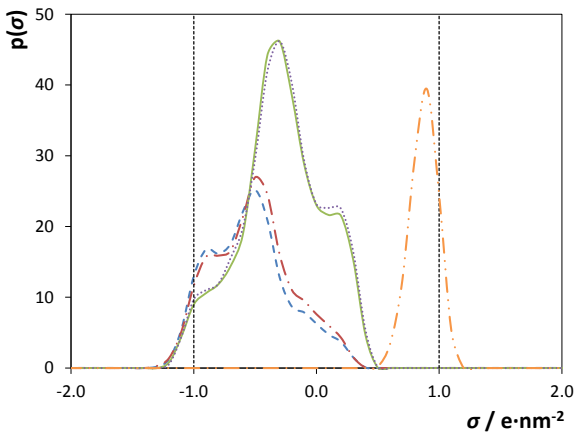

Figure 3.17. Sigma profiles of the cations and anion composing the studied salts: (---), $[C_3C_1pyr]^+$; (— · —), $[C_3C_1pip]^+$; (—), $[N_{4444}]^+$; (····), $[P_{4444}]^+$; and (— · · —), $[PF_6]^-$.

The sigma profiles of all the cations are similar in nature. Peaks are only observed between -1 e·nm^{-2} < σ < 1 e·nm^{-2} which corresponds to a nonpolar character. The higher peak intensity indicates a higher nonpolar character that translates the more hydrophobic nature of the studied salts. Accordingly, the cation core hydrophobic character observed experimentally and according to $[C_3C_1pyr]^+$ < $[C_3C_1pip]^+$ < $[P_{4444}]^+$ was also perceived with the COSMO-RS predictions. Only one exception was detected with $[N_{4444}]^+$, probably due to the very low solubility of the studied salt in water. Nevertheless, the prediction of the correct trend on the influence of salt cations and anions in the phase behaviour using the

COSMO-RS model is of main importance when the goal is a screening of salts solubility before experimental measurements. In spite of the quantitative deviations of the COSMO-RS predictions, this method shows to be a useful tool in predicting the solid-liquid phase behaviour of salts and water, allowing thus a beforehand choice of the cation and anion composing the salt for specific purposes.

CORRELATION FOR THE SOLUBILITY OF THE HEXAFLUOROPHOSPHATE-BASED SALTS IN WATER

Any dissolution process depends upon the free energy change of both the solute and solvent. According to the theory of hydrophobic solvation,[257,258] the aqueous solubility of organic compounds is related with the work required to create a cavity on the solvent to accommodate the solute. The solubility of hydrophobic solutes in water is thus often correlated with their molar volumes. In this context, we have further investigated the effect of the solutes molar volume on the solubility of the [PF_6]-based salts in water. The molar volumes of each salt at 298.15 K were estimated using the COSMO-RS model, and the aqueous solubility experimental data used were those obtained in this work together with other results taken from literature.[6,11] The dependency of the salt solubility in water with the salt molar volume (both properties at 298.15 K) is depicted in Figure 3.18.

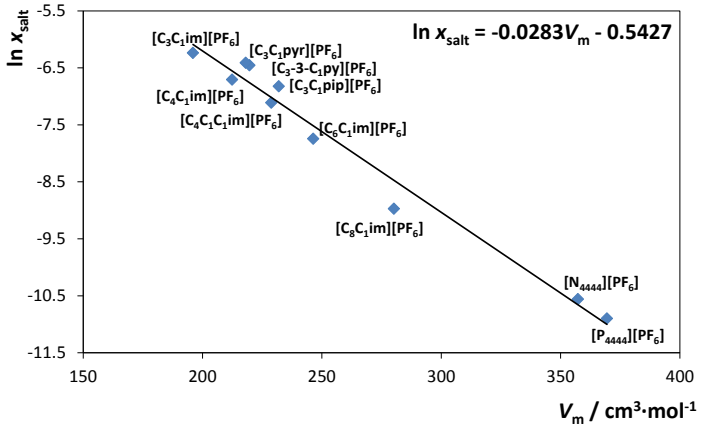

Figure 3.18. Solubility of [PF_6]-based salts in water (expressed as mole fraction of solute) as a function of the salt molar volume. All data are at 298.15 K.

In fact, a very good correlation is observed and covers a wide range of magnitudes regarding the solubility mole fraction data. This type of correlation was already shown

before;[7,10] yet, it is here shown that a large range of solubility of ionic liquids or ionic liquid analogues in water can be estimated only making use of their molar volumes.

3.7. Impact of the cation symmetry on the mutual solubilities between water and imidazolium-based ionic liquids

Mónia A. R. Martins, Catarina M. S. S. Neves, Kiki A. Kurnia, Andreia Luís, Luís M. N. B. F. Santos, Mara G. Freire, Simão P. Pinho and João A. P. Coutinho, Fluid Phase Equilibria 375 (2014) 161-167, DOI: 10.1016/j.fluid.2014.05.013

3.7.1. Abstract

Aiming at the evaluation of the impact of ionic liquids cation symmetry on their phase behaviour, in this work, novel mutual solubilities with water of the symmetric series of $[C_nC_n\text{im}][NTf_2]$ (with n = 1-5) were determined and compared with their isomeric forms of the asymmetric $[C_nC_1\text{im}][NTf_2]$ group. While the solubility of isomeric ionic liquids in water was found to be similar, the solubility of water in ionic liquids follows the same trend up to a maximum cation alkyl side chain length. For $n \geq 4$ in $[C_nC_n\text{im}][NTf_2]$ the solubility of water in the asymmetric ionic liquids is slightly higher than that observed in the symmetric counterparts. The thermodynamic properties of solution and solvation derived from the experimental solubility data of ionic liquids in water at infinite dilution, namely the free Gibbs energy, enthalpy and entropy were used to evaluate the cation symmetry effect on the ionic liquids solvation. It is shown that the solubility of ionic liquids in water is entropically driven and highly influenced by the cation size. Accordingly, it was found that the ionic liquids solubility in water of both the symmetric and asymmetric series depends on their molar volume. Based on these findings, a linear correlation between the logarithm of the solubility of ionic liquids in water and their molar volume is here proposed for the $[NTf_2]$-based ionic liquids at a fixed temperature.

3.7.2. Results and discussion

MUTUAL SOLUBILITIES MEASUREMENTS

The novel experimental solubility data for the series $[C_nC_nim][NTf_2]$ (with n = 1-5), along with the respective standard deviations, are presented in Tables S3.10 and S3.11, in Appendix. The solubility data for the asymmetric imidazolium-based ionic liquids, $[C_nC_1im][NTf_2]$ (with n = 2-8), were previously reported[5] and are here used for comparison purposes. The liquid-liquid phase diagrams of all the $[C_nC_nim][NTf_2]$ ionic liquids studied, along with the $[C_nC_1im][NTf_2]$ previously investigated,[5] are depicted in Figure 3.19.

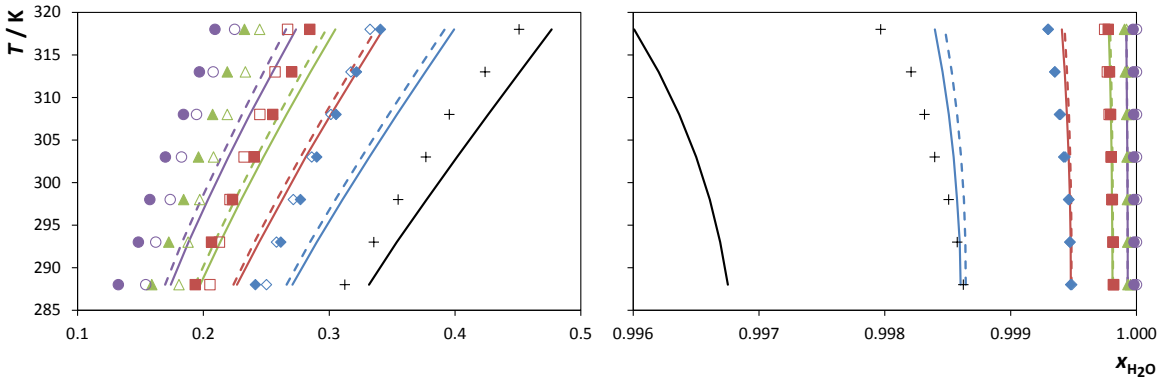

Figure 3.19. Liquid-liquid phase diagrams of water and ILs: (+), $[C_1C_1im][NTf_2]$; (◆), $[C_2C_2im][NTf_2]$; (◇), $[C_3C_1im][NTf_2]$;(■), $[C_3C_3im][NTf_2]$; (□), $[C_5C_1im][NTf_2]$; (▲), $[C_4C_4im][NTf_2]$; (△), $[C_7C_1im][NTf_2]$; (●), $[C_5C_5im][NTf_2]$; and (○), $[C_9C_1im][NTf_2]$. The matching colour full and dashed lines represent, respectively, the COSMO-RS predictions for the ILs containing asymmetric and symmetric cations.

The inspection of Figure 3.19 (and Table S3.10 in Appendix) indicates that the solubility of water in the ionic liquid is always above 0.1 in mole fraction, despite the "hydrophobic" label usually attributed to the $[NTf_2]$-based ionic liquids. On the other hand, the same figure (Figure 3.19 and Table S3.11 in Appendix) also indicates that the mole fraction solubility of ionic liquids in water is in the order of 10^{-3} to 10^{-5}, and therefore the dissolved ionic liquids can be considered at infinite dilution.

Concerning the phase diagrams, two features must be highlighted: *i*) the studied ionic liquids and water binary systems display a common UCST behaviour asymmetrically centred in the low-concentration region of the ionic liquids; *ii*) the mutual solubilities between ionic liquids and water, in both series, decrease with increasing the cation alkyl

side chain of ionic liquids. This is the expectable behaviour given the increasing hydrophobic nature of ionic liquids along with the aliphatic moiety. These features are also observed in the phase behaviour of water with other imidazolium-based ionic liquids combined with the $[BF_4]^-$ or $[PF_6]^-$ anions.[6,12,259]

In order to check the validity of the results obtained, a literature revision was made. Data for the mutual solubilities with water of $[C_1C_1im][NTf_2]$[260] and $[C_2C_2im][NTf_2]$[261] were found and are represented in Figure 3.20 together with the experimental values.

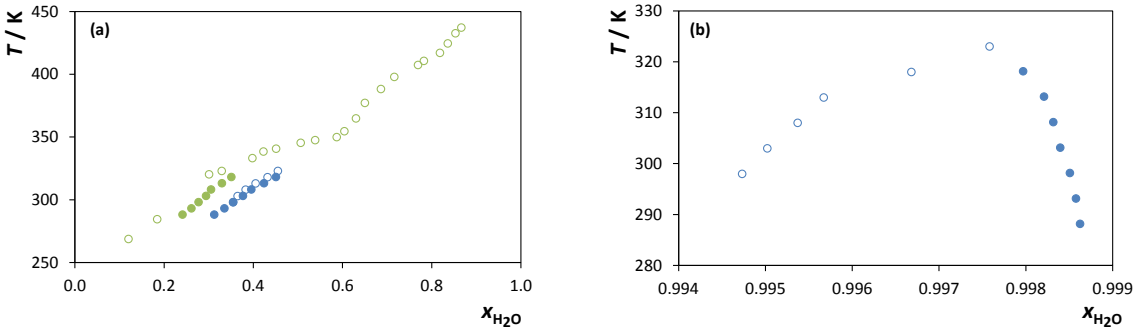

Figure 3.20. Comparison with literature data: (a) IL-rich phase; and (b) water-rich phase. Symbols: (●), $[C_1C_1im][NTf_2]$ this work; (○), $[C_1C_1im][NTf_2]$;[260] (●), $[C_2C_2im][NTf_2]$ this work; and (○), $[C_2C_2im][NTf_2]$.[261]

As can be seen, in the ionic liquid rich phase, Figure 3.20a, the discrepancy is not significant for both ionic liquids, and taking in account the different experimental conditions, it is possible to conclude that the values are in agreement. However, in the water rich-phase, Figure 3.20b, the values presented by Gardas and co-workers[260] are considerably distinct. These data don't present an upper critical solution temperature behaviour as it was expected and as was already proved in some works.[6,12,259] It is worth to say that Domańska and co-workers[261] also presented two points in the water-rich phase, but the temperatures used are much different from the ones used in the present work and, thus, they do not allow a reasonable comparison.

The main goal of this work is to provide a better understanding of the impact of the symmetry of the ionic liquid cation and, to this end, two series of ionic liquids are compared: symmetric and asymmetric ones with the same number of total methylene groups in the alkyl side chains. Figure 3.19 shows that the solubility of water in

$[C_2C_2im][NTf_2]$ and $[C_3C_3im][NTf_2]$ are similar to those of their structural analogues or isomers, $[C_3C_1im][NTf_2]$ and $[C_5C_1im][NTf_2]$, respectively. On the other hand, water presents a somewhat lower solubility in $[C_4C_4im][NTf_2]$ and $[C_5C_5im][NTf_2]$ than on $[C_7C_1im][NTf_2]$ and $[C_9C_1im][NTf_2]$.[9] Thus, for the long alkyl chain length isomers, the ionic liquids with an asymmetric cation are able to dissolve a higher content of water. A symmetry-asymmetry effect was also recently reported for other properties of the same ionic liquids series, such as density and viscosity,[241] volatility,[262] heat capacity,[263,264] surface tension,[265,266] and refractive index.[267]

The solubility of isomeric ionic liquids in water is essentially identical, as shown in Figure 3.19. The solubility of poorly soluble compounds in water, is known to be primarily controlled by their molar volume.[7] Since the molar volume for isomeric ionic liquids is identical, containing either symmetric or asymmetric cations, their solubilities in water are very close. The effect of the molar volume, V_m, on the solubility of ionic liquids in water has been discussed in our previous works.[10,13] The V_m of each ionic liquid at 298.15 K was determined based on experimental density data taken from literature,[241] and the aqueous solubility experimental data used were those obtained in this work along with other results taken from the literature.[5] The dependence of the ionic liquid solubility in the water-rich phase with the ionic liquid molar volume, at 298.15 K, is shown in Figure 3.21.

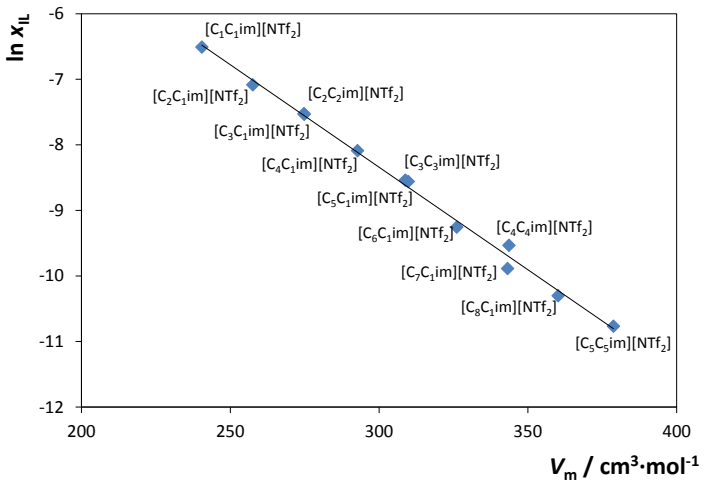

Figure 3.21. Solubility of $[NTf_2]$-based ILs in water (expressed in mole fraction) as function of the IL molar volume: $\ln(x_{IL}) = -0.0313\ V_m + 1.040$; $R^2 = 0.9946$. All data are at 298.15 K.

A very good correlation between the logarithm of the solubility, $\ln(x_{IL})$, and the molar volume, V_m, was obtained while covering a wide range of magnitudes regarding the solubility mole fraction data. Thus, it is here shown that a large range of solubilities of $[NTf_2]$-based ionic liquids in water can be estimated using their molar volumes and the equation provided in Figure 3.21 caption.

THERMODYNAMIC FUNCTIONS OF SOLUTION

To describe the temperature dependence of the experimental mutual solubilities aiming at determining the thermodynamic functions of solution, two correlations were employed. The solubility of water in the IL-rich phase is described by eq 3.1, while the solubility of ionic liquid in the water-rich phase is expressed using eq 3.2.[5,12]

Those parameters and their standard deviations are presented in Table 3.11. It must be stressed that in order to derive eq 3.1, it is assumed that in the temperature interval investigated the change in the standard molar enthalpy of solution of water in the ionic liquid phase is negligible. The proposed correlations present a maximum relative deviation in the experimental mole fraction data of 2% and 3%, for the water-rich and IL-rich phases, respectively.

Table 3.11. Estimated parameters (and respective starndard deviations) for the mole fraction of water in the IL-rich phase and IL in the water-rich phase estimated using eqs 3.1 and 3.2, respectively.

IL	*A*	*B* / K	*C*	*D* / K	*E*
$[C_1C_1im][NTf_2]$	2.65 ± 0.08	-1098 ± 23	-337 ± 83	13938 ± 3744	50 ± 12
$[C_2C_2im][NTf_2]$	2.11 ± 0.09	-1102 ± 28	-359 ± 73	15065 ± 3322	53 ± 11
$[C_3C_3im][NTf_2]$	2.52 ± 0.08	-1197 ± 24	-131 ± 28	4954 ± 1240	19 ± 4
$[C_4C_4im][NTf_2]$	2.12 ± 0.07	-947 ± 34	-462 ± 96	19516 ± 4309	68 ± 14
$[C_5C_5im][NTf_2]$	2.76 ± 0.15	-1372 ± 38	-217 ± 45	8495 ± 2022	31 ± 7

Aiming at exploring the molecular mechanisms behind the solvation phenomena, the molar thermodynamic properties of solution, namely the standard molar Gibbs energy ($\Delta_{sol}G_m^0$), and the enthalpy ($\Delta_{sol}H_m^0$) and entropy ($\Delta_{sol}S_m^0$) of solution were derived. These thermodynamic properties are associated with the changes that occur in the solute neighbourhood when one solute molecule is transferred from an ideal gas phase to a

diluted ideal solution. Because of the solubility of water in the IL-rich phase is large (*cf*. Table S3.10 in Appendix), the associated thermodynamic molar functions at 298.15 K were not determined. The solubility of ionic liquids in water is very small (*cf*. Table S3.11 in Appendix) and can be taken as at infinite dilution, and thus, the solution standard molar functions can be derived using eqs 3.3 to 3.5.[5,12]

At 298.15 K, the standard Gibbs energy of solution of the ionic liquids in water increases with the alkyl chain leading to a lower solubility in water with the increase of the respective aliphatic moieties. The enthalpies of solution derived from experimental data show that the dissolution of ionic liquids in water is an endothermic process, thus leading to an UCST-type of phase diagram. As previously shown, the enthalpies of solution of ionic liquids in water are very little dependent on the alkyl side chain length of the cation,[5] and this trend is also observed with the symmetric $[C_nC_n\text{im}][NTf_2]$ series of ionic liquids. These results confirm that the solubility of ionic liquids in water is entropically driven, as previously observed for $[C_nC_1\text{im}][NTf_2]$[5] and $[PF_6]$-based ionic liquids.[6] Figure 3.22 presents the experimental entropies of $[C_nC_n\text{im}][NTf_2]$, $[C_nC_1\text{im}][NTf_2]$,[5] and $[C_nC_1\text{im}][PF_6]$[6] as function of total methylene groups in the two alkyl side chains, *N*.

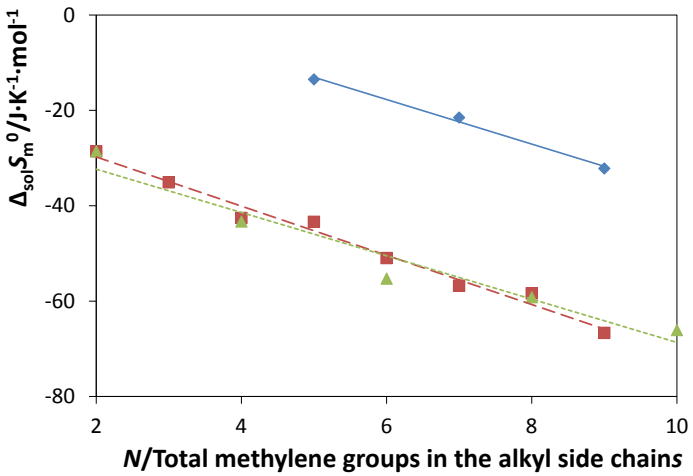

Figure 3.22. Standard molar entropy of solution, $\Delta_{sol}S_m^0$, as function of total methylene groups in the alkyl side chains, *N*, of ILs. Symbols: (◆, solid line), $[C_nC_1\text{im}][PF_6]$,[6] $\Delta_{sol}S_m^0 = -4.7 \cdot N + 10.3$, $R^2 = 0.9931$; (■, dashed line), $[C_nC_1\text{im}][NTf_2]$,[5] $\Delta_{sol}S_m^0 = -5.2 \cdot N + 19.4$, $R^2 = 0.9832$; and (▲, dotted line), $[C_nC_n\text{im}][NTf_2]$, $\Delta_{sol}S_m^0 = -4.5 \cdot N - 23.2$, $R^2 = 0.9459$. The symbols and line represents the $\Delta_{sol}S_m^0$ calculated using eq 3.5 and dependency of $\Delta_{sol}S_m^0$ as function of *N*, respectively. All data are at 298.15 K.

The entropies of solution of these three series of ionic liquids in water exhibit a small decrease in the entropy of solution of approximately -5 $J \cdot K^{-1} \cdot mol^{-1}$ *per* methylene addition to the cation. In addition, the entropies of solution of ionic liquids in water decrease with increasing cation alkyl side chain length, regardless of the anion. Thus, it can be concluded that the decrease of the ionic liquids solubility with the increase of the alkyl side chain length is driven by the linear decrease of the entropy of solution, related with the increase of the cavitation entropy very identical to that the observed in the solvation of linear alkanes and alcohols in water.[268,269]

The conventional standard molar properties of solvation (eqs 3.6 to 3.8) were determined through the reported vapour pressures and the standard molar enthalpy of vaporization of each ionic liquid studied at 298.15 K.[262,270] The reported vapour pressures were used to extrapolate them to 298.15 K using the Clarke and Glew equation. The conventional solvation thermodynamic functions at 298.15 K, and for the ionic liquids studied, are presented in Table 3.12.

Table 3.12. Standard molar properties of solvation of ILs in water at 298.15 K, and respective standard deviations.

	$\Delta_{svt}H^0_m$ / kJ·mol^{-1}	$\Delta_{svt}G^0_m$ / kJ·mol^{-1}	$\Delta_{svt}S^0_m$ / J·K^{-1}·mol^{-1}
$[C_1C_1im][NTf_2]$	-128.8 ± 1.8	-63.775 ± 0.017	-218.1 ± 4.5
$[C_2C_2im][NTf_2]$	-123.3 ± 1.8	-57.017 ± 0.024	-222.3 ± 4.5
$[C_3C_3im][NTf_2]$	-131.3 ± 1.8	-55.226 ± 0.026	-255.1 ± 4.5
$[C_4C_4im][NTf_2]$	-134.8 ± 1.8	-53.867 ± 0.003	-271.4 ± 4.5
$[C_5C_5im][NTf_2]$	-143.6 ± 1.8	-54.087 ± 0.024	-300.3 ± 4.5

The standard molar Gibbs energies of solvation increase with the alkyl chain length (decrease of the ionic liquid solubility in water). The results show, with exception of the outlier ionic liquid $[C_1C_1im][NTf_2]$, a regular decrease of the molar enthalpies and entropies of solvation as a function of the alkyl chain length, highlighting the role of the entropy in the solvation of ionic liquids in water.

COSMO-RS

Figure 3.19 presents the COSMO-RS predicted phase diagrams of the binary mixtures composed of ionic liquids and water. The results obtained with COSMO-RS show an acceptable qualitative agreement with the experimental data, and as previously observed.[5,6,11,13,157] At the water-rich side, the same hydrophobic character increase is observed both in the experimental data and in the predictions. Furthermore, the similar trends of mole fraction solubility of water in symmetric and asymmetric ionic liquids are also well predicted by COSMO-RS. Higher relative deviations were observed in the water-rich phase due to the very low solubility of the studied ionic liquids in water. In spite of the quantitative deviations obtained with COSMO-RS from experimental data, the model is able to correctly display the alkyl chain length and cation symmetry impact in these mutual solubilities. Thus, COSMO-RS proved to be a useful predictive method for the *a priori* screening of ionic liquids to find suitable candidates for a given task, before extensive experimental measurements.

It is worth mentioning that in this work also the latest COSMO file parameterization, BP_TZVP_C30_1301, was used and the results are given in Figure S3.14 in Appendix. Despite the new parameterization being able to correctly predict the trend of water mole fraction in the IL-rich phase, the phase diagram of ionic liquids in the water-rich phase deviates much more from the experimental results. Moreover, the predicted phase diagrams behaviour display a wrong trend with temperature.

3.8. Analysis of the isomerism effect on the mutual solubilities of bis(trifluoromethylsulfonyl)imide-based ionic liquids with water

Mónia A. R. Martins, Catarina M. S. S. Neves, Kiki A. Kurnia, Luís M. N. B. F. Santos, Mara G. Freire, Simão P. Pinho, and João A. P. Coutinho, Fluid Phase Equilibria 381 (2014) 28-35, DOI: 10.1016/j.fluid.2014.08.007

3.8.1. Abstract

The knowledge of the liquid-liquid equilibria between ionic liquids and water is of utmost importance for environmental monitoring, process design and optimization. Therefore, in this work, the mutual solubilities with water, for the ionic liquids combining the 1-methylimidazolium, $[C_1im]^+$; 1-ethylimidazolium, $[C_2im]^+$; 1-ethyl-3-propylimidazolium, $[C_2C_3im]^+$; and 1-butyl-2,3-dimethylimidazolium, $[C_4C_1C_1im]^+$ cations with the bis(trifluoromethylsulfonyl)imide anion, were determined and compared with the isomers of the symmetric 1,3-dialkylimidazolium bis(trifluoromethylsulfonyl)imide ($[C_nC_nim][NTf_2]$, with n = 1-3) and of the asymmetric 1-alkyl-3-methylimidazolium bis(trifluoromethylsulfonyl)imide ($[C_nC_1im][NTf_2]$, with n = 2-5) series of ionic liquids. The results obtained provide a broad picture of the impact of the ionic liquid cation structural isomerism, including the number of alkyl side chains at the cation, on the water-IL mutual solubilities. Despite the hydrophobic behaviour associated to the $[NTf_2]^-$ anion, the results show a significant solubility of water in the IL-rich phase, while the solubility of ionic liquids in the water-rich phase is much lower. The thermodynamic properties of solution indicate that the solubility of ionic liquids in water is entropically driven and highly influenced by the cation size. Using the results obtained here along with those in literature, a correlation between the solubility of $[NTf_2]$-based ionic liquids in water and their molar volume is proposed. The COSMO-RS was also used to estimate the LLE of the investigated systems and proved to be a useful predictive tool for the *a priori* screening of

ionic liquids aiming at finding suitable candidates before extensive experimental measurements.

3.8.2. Results and discussion

MUTUAL SOLUBILITIES MEASUREMENTS

The experimental data for the mutual solubility between water and the studied ionic liquids, along with the respective standard deviations, are given in Table S3.12 in Appendix, and depicted in Figure 3.23.

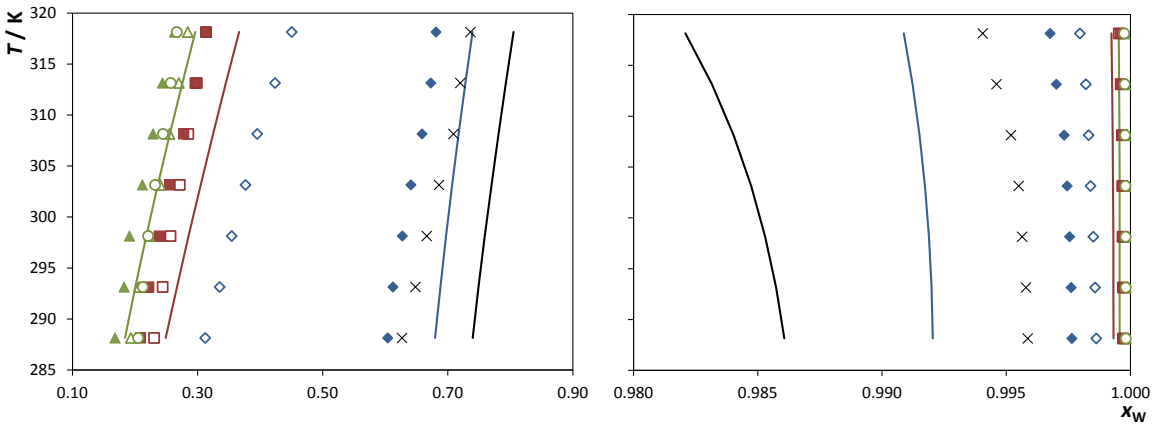

Figure 3.23. Liquid-liquid phase diagram for water and ILs: (✕), $[C_1im][NTf_2]$; (◆), $[C_2im][NTf_2]$; (◇), $[C_1C_1im][NTf_2]$;[15] (■), $[C_2C_3im][NTf_2]$; (□), $[C_4C_1im][NTf_2]$;[5] (▲), $[C_4C_1C_1im][NTf_2]$; (△), $[C_3C_3im][NTf_2]$;[15] and (○), $[C_5C_1im][NTf_2]$.[5] The lines at the same colours represent the COSMO-RS predictions for the compounds measured in this work.

The analysis of the figure reveals a significant mole fraction solubility of water in the IL-rich phase, and above 0.5 for the $[C_1im][NTf_2]$ and $[C_2im][NTf_2]$ ionic liquids. Thus, in spite of the hydrophobic character usually associated to the bis(trifluoromethylsulfonyl)imide anion, it is shown here that mono-substituted ionic liquids dissolve large amounts of water. The change on the nature and acidity of the imidazolium cation by and extra N-H acidic site leads to a saturation limit above 1:1 for the pair water-IL. The water solubility in $[C_2C_3im][NTf_2]$ and $[C_4C_1im][NTf_2]$ is of the same order observed previously in the $[C_nC_1im][NTf_2]$ and $[C_nC_nim][NTf_2]$ series.[5,15] On the opposite side of the phase diagram, the mole fraction solubility of ionic liquids in the water-rich phase is much lower, in the

order of 10^{-3} to 10^{-4}, which may be considered as an almost pure phase with the ionic liquid close to infinite dilution.

In general, and when comparing the data obtained for $[C_1im][NTf_2]$ and $[C_2im][NTf_2]$, the mutual solubilities with water decrease with the increase of the alkyl side chain length of the cation, due to a growth of the ionic liquid hydrophobic character. For all the studied ionic liquids, the mutual solubilities increase with temperature, displaying an upper critical solution temperature behaviour. This behaviour is expectable, and also observed with other imidazolium-based ionic liquids combined with the $[BF_4]^-$ or $[PF_6]^-$ anions.[6,12,259] Watanabe and Katsuta[271] reported the solubility of $[C_4C_1C_1im][NTf_2]$ in water at 298.15 K. The relative deviation to the experimental value measured in this work is only 5%.

Aiming at studying the impact of the structural variation of ionic liquids toward their mutual solubility with water, Figure 3.23 depicts the phase diagrams of the studied ionic liquids along with the corresponding isomers previously reported.[5,15] The ionic liquids studied in this work and the symmetric and asymmetric series with the same number of methylene groups in the alkyl side chains are compared, enabling therefore the investigation of the impact of structural isomers toward their mutual solubilities with water. As depicted in Figure 3.23, the mole fraction solubility of water in the ionic liquid $[C_2C_3im][NTf_2]$ is similar to that of $[C_4C_1im][NTf_2]$. Considering now the ionic liquid $[C_4C_1C_1im][NTf_2]$ with the respective structural isomers, $[C_3C_3im][NTf_2]$ and $[C_5C_1im][NTf_2]$, the trialkyl-substituted ionic liquid presents a lower solubility of water whereas the di-substituted ionic liquids present similar solubility values. The introduction of a third aliphatic moiety substituting the most acidic hydrogen clearly reduces the hydrogen-bonding ability between the imidazolium cation and water with an impact on the water solubility. However, smaller differences are observed for the pair $[C_3C_3im][NTf_2]$ and $[C_5C_1im][NTf_2]$ that contain the same number of aliphatic tails. Moreover, it is interesting to notice the significant differentiation of the solubility of water in $[C_2im][NTf_2]$ and in $[C_1C_1im][NTf_2]$, also structural isomers. The change in the chemical nature of the cation and the presence of a N-H group increases the water solubility in the ionic liquid to a

mole fraction higher than 0.5 (above 1:1, water:IL) that is an indication of a strong affinity and hydrogen-bonding between N-H and H_2O.

The mole fraction solubility of the different ionic liquids in water is presented in Figure 3.23. Also here, as noted in the IL-rich phase, the mole fraction solubility in water of the ionic liquid $[C_2C_3im][NTf_2]$ is similar to that of $[C_4C_1im][NTf_2]$. In the case of the trialkyl-substituted ionic liquid, $[C_4C_1C_1im][NTf_2]$, and their structural isomers, $[C_5C_1im][NTf_2]$ and $[C_3C_3im][NTf_2]$, its solubility in water is slightly larger than the respective isomers, contrary to what happens in the IL-rich phase. The solubility of the di-substituted isomers $[C_3C_3im][NTf_2]$ and $[C_5C_1im][NTf_2]$ is similar as they contain the same number of aliphatic tails. Finally, concerning the solubility in water of $[C_2im][NTf_2]$ and $[C_1C_1im][NTf_2]$, and similar to what observed is the IL-rich phase, a large significant difference can be observed. Once again the strong affinity and hydrogen-bonding between N-H and H_2O increases the ionic liquid solubility in water.

In order to more thoroughly understand the impact of the structural variations of ionic liquids on their mutual solubilities with water, the solubility variations are summarized in Figure 3.24. The ionic liquids investigated in this work, together with the symmetric ($[C_nC_nim][NTf_2]$, with n = 1-3) and asymmetric ($[C_nC_1im][NTf_2]$, with n = 2-5) series are analysed in order to evaluate the variations in the mutual solubilities when adding a methyl group.

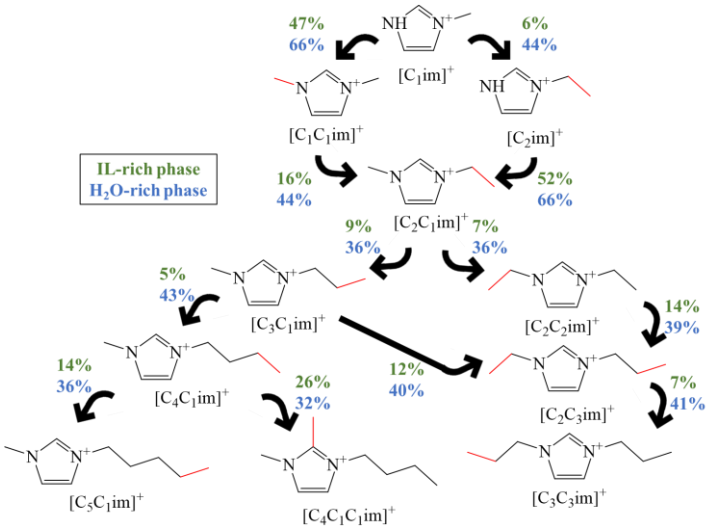

Figure 3.24. Schematic representation of the percent decrease in the mutual solubilities of ILs with water, when introducing a methyl group.

As observed in Figure 3.24, in both phases, whenever a methyl group is introduced, the solubility decreases. In the IL-rich phase, this reduction is within the range 5-16%, if the introduction of the methyl group takes place in the aliphatic chains, and 26-52%, if directly attached to the aromatic ring. Concerning the water-rich phase, the reduction is more pronounced but less distinct; 36-44% for an addition of a methyl to the aliphatic chains, and 32-66% if to the aromatic ring. When the methyl group is added to the aromatic ring, the highest percent decrease correspond to the pair $[C_2im][NTf_2]/[C_2C_1im][NTf_2]$ and the lowest to $[C_4C_1im][NTf_2]/[C_4C_1C_1im][NTf_2]$, *i.e.*, the introduction of a third aliphatic moiety has a less impact that the elimination of the N-H bond.

Concerning the IL-rich phase, when adding a methyl group to $[C_1im][NTf_2]$ in the aliphatic chain the variation is 6%, but, if this addition causes the elimination of the N-H bond, the variation is 47%. In the same way, the variation in the solubility to obtain $[C_2C_1im][NTf_2]$ from a mono-substituted ionic liquid ($[C_2im][NTf_2]$) is much larger than from a di-substituted ionic liquid ($[C_1C_1im][NTf_2]$). The addition of methyl groups to obtain the symmetric and asymmetric series causes a more or less constant variation in the solubility (5-14%), being $[C_4C_1im][NTf_2]/[C_5C_1im][NTf_2]$ the pair where the greatest variation occurs. Lastly the $[C_4C_1im][NTf_2]$, where the introduction of a third aliphatic moiety, to obtain

$[C_4C_1C_1im][NTf_2]$, reduce the hydrogen-bonding ability and, consequently, causes a significant decrease in the solubility.

On the other hand, in the water-rich phase although the changes are larger than in the IL-rich phase, these seem more similar the different isomers. For instance, when adding a methyl group to the mono-substituted ionic liquid, $[C_1im][NTf_2]$, the variations are 44% for the addition to the aliphatic chain, and 66% if the addition takes place directly in the aromatic ring. The addition of a methyl group to $[C_2im][NTf_2]$, to obtain $[C_2C_1im][NTf_2]$, cause a variation of 66% while the addition to $[C_1C_1im][NTf_2]$ causes a variation of only 44%. Again, the addition of methyl groups to obtain the symmetric and asymmetric series, causes approximately constant variations in the solubility (36-43%). Concerning the trialkyl-substituted ionic liquid, $[C_4C_1C_1im][NTf_2]$, the addition of a methyl group to $[C_4C_1im][NTf_2]$ causes merely a reduction of 32% in the ionic liquid solubility. Moreover, it is interesting to note that the variation on the solubility between the pairs $[C_3C_1im][NTf_2]$/$[C_2C_3im][NTf_2]$ and $[C_2C_2im][NTf_2]$/$[C_2C_3im][NTf_2]$ is almost the same in each phase, and four times higher in the water-rich phase.

THERMODYNAMIC FUNCTIONS OF SOLUTION

Aiming at determining the thermodynamic functions of solution, the temperature dependence of the mole fraction solubility was correlated using eqs 3.1 and 3.2.[5,10] For the solubility of water in the IL-rich phase, it can be assumed that the process occurs at constant molar enthalpy of solution, and thus, eq 3.1 can be used. On the other hand, for the solubility of the ionic liquids in water, there is a significant dependence on temperature for the enthalpy of solution, and therefore, eq 3.2 is used.

The fitted parameters as well as their standard deviations are listed in Table S3.13 in Appendix. The maximum relative deviation to the experimental data is 2%, for both the water-rich and the ionic liquid-rich phases.

Solubility is a quantitative measure of the equilibrium composition of a saturated solution. When this equilibrium is established between two liquids, the standard molar thermodynamics functions, such as the Gibbs energy ($\Delta_{sol}G_m^0$), enthalpy ($\Delta_{sol}H_m^0$) and

entropy of solution ($\Delta_{sol}S^0_m$) can be derived from the temperature dependence of the experimental solubility data.[6] These properties were calculated using eqs 3.3-3.5[5,10,219] for the water-rich phase, where the solute could be considered at infinite dilution. In the IL-rich phase, the solubility of water is higher and the associated thermodynamic molar functions cannot be determined. The molar thermodynamic functions for the ionic liquid solution in water were estimated at 298.15 K and are reported in Table 3.13.

Table 3.13. Standard molar properties of solution of ILs in water at 298.15 K, and respective standard deviations.

IL	$\Delta_{sol}H^0_m$ /kJ·mol^{-1}	$\Delta_{sol}G^0_m$ /kJ·mol^{-1}	$\Delta_{sol}S^0_m$ /J·K^{-1}·mol^{-1}
[C_1im][NTf_2]	6.0 ± 1.5	13.475 ± 0.006	-25.0 ± 5.1
[C_2im][NTf_2]	5.2 ± 1.5	14.901 ± 0.008	-32.7 ± 5.1
[C_2C_3im][NTf_2]	5.0 ± 1.5	19.910 ± 0.010	-50.1 ± 5.1
[$C_4C_1C_1$im][NTf_2]	5.1 ± 1.5	21.000 ± 0.017	-53.1 ± 5.1

At 298.15 K, the $\Delta_{sol}H^0_m$ of the studied ionic liquids in water, remains approximately constant with the increase of the aliphatic moiety, because when the ionic liquid is in aqueous solution, the interactions occur mainly with the charged head and are much less dependent on the alkyl chain. The experimental enthalpies of solution also show that the solubilisation of ionic liquids in water is an endothermic process, leading to an upper critical solution temperature behaviour type phase diagram. On the other hand, the standard Gibbs energy of solution increases with the alkyl chain length leading to a lower solubility of the heavier ionic liquids in water. The molar entropies of solution are shown to be negative and dependent on the cation structure, decreasing with increasing the alkyl chain length (approximately -5 J·K^{-1}·mol^{-1} *per* methylene addition to the cation and as shown previously[5–7,10]). Therefore, the solubility of the ionic liquids in water is driven by the entropy of solution; the higher (less negative) entropic change leads to a higher solubility of ionic liquids in water.

The significant increase of solubility of the [C_1im][NTf_2] and [C_2im][NTf_2] in water is also entropically driven, and is a result of the quite significant increase of the entropy of solution of ≈ +25 kJ·K^{-1}·mol^{-l} when compared with their isomers[10,15] and other members of the [NTf_2]-series of ionic liquids, as well as combined with other anions. The significant

increase in the entropy of solution is also related with the expected cation to water interaction via the N-H group that leads to a better solvation interaction with water and to a decrease of the cavitation entropy penalty (more hydrophilic).

COSMO-RS

The predicted phase diagrams of the binary mixtures composed of water and the studied ionic liquids using COSMO-RS are presented in Figure 3.23. The same increase on the hydrophobic character is observed for the experimental data and COSMO predictions. COSMO-RS is thus able to qualitatively predict the trend on the ionic liquids affinity for water. The only exception found was for the prediction of the solubility change with the temperature for the ionic liquid containing the cation $[C_4C_1C_1im]^+$ in water. In opposition to the experimental information, COSMO-RS predicts a solubility decrease with rising temperature. This irregularity can be related to the fact that simple empirical interaction potentials are used in COSMO-RS to describe the weaker interactions of the ionic liquids with water, which is expected to poorly describe their effective complexity.

Figure 3.25 plots the calculated *versus* experimental solubility for several $[NTf_2]$-based ionic liquids, at both rich phases, and at 298.15 K. From the close correlations depicted in Figure 3.25 it can be concluded that COSMO-RS can predict the mutual solubilities between the studied ionic liquids and water.

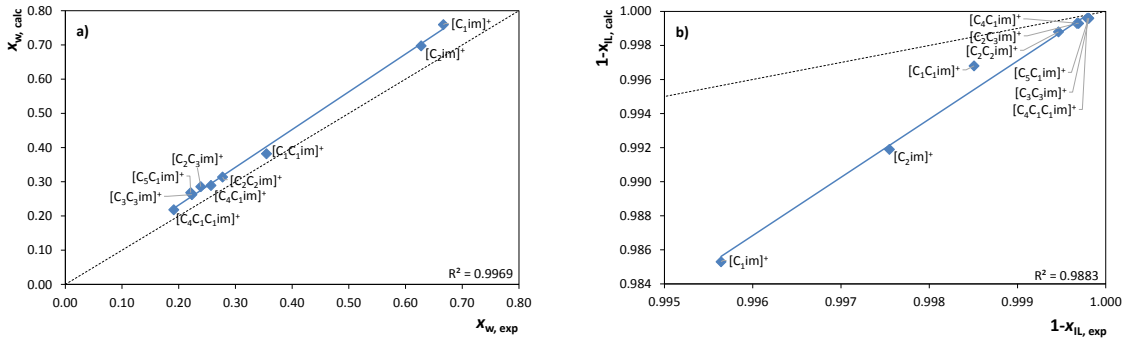

Figure 3.25. Calculated *versus* experimental solubility of bis(trifluoromethylsulfonyl)imide-based ILs at 298.15 K in (a) IL-rich phase and (b) water-rich phase. The solid and dotted lines represent the points correlation and the y = x function, respectively.

It should be pointed out here that the latest COSMO file parameterization, BP_TZVP_C30_1401, was also used to predict the LLE of the binary systems investigated in this work, *cf*. Figure S3.15 in Appendix, presenting a global relative deviations of 35.3% and 2.8% for the solubility of water in ionic liquids and ionic liquids in water, respectively. However, this COSMO-RS parameterization is also unable to correctly describe the solubility change with the temperature for the ionic liquids $[C_4C_1C_1im][NTf_2]$ and $[C_2C_3im][NTf_2]$ in water. With the file parameterization, BP_TZVP_C21_0110 the global relative deviations obtained were 16.8% and 1.2%. Since the latest version of COSMO-RS predicts the phase diagrams with a larger deviation from the experimental results and wrong trends, the oldest version is preferred and was used here. Despite some regular deviations, COSMO-RS shows to be a useful tool in the prediction of the binary systems behaviour, and able to correctly display the alkyl chain length and ionic liquid cation isomeric effect.[5,6,11,13]

CORRELATION FOR THE SOLUBILITY OF BIS(TRIFLUOROMETHYLSULFONYL)IMIDE-BASED IONIC LIQUIDS IN WATER

The solubility of hydrophobic solutes in water, near infinite dilution, is controlled and strongly correlated to their molar volume.[6,7,13] For isomeric ionic liquids, the molar volume is identical and, consequently, the solubilities are essentially the same. In this context, in a previous work[15] the relevance of the solutes molar volume on the solubility of the $[NTf_2]$-based ionic liquids in water, at 298.15 K, and a correlation was proposed. Here, new points were plotted together with the correlation obtained,[15] in order to verify if it can be also used for more diverse systems, as shown in Figure 3.26. The molar volumes were calculated based on density data taken from literature[240–242] and the aqueous solubility data used were those obtained in this work along with data previously published.[5,7,10,15] Data relative to other cations (pyridinium-, pyrrolidinium- and piperidinium-based)[7,10,240,242] combined with the same anion where also included in order to verify the robustness of the correlation proposed.

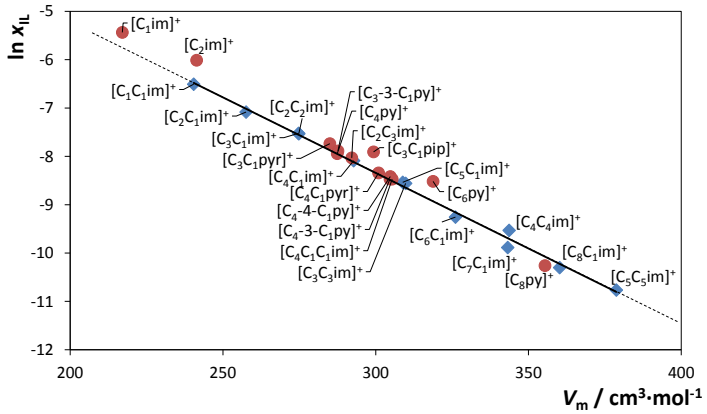

Figure 3.26. Solubility of bis(trifluoromethylsulfonyl)imide-based ILs in water as a function of the IL molar volume: $\ln(x_{IL}) = -0.0313\ V_m + 1.040$; $R^2 = 0.9946$, at 298.15 K. (◆), data used in the correlation; and (●), new data.

Despite the different cations families, the correlation[15] is able to correctly describe the solubility of [NTf_2]-based ionic liquids in water. However, it is observed that cations with different cores, *i.e.*, with a more different chemical nature (like pyridinium-, pyrrolidinium- and piperidinium-based) and the mono-substituted imidazolium ionic liquid deviate more from the proposed correlation that was constructed with di-substituted imidazolium-based fluids only. On Figure 3.26 the isomerism effect can also be analysed and, as can be seen, ionic liquids with the same molar volume present similar solubility in water. Exceptions are only the pair [C_2im][NTf_2]/[C_1C_1im][NTf_2], which is understood due to the elimination of a N-H bond in the imidazolium ring like explored before, and for ionic liquids with a different core than imidazolium, namely [C_3C_1pip][NTf_2] and [C_6py][NTf_2].

3.9. The impact of ionic liquids fluorinated moieties on their thermophysical properties and aqueous phase behaviour

Catarina M. S. S. Neves, Kiki Adi Kurnia, Karina Shimizu, Isabel M. Marrucho, Luís Paulo N. Rebelo, João A. P. Coutinho, Mara G. Freire, José N. Canongia Lopes, Physical Chemistry Chemical Physics 16 (2014) 21340-2134, DOI: 10.1039/C4CP02008A

3.9.1. Abstract

In this work is demonstrated that the presence of fluorinated alkyl chains in ionic liquids is highly relevant in terms of their thermophysical properties and aqueous phase behaviour. The density and viscosity of pure 1-ethyl-3-methylimidazolium tris(pentafluoroethyl)trifluorophosphate, $[C_2C_1im][FAP]$, with that of pure 1-ethyl-3-methylimidazolium hexafluorophosphate, $[C_2C_1im][PF_6]$, at atmospheric pressure and in the (288.15 to 363.15) K temperature range, have been measured and compared. The results show that the density of $[C_2C_1im][PF_6]$ is lower than that of $[C_2C_1im][FAP]$, while the viscosity data reveal the opposite trend. The fluid phase behaviour of aqueous solutions of the two ionic liquids was also evaluated under the same conditions and it was found that the mutual solubilities of $[C_2C_1im][FAP]$ and water are substantially lower than those verified with $[C_2C_1im][PF_6]$. The experimental data were lastly interpreted at a molecular level using Molecular Dynamics (MD) simulation results revealing that the interactions between the ionic liquid ions and the water molecules are mainly achieved *via* the six fluorine atoms of $[PF_6]^-$ and the three analogues in $[FAP]^-$. The loss of three interaction centres when replacing $[PF_6]^-$ by $[FAP]^-$, coupled with the bulkiness and relative inertness of the three perfluoroethyl groups, reduces its mutual solubility with water and also contributes to a lower viscosity displayed by the pure [FAP]-based ionic liquid as related to that of the $[PF_6]$-based compound.

3.9.2. Results and discussion

The main point of the present work is the comparison of the distinct behaviour of two ionic liquids that are somewhat related (same cation and substitution in the anion of three fluorine atoms by three fluorinated ethyl groups), namely $[C_2C_1im][PF_6]$ and $[C_2C_1im][FAP]$, aiming a deeper understanding of the effect of substituting fluorine atoms by fluorinate alkyl chains through the ILs thermophysical properties and aqueous phase behaviour. Figure 3.27 depicts the structures of the ions that compose the investigated ILs. The *cis* and *trans* positions of the C_2F_5- groups and the fluorine atoms in the structure of the $[FAP]^-$ anion of the ionic liquid studied in this work were determined by us by ^{19}F NMR (*cf.* Figure S3.16 in Appendix).

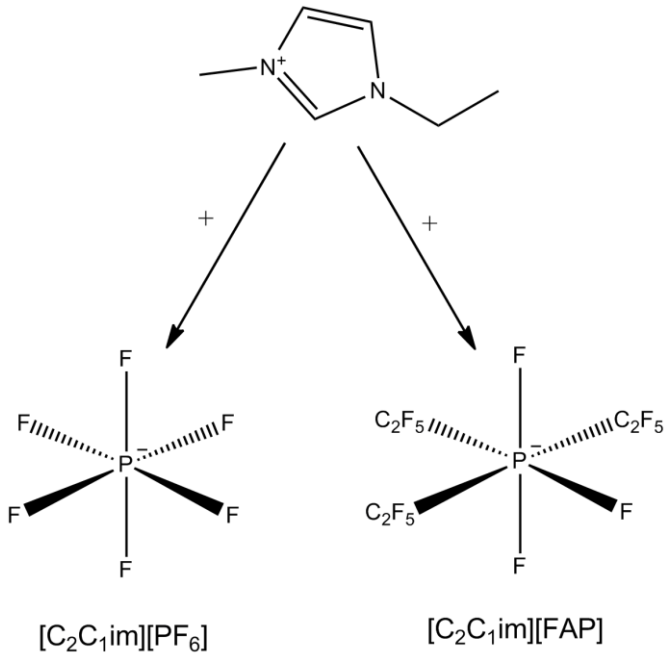

Figure 3.27. Structures of the ions that compose the ILs studied in this work.

MELTING TEMPERATURE

The melting temperature of the dried $[C_2C_1im][PF_6]$, solid at room temperature, was determined by DSC. Only one phase transition was observed in the temperature range evaluated. The melting temperature obtained was 333.83 K that is in good agreement with literature.[215] For the same sample, the enthalpy change at the corresponding melting temperature, from the crystal to the isotropic liquid phase transition, is 17.1 $kJ \cdot mol^{-1}$. The

melting temperature reported for $[C_2C_1im][FAP]$ is 236.15 K,[272] thus significantly lower than that observed for $[C_2C_1im][PF_6]$. This is a result of the larger [FAP] anion which contributes for a reduction of the structural (crystalline) organization of the ions, therefore leading to lower melting temperatures.

DENSITY

The experimental density data for pure and dried ionic liquids are presented in Table S3.14 in Appendix. For $[C_2C_1im][FAP]$ the temperature interval attempted ranges between (278.15 and 363.15) K. Due to the higher melting temperature of $[C_2C_1im][PF_6]$, densities and viscosities were only determined at temperatures above 338.15 K. This work presents, for the first time, experimental density data for $[C_2C_1im][PF_6]$. Figure S3.17 in Appendix depicts the relative deviations between the experimental density data obtained here and literature for $[C_2C_1im][FAP]$.[273–276] The maximum relative deviation between our data and those previously published[273–276] is below 1%.

The experimental density data for the studied ionic liquids are shown in Figure 3.28. The density of the hexafluorophosphate-based ionic liquid is substantially lower than that displayed by $[C_2C_1im][FAP]$ in the temperature range investigated. As far as the volumetric properties are concerned, at 343.15 K, the differences can be mostly ascribed to a higher percentage of heavier atoms in the latter ionic liquid. Conversely, the large difference in the corresponding molar volumes (at 343.15 K, 178.6 $cm^3 \cdot mol^{-1}$ for $[C_2C_1im][PF_6]$ and 338.6 $cm^3 \cdot mol^{-1}$ for $[C_2C_1im][FAP]$) can be attributed to the much higher molar mass of $[C_2C_1im][FAP]$ relative to that of $[C_2C_1im][PF_6]$.

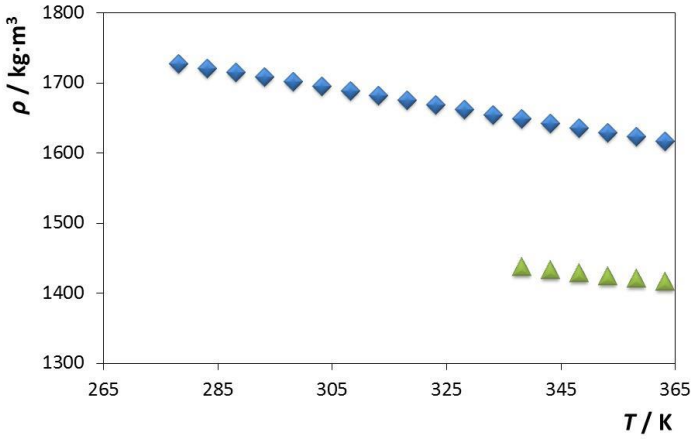

Figure 3.28. Experimental density as a function of temperature and at 0.1 MPa for the ILs: $[C_2C_1im][FAP]$ (◆); $[C_2C_1im][PF_6]$ (▲).

The isobaric thermal expansion coefficient (α_p), which considers the volumetric changes with temperature, was calculated from the fitting of the experimental data using eq 3.10. The thermal expansion coefficients are very close and vary between (5.94 and 7.84) × 10^{-4} K^{-1} for both ionic liquids. $[C_2C_1im][FAP]$ presents a lower thermal expansion coefficient than $[C_2C_1im][PF_6]$. These values are considerably lower than those observed with molecular organic solvents and higher than those of classical molten salts.[277]

VISCOSITY

As for the density measurements, the viscosity data were determined in the temperature range from (278.15 to 363.15) K for the $[C_2C_1im][FAP]$ and from (338.13 to 363.15) K for the $[C_2C_1im][PF_6]$. The experimental results are presented in Table S3.14 in Appendix and in Figure 3.29.

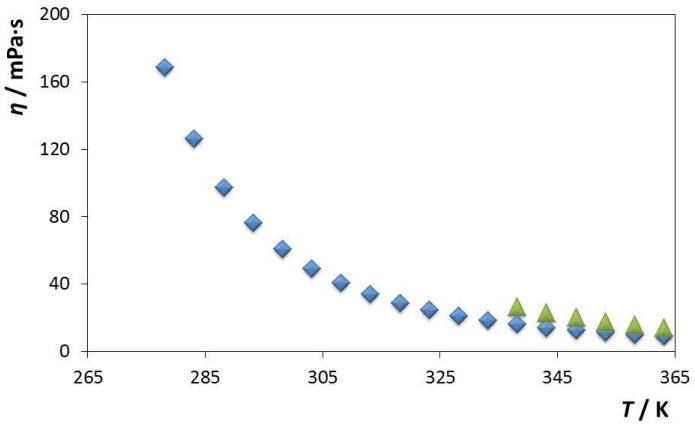

Figure 3.29. Experimental viscosity as a function of temperature and at 0.1 MPa for the ILs: $[C_2C_1im][FAP]$ (◆); $[C_2C_1im][PF_6]$ (▲).

Figure S3.18 in Appendix depicts the relative deviations between this work and literature data for $[C_2C_1im][FAP]$.[273,275] The maximum relative deviation found was 4.3%. Taking into consideration that the viscosity of ionic liquids is highly sensitive to the water content and to the purity level of the sample, it can be stated that our data are in close agreement with literature.[273,275]

Since viscosity is mainly dependent on intermolecular interactions (H-bonding, dispersive and Coulombic interactions), an increase in temperature will substantially decrease the intensity of H-bonding interactions and, therefore, the viscosity decreases with the temperature increase. In general, and at all the temperatures studied, $[C_2C_1im][PF_6]$ is more viscous than $[C_2C_1im][FAP]$, and follows the opposite behaviour to that observed in density results. The charge density in the two ionic liquids and its distribution is quite distinct,[226,236] with an important impact on their viscosity. Moreover, the substitution of 3 F atoms by three perfluoroethyl groups in [FAP]-based ionic liquids leads to a lower viscosity also resulting from weaker cation-anion interactions.

MUTUAL SOLUBILITIES MEASUREMENTS

The measured solubility data and the respective standard deviations are presented in Table S3.15 in Appendix. The representation of the respective phase diagrams is depicted in Figure 3.30.

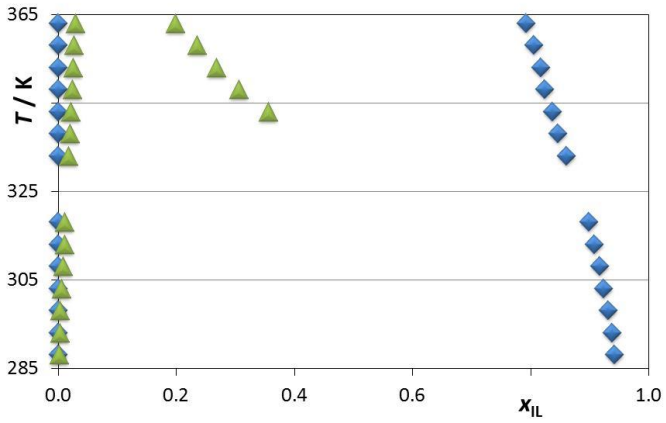

Figure 3.30. Liquid-liquid phase diagram for the binary system composed of water and ILs: $[C_2C_1im][FAP]$ (◆); $[C_2C_1im][PF_6]$ (▲).

The comparison of the results here obtained with those already reported in literature[215,278] is depicted in Figure S3.19 in Appendix. For the aqueous system with $[C_2C_1im][FAP]$, the values obtained in this work are in close agreement with those reported by Domańska et al..[278] Nevertheless, the major differences between authors are observed in the IL-rich phase, and at higher temperatures. In this work, the water content in the IL-rich phase was measured by Karl-Fischer (KF) titration, whereas the values reported in literature were obtained by a dynamic (synthetic) method.[278] On the other hand, the liquid-liquid equilibrium results for $[C_2C_1im][PF_6]$ obtained in this work and those reported in literature[215] display significant differences. This should be mainly related with the purity of the ionic liquid used as well as with the different experimental techniques employed. The solubility values of the ionic liquid in water reported in literature were obtained by KF titration.[215] However, it should be stressed that this method is not the most accurate to determine such large amounts of water at a water-rich phase.

Regarding our results, for both ionic liquids, the mutual solubilities increase with increasing temperature, a fact that suggests an upper critical solution temperature behaviour. The mole fraction solubility of $[C_2C_1im][FAP]$ in water is in the order $\approx 10^{-5}$, while with $[C_2C_1im][PF_6]$ the solubility in water is in the order of $\approx 10^{-3}$. Instead, the water mole fraction solubility in $[C_2C_1im][FAP]$ is around 10^{-2}, and for $[C_2C_1im][PF_6]$ it is in the order of $\approx 10^{-1}$, indicating that both ionic liquids are highly "hygroscopic", as previously

shown for other hydrophobic ionic liquids.[5,6,11,13] Thus, while the water-rich phase can be considered as an almost pure phase with the ionic liquid at infinite dilution, the IL-rich phase presents a significant content of water. Overall, the mutual solubilities between water and ionic liquids are much lower for the ionic liquid composed of the longer aliphatic fluorinated tails. This trend is the opposite of that observed in the liquid-liquid equilibrium of binary mixtures involving fluorinated ionic liquids and perfluorocarbons.[279] Although an upper critical solution temperature is also observed, on the other hand, an increase in the fluorinated chain length of the ionic liquid anion increases the perfluorocarbon solubility.[279]

The extremely skewed phase diagram presented in Figure 3.30 can be re-plotted taking into account: *i*) the large differences between the molar volume (charge density) of the two ionic liquids; and *ii*) between those and the molar volume of water. The phase diagrams given in Figure 3.31 (as a function of the weight and volume fractions occupied by the ionic liquid component, respectively) yield much more symmetrical diagrams that emphasize the much lower mutual solubilities of $[C_2C_1im][FAP]$ and water relative to those of $[C_2C_1im][PF_6]$, both for the water-rich and IL-rich compositions. The diagrams of Figures 3.30 and 3.31 alert for the fact that any comparison between these systems must take into account the intrinsic differences in molar volume of the different components.

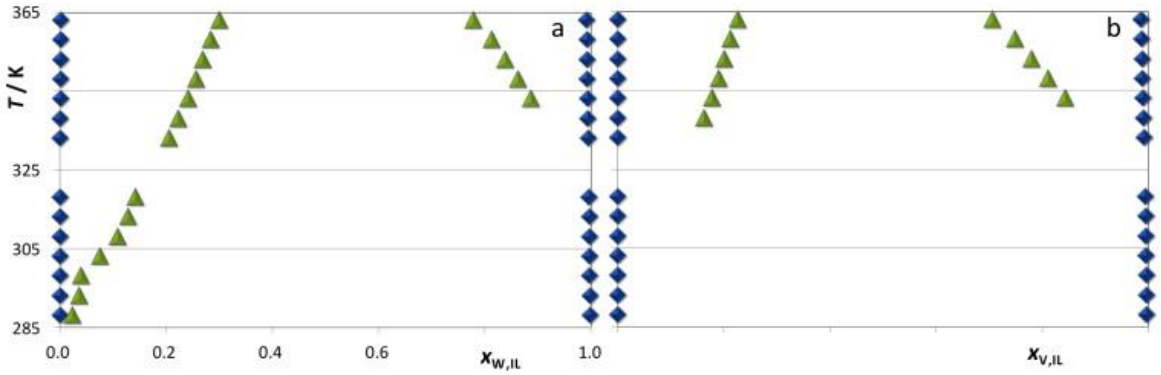

Figure 3.31. Liquid-liquid (*T*-*x*) phase diagrams as a function of (a) weight, $x_{W,IL}$ (b) and volume fraction, $x_{V,IL}$ for the binary system composed of water and $[C_2C_1im][FAP]$ (◆) and $[C_2C_1im][PF_6]$ (▲). For $[C_2C_1im][PF_6]$ the $x_{V,IL}$ was only calculated for temperatures above 338.15 K due to its higher melting point and lack of density data at lower temperatures.

MOLECULAR DYNAMICS SIMULATION

The phase behaviour of the two ionic liquids, namely in binary mixtures with water, were determined by the nature, distribution and density of the interaction centres of the ions that are capable of strong interactions with water molecules (the aromatic hydrogen atoms in the imidazolium cation and the fluorine atoms directly connected to the phosphorus atom of the anion). Several Molecular Dynamics (MD) simulations were performed in order to explore the relation between the phase behaviour in the binary mixtures and the underlying interactions at a molecular level.

Figure 3.32 shows the radial distribution functions between the charged parts of the anions and cations in the pure ionic liquids (continuous lines) and in the water-rich solutions (dotted lines). The grey, red and blue functions are a sort of fingerprint of an ionic liquid: due to the ionic character of the liquid, any given ion will be surrounded by alternating shells of counter-ions and same-charge-ions. This can be appreciated in the snapshots of Figure 3.32c and 3.32d where the polar network of the ionic liquids can be noticed as blue areas (cations) surrounded by red areas (anions) in a three-dimensional and continuous arrangement. Figure 3.32a and 3.32b show the same opposition-of-phase character of the anion-cation (grey) *versus* anion-anion (red) or cation-cation (blue) correlations. This periodicity and its characteristic wavelength is rather different in the two pure ionic liquids and is a measure of the morphology of the polar network in each case: both are continuous but more stretched and string-like in $[C_2C_1im][FAP]$ than in the case of $[C_2C_1im][PF_6]$ (the former has to accommodate the bulky $-C_2F_5$ moieties of its anion – depicted as green space-filled atoms in Figure 3.32d – whereas the latter does not have to). Interestingly, the elongation of the wavelength of the polar network (from shell-to-shell distances of around 0.32 nm in $[C_2C_1im][PF_6]$ to shell-to-shell distances of around 0.40 nm in $[C_2C_1im][FAP]$) corresponds approximately to the ratio of the molar volumes ((0.32 / 0.39)3 ≈ 0.54 ≈ 178.6 / 338.6) of the two pure ionic liquids. In other words, both ionic liquids are characterized by a polar network of the charged parts of their ions but, whereas such network occupies most of the available volume in $[C_2C_1im][PF_6]$, it is more stretched and has to encompass rather large non-polar moieties in the case of $[C_2C_1im][FAP]$.

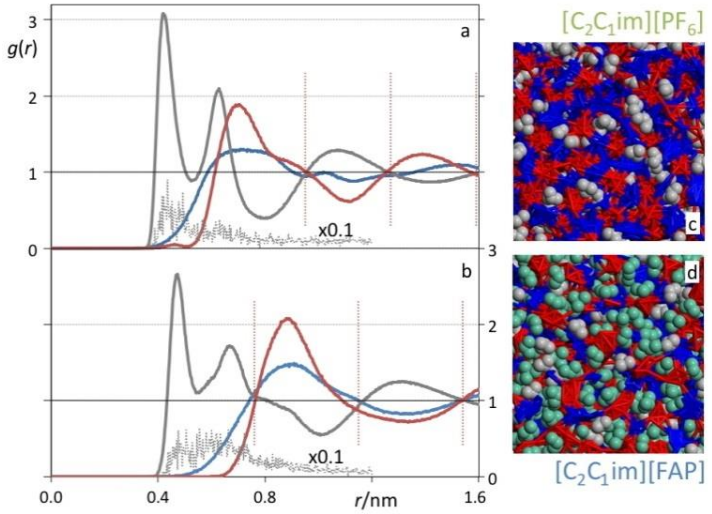

Figure 3.32. Selected radial distribution functions (RDFs), $g(r)$, as a function of distance, r, for the (a) $[C_2C_1im][PF_6]$ and (b) $[C_2C_1im][FAP]$ ILs. Grey lines: RDFs between the imidazolium ring centroid of the cation, im, and the phosphorus atom of the anion, P; blue lines: im-im RDFs; red lines: P-P RDFs. The dotted grey lines correspond to im-P RDFs (with its intensities divided by 10) obtained at infinite dilution in water. The dotted vertical lines show the periodicity of the alternating shells of ions and counter-ions surrounding a given ion. The MD simulation snapshots (c, d) are color-coded to reflect the presence of the charged parts of the cations (blue), the charged parts of the anions (red), the alkyl side chains of the cation (grey), and, in the case of $[C_2C_1im][FAP]$, the perfluoroalkyl chains of the anion (green).

When the ionic liquid ions are diluted in water (by placing just one pair of ions in the midst of hundreds of water molecules in the MD simulations), the corresponding anion-cation RDFs (grey dotted lines in Figure 3.32a and 3.32b) show intense peaks at approximately the same positions of the pure compounds RDFs. The intensity of the peaks (the RDFs have been divided by a factor of ten in order to fit a single graph) are a consequence of the normalization of all RDFs. Whenever the two ions contained in the simulation box interact with each other for longer periods, or more frequently than the values preordained by pure random encounters, such correlations will contribute disproportionately to the first peak of the RDFs. If more ions were to be found in the simulation box, one would expect that these would start to form small ionic clusters in the solution, *i.e.*, a preliminary phase separation process. Nevertheless, it should be stressed that the simulations under such conditions have not been performed since the results do not correspond to single-phase conditions.

Figure 3.33 shows the hydrogen-oxygen RDFs in almost pure water (Figure 3.33a) and of water diluted in the midst of the ionic liquids (Figure 3.33b). Figure 3.33a shows RDFs that

are almost indistinguishable between them and almost identical to that of pure water. The first peak corresponds to the hydrogen bond between two water molecules, the second to the correlation between the oxygen of one of the molecules and the second hydrogen (not H-bonded to that oxygen) of the second water molecule. Unlike the RDFs of the ionic liquids, the RDF of water converges rapidly to unity and does not show any medium-range periodicity. However, the two peaks attest the strength and directionality of the underlying H-bond interactions. The structure of liquid water is a highly distorted random network of hydrogen bonded species.

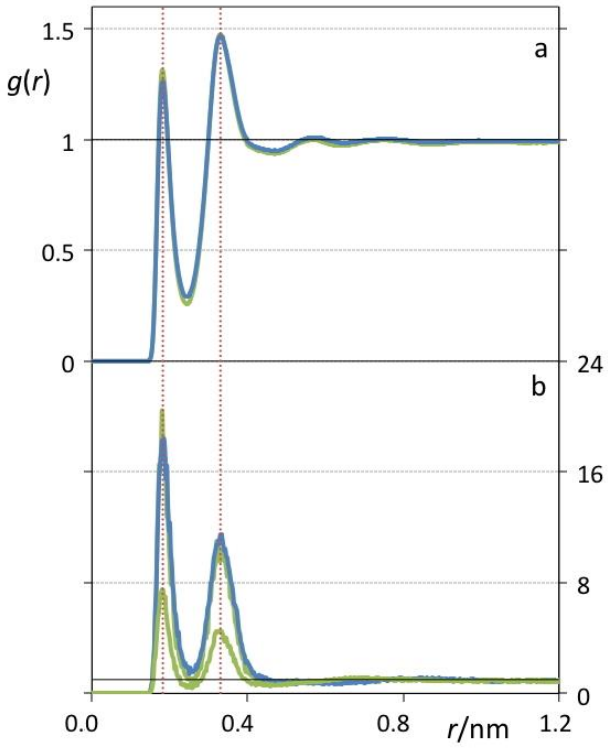

Figure 3.33. Water O-H radial distribution functions (RDFs), $g(r)$, as a function of distance, r. (a) Water-rich $[C_2C_1im][PF_6]$ (green line) and $[C_2C_1im][FAP]$ (blue line) solutions containing one IL ion pair per 600 water molecules. The two lines are nearly superimposed. (b) IL-rich aqueous solutions containing 200 $[C_2C_1im][FAP]$ ion pairs and 20 water molecules (blue line), or 200 $[C_2C_1im][PF_6]$ ion pairs and 20 or 11 water molecules (green lines). One of the green lines (corresponding to the solution with 11 water molecules) is almost superimposed with the blue line.

When water molecules are diluted in the highly organized ionic liquid medium (Figure 3.33b), one sees that water-water hydrogen bonding still occurs, and much more frequently than the values expected based on purely random distributions of water in the ionic liquids. This state of affairs is consistent with possible phase separation at higher

water concentrations. Figure 3.33b also shows another relevant fact: if the water-water RDFs are compared at the same mole concentration of water (20 water molecules in 200 ionic liquid ion pairs), the intensity of the peaks is quite different and larger for the $[C_2C_1im][FAP]$ than for the $[C_2C_1im][PF_6]$ solution. This does not mean that the water-water interactions are more intense in the former ionic liquid than in the latter, just that since the numerical density (number of water molecules *per* volume of solution) is smaller in the $[C_2C_1im][FAP]$ than in the $[C_2C_1im][PF_6]$ solution, the normalization of the RDFs implies that the same number of hydrogen bond contacts in the $[C_2C_1im][FAP]$ aqueous medium produces a more intense peak. This can be proven if one makes the comparison at approximately the same numerical density of water molecules — keeping the 20 water molecules in 200 ionic liquid ion pairs for the $[C_2C_1im][FAP]$ and reducing that number to 11 water molecules in 200 ionic liquid ion pairs for the $[C_2C_1im][PF_6]$ solution. In that case the two RDFs are almost superimposed, implying that if the density of water molecules in the ionic liquid is the same, the amount and intensity of the hydrogen bonds between them is also similar. On one hand, we have to be particularly aware of the implications caused by the large difference in the molar volume of the two ionic liquids, and, on the other hand, the large differences in mutual solubilities of water and the two ionic liquids after the volume effects are discounted must originate in cross interaction (water-IL) differences between the components and not from any significant shift in the self-interactions (water-water or IL-IL).

The correlations between the atoms involved in the cross interactions between the water molecules and the ions that compose the ionic liquids are depicted in Figure 3.34. Panel 3.34a depicts the correlation between the oxygen atom of water and the carbon atom of the imidazolium ring between the two nitrogen atoms (CR) for the IL-rich (solid lines) and water-rich (dotted lines) solutions. Again, the intensity of the first peaks of the solid lines seem to indicate that the cation-water interactions in $[C_2C_1im][FAP]$ (blue solid line) are stronger than those in $[C_2C_1im][PF_6]$ (green solid line). However, this is again an effect caused by the different numerical density of water when diluted in the two ionic liquids: if the intensities of the cross interactions in the water-rich solutions. Panel 3.34b shows the anion-water interactions by depicting the RDFs between the oxygen atom of water and

the phosphorus atom of the anions. The intensity of the two solid peaks (IL-rich solutions) is now very similar and much more intense than the corresponding cation-water interactions; yet, the water-anion interactions in $[C_2C_1im][FAP]$ are weaker than in the corresponding $[C_2C_1im][PF_6]$ solutions if numerical density arguments are invoked. This is further corroborated by the water-rich RDF data. At approximately the same numerical density, the anion-water interactions in the $[C_2C_1im][PF_6]$ solutions are more intense (green dotted peak) than the corresponding interactions in the $[C_2C_1im][FAP]$ solutions (blue dotted peak). This constitutes the greater difference between the two solutions: anion-water interactions (that are the dominant cross interactions in these systems, *cf.* panels a and b of Figure 3.34) with $[FAP]^-$ are weaker than those with $[PF_6]^-$, simply because one has more interaction centres in the former anion (six electronegative fluorine atoms connected to the phosphorus atom) than in the latter. This behaviour can be analysed in Figure 3.34c that shows the RDFs corresponding to the correlation between the hydrogen atoms of the water molecules and the fluorine atoms of the anions connected to the phosphorus atom.

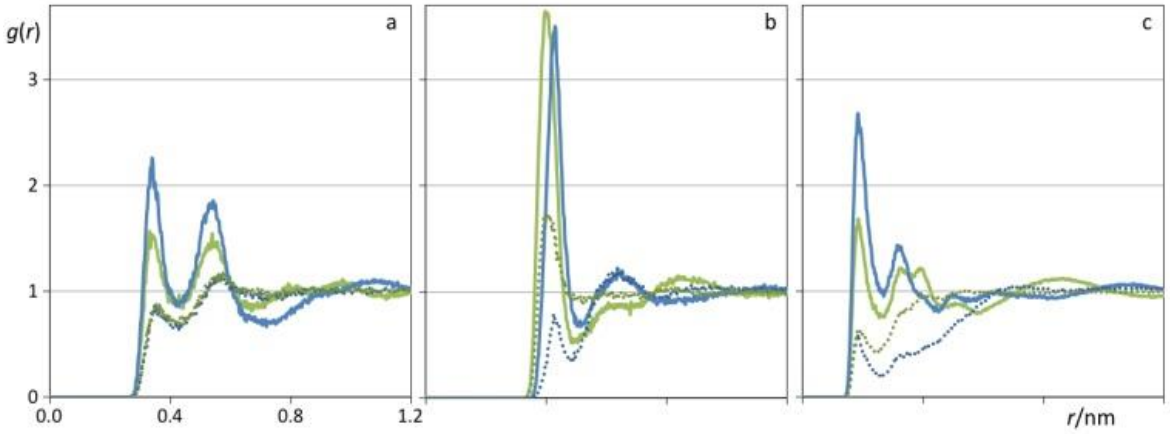

Figure 3.34. Water-IL radial distribution functions (RDFs), $g(r)$, as a function of distance, r. The four lines in each panel correspond to $[C_2C_1im][PF_6]$ IL-rich solutions (solid green), $[C_2C_1im][FAP]$ IL-rich solutions (solid blue), $[C_2C_1im][PF_6]$ water-rich solutions (dotted green) and $[C_2C_1im][FAP]$ water-rich solutions (dotted blue). (a) RDFs between the CR atom (see text) of the cation and the oxygen atom of water; (b) RDFs between phosphorus atom of the anions and the oxygen atom of water; (c) RDFs between three fluorine atoms (see text) of the anions and the hydrogen atom of water.

In order to avoid further numerical density problems, the three fluorine atoms directly attached to the phosphorus atom in $[FAP]^-$ were compared to three of the six fluorine atoms of $[PF_6]^-$. The results in Figure 3.34c show that the intensities of the H-F

interactions are very similar for both ionic liquids if their different molar volumes are taken into account. The first peaks of the dotted lines in the water-rich solutions have almost identical intensities, whereas the first peaks of the solid lines in the IL-rich solutions show larger intensities for the $[C_2C_1im][FAP]$ solutions, due to the normalization effect already discussed for the water-water and cation-water interactions. In other words, individual H(water)-F(anion) interactions are similar in both types of solutions, but the overall water-anion interactions are more intense in $[C_2C_1im][PF_6]$, simply because there are six instead of three available electronegative fluorine atoms.

In respect to the other fluorine atoms in the $[FAP]^-$ ion (those attached to the perfluoroethyl groups), Figure 3.35a shows that the correlations between those groups in pure $[C_2C_1im][FAP]$ or in $[C_2C_1im][FAP]$-rich solutions are not very intense. In fact, they are approximately as intense as those between the terminal methyl groups of the ethyl side chains of the $[C_2C_1im]^+$ cation.[280] These perfluorethyl groups, like their hydrogenated counterparts in the cation, form small non-polar aggregates in the midst of the polar network, confirming the already discussed "stretching" of the polar network and the much large molar volume of $[C_2C_1im][FAP]$. Moreover, Figure 3.35b shows that the interactions between the fluorine atoms of the perfluoroethyl chains and the hydrogen atoms of the water molecules are quite weak. Unlike the H-F RDFs of Figure 3.34c, there are no peaks at distances (*ca.* 0.2 nm) compatible with hydrogen-bonding. The peaks of Figure 3.35b, at distances above 0.4 nm, simply correspond to correlations between the hydrogen atoms of water that are performing hydrogen bonds with the $–PF_3$ fluorine atoms and the neighbouring fluorine atoms of the $–CF_2–$ and $–CF_3$ groups.

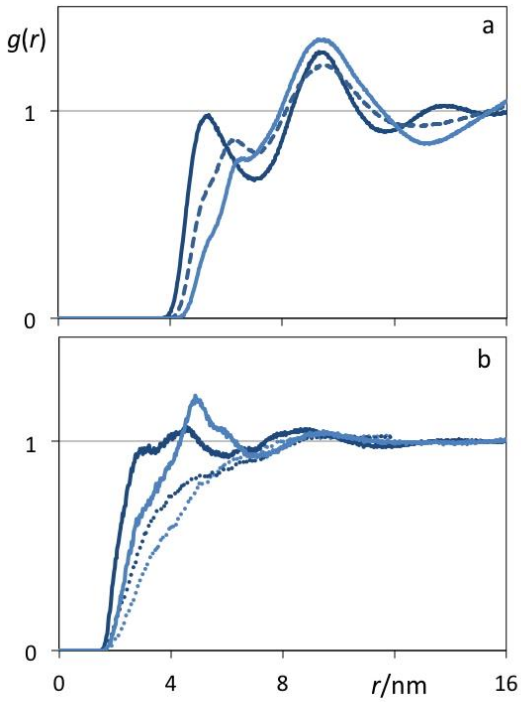

Figure 3.35. (a) Perfluoroethyl-perfluoroethyl radial distribution functions (RDFs), $g(r)$, as a function of distance, r, in $[C_2C_1im][FAP]$ IL-rich solutions. The dark blue line corresponds to correlations between the terminal carbon atoms of the perfluoroethyl groups; the light blue one to correlations between the carbons attached to the phosphorus atom; and the dashed line to correlations between the two types of carbon. (b) water-perfluorethyl radial distribution functions (RDFs), $g(r)$, as a function of distance, r, in $[C_2C_1im][FAP]$ IL-rich solutions (solid lines) and water-rich solutions (dotted lines). The dark blue line corresponds to correlations between the hydrogen atom of water and the $–CF_3$ fluorine atoms of the perfluoroethyl groups; the light blue one to correlations between the hydrogen atom of water and the $–CF_2–$ fluorine atoms of the perfluoroethyl groups.

In summary, the mutual solubilities of $[C_2C_1im][FAP]$ or $[C_2C_1im][PF_6]$ with water can be rationalized taking into account the following facts: *i*) the asymmetrical nature of the immiscibility windows (Figure 3.30) can be "corrected" if one takes into account the different molar volumes of the two ionic liquids (Figure 3.31); *ii*) both pure components are characterized by strong intermolecular interactions. These investigated ionic liquids are electrostatic in nature and lead to a mesoscopic ordered polar network, interspersed with non-polar domains that are much larger in $[C_2C_1im][FAP]$ than in $[C_2C_1im][PF_6]$ (*cf.* Figure 3.32a and 3.32b). Indeed, the formation of three nanosegregated domains (polar, nonpolar, and fluorous) has been already observed in other fluorinated ionic liquids.[281] In the case of water, the liquid phase is characterized by a disordered but tightly connected hydrogen-bonded three-dimensional network (Figure 3.33). In order to mix these two types of components, the cross interactions in the mixture must compensate the partial

loss of the strong interactions within the pure components; *iii*) both systems exhibit immiscibility windows because in neither example the cross interactions are strong enough to disrupt completely the established networks. The immiscibility window of $[C_2C_1im][FAP]$ is much larger than that of $[C_2C_1im][PF_6]$ due to the fact that the most important cross interactions (those between the anion and water, namely the interactions between the fluorine atoms attached to the phosphorus atom and the hydrogen atoms of water) are overall weaker in the former than in the latter ionic liquid (Figure 3.34b). This is a direct result of the six fluorine interaction centres in $[PF_6]^-$ and only three in $[FAP]^-$ (compare Figure 3.35b with Figure 3.34b).

Finally, the direct estimation of the viscosity of ionic liquids using MD is a relatively difficult procedure due to the fact that most of the force-fields commonly used (including CL&P[226,235,236]) are non-polarizable and thus yield diffusion coefficients are sometimes almost one order of magnitude lower than the experimental results. The high viscosity of most ionic liquids also implies unreasonably long simulation runs. Nevertheless, it is possible to infer some conclusions about the viscosity difference between the two neat ionic liquids by reconciling the trends of the self-diffusion coefficients of the two ions with all that was previously discussed concerning their distinct nano-structuration, molar volume and charge density distribution. Nevertheless, it should be remarked that some literature reports already pointed out the correlation between the ionicity of ionic liquids and their physicochemical properties.[282–285] At 338 K, the 8-ns-long MD runs on the pure systems have yielded self-diffusion coefficients of 15 and 5 $m^2 \cdot Ts^{-1}$ for the diffusion of the $[C_2C_1im]^+$ cations in $[C_2C_1im][FAP]$ and $[C_2C_1im][PF_6]$, respectively, and 8 and 3 $m^2 \cdot Ts^{-1}$ for the diffusion of the $[FAP]^-$ and $[PF_6]^-$ anions in $[C_2C_1im][FAP]$ and $[C_2C_1im][PF_6]$, respectively. Even if the uncertainty associated with these values is high and the comparisons are performed on a semi-quantitative basis, the trends — the diffusion coefficients of the ions are three times higher in the [FAP]-based than in the $[PF_6]$-based ionic liquid in spite of the fact that the anions of the former ionic liquid are much bulkier — suggest that the loss of strong interaction centres when one substitutes the $[PF_6]^-$ ion by the $[FAP]^-$ ion does indeed lead to a less coordinated and more flexible polar network.

Albeit the presence of bulkier groups in $[FAP]^-$, this leads to higher ionic mobilities in the [FAP]-based ionic liquid than in its $[PF_6]$-based counterpart.

3.10. Conclusions

New data for physical properties, such as melting temperatures, densities and viscosities, and mutual solubilities with water, of ionic liquids based on different cation families (like imidazolium, pyridinium, pyrrolidinium, piperidinium, phosphonium and ammonium) in combination with the hexafluorophosphate, bis(trifluoromethylsulfonyl)imide and tris(pentafluoroethyl)trifluorophosphate anions were here determined. In addition, the isomerism of the cation and the alkyl chain length was also evaluated.

Despite the hydrophobic label attributed to all ionic liquids here studied, all of them dissolve a large amount of water. In particular, solubilities in the order of 0.5 (in mole fraction) were found for the monosubstituted ionic liquids ($[C_1im][NTf_2]$ and $[C_2im][NTf_2]$). The solubility of the various ionic liquids/salts in water follows the cation order: imidazolium > pyrrolidinium > pyridinium > piperidinium >>> ammonium > phosphonium. The ammonium and phosphonium-based salts are by far less soluble in water with a decrease in one order of magnitude in their mole fraction solubility. It was also found that an increase in the cation side alkyl chain leads to a decrease in the mutual solubilities with water – increase of the ionic liquid hydrophobic character – while the presence of distinct isomers has different effects both on their solubility in water and that of water in ionic liquids. The solubility of both symmetric and asymmetric imidazolium-based ionic liquids in water are comparable as they have similar molar volumes. Indeed, a linear correlation between the logarithm of the solubility of ionic liquids and the respective molar volume was presented and which allows the estimation of solubility data for ionic liquids not experimentally attempted. Considering the anion, the mutual solubilities of water and ionic liquids follows the order: $[PF_6]^- > [NTf_2]^- > [FAP]^-$.

The thermodynamic functions of solution and solvation were also derived, indicating that the solution of the studied ionic liquids in water is entropically driven, and both the symmetric and asymmetric series of ionic liquids display an increase of circa -5 $J \cdot K^{-1} \cdot mol^{-1}$

per methylene addition at the longer aliphatic moiety. This phenomenon is similar to that observed in the alkanes dissolution in water (circa -20 $J \cdot K^{-1} \cdot mol^{-1}$ *per* methylene addition).

The COSMO-RS was used to predict the mutual solubilities of some binary systems and proved to be a valuable *a priori* tool.

New density and viscosity data for pure and water-saturated ionic liquids were reported. It was concluded that the presence of water has a marginal effect on the ionic liquid densities, yet a large impact through their viscosities. Less hydrophobic ionic liquids are more affected due to their larger water contents.

Chapter 4 – Removing Ionic Liquids from Aqueous Solutions using Aqueous Biphasic Systems

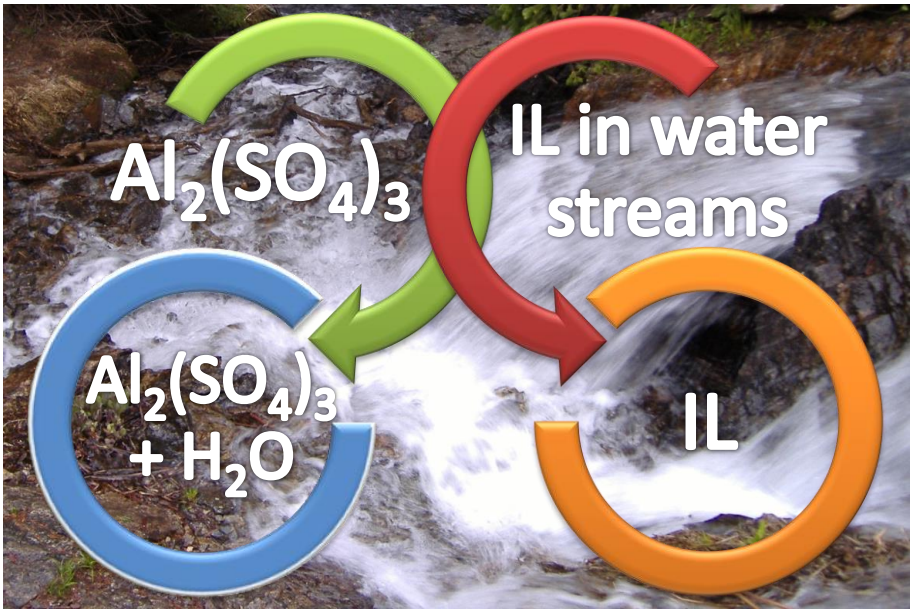

4.1. Introduction

The beneficial use of ionic liquids (ILs) in a diverse range of applications has become increasingly evident.[1,2,286] Their intrinsic non-volatile nature provides the enhanced opportunity to reduce, or even completely eliminate, hazardous and toxic emissions to the atmosphere. However, although ionic liquids cannot contribute to air pollution, they present a non-negligible solubility in water. Consequently, their use in a large scale, either at the academic or industrial level, should also involve a treatment approach aiming at "cleaning" the discarded aqueous effluents, as well as to recover and recycle the ionic liquid used. In this context, it is of vital significance the research and development of novel methods to remove and recover ionic liquids from wastewater streams with the final goal of creating overall "greener" and more sustainable processes.

An approach already described in the literature for the treatment of aqueous solutions contaminated with ionic liquids relays on their physicochemical degradation. This type of treatment addresses the oxidative,[86,87,91] thermal[82] and photocatalytic[19,84,88–90] degradations. These processes are only applicable at diluted solutions and do not allow the recovery of the ionic liquid. Other approach that has been studied for the removal of ionic liquids consists on their adsorption by activated carbon, either commercially available or modified.[92,95,100]

Taking into consideration previous works[68,71,78–81,287,288] which reported aqueous biphasic systems composed of ionic liquids and salting-out species, herein such possibility is explored as an alternative pathway for recovering ionic liquids from aqueous effluents. IL-based aqueous biphasic systems (ABS) are formed when two mutually incompatible, though both miscible with water, ionic liquid/salt aqueous solutions are mixed. Above a critical concentration of those components, spontaneous phase separation takes place. The pioneer work of Rogers and co-workers[71] demonstrated that the addition of a "kosmotropic" salt (like K_3PO_4) to an aqueous ionic liquid solution of a given ionic liquid can induce the phase separation. After this proof of principle, several IL-based ABS were further tested[78–81] with the aim of recovering ionic liquids from aqueous effluents. Deng

et al.[80] presented the recovery of 1-allyl-3-methylimidazolium chloride with three inorganic salts: K_3PO_4, K_2HPO_4 and K_2CO_3. They found that, for the same concentration of salt, the recovery efficiency of the ionic liquid follows the order: K_3PO_4 > K_2HPO_4 > K_2CO_3,[80] which is in good agreement with the Hofmeister series.[76] The authors[80] also concluded that the increase of the concentration of the salt increases the recovery efficiency of the ionic liquid. They reached a maximum recovery efficiency of 96.80% using 46.48 wt% of K_2HPO_4.[80] In the same line of research, Li et al.[81] studied the effect of some sodium-based salts to recover the ionic liquid 1-butyl-3-methylimidazolium tetrafluoroborate from aqueous media. The salts used were Na_3PO_4, Na_2CO_3, Na_2SO_4, NaH_2PO_4 and NaCl, and the highest extraction efficiency (98.77%) was achieved with 16.94 wt% of Na_2CO_3.[81] In a different perspective, and with the goal of reducing the use of charged species to recuperate ionic liquids from aqueous solutions, Wu et al.[78,79] reported the recovery of different ionic liquids from aqueous solutions making use of carbohydrates. A recovery efficiency of 65% of 1-allyl-3-methylimidazolium bromide and 63% of 1-allyl-3-methylimidazolium chloride was achieved by the addition of sucrose.[79] On the other hand, with a distinct ionic liquid, 1-butyl-3-methylimidazolium tetrafluoroborate, and changing the sugar, the recovery efficiencies observed were higher, but still not satisfactory: 74% with sucrose, 72% with xylose, 64% with fructose and 61% with glucose.[78] Despite the possibility of employing carbohydrates to remove ionic liquids from aqueous media, one must be aware that it increases the amount of organic matter in the aqueous streams if large scale applications are envisaged. In addition, the tests with tetrafluoroborate-based ionic liquids must be carried out with special care since these fluids suffer hydrolysis in contact with water.[27]

Taking into account these previous results,[78–81] the ability of two strong salting-out inducing species – $Al_2(SO_4)_3$ and $AlK(SO_4)_2$ – to create ABS and to recover ionic liquids from aqueous solutions were tested. Besides the strong salting-out aptitude of these salts (according to the Hofmeister series[76]) that may easily induce the phase separation of ionic liquids from aqueous media, they are actually used in water treatment processes.[289] According to the USEPA (United States Environmental Protection Agency), alum, chlorine, lime and coagulant aids can be added directly to the public water storage and distribution

systems to treat water, and make it suitable for public consumption.[289] Therefore, in this work, ABS based on aluminium-based salts with different ionic liquids were studied with the goal of developing improved systems for the removal and recovery of ionic liquids from aqueous streams.

4.2. Experimental procedure

4.2.1. Materials

Several ABS composed of the following ionic liquids: 1-ethyl-3-methylimidazolium trifluoromethanesulfonate (triflate), $[C_2C_1im][CF_3SO_3]$, purity 99 wt%; 1-butyl-3-methylimidazolium trifluoromethanesulfonate (triflate), $[C_4C_1im][CF_3SO_3]$, purity 99 wt%; 1-butyl-3-methylimidazolium tosylate, $[C_4C_1im][Tos]$, purity 98 wt%; 1-butyl-3-methylimidazolium dicyanamide, $[C_4C_1im][N(CN)_2]$, purity > 98 wt%; 1-octylpyridinium dicyanamide, $[C_8py][N(CN)_2]$, purity > 98 wt%; 1-benzyl-3-methylimidazolium ethylsulphate, $[(C_7H_7)C_1im][C_2H_5SO_4]$, purity 98 wt%; tri(isobutyl)methylphosphonium tosylate, $[P_{i(444)1}][Tos]$, purity 98 wt%; tetrabutylphosphonium bromide, $[P_{4444}]Br$, purity 95 wt%; tetrabutylphosphonium chloride, $[P_{4444}]Cl$, purity 97 wt%; tributylmethylphosphonium methylsulphate, $[P_{4441}][CH_3SO_4]$, purity 96-98 wt% were investigated in this work. The structures of the ionic liquids that were successfully removed are depicted in Figure 4.1.

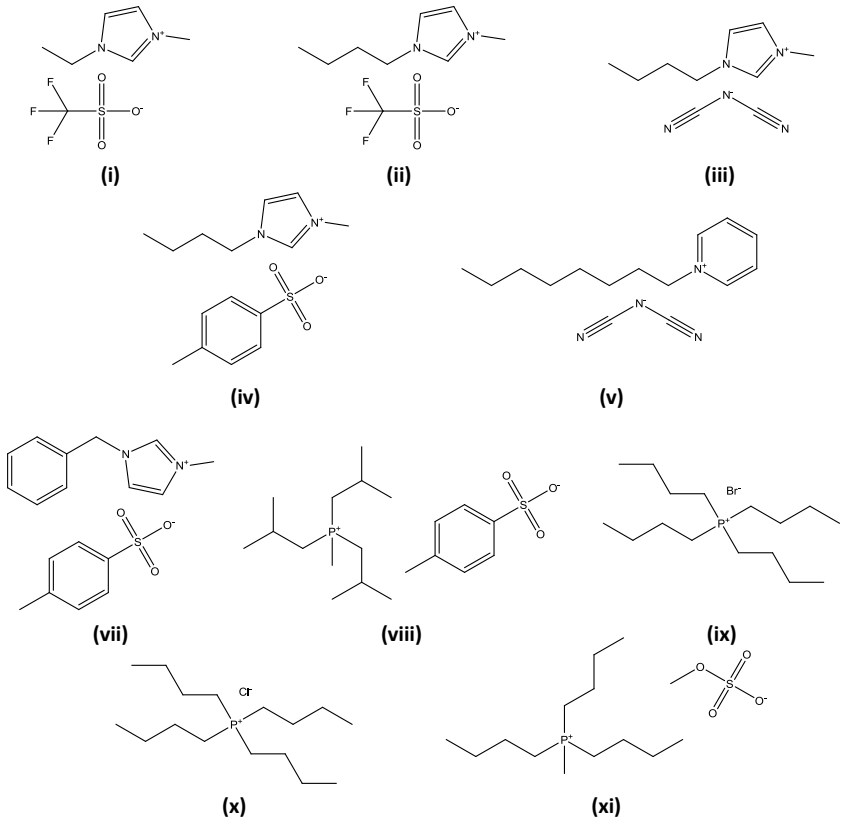

Figure 4.1. Chemical structures of the ILs used to form ABS: (i) $[C_2C_1im][CF_3SO_3]$; (ii) $[C_4C_1im][CF_3SO_3]$; (iii) $[C_4C_1im][N(CN)_2]$; (iv) $[C_4C_1im][Tos]$; (v) $[C_8py][N(CN)_2]$; (vi) $[(C_7H_7)C_1im][C_2H_5SO_4]$; (vii) $[P_{i(444)1}][Tos]$; (viii) $[P_{4444}]Br$; (ix) $[P_{4444}]Cl$; (x) $[P_{4441}][CH_3SO_4]$.

All imidazolium- and pyridinium-based ionic liquids were purchased from Iolitec. The phosphonium-based ionic liquids were kindly supplied by Cytec Industries Inc. To reduce the volatile impurities contents to negligible values, individual samples of ionic liquids were further purified under constant agitation at vacuum and at moderate temperature (343 K) for a minimum of 24 h. After this purification approach, the purity of each ionic liquid was checked by ^{1}H and ^{13}C NMR spectra, and ^{19}F and ^{31}P NMR spectra whenever applicable, and found to be according to the purities given by the suppliers.

The inorganic salts $Al_2(SO_4)_3$ and $AlK(SO_4)_2.12H_2O$ were acquired from Himedia (purity ≥ 98.0 wt%) and from Carlo Erba (purity ≥ 99.5 wt%), respectively. The water employed was double distilled, passed across a reverse osmosis system and further treated with a Milli-Q plus 185 water purification equipment. The buffers used in the calibration of the pH meter equipment were solutions with pH values of 4.00 and 7.00, acquired from Panreac. In order to calibrate the conductivity meter, standard solutions of KCl with concentrations

of 0.1 and 0.01 M were diluted from a standard solution of 1 M supplied by Mettler Toledo and used.

4.2.2. Methods

PHASE DIAGRAMS AND TIE-LINES

Aqueous solutions of $Al_2(SO_4)_3$ at ≈ 36 wt% and $AlK(SO_4)_2$ at ≈ 7 wt%, and aqueous solutions of the different hydrophilic ionic liquids at ≈ 90 wt%, were prepared and used for the determination of the ternary phase diagrams. Note that for the salt $AlK(SO_4)_2$ the concentrations reported on the phase diagrams were calculated without the contribution of the water complexed with the salt. The solubility curves were determined at 298 (± 1) K and at atmospheric pressure through the cloud point titration method, as previously described.[68,126,287] Drop-wise addition of each aqueous inorganic salt solution to each ionic liquid aqueous solution, or vice-versa, was carried out until the detection of a cloudy point (liquid-liquid biphasic solution), followed by drop-wise addition of ultra-pure water until the observation of a clear and limpid solution (fitting into the monophasic regime). Drop-wise additions were carried out under constant stirring. The ternary systems compositions were determined by weight quantification of all components within ± 10^{-4} g (using an analytical balance, Mettler Toledo Excellence XS205 Dual Range). With the salt $AlK(SO_4)_2.12H_2O$ only the ionic liquids $[C_8py][N(CN)_2]$ and $[C_4C_1im][CF_3SO_3]$ were found to undergo liquid-liquid demixing. The composition of the phase diagrams are reported in Tables S4.1 and S4.2 in Appendix.

The experimental binodal curves were fitted according to according to,

$$[IL] = A\exp\left[(B\times[Salt]^{0.5}) - (C\times[Salt]^{3})\right] \quad (4.1)$$

where [IL] and [Salt] are the ionic liquid and salt weight fraction percentage, respectively, and *A*, *B* and *C* are fitted constants obtained by the regression.

Tie-lines (TLs) were determined by a gravimetric method originally proposed by Merchuk et al..[290] For that purpose, ternary mixtures of known total composition at the biphasic

region and composed of ionic liquid + salt + water were gravimetrically prepared within ± 10^{-4} g, vigorously agitated, and left to equilibrate for at least 12 h at 298 (± 1) K, aiming at a complete separation of both phases. After a careful separation step, both ionic liquid and salt phases were weighed within ± 10^{-4} g. Each TL was determined by a mass balance approach through the relationship between the IL-rich mass phase composition and the overall system composition, and for which the following system of four equations (eqs 4.2 – 4.5) and four unknown values ($[IL]_{IL}$, $[IL]_{Salt}$, $[Salt]_{IL}$ and $[Salt]_{Salt}$) was solved:[290]

$$[IL]_{IL} = A\exp\left[(B\times[Salt]_{IL}^{0.5}) - (C\times[Salt]_{IL}^{3})\right] \quad (4.2)$$

$$[IL]_{Salt} = A\exp\left[(B\times[Salt]_{Salt}^{0.5}) - (C\times[Salt]_{Salt}^{3})\right] \quad (4.3)$$

$$[IL]_{IL} = \frac{[IL]_{M}}{\alpha} - \frac{1-\alpha}{\alpha}\times[IL]_{Salt} \quad (4.4)$$

$$[Salt]_{IL} = \frac{[Salt]_{M}}{\alpha} - \frac{1-\alpha}{\alpha}\times[Salt]_{Salt} \quad (4.5)$$

where “IL”, “Salt” and “M” designate the IL-rich phase, the salt-rich phase and the mixture, respectively; [Salt] and [IL] represent, respectively, the weight fraction percentage of salt and ionic liquid; and α is the ratio between the mass of the IL-rich phase and the total mass of the mixture. The system solution results in the concentration (wt%) of the ionic liquid and inorganic salt in the IL- and salt-rich phases, and thus, TLs can be simply represented.

For the calculation of individual tie-line lengths (TLLs), the following equation was employed:

$$\sqrt{([Salt]_{IL} - [Salt]_{Salt})^2 + ([IL]_{IL} - [IL]_{Salt})^2} \quad (4.6)$$

where “IL” and “Salt” symbolize, respectively, the IL- and salt-rich phases, and [Salt] and [IL] are the weight fraction percentage of inorganic salt and ionic liquid, as described before.

The critical point (the mixture composition at which the composition of the two aqueous phases becomes identical) of each system was also estimated.[55,56] This was accomplish by extrapolating the TL slopes of individual systems followed by a further fitting using eq 4.7,

$$[IL] = f[Salt] + g \quad (4.7)$$

where [IL] and [Salt] are the concentration of ionic liquid and salt in weight fraction percentage, respectively, and f and g are the fitting parameters. The parameters values obtained and respective correlation coefficient (R^2) are reported in Table S4.3 in Appendix.

The thermophysical properties of the coexisting phases, namely pH, conductivity, density and viscosity, were determined for total mixture compositions of 40 wt% of ionic liquid + 15 wt% of $Al_2(SO_4)_3$ + 45 wt% of water, and 51 wt% of ionic liquid + 2 wt% of $AlK(SO_4)_2$ + 45 wt% of water. For such mixture compositions, the respective TLs were determined in order to known the composition of each aqueous phase.

pH AND CONDUCTIVITY

The pH and conductivity measurements (± 0.02 and ± 0.5%, respectively) of the IL-rich and inorganic-salt-rich aqueous phases were measured at 298 (± 1) K using a Mettler Toledo S47 SevenMulti™ dual meter pH / conductivity equipment. The calibration of the pH meter was carried out with two different buffers with pH values of 4.00 and 7.00, while the calibration of the conductivity meter was carried out with KCl aqueous solutions.

DENSITY AND VISCOSITY

Density and viscosity measurements were performed at atmospheric pressure and in the temperature range between (298.15 and 328.15) K for both the IL-rich and inorganic-salt-rich phases (the complete data with the dependence on temperature are available in Table S4.1 in Appendix), using an automated SVM 3000 Anton Paar rotational Stabinger viscometer-densimeter. The SVM 3000 Anton Paar rotational Stabinger viscometer-densimeter uses Peltier elements for fast and efficient thermostatization. Further details

regarding the operation system can be found elsewhere.[216,291] The uncertainty in temperature is within ± 0.02 K, the relative uncertainty for the dynamic viscosity is ± 0.35% and the absolute uncertainty for the density is ± 5 × 10^{-4} g·cm^{-3}.

ULTRAVIOLET-VISIBLE SPECTROSCOPY / INDUCTIVELY COUPLED PLASMA-OPTICAL EMISSION SPECTROMETRY / FOURIER TRANSFORM INFRARED SPECTROSCOPY

The TL compositions for systems with the ionic liquids [$P_{i(444)1}$][Tos] and [C_4C_1im][$N(CN)_2$] were confirmed, aiming at checking that there is no ion exchange among the phases, by Ultraviolet-Visible (UV-Vis) spectroscopy, ICP-OES (Inductively Coupled Plasma-Optical Emission Spectrometry) and FTIR (Fourier Transform Infrared) spectroscopy. The amount of imidazolium- and tosylate-based ionic liquids in each aqueous phase was determined by UV-spectroscopy using a SHIMADZU UV-1700 Pharma-Spec Spectrophotometer at a wavelength of 211 and 222 nm (using calibration curves previously established), respectively. The aluminium and phosphonium content at the coexisting phases was quantified by ICP-OES using a Jobin Yvon 70 plus, power 880 W, under a plasma gas flow of 16 mL/min and pressure of 2.6 bar. The FTIR spectra, with a resolution of 4 cm^{-1}, were obtained using a Perkin Elmer BX spectrometer operating in the attenuated total reflection (ATR) mode (equipped with a single horizontal Golden Gate ATR cell).

4.3. Improved recovery of ionic liquids from contaminated aqueous streams using aluminium-based salts

Catarina M. S. S. Neves, Mara G. Freire and João A. P. Coutinho, RSC Advances 2 (2012) 10882-10890, DOI: 10.1039/C2RA21535G

4.3.1. Abstract

The number of applications involving ionic liquids has dramatically increased in the past few years, and their production and use in a large scale will inevitably lead to their dispersion into water streams (either by wastewater disposal or accidental leakage). Studies on the removal and recovery of ionic liquids from wastewater streams are

therefore of crucial importance, yet particularly scarce. In this work, the use of aluminium salts is proposed to concentrate and remove ionic liquids from aqueous solutions. Two aluminium-based salts ($Al_2(SO_4)_3$ and $AlK(SO_4)_2.12H_2O$) were used to treat various aqueous solutions of ionic liquids containing imidazolium-, pyridinium- and phosphonium-based fluids. All the ternary systems studied were additionally characterized by measuring some of their tie-lines and tie-line lengths. The physical properties of the coexisting phases, namely density, viscosity, conductivity and pH values were also determined to fully characterize and gather a broader picture on the applicability of these systems. The gathered results show the enhanced ability of these salts to remove and recover ionic liquids from aqueous media. The minimum recovery efficiency achieved was 96%, whereas for a large array of systems recoveries of circa 100% of ionic liquid were attained. The residual concentrations of ionic liquids in water range from 0.01 to 6 wt%. The results reported disclose a novel promising technique for the recovery and treatment of aqueous effluents contaminated with ionic liquids by using salts commonly employed in water treatment processes, allowing thus its easy scale-up and adaptation to new processes involving ionic liquids.

4.3.2. Results and discussion

The ternary phase diagrams of the two salts ($Al_2(SO_4)_3$ and $AlK(SO_4)_2$) and a large array of ionic liquids were firstly determined to obtain a wide characterization of these novel ABS. Contrarily to previous works,[78–81] a large array of ionic liquids was studied here. The ionic liquids investigated, and that could be recovered from aqueous solutions by the addition of the $Al_2(SO_4)_3$, were $[C_2C_1im][CF_3SO_3]$, $[C_4C_1im][CF_3SO_3]$, $[C_4C_1im][Tos]$, $[C_4C_1im][N(CN)_2]$, $[C_8py][N(CN)_2]$, $[(C_7H_7)C_1im][C_2H_5SO_4]$, $[P_{i(4441)}][Tos]$, $[P_{4444}]Br$, $[P_{4444}]Cl$ and $[P_{1444}][CH_3SO_4]$. On the other hand, with $AlK(SO_4)_2.12H_2O$, from the series of ionic liquids investigated, only $[C_4C_1im][CF_3SO_3]$ and $[C_8py][N(CN)_2]$ could be recovered. Moreover, the ionic liquids $[C_4C_1im]Br$, $[C_4C_1im][C_2H_5SO_4]$ and $[C_8C_1im]Cl$ were also tested and found to be not sufficiently “hydrophobic” to undergo liquid-liquid demixing in the presence of the acidic aqueous solution of $Al_2(SO_4)_3$. Since we are dealing with acidic aqueous solutions, only a limited range of ionic liquids is capable of creating ABS, as shown in a previous work

where a critical assessment regarding the formation of IL-based ABS under acidic media was provided.[70] Besides the salting-out ability of the inorganic salt, the pH of the aqueous solution seems to play an important role on the formation of IL-based ABS.

The experimental solubility phase diagrams obtained, at 298 K and at atmospheric pressure, for the ternary systems composed of ionic liquid + salt + water are presented in Figure 4.2.

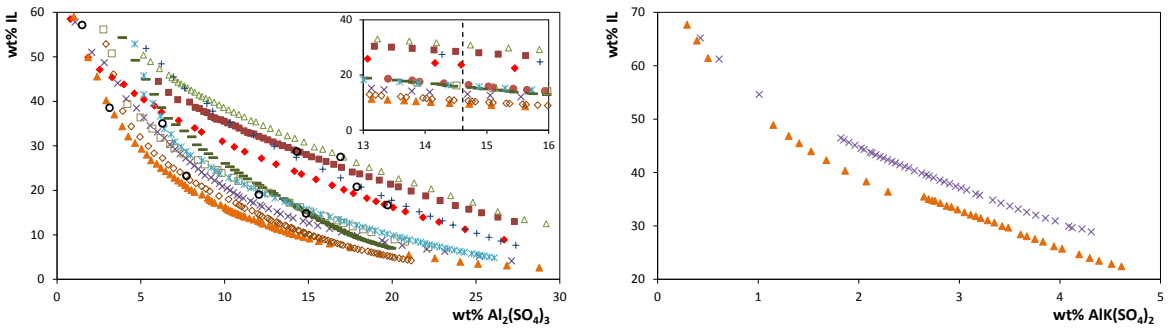

Figure 4.2. Ternary phase diagrams for systems composed of IL + aluminium-based salt + water at 298 K and atmospheric pressure (weight fraction units): ■, $[C_2C_1im][CF_3SO_3]$; ×, $[C_4C_1im][CF_3SO_3]$; +, $[C_4C_1im][Tos]$; ◆, $[C_4C_1im][N(CN)_2]$; ▲, $[C_8py][N(CN)_2]$; △, $[(C_7H_7)C_1im][C_2H_5SO_4]$; ▬, $[P_{i(444)1}][Tos]$; ◇, $[P_{4444}]Br$; ✳, $[P_{4444}]Cl$; □, $[P_{4441}][CH_3SO_4]$; ○, critical point.

The phase diagrams are separated by salts, and reported in weight fraction percentage units (the phase diagrams in molality units are provided in Figure S4.1 in Appendix). Aiming at providing a general trend and to allow the reader to know the mass fraction content at a given point, Table 4.1 presents the parameters obtained by regression of the experimental binodal curves (in weight fraction percentage units) by the application of eq 4.1.[290] In general, good correlation coefficients were obtained which indicate the reliability of eq 4.1 in describing the experimental data.

The larger the biphasic region, the higher is the ability of the salt to recover and remove the ionic liquid from solution. From the gathered data, the tendency of the $Al_2(SO_4)_3$ to recover the ionic liquids follows the order: $[C_8py][N(CN)_2]$ > $[P_{4444}]Br$ > $[C_4C_1im][CF_3SO_3]$ > $[P_{i(444)1}][Tos]$ ≈ $[P_{4441}][CH_3SO_4]$ ≈ $[P_{4444}]Cl$ > $[C_4C_1im][N(CN)_2]$ > $[C_4C_1im][Tos]$ > $[C_2C_1im][CF_3SO_3]$ > $[(C_7H_7)C_1im][C_2H_5SO_4]$. Concerning the $AlK(SO_4)_2$ salt, $[C_8py][N(CN)_2]$ is more easily removed from solution than $[C_4C_1im][CF_3SO_3]$. Although this latter salt could

only salt-out two of the studied ionic liquids it has the advantage that the concentration necessary to promote ABS, and consequently to remove ionic liquids from water streams, is lower than that required by using $Al_2(SO_4)_3$. In general, the trends found for the ionic liquids ability in creating ABS are in good agreement with our previous works using distinct inorganic salts.[67–70] For these different salts, concentrations of ≈ 22 wt% of Na_2SO_4[70] or ≈ 40 wt% of K_3PO_4[67–69] were needed to salt-out the different ionic liquids.

Table 4.1. Parameters used for the regression of the experimental data by eq 4.1 and respective standard deviation, σ, and correlation coefficient, R^2, for each IL + salt + H_2O system at 298 K.

IL	$A \pm \sigma$	$B \pm \sigma$	10^5 ($C \pm \sigma$)	R^2
	$Al_2(SO_4)_3$			
$[C_2C_1im][CF_3SO_3]$	84 ± 1	-0.267 ± 0.004	2.4 ± 0.1	0.9994
$[C_4C_1im][CF_3SO_3]$	102 ± 3	-0.469 ± 0.013	6.6 ± 0.1	0.9888
$[C_4C_1im][Tos]$	118 ± 2	-0.355 ± 0.007	4.0 ± 0.2	0.9994
$[C_4C_1im][N(CN)_2]$	73 ± 1	-0.259 ± 0.003	4.2 ± 0.1	0.9992
$[C_8py][N(CN)_2]$	111 ± 1	-0.598 ± 0.004	3.8 ± 0.4	0.9983
$[(C_7H_7)C_1im][C_2H_5SO_4]$	91 ± 1	-0.265 ± 0.002	2.3 ± 0.1	0.9998
$[P_{i(444)1}][Tos]$	154 ± 4	-0.534 ± 0.010	8.6 ± 0.4	0.9977
$[P_{4444}]Br$	151 ± 6	-0.666 ± 0.016	4.2 ± 0.8	0.9912
$[P_{4444}]Cl$	145 ± 6	-0.564 ± 0.014	2.3 ± 0.3	0.9958
$[P_{4441}][CH_3SO_4]$	132 ± 7	-0.551 ± 0.023	1.5 ± 1.1	0.9874
	$AlK(SO_4)_2$			
$[C_4C_1im][CF_3SO_3]$	89 ± 1	-0.473 ± 0.002	1.9 ± 0.1	0.9998
$[C_8py][N(CN)_2]$	92 ± 1	-0.579 ± 0.009	1.6 ± 0.2	0.9972

The tie-lines (TLs) and tie-line lengths (TLLs) for each system were also determined at 298 K. The consistency of the TLs was further checked using the Othmer-Tobias[165] and Bancroft[292] correlations – the correlation of each system is provided in Figures S4.2 and S4.3 in Appendix. The total mixture compositions, the weight fraction percentage compositions of the coexisting phases (TLs), and the respective TLLs, are reported in Table 4.2.

Table 4.2. Weight fraction percentage of IL and salt (wt%) in the total mixture and in the IL-rich and salt-rich phases, at 298 K, and respective values of TLL. The percentage recovery efficiency of each IL at a given TL is given as %*R*.

IL	weight fraction percentage / wt%						TLL	%*R*
	$[IL]_{IL}$	$[Salt]_{IL}$	$[IL]_{M}$	$[Salt]_{M}$	$[IL]_{Salt}$	$[Salt]_{Salt}$		
	$Al_2(SO_4)_3$							
$[C_2C_1im][CF_3SO_3]$	56.84	2.21	44.96	9.96	6.10	35.34	60.60	97.1
	63.19	1.19	45.00	13.01	3.44	40.02	71.27	97.9
	68.32	0.64	45.08	15.85	1.89	44.14	79.41	98.7
	60.20	1.62	39.82	15.04	4.20	38.48	67.04	96.4
$[C_4C_1im][CF_3SO_3]$	73.51	0.47	44.97	9.96	4.49	23.43	72.74	96.1
	76.21	0.37	44.96	13.02	1.10	30.77	81.02	99.0
	82.14	0.20	44.92	15.90	0.41	34.67	88.70	99.7
$[C_4C_1im][Tos]$	57.09	4.10	45.06	13.00	0.20	46.16	70.75	99.9
	61.49	3.31	44.98	15.88	0.06	50.08	77.21	100.0
	54.02	4.74	40.10	15.00	0.33	44.31	66.69	99.8
$[C_4C_1im][N(CN)_2]$	58.66	0.68	45.09	9.94	0.95	40.04	69.85	99.6
	63.53	0.27	44.90	13.03	0.41	43.51	76.51	99.8
	69.30	0.03	44.98	15.88	0.28	45.01	82.38	99.8
	61.45	0.42	40.12	14.96	0.62	41.87	73.61	99.5
$[C_8py][N(CN)_2]$	59.03	1.12	24.99	14.98	3.69	23.66	59.75	91.1
	66.54	0.73	45.04	9.95	1.94	28.41	70.29	98.8
	70.82	0.57	45.08	12.99	0.72	34.41	77.84	99.6
	75.38	0.42	44.98	15.88	0.31	38.60	84.22	99.8
$[(C_7H_7)C_1im][C_2H_5SO_4]$	53.66	4.01	45.02	9.98	5.46	37.35	58.61	98.1
	59.88	2.54	44.70	13.10	2.92	42.15	69.38	98.4
	65.37	1.59	44.95	15.99	1.44	46.67	78.22	99.0
	56.77	3.21	39.86	15.03	3.82	40.20	64.58	97.1
$[P_{i(444)1}][Tos]$	56.15	3.53	45.16	9.93	0.10	36.17	64.86	100.0
	61.88	2.89	44.87	13.04	0.02	39.81	72.04	100.0
	67.99	2.32	44.80	15.93	0.01	42.22	78.82	100.0
$[P_{4444}]Br$	63.40	1.69	44.94	9.97	1.37	29.51	67.98	99.2
	70.60	1.30	45.05	13.00	0.68	33.32	76.91	99.5
	76.70	1.03	44.82	15.93	0.33	36.72	84.30	99.7
$[P_{4444}]Cl$	55.46	2.90	37.49	14.03	1.59	36.28	63.37	98.6
	55.44	2.90	44.85	10.00	1.01	39.42	65.55	99.6
	60.13	2.43	44.90	12.98	0.50	43.71	72.53	99.8
$[P_{4441}][CH_3SO_4]$	58.34	2.21	44.95	9.97	2.81	34.38	64.18	98.7
	63.89	1.75	44.76	13.07	1.81	38.49	72.13	98.9

	70.16	1.33	45.03	15.87	1.33	41.14	79.52	99.1
	61.75	1.91	40.11	14.97	1.91	38.00	69.88	98.4
	$AlK(SO_4)_2$							
$[C_4C_1im][CF_3SO_3]$	61.21	0.61	51.00	2.18	4.77	9.27	57.11	97.4
$[C_8py][N(CN)_2]$	68.62	0.26	50.99	2.18	6.00	15.86	53.07	95.8

In addition, the critical point of each system (the mixture composition for which the composition of the two aqueous phases are equal) is presented in Table 4.3. Due to the low solubility of the salt $AlK(SO_4)_2$ in water it was only possible to have one TL for each system. Therefore the calculation of the critical points was not carried out with this type-based systems. As an example, Figure 4.3 depicts the results obtained for the system composed of $[P_{4444}]Br + Al_2(SO_4)_3 + H_2O$.

Table 4.3. Critical point of each system composed of IL + $Al_2(SO_4)_3$ + H_2O at 298 K.

IL	Critical Point / wt%	
	[IL]	[Salt]
$[C_2C_1im][CF_3SO_3]$	14.32	28.72
$[C_4C_1im][CF_3SO_3]$	1.49	57.15
$[C_4C_1im][Tos]$	17.88	20.79
$[C_4C_1im][N(CN)_2]$	19.72	16.68
$[C_8py][N(CN)_2]$	3.13	38.55
$[(C_7H_7)C_1im][C_2H_5SO_4]$	16.91	27.50
$[P_{i(444)1}][Tos]$	14.86	14.78
$[P_{4444}]Br$	7.72	23.25
$[P_{4444}]Cl$	35.03	6.29
$[P_{4441}][CH_3SO_4]$	12.05	19.04

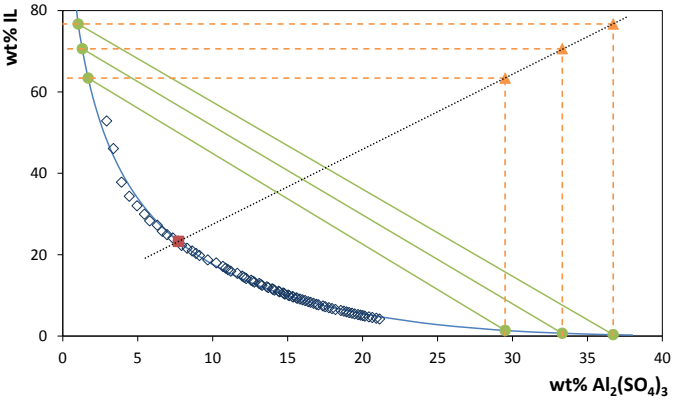

Figure 4.3. Binodal curve, TLs and critical point for the system composed of $[P_{4444}]Br + Al_2(SO_4)_3 + H_2O$ at 298 K: ◇, experimental binodal data; ●, TL data; ▲, TLs relation; ■, critical point.

Aiming at exploring the viability of the proposed systems for wastewater treatment and to recover ionic liquids from aqueous effluents, Table 4.2 presents the values of the recovery efficiencies of the various ionic liquids determined according to,

$$\%R = \frac{[IL]_{IL} \times m_{IL}}{[IL]_{IL} \times m_{IL} + [IL]_{Salt} \times m_{Salt}} \times 100 \quad (4.8)$$

where "IL" and "Salt" symbolize, respectively, the IL- and salt-rich phases, [Salt] and [IL] are the weight fraction percentage of inorganic salt and ionic liquid, and *m* is the mass of each phase.

For an easier analysis of the recovery efficiencies of all ionic liquids, all the gathered results are depicted in Figures 4.4 and 4.5. Figure 4.4 shows the results for phosphonium- and pyridinium-based ionic liquids, whereas Figure 4.5 illustrates the effect of the ionic liquid anion and cation composing imidazolium-based fluids.

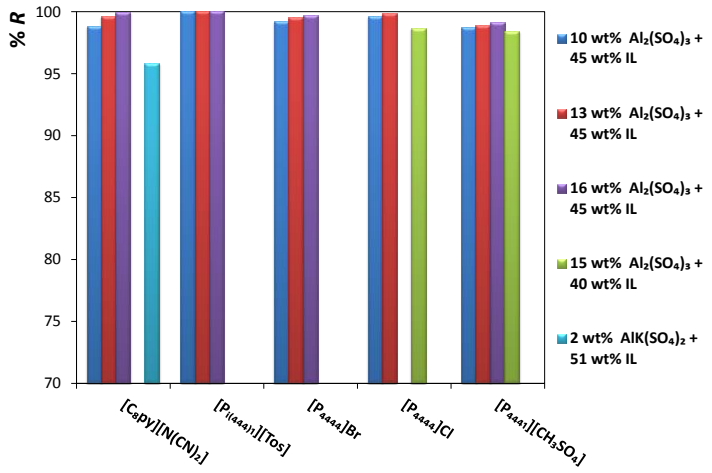

Figure 4.4. Percentage recovery efficiencies (%*R*) of phosphonium- and pyridinium-based ILs at diverse mixture compositions.

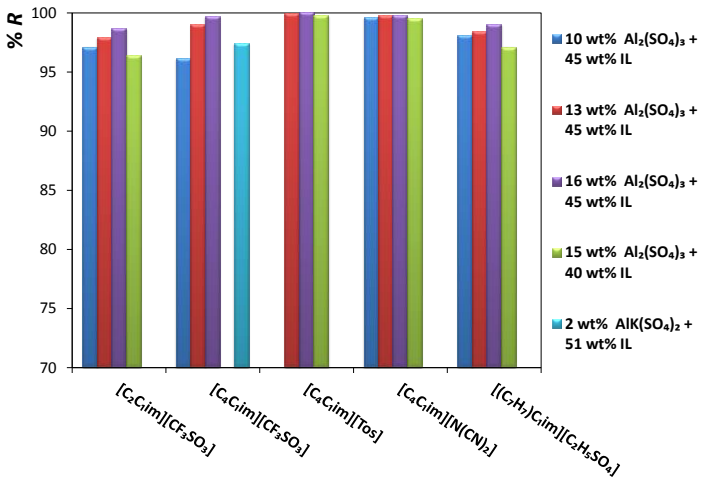

Figure 4.5. Percentage recovery efficiencies (%*R*) of imidazolium-based ILs at diverse mixture compositions.

Figures 4.4 and 4.5, and Table 4.2, show that remarkable results on the recovery of ionic liquids from aqueous media can be obtained. The recovery efficiencies of the diverse ionic liquids are always above 96% and for a large number of systems circa 100% of recuperation was achieved. In particular, the fluids $[C_4C_1im][Tos]$, $[P_{i(444)1}][Tos]$ and $[C_4C_1im][N(CN)_2]$ show recovery efficiencies above 99.5%, and for $[C_4C_1im][N(CN)_2]$ the amount of inorganic salt at the IL-rich phase is inferior to 0.7 wt%. In addition, the ionic liquid concentration in the salt-rich phase is low, and ranges from 0.01 wt% with $[P_{i(444)1}][Tos]$ to 6.10 wt% with $[C_2C_1im][CF_3SO_3]$, both with the salt $Al_2(SO_4)_3$. For a fixed concentration of ionic liquid, and increasing the concentration of inorganic salt, there is an increase on the recovery efficiency of the ionic liquid, as depicted in Figures 4.4 and 4.5. These results agree with the observations reported before by other authors.[80,81] Regarding the $AlK(SO_4)_2$, the recoveries of the ionic liquids are also high (97.4% for $[C_4C_1im][CF_3SO_3]$ and 95.8% for $[C_8py][N(CN)_2]$), and remarkably they were achieved using only 2 wt% of salt in the total mixture composition. The main handicap of this salt is its inability to promote ABS with a larger matrix of ionic liquids.

The results gathered show that it is possible, by a proper selection of the salting-out species used, to achieve an enhanced recovery of ionic liquids from aqueous solutions. Previous works reported recovery efficiencies of ionic liquids substantially lower: 61-74% with carbohydrates[78,79] and 96.80% with the addition of 46.48 wt% of K_2HPO_4[287] or 98.77% with the addition of 16.94 wt% of Na_2CO_3.[81] With aluminium-based salts,

commonly used in water treatment processes, the recovery efficiencies of ionic liquids are greatly improved. Moreover, the amount of inorganic salt used in this work is substantially lower than those previously reported with other salts.[80,81]

Based on the enhanced recovery efficiencies obtained, the use of aluminium-based two-phase systems, and their scale-up and adaptation to new processes involving ionic liquids, is straightforwardly envisaged. A graphical representation of the process configuration is depicted Figure 4.6. This process was tested with the ionic liquid [$P_{i(444)1}$][Tos] in several recovery cycles, and the results obtained are depicted in Figure 4.7. For each cycle, the recovery is always circa to 100% and proves the recyclability of the inorganic salt.

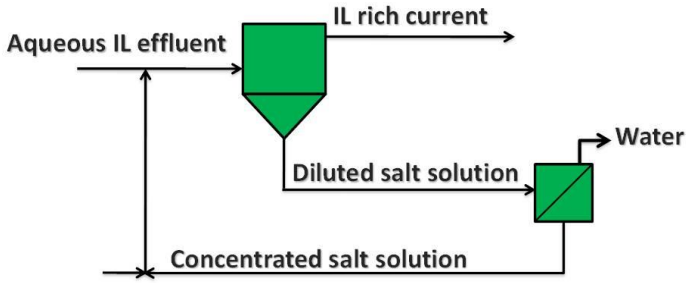

Figure 4.6. Configuration of the global process for the recovery of ILs from aqueous effluents.

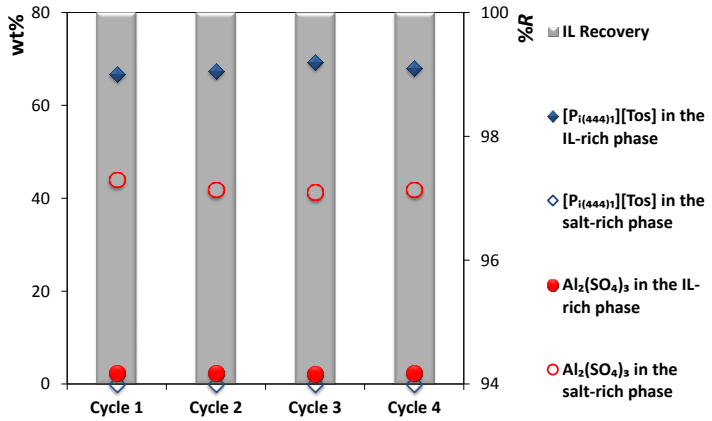

Figure 4.7. Recovery of [$P_{i(444)1}$][Tos] in several cycles using 16 wt% $Al_2(SO_4)_3$ + 45 wt% IL, and concentration of salt and IL in both aqueous phases at the end of each cycle.

Since we are dealing with two charged species, one of the main concerns is the possibility of ion exchange. Therefore, aiming at evaluating if any ion exchange is occurring during the formation of ABS and further phase separation – to check if the ionic liquid recovered is a non-contaminated fluid – several analytical and spectroscopic techniques were

applied to the characterization of the recovered coexisting phases of the systems composed of $[P_{i(444)1}][Tos]$ and $[C_4C_1im][N(CN)_2]$. The detection of the sulphate anion was carried out with Fourier Transform Infrared spectroscopy. The Al^{3+} and $[P_{i(444)1}]^+$ cations, at both aqueous phases, were quantified by Inductively Coupled Plasma Optical Emission Spectrometry. The imidazolium cation and tosylate anion contents were quantified by UV-Vis spectroscopy. From the results obtained we can guarantee that there is no ion exchange in these systems, and that the amount of each ion at each phase is in good agreement with those estimated from the tie-lines.

The thermophysical properties of the coexisting phases are of crucial relevance to evaluate the applicability and potential scale up of the process here proposed. Therefore, the density, viscosity, conductivity and pH values of the coexisting phases were measured for ABS composed of 15 wt% of $Al_2(SO_4)_3$ + 45 wt% of water + 40 wt% of ionic liquid, and 2 wt% of $AlK(SO_4)_2$ + 45 wt% of water + 51 wt% of ionic liquid. The data obtained at 298 K are reported in Table 4.4. The compositions of each phase correspond to the TLs compositions reported in Table 4.2.

The results obtained indicate that for almost all systems the two phases present low pH values. Although these low pH values are a result of the acidic nature of the inorganic salt by itself (pH = 2.12 for an aqueous solution with 15 wt% of $Al_2(SO_4)_3$ and pH = 3.15 for an aqueous solution with 5 wt% of $AlK(SO_4)_2$), the influence of the ionic liquid is also noted. The greatest impact is shown in ABS containing ionic liquids with the alkaline anion $[N(CN)_2]^-$ that increases the pH values of the phases (albeit remaining acidic). This trend was previously verified by us with a distinct inorganic salt and a broad number of ionic liquids.[70]

The conductivity of the coexisting phases in IL-based ABS is here reported for the first time. This property is also crucial since it reflects the charge density of the phase and the mobility of the ions in aqueous solutions. The values obtained range between (10.5 and 46.4) $mS \cdot cm^{-1}$ for $[P_{i(444)1}][Tos]$ and $[CF_3SO_3]$-based ionic liquids, respectively, in the IL-rich phase and with the salt $Al_2(SO_4)_3$. Regarding the salt-rich phase the values range between

6.20 mS·cm^{-1} for [C_4C_1im][Tos] and 32.0 mS·cm^{-1} for the system composed of [C_4C_1im][CF_3SO_3] and $AlK(SO_4)_2$.

Table 4.4. Experimental data of pH, conductivity (κ), density (ρ) and viscosity (η) of the coexisting phases in diverse ABS composed of 40 wt% of IL + 15 wt% of $Al_2(SO_4)_3$ + 45 wt% of H_2O or 51 wt% of IL + 2 wt% of $AlK(SO_4)_2$ + 47 wt% of H_2O at 298 K.

IL	Phase	pH	κ / (mS·cm^{-1})	ρ / (g·cm^{-3})	η / (mPa·s)
			$Al_2(SO_4)_3$		
[C_2C_1im][CF_3SO_3]	IL	1.72	46.4	1.2394	3.7823
	Salt	1.63	13.7	1.2911	12.214
[C_4C_1im][CF_3SO_3]	IL	1.84	46.4	1.2374	3.7387
	Salt	1.72	19.7	1.2899	12.128
[C_4C_1im][Tos]	IL	2.58	13.4	1.1355	9.3852
	Salt	1.58	6.20	1.2969	15.568
[C_4C_1im][$N(CN)_2$]	IL	4.82	44.1	1.0415	4.5958
	Salt	2.53	13.5	1.3135	17.177
[C_8py][$N(CN)_2$]	IL	5.07	24.6	1.0105	11.372
	Salt	2.61	17.9	1.2630	8.8931
[(C_7H_7)C_1im][$C_2H_5SO_4$]	IL	1.81	20.3	1.1642	6.9866
	Salt	1.51	13.2	1.3061	15.242
[$P_{i(444)1}$][Tos]	IL	1.45	10.5	1.0709	14.363
	Salt	0.98	13.2	1.2802	10.527
[P_{4444}]Br	IL	1.23	15.8	1.0591	19.382
	Salt	1.00	21.0	1.2696	8.1799
[P_{4444}]Cl	IL	1.35	21.6	0.9999	12.795
	Salt	1.20	7.78	1.2928	13.020
[P_{4441}][CH_3SO_4]	IL	1.87	12.8	1.0495	10.385
	Salt	1.52	7.94	1.3045	14.579
			$AlK(SO_4)_2$		
[C_4C_1im][CF_3SO_3]	IL	3.83	29.2	1.1632	3.9547
	Salt	3.03	32.0	1.0596	1.3749
[C_8py][$N(CN)_2$]	IL	5.77	25.4	1.0088	6.921
	Salt	3.74	18.8	1.0396	1.6005

The density and viscosity are relevant properties when envisaging the application of these systems in a large scale at an industrial level. Concerning the $Al_2(SO_4)_3$, the viscosity of the IL-rich phase ranges from 3.74 mPa·s for the system containing [C_4C_1im][CF_3SO_3] to 19.4 mPa·s for the system composed of [P_{4444}]Br. On the other hand, in the salt-rich phase, the

values range between (8.18 and 17.2) mPa·s for the ionic liquids $[P_{4444}]Br$ and $[C_4C_1im][N(CN)_2]$, respectively. Albeit it was expected the IL-rich phase to be more viscous, this is not observed for most of the systems evaluated. Indeed, this trend is only verified in the systems composed of $[C_8py][N(CN)_2]$, $[P_{4444}]Br$ and $[P_{i(444)1}][Tos]$. These ionic liquids present a larger biphasic region and, consequently, their concentration at the salt-rich phase is smaller when compared with other ionic liquids. This can also be explained by the amount of water at the coexisting phases, since these systems present lower water contents at the IL-rich phase. Comparing the viscosity of $[C_4C_1im][CF_3SO_3]$-based ABS formed with other salts[291] and sugars,[287] the data here reported indicate slightly higher viscosities, albeit well below to those displayed by common polymer-based ABS.[293–295] With the salt $AlK(SO_4)_2$, the viscosity is higher for the IL-rich phase (3.95 mPa·s for the system containing $[C_4C_1im][CF_3SO_3]$ and 6.92 mPa·s for the system with $[C_8py][N(CN)_2]$) when compared with the salt-rich phase, and is generally lower when compared with those displayed by the salt $Al_2(SO_4)_3$.

The density data shows that, for almost all systems, the salt-rich phase is denser than the IL-rich phase. The exception to that rule is the system with $[C_4C_1im][CF_3SO_3]$ and $AlK(SO_4)_2$, and where an inversion of the phases was observed. These results are in close agreement with other systems previously reported.[67,288,293] This is a direct consequence of the low concentration of salt at the IL-rich phase and of the high density of the fluorinated ionic liquid.[287] The values for the IL-rich phase range from 1.00 $g \cdot cm^{-3}$ for the system containing the $[P_{4444}]Cl$ and 1.24 $g \cdot cm^{-3}$ for system employing the $[C_2C_1im][CF_3SO_3]$. For the salt-rich phase the values range between 1.04 $g \cdot cm^{-3}$ for the system with $[C_8py][N(CN)_2]$ + $AlK(SO_4)_2$ and 1.31 $g \cdot cm^{-3}$ for the aqueous system composed of $[C_4C_1im][N(CN)_2]$ + $Al_2(SO_4)_3$. In general, the systems here reported present lower densities than the ones already reported in literature and making use of ionic liquids and distinct salts,[69,291] as well as those involving polymers.[293–295]

4.4. Conclusions

This work discloses a novel and efficient method to remove and recover ionic liquids from contaminated water streams. It makes use of the strong salting-out inducing ability of aluminium-based salts to create ABS that allow the removal of hydrophilic ionic liquids from diluted aqueous solutions by concentrating them into a second liquid phase. Aiming at gathering a broader picture on the amount of salts necessary to treat the contaminated effluents, the ternary phase diagrams, critical points, TLs and TLLs were determined at 298 K. The addition of $Al_2(SO4)_3$ and $AlK(SO_4)_2$ to aqueous solutions containing ionic liquids leads, for most of the systems, to a recovery efficiency of *circa* 100%, while reducing the ionic liquid concentration in the aqueous solution from 45 wt% to values around 1 wt%. By applying several cycles in the process here proposed, it was possible to guarantee that the salt can be recycled and the ionic liquid is completely recovered.

The results here obtained constitute the first report on a complete recovery of ionic liquids from aqueous solutions making use of inorganic salts already used in water treatment processes, and could represent a major contribution for the development of industrial processes based in ionic liquids.

Chapter 5 – Removing Ionic Liquids from Aqueous Solutions by Adsorption

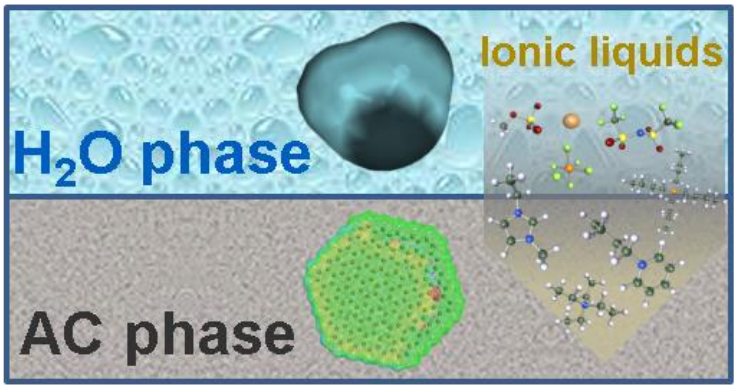

5.1. Introduction

As it is well-known, the intrinsic non-volatile nature of ionic liquids (ILs) provides an opportunity to reduce, or even completely eliminate, hazardous and toxic emissions to the atmosphere. However, the application of ionic liquids at industrial scale may involve an environmental risk resulting from their transport, storage and, even ionic liquids cannot contribute to air pollution, they present a non-negligible solubility in water,[5–7,10,11,157] and their release into aquatic media raises serious environmental concerns.[64,108] Therefore, the search of novel methods/techniques to remove ionic liquids from aqueous environments is of outmost importance. There are some previous studies regarding the removal of ionic liquids from aqueous streams.[44,83,92,95,98–100,102,296–308] Amongst those, some of them use destructive methods such as advanced oxidation[83,296,297] or biological treatments.[44,299,300] However, when envisaging sustainable technologies, the degradation of ionic liquids should be avoided and they should be recovered and recycled instead.[108] There are also some non-destructive methods already reported in the literature, such as distillation,[301] crystallization,[302] nanofiltration,[303] pervaporation,[304] phase separation[298] and adsorption.[95] Among the non-destructive techniques, the adsorption onto activated carbon (AC) proved to be able to remove different ionic liquids from aqueous solutions.[95,98,99,308] Anthony et al.[92] were the first to propose the use of activated carbon for the adsorption of 1-butyl-3-methylimidazolium hexafluorophosphate. More recently, Palomar and co-workers[95,100] reported a detailed study on the adsorption of different ionic liquids into activated carbon. Besides the adsorption step, the recovery of the ionic liquid was further attempted by the addition of acetone.[95]

ACs are interesting candidates among other adsorbents[309] due to their high surface area, surface chemistry tailoring, harmfulness to the environment and easy handling in operation.[310] Previous adsorption equilibrium studies[98–100] confirmed that the structural properties and chemical surface of the AC can be conveniently modified to adsorb efficiently imidazolium-based ionic liquids with different chemical nature, indicating the viability of ionic liquid adsorption from a thermodynamic point of view.

Therefore, the investigation of ionic liquid adsorption onto AC in aqueous solution is here extended by measuring the equilibrium isotherms of different ionic liquids based on 6 cation families (imidazolium, pyridinium, ammonium, phosphonium, piperidinium and pyrrolidinium), including different lengths of alkyl side chains and 6 different anions. Expanding the range of ionic liquids studied in previous works[95,99] to a total of 48, it was possible an exhaustive study of the structure influence in the adsorption of ionic liquids onto AC. The main objective is to analyse the influence of structural ionic liquid elements on the adsorption capacity of a commercial AC to recover the ionic liquid solute from water solution.

Nevertheless, unlike for hydrophobic ionic liquids, for hydrophilic compounds this method is not as effective due to the low polarity of the AC surface.[95,308] It is well-known that the addition of salting-out species to aqueous media, like inorganic or organic salt ions, leads to a decrease on the solubility of hydrophobic ionic liquids in water,[66] and can even induce phase separation with hydrophilic or completely water-soluble ionic liquids.[65] Therefore, the salting-out ability of an inorganic salt, Na_2SO_4, a strong salting-out inducing salt that does not change the medium pH when dissolved in aqueous medium,[66,70] was evaluated on the adsorption of different ionic liquids (hydrophobic and hydrophilic) onto AC. It was already shown that Na_2SO_4 can promote the phase separation when combined with hydrophilic ionic liquids in aqueous solutions,[70] and that it can decrease the solubility of highly hydrophobic and fluorinated ionic liquids in water.[66]

In order to complement the experimental measurements, the COnductor like Screening MOdel for Real Solvents (COSMO-RS), a quantum chemical-based prediction model, which provides thermodynamic property estimations and intermolecular interaction analysis, was used to well understand the equilibrium data of the ionic liquid distribution between AC and water phases from a molecular point of view, and to better evaluate the salt effect in the adsorption of ionic liquids onto AC.

5.2. Experimental procedure

5.2.1. Materials

The ionic liquids used in this study as adsorbates were in the highest purity available. The ionic liquids were used without previous purification. Table 5.1 provides a list of the ionic liquids used in this study, their source and purity. The structures of the ionic liquids used are depicted in Figure 5.1.The purity of all ionic liquids was also confirmed by ^{1}H and ^{13}C NMR, and ^{19}F and ^{31}P NMR whenever applicable.

Table 5.1. Name, acronym, purity and supplier of the ILs used in this work.

IL		Purity (%)	Supplier	Structure
Name	Acronym			
1-methyl-1-propylpiperidinium bis(trifluoromethylsulfonyl)imide	$[C_3C_1pip][NTf_2]$	99	Iolitec	(i)
3-methyl-1-propylpyridinium bis(trifluoromethylsulfonyl)imide	$[C_3\text{-}3\text{-}C_1py][NTf_2]$	99	Iolitec	(ii)
1-butyl-3-methylpyridinium bis(trifluoromethylsulfonyl)imide	$[C_4\text{-}3\text{-}C_1py][NTf_2]$	99	Iolitec	(iii)
1-methyl-1-propylpyrrolidinium bis(trifluoromethylsulfonyl)imide	$[C_3C_1pyr][NTf_2]$	99	Iolitec	(iv)
1-ethylimidazolium bis(trifluoromethylsulfonyl)imide	$[C_2im][NTf_2]$	98	Iolitec	(v)
1,3-dimethylimidazolium bis(trifluoromethylsulfonyl)imide	$[C_1C_1im][NTf_2]$	99	Iolitec	(vi)
1,3-diethylimidazolium bis(trifluoromethylsulfonyl)imide	$[C_2C_2im][NTf_2]$	99	Iolitec	(vii)
1,3-dipropylimidazolium bis(trifluoromethylsulfonyl)imide	$[C_3C_3im][NTf_2]$	98	Iolitec	(viii)
1-ethyl-3-propylimidazolium bis(trifluoromethylsulfonyl)imide	$[C_2C_3im][NTf_2]$	99	Iolitec	(ix)
1-ethyl-3-methylimidazolium bis(trifluoromethylsulfonyl)imide	$[C_2C_1im][NTf_2]$	99	Iolitec	(x)
1-methyl-3-propylimidazolium bis(trifluoromethylsulfonyl)imide	$[C_3C_1im][NTf_2]$	99	Iolitec	(xi)
1-butyl-3-methylimidazolium bis(trifluoromethylsulfonyl)imide	$[C_4C_1im][NTf_2]$	99	Iolitec	(xii)
1-methyl-3-pentylimidazolium bis(trifluoromethylsulfonyl)imide	$[C_5C_1im][NTf_2]$	99	Iolitec	(xiii)

1-butyl-3-methylimidazolium trifluoromethanesulfonate (triflate)	$[C_4C_1im][CF_3SO_3]$	99	Iolitec	(xiv)
1-butyl-3-methylimidazolium methanesulfonate	$[C_4C_1im][CH_3SO_3]$	99	Iolitec	(xv)
-butyl-3-methylimidazolium chloride	$[C_4C_1im]Cl$	99	Iolitec	(xvi)
Tetrabutylammonium chloride	$[N_{4444}]Cl$	97	Sigma-Aldrich	(xvii)
Tetrabutylphosphonium chloride	$[P_{4444}]Cl$	97	Cytec	(xviii)
1-butyl-3-methylimidazolium tosylate	$[C_4C_1im][Tos]$	98	Iolitec	(xix)
tri(isobutyl)methylphosphonium tosylate	$[P_{i(444)1}][Tos]$	98	Cytec	(xx)
1-butyl-3-methylimidazolium methylsulphate	$[C_4C_1im][CH_3SO_4]$	95	Iolitec	(xxi)
1-butyl-3-methylimidazolium octylsulphate	$[C_4C_1im][C_8H_{17}SO_4]$	95	Iolitec	(xxii)
1-butyl-3-methylimidazolium acetate	$[C_4C_1im][CH_3CO_2]$	95	Sigma-Aldrich	(xxiii)
1-ethylpyridinium hexafluorophosphate	$[C_2py][PF_6]$	99	Iolitec	(xxiv)
1-hexylpyridinium hexafluorophosphate	$[C_6py][PF_6]$	99	Iolitec	(xxv)

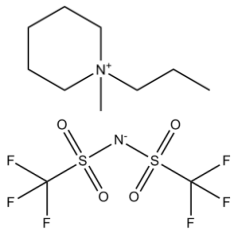

(i)

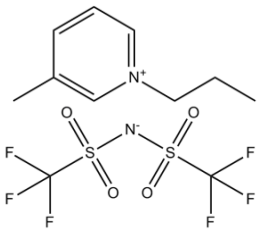

(ii)

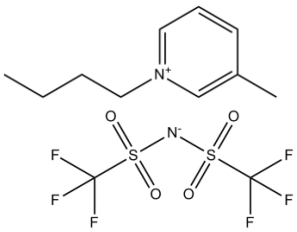

(iii)

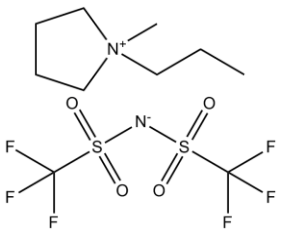

(iv)

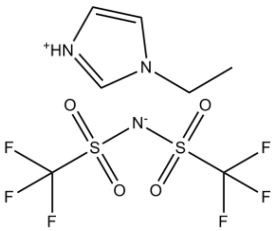

(v)

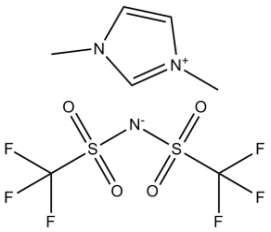

(vi)

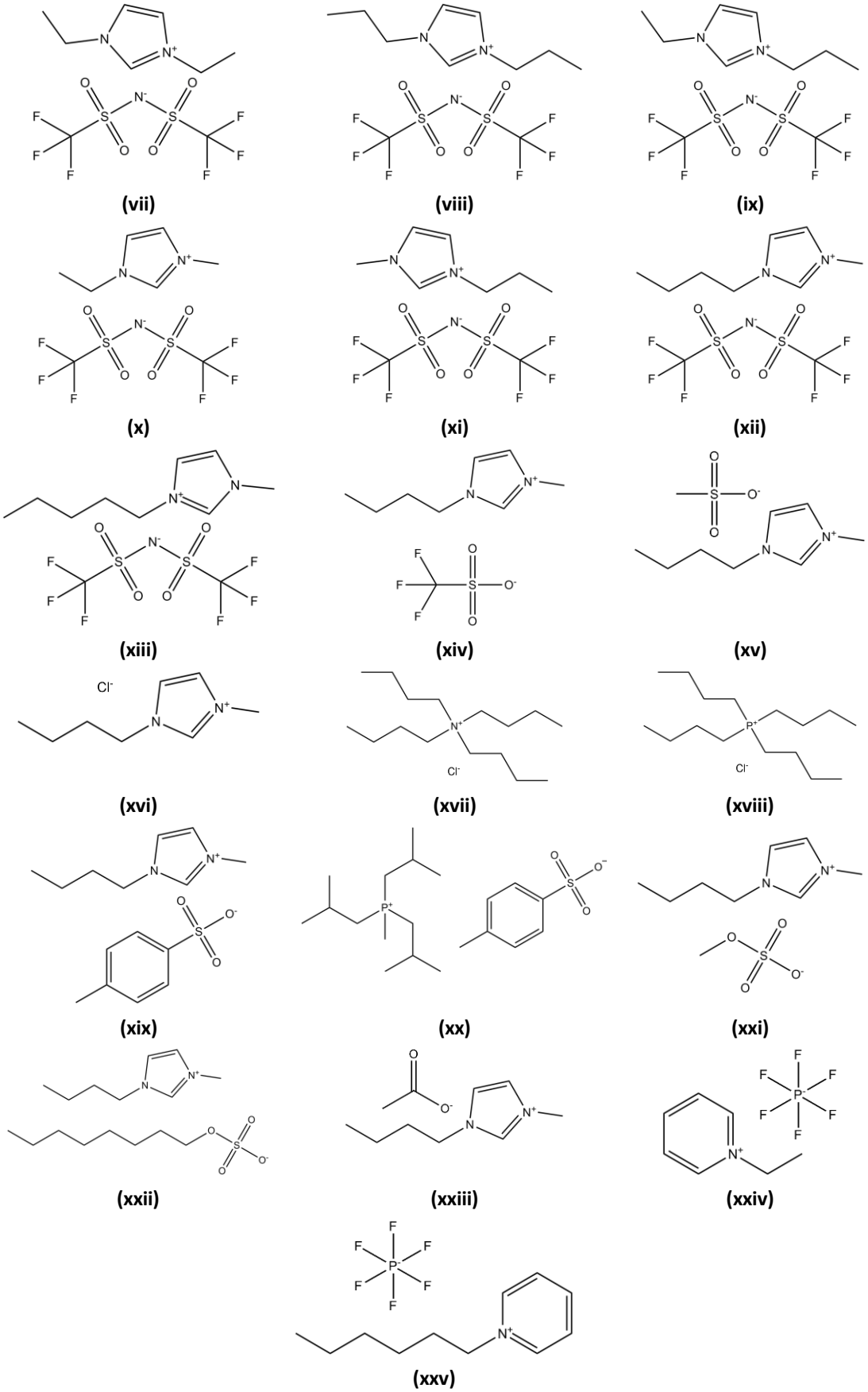

Figure 5.1. Chemical structures of the ILs here studied.

The inorganic salt sodium sulphate (Na_2SO_4) was acquired from Sigma-Aldrich with a mass fraction purity above 99%. The commercial AC was supplied by Merck (AC-MkU) and was used as adsorbent. The AC used in this work has a surface BET area of 927 $m^2 \cdot g^{-1}$ with high micropore volume contribution ($V_{microp.}$ = 0.36 $cm^3 \cdot g^{-1}$ and $V_{mesop.}$ = 0.14 $cm^3 \cdot g^{-1}$) and a relatively low concentration of surface functional groups, as reported before.[311]

5.2.2. Methods

ADSORPTION

The experiments were conducted in glass bottles (100 mL) at 308 K, using 50 mL of water or of each salt solution with the ionic liquid in a concentration ranging from 100 to 500 $mg \cdot L^{-1}$. The ionic liquid concentrations used are below of ionic liquid saturation in water.[5–7,13,15] The concentrations of the different salt solutions varied between 0.28 and 1.76 $mol \cdot kg^{-1}$. Then 12.5 mg of AC was added to the water or aqueous salt solutions and placed in an orbital incubator (Julabo Shake Temp, model SW-22) at 200 rpm, and left for, at least, four days. This time proved to be the minimum time necessary to reach the equilibrium.[95] After this period, the samples were removed and the ionic liquids content was quantified. The concentration of imidazolium-, pyridinium- and tosylate-based ionic liquids was determined by UV spectroscopy (Varian, model Cary 1E) at 212, 266 and 222 nm, respectively. The concentration of ammonium, phosphonium-, pyrrolidinium- and piperidinium-based ionic liquids were determined by conductivity measurements (with an uncertainty of ± 0.02), at room temperature, using a Mettler Toledo S47 SevenMulti™ dual meter pH/conductivity equipment.[13] In both methods, the quantification was achieved through calibration curves previously established. The data obtained was fitted with the Langmuir model (eq 5.1),

$$q_e = \frac{q_{max} \times B \times C_e}{1 + B \times C_e} \quad (5.1)$$

where B ($L \cdot mmol^{-1}$) and q_{max} ($mmol \cdot g^{-1}$) are empirical coefficients of the Langmuir equation, C_e ($mmol \cdot L^{-1}$) is the equilibrium concentration of adsorbate in the fluid phase and q_e ($mmol \cdot g^{-1}$) is the equilibrium concentration of adsorbate in the solid phase.[95]

The apparent distribution coefficients (K_d, L·kg^{-1}) of each system were calculated taking into consideration eq 5.2:

$$K_d = \frac{q_e}{C_e} \times 1000 \quad (5.2)$$

This coefficient evaluates the capacity of AC for the adsorption of different ionic liquids at the same equilibrium concentration.

COSMO-RS

The molecular geometry of all molecular models (AC, water, ions of the Na_2SO_4 salt and ion-paired structures of ionic liquids) were optimized at B3LYP/6-31++G** computational level[312,313] in the ideal gas-phase using quantum chemical Gaussian03 package.[312,313] The ionic liquid adsorptive capacity was described by an ion-pair structure, the aqueous media by individual water molecule and AC adsorbent by a mixture of two AC structures[95] in a 90/10 molar AC/AC-OH ratio, in order to introduce in the simulation the measured concentration of oxygenated groups of the MkU activated carbon.[98,100] Vibrational frequency calculations were performed for each case to confirm the presence of an energy minimum. Then, the standard procedure was applied for COSMO-RS calculations, which consists of two steps: first, Gaussiano03 was used to compute the COSMO files. The ideal screening charges on the molecular surface for each species were calculated by the continuum solvation COSMO model using BVP86/TZVP/DGA1 level of theory.[313,314] Subsequently, COSMO files were used as an input in COSMOtherm[315] code to calculate the thermodynamic properties of the binary IL-AC/H_2O mixtures [Interaction energy between ionic liquid and AC ($E_{IL\text{-}AC}$) or H_2O ($E_{IL\text{-}H2O}$)] and the ternary systems involved in the adsorption phenomena [Partition coefficient of ionic liquid between water and AC phases, log(P)]. The AC/water partition coefficient, log$P$, of ionic liquid at infinite dilution was calculated by COSMO-RS at 298 K.

The octanol–water partition coefficient (K_{ow}) and AC/water/salt partition coefficient (P) of each ionic liquid at infinite dilution was calculated with COSMO-RS at 308 K. According to the quantum method chosen, the functional and the basis set, the corresponding

parameterization (BP_TZVP_C30_0210 and BP_TZVP_ C30_1201[315], for IL/H_2O and IL/salt solutions systems, respectively) for COSMO-RS calculations in COSMOtherm code was used.

5.3. Composition and structural effects on the adsorption of ionic liquids onto activated carbon

Jesús Lemus, Catarina M. S. S. Neves, Carlos F. C. Marques, Mara G. Freire, João A. P. Coutinho and Jose Palomar, Environmental Science: Processes & Impacts 15 (2013) 1752-1759, DOI: 10.1039/C3EM00230F

5.3.1. Abstract

The applications and variety of ionic liquids have increased during the last years, and their use at large scale will require their removal/recovery from wastewater streams. Adsorption on ACs has been recently proposed for this purpose and this work presents a systematic analysis of the influence of the ionic liquid structure (cation side chain, head group, anion type and the presence of functional groups) on its adsorption onto commercial AC from water solution. It has been here experimentally measured the adsorption of 21 new ionic liquids, which includes imidazolium-, pyridinium-, pyrrolidinium-, piperidinium-, phosphonium- and ammonium-based cations and different hydrophobic and hydrophilic anions. This contribution allows to expand the range of ionic liquid compounds studied in previous works, and permits a better understanding of the influence of the ionic liquids structure in the adsorption on the AC. In addition, the COSMO-RS method was used to analyse the measured adsorption isotherms, allowing understanding the role of the cationic and anionic structure in the adsorption process, in terms of the different interactions between the ionic liquid compound and AC surface/water solvent. The results of this work provide new insights for the development of adsorption as an effective operation to remove/recover ionic liquids with very different chemical nature from water solution.

5.3.2. Results and discussion

The adsorption from water solution of 21 ionic liquids onto a commercial AC (AC-MkU), with high micropore volume contribution and a relatively low concentration of surface functional groups,[311] was measured and compared with the adsorption results of other 36 ionic liquids.[95,99] This AC-MkU was previously reported as an effective adsorbent to remove imidazolium ionic liquids from aqueous solution, being its adsorption capacity strongly determined by the hydrophobic/hydrophilic character of the anion and the cation constituting the ionic liquid, as consequence of the different interactions such as polar, van der Waals and hydrogen bonding.[95,99] The wide range of ionic liquids investigated in the current study allows a systematic evaluation of the influence of the cation family, anionic and cationic substituents and type of anion on the adsorption of the ionic liquid onto AC-MkU.

Figure 5.2 shows the adsorption isotherms at 308 K of four ionic liquids with common anion ($[NTf_2]^-$) and alkyl side chains (C_3C_1) and different head group, as representative cases of pyridinium, imidazolium, pyrrolidinium and piperidinium families. The results indicate that ionic liquids with cation based on aromatic ring present higher adsorption capacity than the corresponding aliphatic ones, following the order pyridinium > imidazolium > pyrrolidinium > piperidinium.

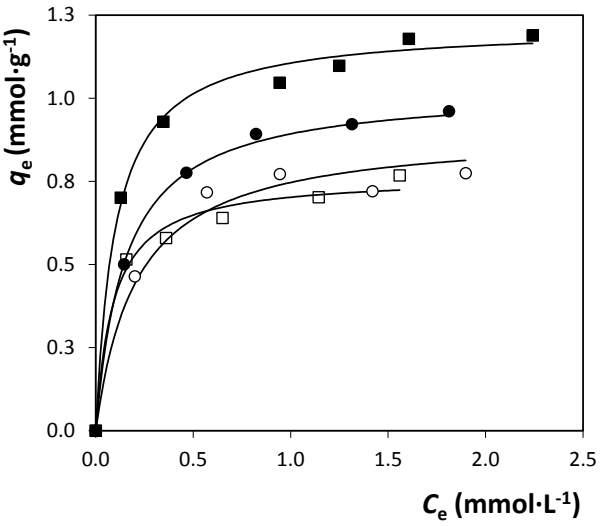

Figure 5.2. Experimental equilibrium data (dots) and Langmuir fits (curves) for the adsorption isotherms onto AC-MkU at 308 K of (□), $[C_3C_1pip][NTf_2]$; (○), $[C_3C_1pyr][NTf_2]$; (●), $[C_3C_1im][NTf_2]$ and (■), $[C_3\text{-}3\text{-}C_1py][NTf_2]$.

Other factor to take into account is the number and size of the alkyl chain substituents on the cation. The adsorption isotherms presented in Figure 5.3 allow the evaluation of the effect of these structural differences on the adsorption for a series of $[C_nC_nim][NTf_2]$ with different chain lengths. The results show that the increase of the number of carbon atoms in the alkyl chain of the imidazolium cation increase the adsorption with a maximum value for $[C_5C_1im][NTf_2]$, for the cases studied. The adsorption seems to be proportional to the molar volume of the cation, relating the total number of carbon atoms in its substituents, that presents similar adsorption on AC-MkU ($C_1C_1 \approx C_2$, $C_3C_1 \approx C_2C_2$, $C_4C_1 \approx C_2C_3$ and $C_5C_1 \approx C_3C_3$), with the asymmetric cations being slightly more adsorbed onto AC-MkU.

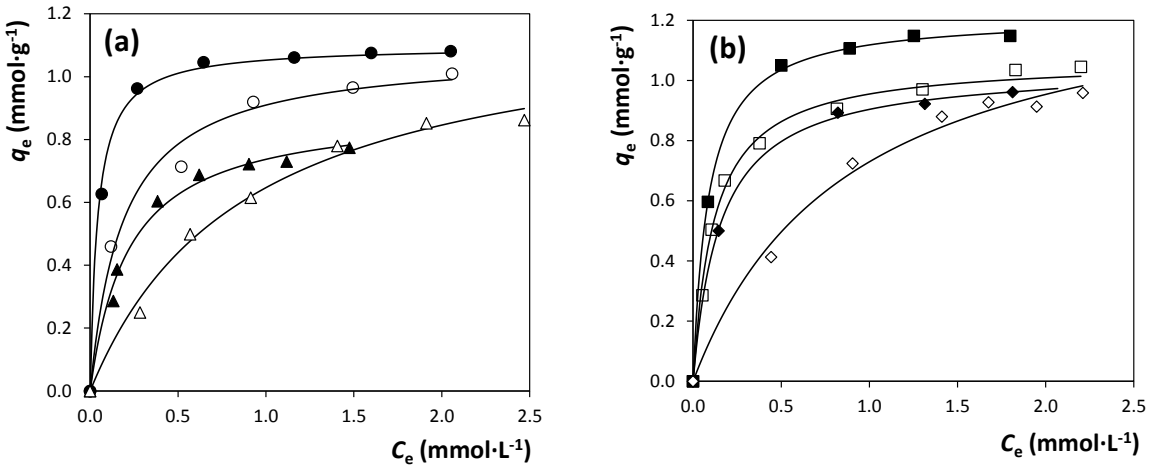

Figure 5.3. Experimental equilibrium data (dots) and Langmuir fits (curves) for the adsorption isotherms onto AC-MKU at 308 K of $[NTf_2]$-based ILs using as cation: (△),$[C_1C_1im]^+$; (▲), $[C_2C_2im]^+$; (○), $[C_2C_3im]^+$; (●), $[C_3C_3im]^+$; (◇),$[C_2im]^+$; (◆), $[C_3C_1im]^+$; (□), $[C_4C_1im]^+$ and (■), $[C_5C_1im]^+$.

The functionalization on the anion was investigated in order to establish what characteristics produce ionic liquids with a higher affinity towards the AC. Figure 5.4a shows the measured adsorption isotherms at 308 K for five $[C_4C_1im][X]$ ionic liquids. Concerning the sulfonate-based anions $[R\text{-}SO_3]$, it is possible to observe that the benzyl substituent ($[Tos]^-$) promotes the highest uptake, followed by the CF_3- ($[CF_3SO_3]^-$, triflate) and the CH_3- ($[CH_3SO_3]^-$, methylsulfonate). Similar substituent effects are observed for acetate-based ([R-COO]) anions (Figure 5.4a), but with a much less remarkable effect. Figure 5.4b shows that an increment in the number of carbon atoms in the alkyl chain of the anion (for example, from methylsulphate to octylsulphate) enhances remarkably the adsorption capacity in a way similar to that of increasing the length of the alkyl chain of the imidazolium cation with common anion (such as from $[C_2C_1im]Cl$ to $[C_8C_1im]Cl$ as shown in Figure 5.4b). Moreover, it is found that the presence of aromatic substituents in the cation (as in $[(C_7H_7)C_1im]Cl$) also leads to higher adsorption capacities onto AC-MkU (Figure 5.4b), in a similar effect observed when this substituent is located in the anion.

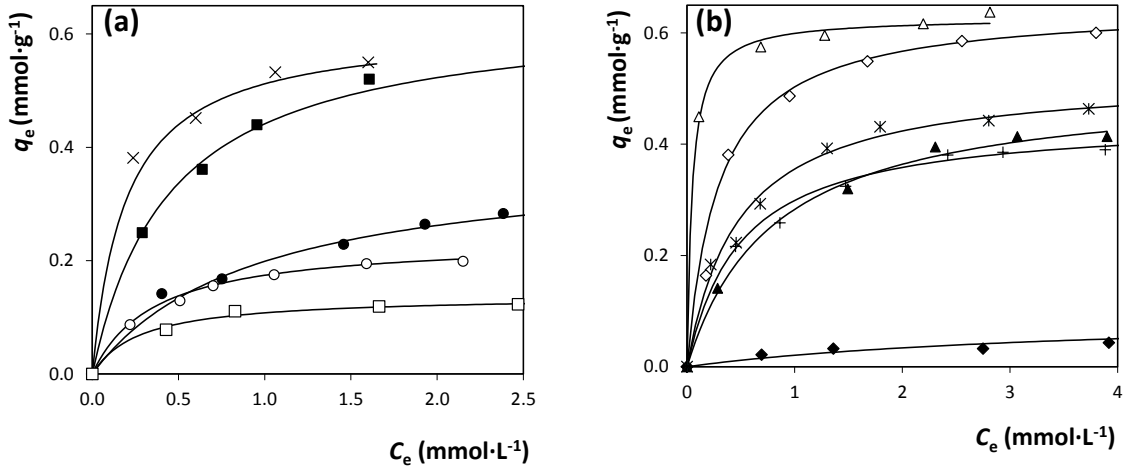

Figure 5.4. Experimental equilibrium data (dots) and Langmuir fits (curves) for the adsorption isotherms onto AC-MkU at 308 K of (×), $[C_4C_1im][Tos]$; (■), $[C_4C_1im][CF_3SO_3]$;[95] (●), $[C_4C_1im][CF_3CO_2]$ (1-butyl-3-methylimidazolium trifluoroacetate);[95] (○), $[C_4C_1im][CH_3CO_2]$; (□), $[C_4C_1im][CH_3SO_3]$;[95] (△), $[C_4C_1im][C_8H_{17}SO_4]$; (◇), $[C_8C_1im]Cl$;[95] (∗), $[(C_7H_7)C_1im]Cl$;[95] (▲), $[C_4C_1im][CH_3SO_4]$; (+), $[C_6C_1im]Cl$ and (◆), $[C_2C_1im]Cl$.[99]

Finally, Figure 5.5 shows a summary of the effects of the anion on ionic liquid adsorption for various cation families in terms of the apparent adsorption coefficient (K_d) obtained from the experimental isotherms at 308 K with AC-MkU. It can be appreciated that ionic liquids based on hydrophobic anion as $[NTf_2]^-$ and $[PF_6]^-$ present the highest absorption, independent of the cation, which indicates a major influence of the anion nature on the adsorption of ionic liquids by ACs from aqueous solution. However, the type of cation also clearly affects the amount of ionic liquid adsorbed by AC-MkU, where a more efficient adsorption is achieved when the hydrophobic or the aromatic character of the cation is increased.

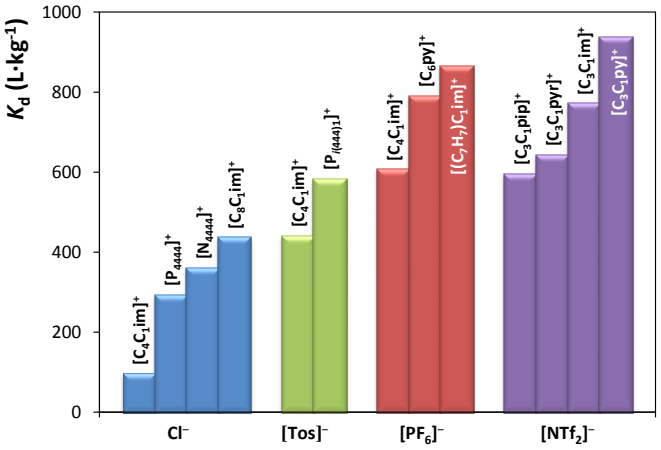

Figure 5.5. Comparison of K_d (obtained when C_e = 1.2 mmol·L^{-1} on AC-MkU at 308 K) for different ILs.

In order to better understand the adsorption behaviour of the ionic liquids from aqueous solutions onto ACs, an analysis based on the COSMO-RS method was carried out. Table 5.2 reports the COSMO-RS predicted values of molecular volume (Å^3) of the ionic liquids, the partition coefficients, log(*P*), of ionic liquid between AC and H_2O phases at infinite dilution, and the experimentally obtained apparent adsorption coefficient (K_d) values onto the AC-MkU at 308 K for the 48 ionic liquids studied so far,[95,99] arranged by experimental adsorption capacity. Figure 5.6 compares the experimental K_d and the theoretical log(*P*) values for 32 imidazolium-based ionic liquids with molecular volume under 0.4 nm^3, since it is reported that ionic liquids with higher molecular size present lower adsorption onto AC due to steric effects.[99] The results show a good correlation between experimental and theoretical values for the wide array of 33 ionic liquid compounds, indicating the suitability of COSMO-RS approach to describe the adsorption behaviour of ionic liquids onto ACs from aqueous solution.

Table 5.2. Supplier, molecular volume, log(*P*) of IL calculated by COSMO-RS and experimental K_d, (obtained for the C_e = 1.2 mmol·L^{-1} at 308 K using AC-MkU as adsorbent) of checked ILs.

IL	Volume (Å^3)	Log(*P*)	K_d (L·kg^{-1})	IL	Volume (Å^3)	Log(*P*)	K_d (L·kg^{-1})
[C_8C_1im][PF_6]	389	3.860	*1008*	[C_4C_1im][PF_6]	303	2.061	*605*
[C_5C_1im][NTf_2]	439	4.418	*945*	[C_3C_1pip][NTf_2]	427	2.763	593
[C_3-3-C_1py][NTf_2]	406	2.343	936	[C_1C_1im][NTf_2]	352	2.915	587
[C_3C_3im][NTf_2]	434	4.191	883	[$P_{i(4441)}$][Tos]	518	3.723	582
[$C_{10}C_1$im][PF_6]	432	4.601	*869*	[C_2C_1im][PF_6]	259	1.273	*528*
[(C_7H_7)C_1im][PF_6]	354	3.523	*864*	[(C_7H_7)C_1im][BF_4]	298	1.131	*515*

$[C_{10}C_1im][BF_4]$	402	3.036	*859*	$[C_4C_1im][C_8H_{17}SO_4]$	451	3.089	503
$[C_6C_1im][PF_6]$	346	2.832	*858*	$[C_6C_1im][BF_4]$	316	1.172	*465*
$[C_{12}C_1im]Cl$	408	3.914	*825*	$[C_4C_1im][Tos]$	363	1.561	439
$[C_4C_1im][NTf_2]$	420	4.002	*810*	$[C_8C_1im]Cl$	322	1.490	*435*
$[C_6C_1im][NTf_2]$	463	4.740	*801*	$[N_{4444}]Cl$	420	3.178	358
$[C_6py][PF_6]$	339	2.418	790	$[(C_7H_7)C_1im]Cl$	265	-0.423	*313*
$[C_4C_1C_1im][PF_6]$	335	-0.150	*781*	$[P_{4444}]Cl$	425	4.116	292
$[C_2C_3im][NTf_2]$	412	3.947	778	$[C_2py][PF_6]$	251	0.889	278
$[C_{14}C_1im]Cl$	451	4.784	*775*	$[C_6C_1im]Cl$	279	0.585	*264*
$[C_8C_1im][BF_4]$	359	2.112	*772*	$[C_4C_1im][CF_3SO_3]$	317	1.496	*258*
$[C_3C_1im][NTf_2]$	398	3.559	*770*	$[C_4C_1im][CH_3SO_4]$	300	0.048	254
$[C_{16}C_1im]Cl$	494	4.729	*733*	$[C_4C_1im][BF_4]$	273	0.289	*240*
$[C_{12}C_1im][BF_4]$	445	3.965	*729*	$[C_4C_1im][CF_3CO_2]$	310	2.275	*180*
$[C_2im][NTf_2]$	349	3.641	722	$[C_4C_1im][CH_3CO_2]$	268	2.108	127
$[C_{10}C_1im]Cl$	365	2.027	*655*	$[C_4C_1im]Cl$	236	-0.420	*96*
$[C_2C_2im][NTf_2]$	395	3.473	652	$[C_2C_1im][BF_4]$	229	-0.389	*74*
$[C_3C_1pyr][NTf_2]$	408	2.900	641	$[C_4C_1im][CH_3SO_3]$	289	-0.158	*58*
$[C_2C_1im][NTf_2]$	376	3.175	*633*	$[C_2C_1im]Cl$	192	-1.242	*20*

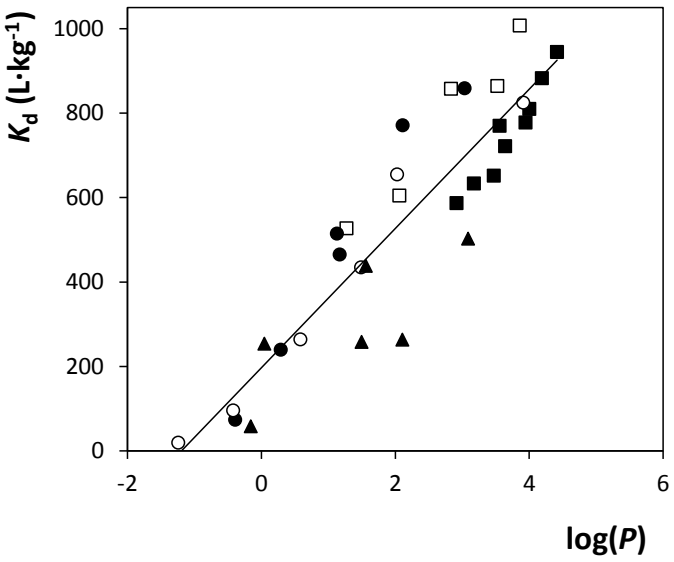

Figure 5.6. Experimental K_d *versus* predicted log(*P*) by COSMO-RS for 32 ILs with molecular volume under 0.4 nm^3 using AC-MkU as adsorbent at 308K: (■), $[NTf_2]^-$; (□), $[PF_6]^-$; (●), $[BF_4]^-$, (○), Cl^- and (▲), others.

Besides the partition coefficient, the COSMO-RS allows the discrimination between the contribution of polar-Misfit, H-bonding and van der Waals forces to the interaction energy between the ionic liquid and AC ($E_{IL\text{-}AC}$) and H_2O ($E_{IL\text{-}H2O}$) components involved in

the adsorption process. Figures 5.7 to 5.11 describe the influence of the ionic liquid structural components in the interaction energy of ionic liquid solute with the pure AC ($E_{IL\text{-}AC}$) and H_2O ($E_{IL\text{-}H2O}$) species predicted by COSMO-RS, which is related to the corresponding experimental values of K_d adsorption capacity parameter for each ionic liquid studied.

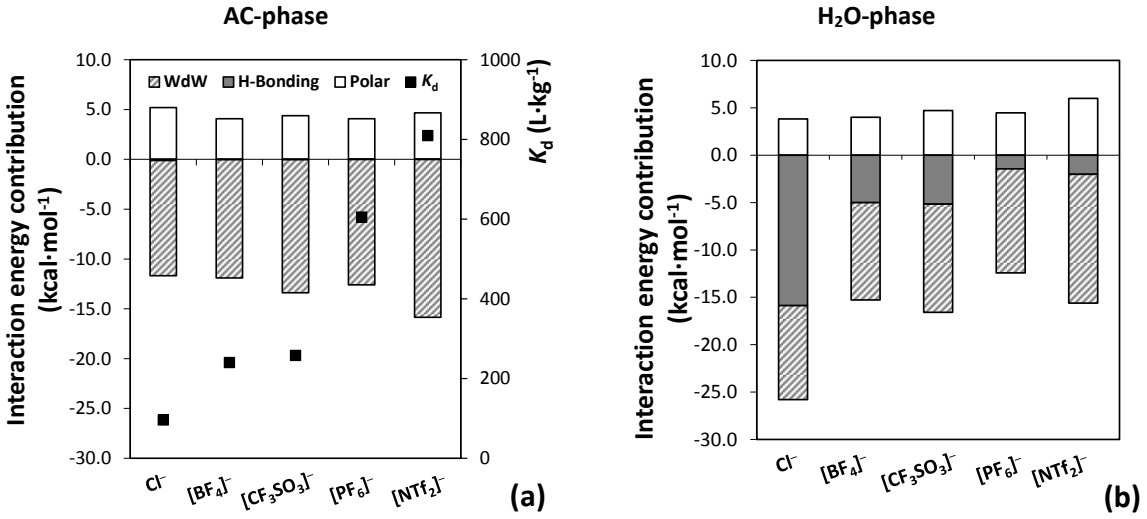

Figure 5.7. Predicted COSMO-RS contributions to interaction energies of (a) IL-AC and (b) IL–water for $[C_4C_1im]^+$ based ILs with Cl^-, $[BF_4]^-$, $[CF_3SO_3]^-$, $[PF_6]^-$ and $[NTf_2]^-$ anions.

Figure 5.7 shows the results obtained for a series of anions with common $[C_4C_1im]$ cation. It can be observed that attractive van der Waals forces dominate the interaction between the ionic liquid adsorbate and the AC adsorbent, being obtained higher adsorption capacities of AC-MkU, quantified in terms of experimental K_d, for more hydrophobic anion-based ionic liquids. This is in good agreement with the increasing attractive van der Waals interactions between ionic liquid and the AC surface, described by COSMO-RS. This result is consistent with the enhanced adsorption capacity of hydrophilic ionic liquid achieved with chemically treated ACs, which presented higher concentration of oxygenated groups in the adsorbent surface.[99] Therefore, the variation in the anion with remarkably different polarities is translated into different uptakes, where ionic liquids with hydrophobic anions ($[NTf_2]^-$ or $[PF_6]^-$) show much higher adsorption by AC-MkU than hydrophilic ionic liquids (Cl^- or $[BF_4]^-$, tetrafluoroborate), due to the stronger attractive

van der Waals between ionic liquid and AC, and the absence of hydrogen bonding interactions between ionic liquid and H_2O.

The results of the COSMO-RS analysis of the cation family effect using series of ionic liquids with common hydrophobic ($[NTf_2]^-$) or hydrophilic (Cl^-) anion are reported in Figure 5.8. It can be concluded again that the favourable van der Waals interactions between ionic liquids and AC control the adsorption of the ionic liquids onto the AC-MkU. On the other hand, as it was explained above, favourable hydrogen bonding between chlorine-based ionic liquids and water molecules lead to lower K_d values than in the case of $[NTf_2]^-$-based ionic liquids. For these later, aromatic cations (imidazolium and pyridinium) present higher uptake than cations with aliphatic rings (piperidinium and pyrrolidinium). The COSMO-RS analysis does not provide an explanation for this effect, since similarly IL-AC van der Waals interactions were predicted for all the cations. On the other hand, a better removal of the chlorine-based ionic liquids from water is clearly achieved by adsorption when increasing the hydrophobic nature of the cation, from nitrogen heterocyclic-based cations to ammonium and phosphonium tetraalkyl-substituted cations. COSMO-RS analysis indicates that this effect should be assigned to the favourable cation-AC van de Waals interaction rather than hydrogen bonding anion–water interactions.

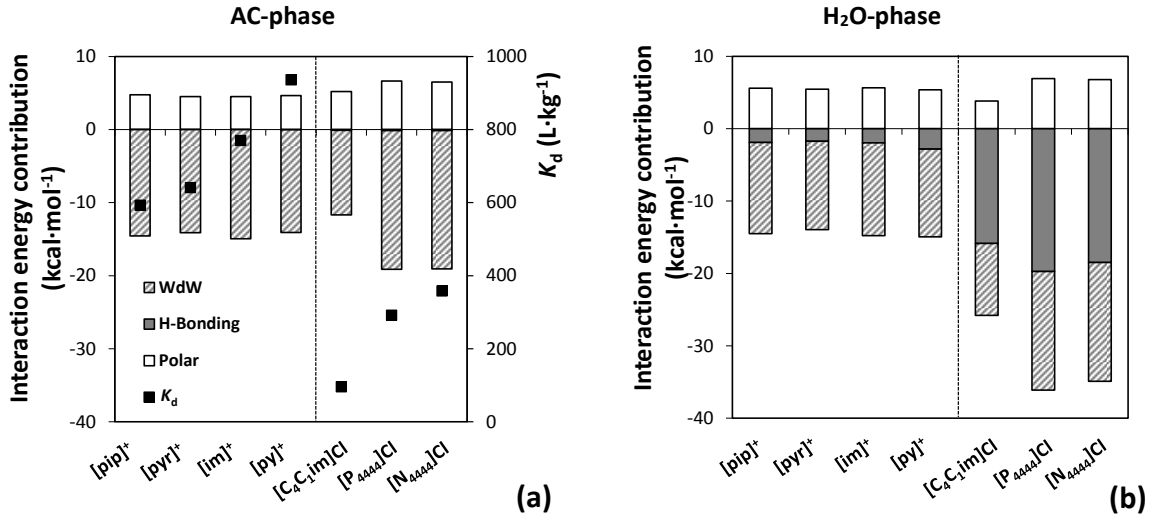

Figure 5.8. Predicted COSMO-RS contributions to interaction energies of (a) IL-AC and (b) IL-water for $[NTf_2]^-$ and Cl^--based ILs with different cation families.

The effects of the substituents in the cation and the anion of ionic liquid on adsorption effectiveness were also considered in the COSMO-RS analysis. Figure 5.9 shows, for the imidazolium cation series, based on a common [NTf_2] anion that increasing the number of carbon atoms in the alkyl chain induces higher attractive interaction energies between the ionic liquid and the AC surface, that is consistent with the higher ionic liquid adsorption measured.

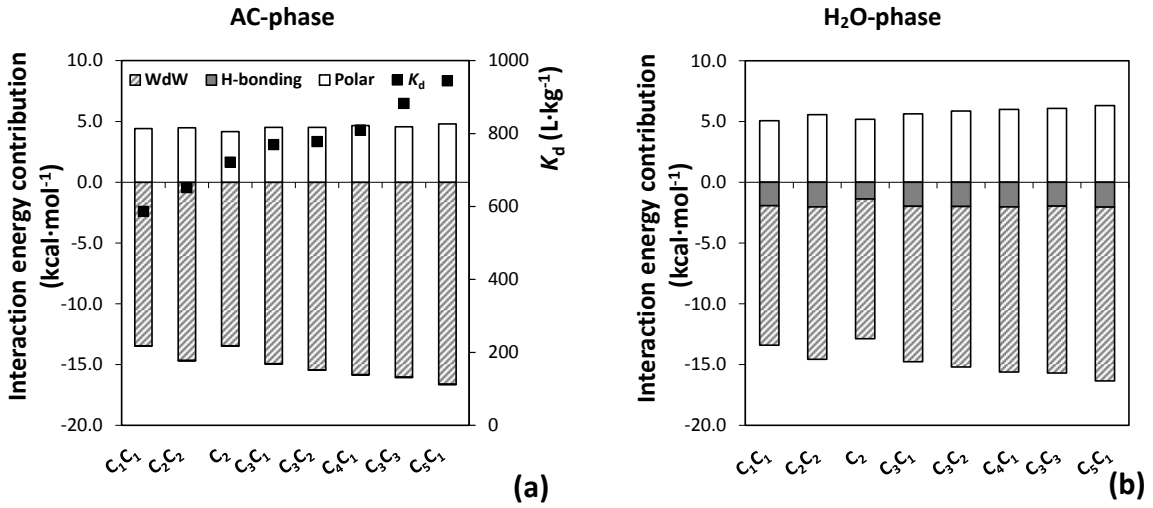

Figure 5.9. Predicted COSMO-RS contributions to interaction energies of IL-AC (a) and IL-water (b) for [$C_nC_m$im][NTf_2] based ILs with different alkyl chain substituents.

Similarly, Figure 5.10 shows that modifying the substituent of the anion for the case of ionic liquids with sulfonate- and acetate-based anions also leads to changes in the interactions between ionic liquid, AC and H_2O components involved in adsorption process, with the attractive van der Waals interactions increasing in the order $C_6H_5^-$ > CF_3^- > CH_3^-, consistently with the adsorption trends described by the K_d values. On the other hand, the significant hydrogen bonding between sulfonate- and acetate-based ionic liquids and water molecules also determines the adsorption thermodynamics, leading to low K_d values, close to those of hydrophilic chlorine-based ionic liquids.

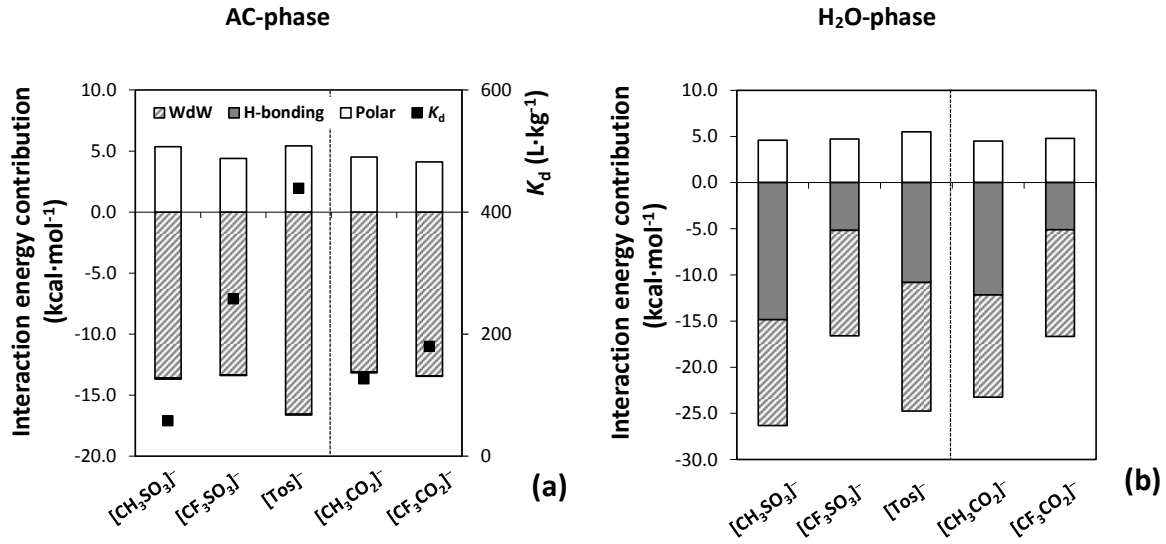

Figure 5.10. Predicted COSMO-RS contributions to interaction energies of (a) IL-AC and (b) IL-water for $[C_4C_1im]^+$ based ILs with differently substituted anion.

The addition of an aromatic substituent (as benzyl) to the cation also enhances the adsorption of ionic liquid onto AC-MkU as showed in Figure 5.11. It seems that the substituents in the cationic or anionic structures of ionic liquids also drive the adsorption uptake. Higher uptakes are achieved for ionic liquids with the benzyl substituent than with a C_6 alkyl chain; or with ionic liquids based on anions substituted with $[CF_3SO_3]^-$ than those substituted with $[CH_3SO_3]^-$ groups.

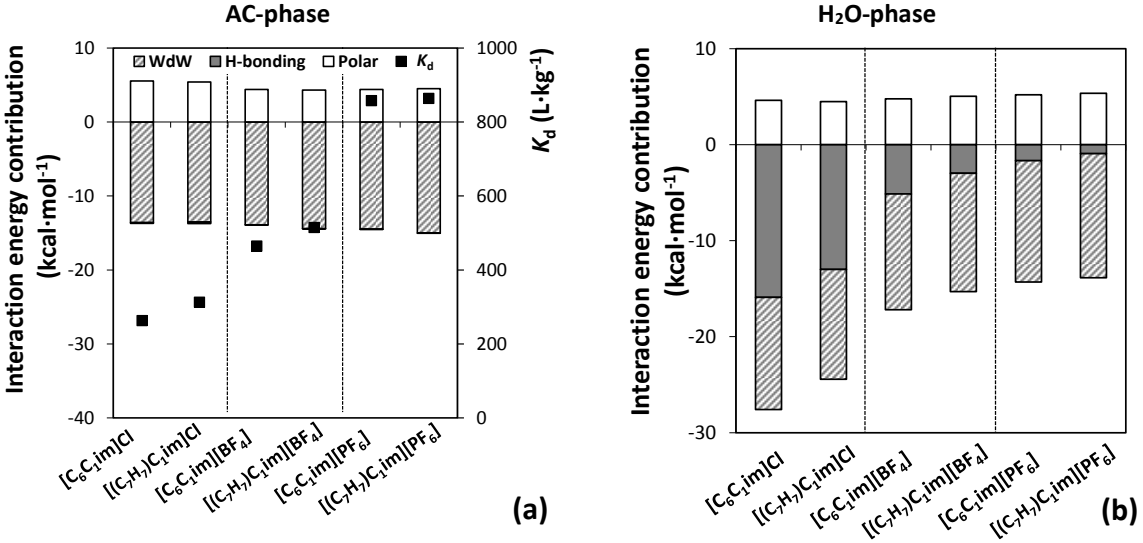

Figure 5.11. Predicted COSMO-RS contributions to interaction energies of (a) IL-AC and (b) IL-water for $[C_6C_1im]^+$ or $[(C_7H_7)C_1im]^+$ based ILs with Cl^-, $[BF_4]^-$ or $[PF_6]^-$ anions.

In summary, the experimental and theoretical results of this work allowed a detailed analysis of the effect on the adsorption of the structural elements of the ionic liquid as cation nature, cation and anion substituents and the anion nature, providing new insights in the development of the ionic liquids adsorption on AC from aqueous phase.

5.4. Enhancing the adsorption of ionic liquids onto activated carbon by the addition of inorganic salts

Catarina M.S.S. Neves, Jesús Lemus, Mara G. Freire, Jose Palomar and João A.P. Coutinho, Chemical Engineering Journal 252 (2014) 305-310, DOI: 10.1016/j.cej.2014.05.009

5.4.1. Abstract

Most ionic liquids are either water soluble or present a non-negligible miscibility with water that may cause some harmful effects upon their release into the environment. Among other methods, adsorption of ionic liquids onto AC has shown to be an effective technique to remove these compounds from aqueous solutions. However, this method has proved to be viable only for hydrophobic ionic liquids rather than for the hydrophilic that, being water soluble, have a larger tendency for contamination. In this context, an alternative approach using the salting-out ability of inorganic salts is here proposed to enhance the adsorption of hydrophilic ionic liquids onto activated carbon. The effect of the concentrations of Na_2SO_4 on the adsorption of five ionic liquids onto AC was investigated. A wide range of ionic liquids that allow the inspection of the ionic liquid cation family (imidazolium- and pyridinium-based) and the anion nature (accounting for its hydrophilicity and fluorination) through the adsorption onto AC was studied. In general, it is shown that the use of Na_2SO_4 enhances the adsorption of ionic liquids onto AC. In particular, this effect is highly relevant when dealing with hydrophilic ionic liquids that are those that are actually poorly removed by AC. In addition, the COSMO-RS was used aiming at complementing the experimental data obtained. This work contributes with the development of novel methods to remove ionic liquids from water streams aiming at creating “greener” processes.

5.4.2. Results and discussion

The adsorption isotherms of the ionic liquids $[C_4C_1im]Cl$, $[C_4C_1im][CH_3SO_3]$, $[C_4C_1im][CF_3SO_3]$, $[C_4C_1im][NTf_2]$ and $[C_4\text{-}3\text{-}C_1py][NTf_2]$ at 308 K onto commercial AC-MkU, measured with different concentrations of Na_2SO_4 in solution, are depicted in Figure 5.12.

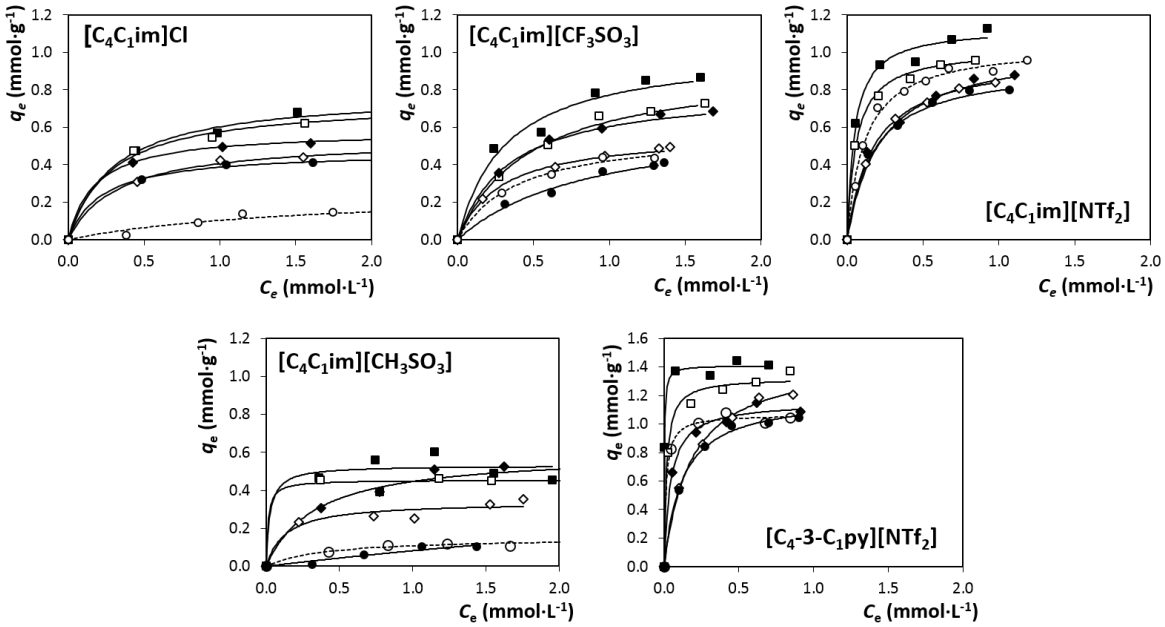

Figure 5.12. Experimental data (symbols) and Langmuir fitting (eq 5.1) (lines) for the adsorption equilibrium of the ILs onto AC-MkU at 308 K, at several salt concentrations: (○), no salt; (●), $[Na_2SO_4]$ = 0.28 mol·kg^{-1}; (◇), $[Na_2SO_4]$ = 0.70 mol·kg^{-1}; (◆), $[Na_2SO_4]$ = 1.06mol·kg^{-1}; (□),$[Na_2SO_4]$ = 1.41 mol·kg^{-1}; (■), $[Na_2SO_4]$ = 1.76 mol·kg^{-1}.

The ionic liquids $[C_4C_1im]Cl$, $[C_4C_1im][CH_3SO_3]$ and $[C_4C_1im][CF_3SO_3]$ are hydrophilic, and they are completely miscible in water at temperatures close to 308 K. The solubilities of $[C_4C_1im][NTf_2]$ and $[C_4\text{-}3\text{-}C_1py][NTf_2]$ in water at 308.15 K are 3.44×10^{-4} and 2.30×10^{-4} (in mole fraction), respectively.[5,10]

The results here obtained show different adsorption capacities attending to both the nature of the ionic liquid and the amount of salt in solution. For comparison purposes, B and q_{max} empirical coefficients of the Langmuir model (eq 5.1) and the apparent distribution coefficients (K_d, eq 5.2), obtained from the experimental adsorption data, are reported in Table 5.3.

Table 5.3. Empirical coefficients obtained from the Langmuir model fitting and K_d coefficients estimated at C_e = 1.2 mmol·L^{-1} for the different ILs studied.

IL	[Na_2SO_4] (mol·kg^{-1})	q_{max} (mmol·g^{-1})	B (L·mmol^{-1})	R^2	K_d (L·kg^{-1})
[C_4C_1im]Cl	No salt	0.26	0.64	0.900	95
	0.28	0.47	4.52	0.999	332
	0.70	0.54	3.02	0.997	353
	1.06	0.58	5.76	0.997	422
	1.41	0.74	3.54	0.961	498
	1.76	0.78	3.31	0.993	522
[C_4C_1im][CH_3SO_3]	No salt	0.13	3.94	0.973	92
	0.28	0.72	0.13	0.924	80
	0.70	0.34	7.54	0.939	254
	1.06	0.60	2.94	0.969	388
	1.41	0.45	78.04	0.977	374
	1.76	0.53	39.79	0.899	433
[C_4C_1im][CF_3SO_3]	No salt	0.58	2.56	0.990	367
	0.28	0.67	1.12	0.988	318
	0.70	0.57	3.52	0.997	385
	1.06	0.81	2.96	0.999	525
	1.41	0.93	2.10	0.995	556
	1.76	1.02	3.17	0.978	670
[C_4C_1im][NTf_2]	No salt	1.04	8.71	0.992	794
	0.28	0.93	5.91	0.981	680
	0.70	0.99	5.73	0.999	719
	1.06	1.04	4.57	0.933	734
	1.41	1.02	16.99	0.964	809
	1.76	1.13	20.86	0.988	908
[C_4-3-C_1py][NTf_2]	No salt	1.10	75.71	0.995	906
	0.28	1.20	8.41	0.997	909
	0.70	1.47	5.69	0.997	1068
	1.06	1.15	23.72	0.991	929
	1.41	1.32	61.70	0.989	1088
	1.76	1.41	406.48	0.458	1173

In general, and for the imidazolium-based ionic liquids, the anion influence on their adsorption capacity onto AC follows the order: Cl^- ≈ $[CH_3SO_3]^-$ < $[CF_3SO_3]^-$ < $[NTf_2]^-$. This trend is in good agreement with the results already reported in the literature,[95] and

reveals that the adsorption of ionic liquids onto AC is progressively more favourable with the increase on the anion hydrophobicity. On the other hand, taking into consideration the ionic liquid cation family, the pyridinium adsorbs more onto AC than the imidazolium-based counterpart. This pattern is also related to the higher hydrophobic character of the pyridinium cation that although being aromatic consists on a 6-sided ring whereas the imidazolium cation is a 5-sided aromatic ring.[308]

In Figure 5.13 it is shown the ratio between the K_d obtained in mixtures with salt to that with no salt. This ratio quantifies thus the relative influence of the salt, and salt concentration, on the adsorption of the different ionic liquids onto AC.

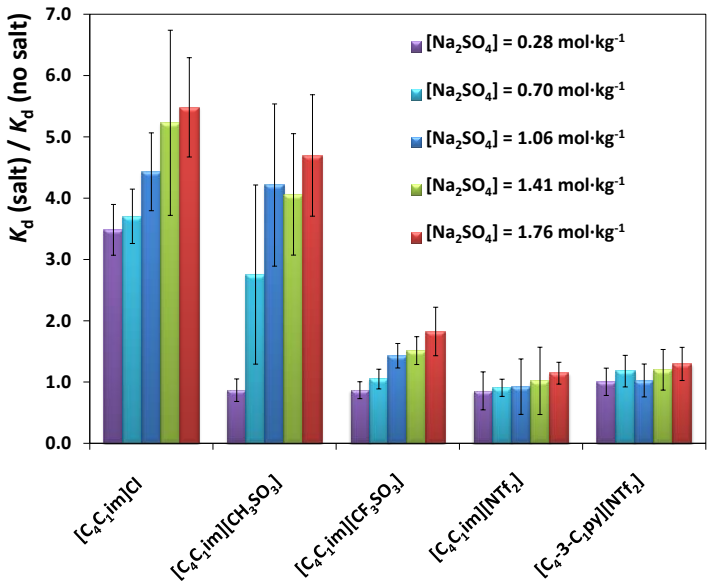

Figure 5.13. Ratio between the K_d values in the presence of salt to that with no salt at different concentrations and for the several ILs investigated.

It is remarkable that, in general, the presence of the inorganic and salting-out salt in aqueous solution enhances the adsorption of the different ionic liquids onto AC. In addition, the salt influence is much more noticeable in the systems including ionic liquids with a more hydrophilic nature, and following the trend: $[C_4C_1im]Cl$ > $[C_4C_1im][CH_3SO_3]$ > $[C_4C_1im][CF_3SO_3]$ > $[C_4C_1im][NTf_2]$ > $[C_4\text{-}3\text{-}C_1py][NTf_2]$. With the $[C_4C_1im]Cl$ and $[C_4C_1im][CH_3SO_3]$ ionic liquids, the K_d value increases up to 5.5 times by the salt addition. Furthermore, it was also found that increasing the salt concentration leads to an increase

on the adsorption of hydrophilic ionic liquids (such as $[C_4C_1im]Cl$ and $[C_4C_1im][CH_3SO_3]$). The salting-out phenomenon, particularly for the more hydrophilic ionic liquids, leads to a decrease on the solubility of the ionic liquids in water and therefore favours the partition to, and enhance their adsorption onto AC.[66] Although mainly an entropic effect, the formation of salt-ion-hydration complexes leads to the dehydration of the ionic liquid solute and to an increase on the surface tension of the cavity that is responsible for the observed salting-out phenomenon of the salt over the ionic liquid.[66,127] Nevertheless, at low salt concentrations, the opposite behaviour is sometimes observed, and the adsorption of some ionic liquids decrease in presence of the salt. This salting-in effect was previously observed for other ionic liquids, and is common with proteins or other charged molecules, at low salt concentrations.[66] In contrast, the presence of salt does not improve significantly the adsorption of the most hydrophobic ionic liquids ($[NTf_2]$-based ionic liquids) onto AC. As reported before,[100] the available pore volume of the AC-MkU adsorbent at maximum capacity should be almost nearly filled by these hydrophobic ionic liquids. For this reason, the presence of salt does not improve the adsorption of the $[NTf_2]$-based ionic liquids onto this specific AC since its saturation was already reached.

To complete the current analysis and to better interpret the gathered experimental data, the COSMO-RS was used to estimate the partition coefficient (*P*) of the different ionic liquids, at infinite dilution, and between AC and the diverse aqueous phases at increasing concentrations of Na_2SO_4. The log *P* has been already reported as a reference quantitative parameter of the affinity of each ionic liquid for AC when in aqueous solutions.[308] Figure 5.14a depicts the log *P* values for the five studied ionic liquids obtained by COSMO-RS while specifying in all the calculations the increasing salt concentration used in the experiments. For comparison purposes, Figure 5.14a also includes the experimental K_d values obtained for each ionic liquid in the absence of salt. In Figure 5.14b it is depicted the ratio between the *P* value in the presence and in absence of salt obtained by COSMO-RS.

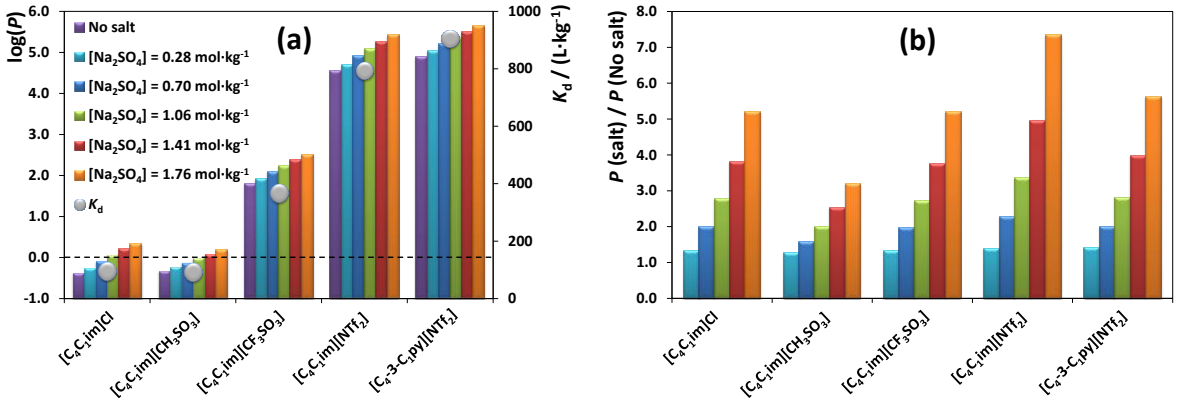

Figure 5.14. (a) log(*P*) predicted by COSMO-RS for the ILs studied with different salt concentrations using the AC molecular model and experimental K_d values for these ILs on AC-MkU without salt; (b) effect of the salt concentration on the *P* ratio predicted by COSMO-RS.

COSMO-RS correctly predicts the influence of the ionic liquid chemical structure onto their AC adsorption capacity, since log(*P*) values increase with the increase on the K_d values and with the hydrophobicity of the ionic liquid solute. In addition, COSMO-RS estimations reasonably reproduce the influence of the Na_2SO_4 salt on the ionic liquids adsorption onto AC. Higher values of log(*P*) are obtained when increasing the salt concentration in aqueous media. However, as expectable, the COSMO-RS approach is not able to correctly describe the effects of lower salt concentrations on hydrophobic ionic liquids ([NTf_2]-based), since aspects as the available pore volume of exhausted AC adsorbent cannot be included in its respective calculations.

In summary, it is here demonstrated, for the first time, that AC can be also used as an effective adsorbent for hydrophilic ionic liquids present at low concentrations in aqueous media if inorganic salts are concomitantly used to promote a salting-out phenomenon and enhance the partition towards the AC.

5.5. Conclusions

The adsorption onto AC proved to be a potential non-destructive method to remove low concentrations of ionic liquids from aqueous solutions.

In this work the study of the influence of the chemical structure of ionic liquids on their adsorption from water onto a commercial activated carbon AC-MkU was evaluated. For that purpose, equilibrium adsorption measurements for 21 different ionic liquids were carried out with the aim of extending the number of compounds studied previously to a wide sample of 48 ionic liquids, which includes a variety of anions (11) and cations (20), from imidazolium, pyridinium, ammonium, phosphonium, piperidinium and pyrrolidinium families. It permitted to analyse the effect of the different structural elements of an ionic liquid, such as the head group cation, anion substituents and nature, on the adsorption. In addition, a COSMO-RS analysis was performed to analyse the interaction energies between ionic liquid and AC / H_2O components involved in adsorption process.

The results obtained show that the ionic liquid family has a remarkably influence on the adsorption of ionic liquid by AC, being observed higher uptakes in the order ammonium > phosphonium > pyridinium > imidazolium > pyrrolidinium > piperidinium, when the head group of the cation promoted attractive van der Waals interactions between the ionic liquid and AC surface. On the other hand, it was also concluded that the substituents of the cation or the anion can also lead to different adsorptions onto AC. Thus, increasing the number of the carbon atoms in the alkyl chains, linked to the cation or the anion, results in higher adsorption coefficients of ionic liquid between AC and H_2O phases, due to enhanced IL–AC interactions. Other substituents in the cationic or anionic structures of ionic liquids also drive into different uptake. Thus, higher uptakes are found for ionic liquids with benzyl substituents than the corresponding ionic liquids with linear alkyl chain; or with ionic liquids based on anions substituted with CF_3- than those substituted with CH_3- groups. Finally, the variation on the anion with remarkably different polarities is translated into different results, where ionic liquids with hydrophobic anions ($[NTf_2]^-$ or $[PF_6]^-$) show much higher adsorption onto AC-MkU than hydrophilic ionic liquids (Cl^- or $[BF_4]^-$), due to the stronger attractive van der Waals interactions between ionic liquid and AC, and the absence of hydrogen bonding interactions between ionic liquid and H_2O.

Since this method showed not to be so effective for hydrophilic ionic liquids, also in this work, the addition of a salting-out inorganic salt (Na_2SO_4) was used to improve the

adsorption of different ionic liquids onto AC. The results obtained show that the K_d values of hydrophilic ionic liquids, such as $[C_4C_1im]Cl$ and $[C_4C_1im][CH_3SO_3]$, increase up to 5.5 times in the presence of the salt. This new approach can be envisaged as a promising route for reducing the pollution of aqueous streams resulting from industrial processes where ionic liquids are employed.

Chapter 6 – Final Remarks and Future Work

Ionic liquids are a recent class of solvents that have been widely studied in both academic and industrial fields. Their outstanding properties, such as negligible vapour pressures and the possibility of tailoring their properties for a specific task by an adequate combination of their ions, makes them good candidates for a wide range of applications. Two different works proposing the use of ionic liquids aiming at improving the performance of eventual industrial processes are proposed in Chapter 2. However, when envisaging large-scale applications ionic liquids will inevitably end in aqueous streams. In this context, the mutual solubilities of hydrophobic, but also hygroscopic, ionic liquids were determined to infer on their saturation values. A wide range of structural effects was evaluated through their mutual solubilities with water. The results obtained were then supported at a molecular-level by molecular dynamics simulations. COSMO-RS was also employed to evaluate its prediction ability.

Besides the importance on the knowledge of the ionic liquid solubility values in water, it is still of vital importance to treat and to remove them from aqueous streams. With this goal in mind, two different processes to remove ionic liquids from aqueous streams were proposed. The first process, described in Chapter 4, shown to be adequate to remove large amounts of hydrophilic ionic liquids. Moreover, the recovery of the ionic liquid was also demonstrated allowing its further reutilization. The second process, which relays on the adsorption of ionic liquids onto activated carbon, proved to be a promising method to remove only low concentrations of ionic liquids. This method showed to be more effective for hydrophobic ionic liquids, and for that reason a salting-out salt, Na_2SO_4, was added to the systems and proved to improve the adsorption of the hydrophilic ones.

Since ionic liquids are composed of different cations and anions, and each combination results in a distinct solvent with different properties, the continuous and future investigations on their liquid-liquid phase behaviour with water is of extreme importance. On the other hand, processes for the removal and recovery of ionic liquids should be studied in more detail and improved. Even if the method based on aqueous biphasic systems proved to be effective for the ionic liquids studied, there are still some limitations, namely the limited number of ionic liquids that can form two phases with

aluminium-based salts. And even if these salts are already used in water treatment processes, there are other organic and biodegradable salts that should be tested for this purpose. Finally, it was demonstrated that the adsorption of ionic liquids onto activated carbon is effective; yet, the finding of a novel approach to remove these compounds from the activated carbon is still in need. In addition, the knowledge of the mechanisms of the ionic liquid adsorption should be better understood in order to develop and/or modify the materials aiming at improving their adsorption capability.

References

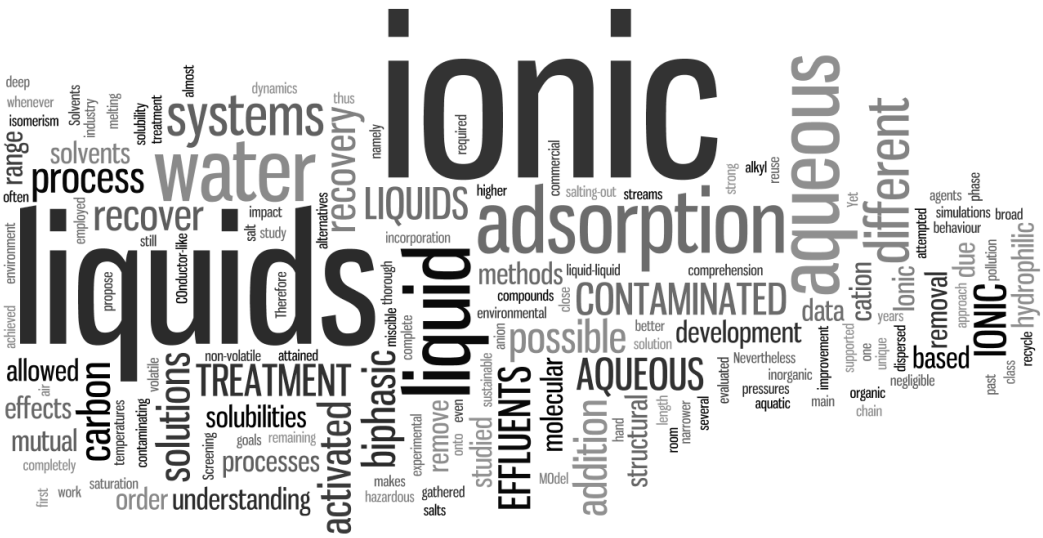
ionic
liquids
liquid
adsorption
aqueous
different
water
systems
process
solvents
recover
recovery
LIQUIDS
CONTAMINATED
AQUEOUS
EFFLUENTS
possible
development
methods
data
cation
ionic
removal
based
IONIC
hydrophilic
solutions
TREATMENT
carbon
activated
biphasic
molecular
addition
structural
solubilities
processes
understanding
order
mutual
effects
allowed
remove
studied
range
deep
whenever
isomerism
Solvents
industry
melting
solubility
treatment
almost
dynamics
thus
namely
required
commercial
salting-out
streams
higher
alkyl
reuse
strong
Yet
agents
phase
simulations
broad
behaviour
attempted
due
pollution
approach
recycle
class
past
negligible
dispersed
organic
chain
unique
one
supported
improvement
inorganic
pressures
aquatic
main
Nevertheless
evaluated
several
narrower
length
room
hand
even
onto
experimental
remaining
goals
Screening
saturation
work
first
completely
temperatures
contaminating
volatile
air
non-volatile
attained
Therefore
impact
salt
study
still
COnductor-like
employed
propose
environment
achieved
often
alternatives
incorporation
miscible
thorough
complete
anion
sustainable
environmental
compounds
close
liquid-liquid
comprehension
better
solution
MOdel
makes
hazardous
gathered
salts

1. M. J. Earle, J. M. S. S. Esperança, M. A. Gilea, J. N. Canongia Lopes, L. P. N. Rebelo, J. W. Magee, K. R. Seddon, and J. A. Widegren, *Nature*, 2006, **439**, 831–834.
2. N. V Plechkova and K. R. Seddon, *Chem. Soc. Rev.*, 2008, **37**, 123–150.
3. R. D. Rogers and K. R. Seddon, *Science*, 2003, **302**, 792–793.
4. A. Bosmann, L. Datsevich, A. Jess, A. Lauter, C. Schmitz, and P. Wasserscheid, *Chem. Commun.*, 2001, 2494–2495.
5. M. G. Freire, P. J. Carvalho, R. L. Gardas, I. M. Marrucho, L. M. N. B. F. Santos, and J. A. P. Coutinho, *J. Phys. Chem. B*, 2008, **112**, 1604–1610.
6. M. G. Freire, C. M. S. S. Neves, P. J. Carvalho, R. L. Gardas, A. M. Fernandes, I. M. Marrucho, L. M. N. B. F. Santos, and J. A. P. Coutinho, *J. Phys. Chem. B*, 2007, **111**, 13082–13089.
7. M. G. Freire, C. M. S. S. Neves, S. P. M. Ventura, M. J. Pratas, I. M. Marrucho, J. Oliveira, J. A. P. Coutinho, and A. M. Fernandes, *Fluid Phase Equilib.*, 2010, **294**, 234–240.
8. C. M. S. S. Neves, K. A. Kurnia, K. Shimizu, I. M. Marrucho, L. P. N. Rebelo, J. A. P. Coutinho, M. G. Freire, and J. N. C. Lopes, *Phys. Chem. Chem. Phys.*, 2014, **16**, 21340–21348.
9. K. A. Kurnia, C. M. S. S. Neves, L. M. N. B. F. Santos, M. G. Freire, and J. A. P. Coutinho, 2014, unpublished data.
10. M. G. Freire, C. M. S. S. Neves, K. Shimizu, C. E. S. Bernardes, I. M. Marrucho, J. A. P. Coutinho, J. N. Canongia Lopes, and L. P. N. Rebelo, *J. Phys. Chem. B*, 2010, **114**, 15925–15934.
11. C. M. S. S. Neves, M. L. S. Batista, A. F. M. Cláudio, L. M. N. B. F. Santos, I. M. Marrucho, M. G. Freire, and J. A. P. Coutinho, *J. Chem. Eng. Data*, 2010, **55**, 5065–5073.
12. F. M. Maia, O. Rodríguez, and E. A. Macedo, *Fluid Phase Equilib.*, 2010, **296**, 184–191.
13. C. M. S. S. Neves, A. R. Rodrigues, K. A. Kurnia, J. M. S. S. Esperança, M. G. Freire, and J. A. P. Coutinho, *Fluid Phase Equilib.*, 2013, **358**, 50–55.
14. M. A. R. Martins, C. M. S. S. Neves, K. A. Kurnia, L. M. N. B. F. Santos, M. G. Freire, S. P. Pinho, and J. A. P. Coutinho, *Fluid Phase Equilib.*, 2014, **381**, 28–35.
15. M. A. R. Martins, C. M. S. S. Neves, K. A. Kurnia, A. Luís, L. M. N. B. F. Santos, M. G. Freire, S. P. Pinho, and J. A. P. Coutinho, *Fluid Phase Equilib.*, 2014, **375**, 161–167.
16. K. A. Kurnia, T. E. Sintra, C. M. S. S. Neves, K. Shimizu, J. N. Canongia Lopes, F. Gonçalves, S. P. M. Ventura, M. G. Freire, L. M. N. B. F. Santos, and J. A. P. Coutinho, *Phys. Chem. Chem. Phys.*, 2014, **16**, 19952–63.
17. M. Królikowska, *Fluid Phase Equilib.*, 2014, **361**, 273–281.
18. D. J. Gorman-Lewis and J. B. Fein, *Environ. Sci. Technol.*, 2004, **38**, 2491–2495.
19. P. Stepnowski, *Aust. J. Chem.*, 2005, **58**, 170–173.
20. P. Stepnowski, W. Mrozik, and J. Nichthauser, *Environ. Sci. Technol.*, 2007, **41**, 511–516.
21. J. J. Beaulieu, J. L. Tank, and M. Kopacz, *Chemosphere*, 2008, **70**, 1320–1328.
22. M. Markiewicz, A. Markowska, J. Hupka, R. Aranowski, and C. Jungnickel, *Environ. Prot. Eng.*, 2009, **35**, 53–64.
23. M. Matzke, K. Thiele, A. Müller, and J. Filser, *Chemosphere*, 2009, **74**, 568–574.

24. S. Studzinska, M. Sprynskyy, and B. Buszewski, *Chemosphere*, 2008, **71**, 2121–2128.
25. S. Kowalska and B. Buszewski, *J. Sep. Sci.*, 2006, **29**, 2625–2634.
26. B. Buszewski, S. Kowalska, and P. Stepnowski, *J. Sep. Sci.*, 2006, **29**, 1116–1125.
27. M. G. Freire, C. M. S. S. Neves, I. M. Marrucho, J. A. P. Coutinho, and A. M. Fernandes, *J. Phys. Chem. A*, 2009, **114**, 3744–3749.
28. OECD guideline for testing of chemicals; adopted by council July 1992—ready biodegradability.
29. OECD 301, Adopted by the Council on 17th July 1992; Ready, 2006.
30. N. S. Battersby, *Chemosphere*, 1997, **34**, 1813–1822.
31. OECD guideline for testing of chemicals, proposal for a new guideline 310—ready biodegradability— CO2 in sealed vessels (Headspace Test), 2003.
32. OECD guideline for testing of chemicals. Method 309: Aerobic mineralisation in surface water— simulation biodegradation test, 2004.
33. ASTMStandardDS988-03, Annual Book of ASTM Standards, ASTM International, Pennsylvania, USA, 2004, vol. 08.03.
34. N. Gathergood, M. T. Garcia, and P. J. Scammells, *Green Chem.*, 2004, **6**, 166–175.
35. N. Gathergood and P. J. Scammells, *Aust. J. Chem.*, 2002, **55**, 557–560.
36. R. S. Boethling, in *Designing Safer Chemicals*, American Chemical Society, 1996, vol. 640, pp. 156–171.
37. R. S. Boethling, in *Cationic Surfactants: Analytical and Biological Evaluation, Surfactant Science Series*, eds. J. Cross and E. J. Singer, Marcel Decker, Inc., New York, 1994, pp. 95–135.
38. M. T. Garcia, N. Gathergood, and P. J. Scammells, *Green Chem.*, 2005, **7**, 9–14.
39. N. Gathergood, P. J. Scammells, and M. T. Garcia, *Green Chem.*, 2006, **8**, 156–160.
40. S. Kumar, W. Ruth, B. Sprenger, and U. Kragl, *Chim. Oggi-Chemistry Today*, 2006, **24**, 24–26.
41. M. Stasiewicz, E. Mulkiewicz, R. Tomczak-Wandzel, J. Kumirska, E. M. Siedlecka, M. Golebiowski, J. Gajdus, M. Czerwicka, and P. Stepnowski, *Ecotoxicol. Environ. Saf.*, 2008, **71**, 157–165.
42. S. Stolte, S. Abdulkarim, J. Arning, A.-K. Blomeyer-Nienstedt, U. Bottin-Weber, M. Matzke, J. Ranke, B. Jastorff, and J. Thoming, *Green Chem.*, 2008, **10**, 214–224.
43. HACH LANGE GMBH, Dr. Lange BOD5-BioKIT LZC 555, 97/ 10 edn, 1997.
44. J. Neumann, O. Grundmann, J. Thoming, M. Schulte, and S. Stolte, *Green Chem.*, 2010, **12**, 620–627.
45. A. Esquivel-Viveros, F. Ponce-Vargas, P. Esponda-Aguilar, L. A. Prado-Barragan, M. Gutierrez-Rojas, G. J. Lye, and S. Huerta-Ochoa, *Rev. Mex. Ing. Quim.*, 2009, **8**, 163–168.
46. C. Zhang, H. Wang, S. V Malhotra, C. J. Dodge, and A. J. Francis, *Green Chem.*, 2010, **12**, 851–858.
47. F. Atefi, M. T. Garcia, R. D. Singer, and P. J. Scammells, *Green Chem.*, 2009, **11**, 1595–1604.

48. A. S. Wells and V. T. Coombe, *Org. Process Res. Dev.*, 2006, **10**, 794–798.

49. Y. Yu, X. Lu, Q. Zhou, K. Dong, H. Yao, and S. Zhang, *Chem. – A Eur. J.*, 2008, **14**, 11174–11182.

50. R. S. Boethling, E. Sommer, and D. DiFiore, *Chem. Rev.*, 2007, **107**, 2207–2227.

51. E. Grabinska-Sota and A. Dmuchowski, *Przem. Chem.*, 2008, **87**, 388–391.

52. C. Pretti, M. Renzi, S. E. Focardi, A. Giovani, G. Monni, B. Melai, S. Rajamani, and C. Chiappe, *Ecotoxicol. Environ. Saf.*, 2011, **74**, 748–753.

53. J. Ranke, S. Stolte, R. Störmann, J. Arning, and B. Jastorff, *Chem. Rev.*, 2007, **107**, 2183–2206.

54. J. Arning, S. Stolte, A. Boschen, F. Stock, W.-R. Pitner, U. Welz-Biermann, B. Jastorff, and J. Ranke, *Green Chem.*, 2008, **10**, 47–58.

55. M. Matzke, S. Stolte, K. Thiele, T. Juffernholz, J. Arning, J. Ranke, U. Welz-Biermann, and B. Jastorff, *Green Chem.*, 2007, **9**, 1198–1207.

56. A. C. Skladanowski, P. Stepnowski, K. Kleszczynski, and B. Dmochowska, *Environ. Toxicol. Pharmacol.*, 2005, **19**, 291–296.

57. M. Yu, S.-M. Li, X.-Y. Li, B.-J. Zhang, and J.-J. Wang, *Ecotoxicol. Environ. Saf.*, 2008, **71**, 903–908.

58. P. Nockemann, B. Thijs, K. Driesen, C. R. Janssen, K. Van Hecke, L. Van Meervelt, S. Kossmann, B. Kirchner, and K. Binnemans, *J. Phys. Chem. B*, 2007, **111**, 5254–5263.

59. S. P. M. Ventura, A. M. M. Gonçalves, F. Gonçalves, and J. A. P. Coutinho, *Aquat. Toxicol.*, 2010, **96**, 290–297.

60. S. P. M. Ventura, A. M. M. Gonçalves, T. Sintra, J. Pereira, F. Gonçalves, and J. P. Coutinho, *Ecotoxicology*, 2013, **22**, 1–12.

61. S. P. M. Ventura, C. S. Marques, A. A. Rosatella, C. A. M. Afonso, F. Gonçalves, and J. A. P. Coutinho, *Ecotoxicol. Environ. Saf.*, 2012, **76**, 162–168.

62. S. P. M. Ventura, F. A. e Silva, A. M. M. Gonçalves, J. L. Pereira, F. Gonçalves, and J. A. P. Coutinho, *Ecotoxicol. Environ. Saf.*, 2014, **102**, 48–54.

63. S. P. M. Ventura, M. Gurbisz, M. Ghavre, F. M. M. Ferreira, F. Gonçalves, I. Beadham, B. Quilty, J. A. P. Coutinho, and N. Gathergood, *ACS Sustain. Chem. Eng.*, 2013, **1**, 393–402.

64. M. Petkovic, K. R. Seddon, L. P. N. Rebelo, and C. Silva Pereira, *Chem. Soc. Rev.*, 2011, **40**, 1383–1403.

65. M. G. Freire, A. F. M. Cláudio, J. M. M. Araújo, J. A. P. Coutinho, I. M. Marrucho, J. N. Canongia Lopes, and L. P. N. Rebelo, *Chem. Soc. Rev.*, 2012, **41**, 4966–4995.

66. M. G. Freire, P. J. Carvalho, A. M. S. Silva, L. M. N. B. F. Santos, L. P. N. Rebelo, I. M. Marrucho, and J. A. P. Coutinho, *J. Phys. Chem. B*, 2009, **113**, 202–211.

67. S. P. M. Ventura, C. M. S. S. Neves, M. G. Freire, I. M. Marrucho, J. Oliveira, and J. A. P. Coutinho, *J. Phys. Chem. B*, 2009, **113**, 9304–9310.

68. C. M. S. S. Neves, S. P. M. Ventura, M. G. Freire, I. M. Marrucho, and J. A. P. Coutinho, *J. Phys. Chem. B*, 2009, **113**, 5194–5199.

69. C. L. S. Louros, A. F. M. Cláudio, C. M. S. S. Neves, M. G. Freire, I. M. Marrucho, J. Pauly, and J. A. P. Coutinho, *Int. J. Mol. Sci.*, 2010, **11**, 1777–1791.

70. A. F. M. Cláudio, A. M. Ferreira, S. Shahriari, M. G. Freire, and J. A. P. Coutinho, *J. Phys. Chem. B*, 2011, **115**, 11145–11153.

71. K. E. Gutowski, G. A. Broker, H. D. Willauer, J. G. Huddleston, R. P. Swatloski, J. D. Holbrey, and R. D. Rogers, *J. Am. Chem. Soc.*, 2003, **125**, 6632–6633.

72. S. Shahriari, L. C. Tomé, J. M. M. Araújo, L. P. N. Rebelo, J. A. P. Coutinho, I. M. Marrucho, and M. G. Freire, *RSC Adv.*, 2013, **3**, 1835–1843.

73. S. Shahriari, C. M. S. S. Neves, M. G. Freire, and J. A. P. Coutinho, *J. Phys. Chem. B*, 2012, **116**, 7252–7258.

74. M. T. Zafarani-Moattar and S. Hamzehzadeh, *J. Chem. Eng. Data*, 2007, **52**, 1686–1692.

75. Y. Pei, J. Wang, L. Liu, K. Wu, and Y. Zhao, *J. Chem. Eng. Data*, 2007, **52**, 2026–2031.

76. F. Hofmeister, *Arch. Exp. Pathol. Pharmakol.*, 1888, **24**, 247–260.

77. N. J. Bridges, K. E. Gutowski, and R. D. Rogers, *Green Chem.*, 2007, **9**, 177–183.

78. B. Wu, Y. Zhang, and H. Wang, *J. Phys. Chem. B*, 2008, **112**, 6426–6429.

79. B. Wu, Y. M. Zhang, and H. P. Wang, *J. Chem. Eng. Data*, 2008, **53**, 983–985.

80. Y. Deng, T. Long, D. Zhang, J. Chen, and S. Gan, *J. Chem. Eng. Data*, 2009, **54**, 2470–2473.

81. C. Li, J. Han, Y. Wang, Y. Yan, J. Pan, X. Xu, and Z. Zhang, *J. Chem. Eng. Data*, 2010, **55**, 1087–1092.

82. W. H. Awad, J. W. Gilman, M. Nyden, R. H. Harris, T. E. Sutto, J. Callahan, P. C. Trulove, H. C. DeLong, and D. M. Fox, *Thermochim. Acta*, 2004, **409**, 3–11.

83. P. Stepnowski and A. Zaleska, *J. Photochem. Photobiol. A Chem.*, 2005, **170**, 45–50.

84. L. Berthon, S. I. Nikitenko, I. Bisel, C. Berthon, M. Faucon, B. Saucerotte, N. Zorz, and P. Moisy, *Dalton Trans.*, 2006, 2526–2534.

85. X. Li, J. Zhao, Q. Li, L. Wang, and S. C. Tsang, *Dalton Trans.*, 2007, 1875–1880.

86. E. M. Siedlecka, W. Mrozik, Z. Kaczynski, and P. Stepnowski, *J. Hazard. Mater.*, 2008, **154**, 893–900.

87. E. M. Siedlecka, M. Golebiowski, J. Kumirska, and P. Stepnowski, *Chem. Anal. (Warsaw)*, 2008, **53**, 943–951.

88. T. Itakura, K. Hirata, M. Aoki, R. Sasai, H. Yoshida, and H. Itoh, *Environ. Chem. Lett.*, 2009, **7**, 343–345.

89. T. Itakura, R. Sasai, and H. Itoh, *Water Res.*, 2005, **39**, 2543–2548.

90. T. Itakura, R. Sasai, and H. Itoh, *Bull. Chem. Soc. Jpn.*, 2006, **79**, 1303–1307.

91. E. Siedlecka and P. Stepnowski, *Environ. Sci. Pollut. Res.*, 2009, **16**, 453–458.

92. J. L. Anthony, E. J. Maginn, and J. F. Brennecke, *J. Phys. Chem. B*, 2001, **105**, 10942–10949.

93. D. Chatzopoulos and A. Varma, *Chem. Eng. Sci.*, 1995, **50**, 127–141.

94. D. Chatzopoulos, A. Varma, and R. L. Irvine, *AIChE J.*, 1993, **39**, 2027–2041.

95. J. Palomar, J. Lemus, M. A. Gilarranz, and J. J. Rodriguez, *Carbon N. Y.*, 2009, **47**, 1846–1856.

96. T. Welton, *Chem. Rev.*, 1999, **99**, 2071–2084.

97. J. P. Hallett and T. Welton, *Chem. Rev.*, 2011, **111**, 3508–3576.

98. J. Lemus, J. Palomar, M. A. Gilarranz, and J. J. Rodriguez, *Ind. Eng. Chem. Res.*, 2013, **52**, 2969–2976.

99. J. Lemus, J. Palomar, F. Heras, M. A. Gilarranz, and J. J. Rodriguez, *Sep. Purif. Technol.*, 2012, **97**, 11–19.

100. J. Lemus, J. Palomar, M. A. Gilarranz, and J. J. Rodriguez, *Adsorption*, 2011, **17**, 561–571.

101. X. Qi, L. Li, Y. Wang, N. Liu, and R. L. Smith, *Chem. Eng. J.*, 2014, **256**, 407–414.

102. X. Qi, L. Li, T. Tan, W. Chen, and R. L. Smith, *Environ. Sci. Technol.*, 2013, **47**, 2792–2798.

103. X.-D. Hou, Q.-P. Liu, T. J. Smith, N. Li, and M.-H. Zong, *PLoS One*, 2013, **8**, e59145.

104. K. D. Weaver, H. J. Kim, J. Sun, D. R. MacFarlane, and G. D. Elliott, *Green Chem.*, 2010, **12**, 507–513.

105. T. P. Thuy Pham, C.-W. Cho, and Y.-S. Yun, *Water Res.*, 2010, **44**, 352–372.

106. K. S. Egorova and V. P. Ananikov, *ChemSusChem*, 2014, **7**, 336–360.

107. M. Hirata-Koizumi, S. Fujii, A. Ono, A. Hirose, T. Imai, K. Ogawa, M. Ema, and A. Nishikawa, *Reprod. Toxicol.*, 2011, **31**, 219–230.

108. J. F. Fernandez, J. Neumann, and J. Thoming, *Curr. Org. Chem.*, 2011, **15**, 1992–2014.

109. L. Ford, J. R. Harjani, F. Atefi, M. T. Garcia, R. D. Singer, and P. J. Scammells, *Green Chem.*, 2010, **12**, 1783–1789.

110. D. Coleman and N. Gathergood, *Chem. Soc. Rev.*, 2010, **39**, 600–637.

111. D. Costill, G. Dalsky, and W. Fink, *Med. Sci. Sports Exerc.*, 1978, **10**, 155–158.

112. D. Essig, D. Costill, and P. Van Handel, *Int. J. Sports Med.*, 1980, **01**, 86–90.

113. U. Flenker and W. Schänzer, *Eur. J. Sport Sci.*, 2001, **1**, 1–5.

114. M. Schmidt and M. Roth, in *Analytical Toxicology for Clinical, Forensic and Pharmaceutical Chemists (Clincal Biochemistry)*, eds. R. A. Maes and H. Brandenberger, Walter De Gruyter & Co., Berlin, 1997, pp. 3–16.

115. J. Chamberlain, in *The Analysis of Drugs in Biological Fluids*, CRC Press, Florida, 2nd edn., 1995, pp. 205–224.

116. C. He, S. Li, H. Liu, K. Li, and F. Liu, *J. Chromatogr. A*, 2005, **1082**, 143–149.

117. S. Li, C. He, H. Liu, K. Li, and F. Liu, *J. Chromatogr. B. Analyt. Technol. Biomed. Life Sci.*, 2005, **826**, 58–62.

118. P.-A. Albertsson, in *Partitioning of cell particles and macromolecules in polymer two-phase systems*, Wiley-Interscience, New York, 3rd edn., 1986, pp. 12–18.

119. J. G. Huddleston, H. D. Willauer, S. T. Griffin, and R. D. Rogers, *Ind. Eng. Chem. Res.*, 1999, **38**, 2523–2539.

120. H. D. Willauer, J. G. Huddleston, and R. D. Rogers, *Ind. Eng. Chem. Res.*, 2002, **41**, 1892–1904.

121. Z. Zhu, Y. Guan, and M. Li, *J. Chem. Ind. Eng.*, 2001, **52**, 1039–1048.

122. Y. Chen, Y. Wang, Q. Cheng, X. Liu, and S. Zhang, *J. Chem. Thermodyn.*, 2009, **41**, 1056–1059.

123. Y. Pei, J. Wang, K. Wu, X. Xuan, and X. Lu, *Sep. Purif. Technol.*, 2009, **64**, 288–295.

124. Z. Du, Y.-L. Yu, and J.-H. Wang, *Chem. - A Eur. J.*, 2007, **13**, 2130–2137.

125. Q. Liu, J. Yu, W. Li, X. Hu, H. Xia, H. Liu, and P. Yang, *Sep. Sci. Technol.*, 2006, **41**, 2849–2858.

126. M. Domínguez-Pérez, L. I. N. Tomé, M. G. Freire, I. M. Marrucho, O. Cabeza, and J. A. P. Coutinho, *Sep. Purif. Technol.*, 2010, **72**, 85–91.

127. M. G. Freire, C. M. S. S. Neves, A. M. S. Silva, L. M. N. B. F. Santos, I. M. Marrucho, L. P. N. Rebelo, J. K. Shah, E. J. Maginn, and J. A. P. Coutinho, *J. Phys. Chem. B*, 2010, **114**, 2004–2014.

128. J. R. Trindade, Z. P. Visak, M. Blesic, I. M. Marrucho, J. A. P. Coutinho, J. N. Canongia Lopes, and L. P. N. Rebelo, *J. Phys. Chem. B*, 2007, **111**, 4737–4741.

129. V. Najdanovic-Visak, J. N. Canongia Lopes, Z. P. Visak, J. Trindade, and L. P. N. Rebelo, *Int. J. Mol. Sci.*, 2007, **8**, 736–748.

130. J. N. Canongia Lopes and L. P. N. Rebelo, *Chim. Oggi-Chemistry Today*, 2007, **25**, 37–39.

131. J. Sangster, in *Octanol-Water Partition Coefficients: Fundamentals and Physical Chemistry*, John Wiley & Sons, Ltd., Chichester, 1997, pp. 19–56.

132. L. P. N. Rebelo, J. N. Canongia Lopes, J. M. S. S. Esperança, H. J. R. Guedes, J. Łachwa, V. Najdanovic-Visak, and Z. P. Visak, *Acc. Chem. Res.*, 2007, **40**, 1114–1121.

133. E. Gnansounou and A. Dauriat, *Bioresour. Technol.*, 2010, **101**, 4980–4991.

134. H. J. Huang, S. Ramaswamy, U. W. Tschirner, and B. V Ramarao, *Sep. Purif. Technol.*, 2008, **62**, 1–21.

135. L. M. Vane, *Biofuels, Bioprod. Biorefin.*, 2008, **2**, 553–588.

136. M. Martín and I. E. Grossmann, *ESCAPE20*, 2010.

137. W. Arlt, M. Seiler, C. Jork, and T. Sheneider, Patent: DE 10114734, DE 10136614, WO 2002074718.

138. M. Seiler, C. Jork, A. Kavarnou, W. Arlt, and R. Hirsch, *AIChE J.*, 2004, **50**, 2439–2454.

139. N. Calvar, B. González, E. Gómez, and Á. Domínguez, *J. Chem. Eng. Data*, 2008, **53**, 820–825.

140. W. Geng, L. Z. Zhang, D. S. Deng, Y. Ge, and J. B. Ji, *J. Chem. Eng. Data*, 2010, **55**, 1679–1683.

141. A. V Orchilles, P. J. Miguel, E. Vercher, and A. Martinez-Andreu, *J. Chem. Eng. Data*, 2010, **55**, 1669–1674.

142. C. F. Poole and S. K. Poole, *J. Chromatogr. A*, 2010, **1217**, 2268–2286.

143. T. M. Boudreau and G. A. Hill, *Process Biochem.*, 2006, **41**, 980–983.

144. A. G. Fadeev and M. M. Meagher, *Chem. Commun.*, 2001, 295–296.

145. R. P. Swatloski, A. E. Visser, W. M. Reichert, G. A. Broker, L. M. Farina, J. D. Holbrey, and R. D. Rogers, *Green Chem.*, 2002, **4**, 81–87.

146. V. Najdanovic-Visak, J. M. S. S. Esperança, L. P. N. Rebelo, M. Nunes da Ponte, H. J. R. Guedes, K. R. Seddon, and J. Szydlowski, *Phys. Chem. Chem. Phys.*, 2002, **4**, 1701–1703.

147. V. Najdanovic-Visak, A. Serbanovic, J. Esperanca, H. J. R. Guedes, L. P. N. Rebelo, and M. N. da Ponte, *Chemphyschem*, 2003, **4**, 520–522.

148. V. Najdanovic-Visak, L. P. N. Rebelo, and M. Nunes da Ponte, *Green Chem.*, 2005, **7**, 443–450.

149. A. Chapeaux, L. D. Simoni, T. S. Ronan, M. A. Stadtherr, and J. F. Brennecke, *Green Chem.*, 2008, **10**, 1301–1306.

150. C. J. Bradaric, A. Downard, C. Kennedy, A. J. Robertson, and Y. Zhou, *Green Chem.*, 2003, **5**, 143–152.

151. U. Domańska and L. M. Casás, *J. Phys. Chem. B*, 2007, **111**, 4109–4115.

152. U. Domańska and K. Paduszyński, *J. Phys. Chem. B*, 2008, **112**, 11054–11059.

153. U. Domańska and K. Paduszyński, *Fluid Phase Equilib.*, 2009, **278**, 90–96.

154. U. Domańska and K. Paduszyński, *J. Chem. Thermodyn.*, 2010, **42**, 707–711.

155. L. I. N. Tomé, R. L. Gardas, P. J. Carvalho, M. J. Pastoriza-Gallego, M. M. Piñeiro, and J. A. P. Coutinho, *J. Chem. Eng. Data*, 2011, **56**, 2205–2217.

156. C. M. S. S. Neves, P. J. Carvalho, M. G. Freire, and J. A. P. Coutinho, *J. Chem. Thermodyn.*, 2011, **43**, 948–957.

157. M. G. Freire, P. J. Carvalho, R. L. Gardas, L. M. N. B. F. Santos, I. M. Marrucho, and J. A. P. Coutinho, *J. Chem. Eng. Data*, 2008, **53**, 2378–2382.

158. P. J. Carvalho, V. H. Álvarez, I. M. Marrucho, M. Aznar, and J. a. P. Coutinho, *J. Supercrit. Fluids*, 2010, **52**, 258–265.

159. P. J. Carvalho and J. A. P. Coutinho, *J. Phys. Chem. Lett.*, 2010, **1**, 774–780.

160. S. P. M. Ventura, J. Pauly, J. L. Daridon, J. A. Lopes da Silva, I. M. Marrucho, A. M. A. Dias, and J. A. P. Coutinho, *J. Chem. Thermodyn.*, 2008, **40**, 1187–1192.

161. F. S. Oliveira, M. G. Freire, M. J. Pratas, J. Pauly, J. L. Daridon, I. M. Marrucho, and J. A. P. Coutinho, *J. Chem. Eng. Data*, 2010, **55**, 662–665.

162. R. Ahlrichs, M. Bär, M. Häser, H. Horn, and C. Kölmel, *Chem. Phys. Lett.*, 1989, **162**, 165–169.

163. A. Schäfer, A. Klamt, D. Sattel, J. C. W. Lohrenz, and F. Eckert, *Phys. Chem. Chem. Phys.*, 2000, **2**, 2187–2193.

164. A. Schäfer, C. Huber, and R. Ahlrichs, *J. Chem. Phys.*, 1994, **100**, 5829–5835.

165. D. Othmer and P. Tobias, *Ind. Eng. Chem.*, 1942, **34**, 693–696.

166. J. D. Seader and E. J. Henley, Separation Process Principles, John Wiley & Sons, New York, 1998.

167. X. S. Hu, J. Yu, and H. Z. Liu, *J. Chem. Eng. Data*, 2006, **51**, 691–695.

168. F. Eckert and A. Klamt, *AIChE J.*, 2002, **48**, 369–385.

169. A. Klamt, *J. Phys. Chem.*, 1995, **99**, 2224–2235.

170. A. Klamt, COSMO-RS from quantum chemistry to fluid phase thermodynamics and drug design, Elsevier, Amsterdam; Boston, 2005.

171. A. Klamt and F. Eckert, *Fluid Phase Equilib.*, 2000, **172**, 43–72.

172. A. Klamt and G. Schuurmann, *J. Chem. Soc. Perkin Trans. 2*, 1993, **0**, 799–805.

173. U. Domanska, A. Pobudkowska, and F. Eckert, *J. Chem. Thermodyn.*, 2006, **38**, 685–695.

174. U. Domańska, A. Pobudkowska, and F. Eckert, *Green Chem.*, 2006, **8**, 268–276.

175. M. G. Freire, L. M. N. B. F. Santos, I. M. Marrucho, and J. A. P. Coutinho, *Fluid Phase Equilib.*, 2007, **255**, 167–178.

176. M. G. Freire, S. P. M. Ventura, L. M. N. B. F. Santos, I. M. Marrucho, and J. A. P. Coutinho, *Fluid Phase Equilib.*, 2008, **268**, 74–84.

177. K. Marsh, A. Deev, A. Wu, E. Tran, and A. Klamt, *Korean J. Chem. Eng.*, 2002, **19**, 357–362.

178. K. Sahandzhieva, D. Tuma, S. Breyer, Á. Pérez-Salado Kamps, and G. Maurer, *J. Chem. Eng. Data*, 2006, **51**, 1516–1525.

179. C. T. Wu, K. N. Marsh, A. V Deev, and J. A. Boxall, *J. Chem. Eng. Data*, 2003, **48**, 486–491.

180. T. Banerjee, K. K. Verma, and A. Khanna, *AIChE J.*, 2008, **54**, 1874–1885.

181. A. A. P. Kumar and T. Banerjee, *Fluid Phase Equilib.*, 2009, **278**, 1–8.

182. Z. G. Lei, W. Arlt, and P. Wasserscheid, *Fluid Phase Equilib.*, 2007, **260**, 29–35.

183. M. G. Freire, P. J. Carvalho, L. M. N. B. F. Santos, L. R. Gomes, I. M. Marrucho, and J. A. P. Coutinho, *J. Chem. Thermodyn.*, 2010, **42**, 213–219.

184. A. R. Ferreira, M. G. Freire, J. C. Ribeiro, F. M. Lopes, J. G. Crespo, and J. A. P. Coutinho, *Ind. Eng. Chem. Res.*, 2011, **50**, 5279–5294.

185. H. Renon and J. M. Prausnitz, *AIChE J.*, 1968, **14**, 135–144.

186. L. D. Simoni, J. F. Brennecke, and M. A. Stadtherr, *Ind. Eng. Chem. Res.*, 2009, **48**, 7246–7256.

187. L. D. Simoni, A. Chapeaux, J. F. Brennecke, and M. A. Stadtherr, *Ind. Eng. Chem. Res.*, 2009, **48**, 7257–7265.

188. L. D. Simoni, Y. Lin, J. F. Brennecke, and M. A. Stadtherr, *Fluid Phase Equilib.*, 2007, **255**, 138–146.

189. L. D. Simoni, Y. Lin, J. F. Brennecke, and M. A. Stadtherr, *Ind. Eng. Chem. Res.*, 2007, **47**, 256–272.

190. J. M. Sørensen, T. Magnussen, P. Rasmussen, and A. Fredenslund, *Fluid Phase Equilib.*, 1979, **3**, 47–82.

191. Y. Song and C.-C. Chen, *Ind. Eng. Chem. Res.*, 2009, **48**, 7788–7797.

192. L. D. Simoni, A. Chapeaux, J. F. Brennecke, and M. A. Stadtherr, *Comput. Chem. Eng.*, 2010, **34**, 1406–1412.

193. M. Matsumura and H. Märkl, *Appl. Microbiol. Biotechnol.*, 1984, **20**, 371–377.

194. M. Roza and E. Maus, in *Distillation & Absorption*, ed. E. Sørenson, IChemE, Rugby, 2006.

195. http://www.il-eco.uft.uni-bremen.de, accessed December 3rd, 2010.

196. D. J. Couling, R. J. Bernot, K. M. Docherty, J. K. Dixon, and E. J. Maginn, *Green Chem.*, 2006, **8**, 82–90.

197. D. Rabari and T. Banerjee, *Fluid Phase Equilib.*, 2013, **355**, 26–33.

198. S. E. Davis and S. A. Morton, *Sep. Sci. Technol.*, 2008, **43**, 2460–2472.

199. G. Severa, G. Kumar, M. Troung, G. Young, and M. J. Cooney, *Sep. Purif. Technol.*, 2013, **116**, 265–270.

200. T. Banerjee, M. K. Singh, R. K. Sahoo, and A. Khanna, *Fluid Phase Equilib.*, 2005, **234**, 64–76.

201. A. Haghtalab and P. Mahmoodi, *Fluid Phase Equilib.*, 2010, **289**, 61–71.

202. Z. Lei, C. Dai, X. Liu, L. Xiao, and B. Chen, *Ind. Eng. Chem. Res.*, 2012, **51**, 12135–12144.

203. Z. Lei, J. Zhang, Q. Li, and B. Chen, *Ind. Eng. Chem. Res.*, 2009, **48**, 2697–2704.

204. C. Pretti, C. Chiappe, D. Pieraccini, M. Gregori, F. Abramo, G. Monni, and L. Intorre, *Green Chem.*, 2006, **8**, 238–240.

205. M. H. Fatemi and P. Izadiyan, *Chemosphere*, 2011, **84**, 553–563.

206. M. McLaughlin, M. J. Earle, M. A. Gîlea, B. F. Gilmore, S. P. Gorman, and K. R. Seddon, *Green Chem.*, 2011, **13**, 2794–2800.

207. X. Wang, C. A. Ohlin, Q. Lu, Z. Fei, J. Hu, and P. J. Dyson, *Green Chem.*, 2007, **9**, 1191–1197.

208. A. García-Lorenzo, E. Tojo, J. Tojo, M. Teijeira, F. J. Rodríguez-Berrocal, M. P. González, and V. S. Martínez-Zorzano, *Green Chem.*, 2008, **10**, 508–516.

209. C.-W. Cho, Y.-C. Jeon, T. P. T. Pham, K. Vijayaraghavan, and Y.-S. Yun, *Ecotoxicol. Environ. Saf.*, 2008, **71**, 166–171.

210. S. P. M. Ventura, R. L. Gardas, F. Gonçalves, and J. A. P. Coutinho, *J. Chem. Technol. Biotechnol.*, 2011, **86**, 957–963.

211. C. Pretti, C. Chiappe, I. Baldetti, S. Brunini, G. Monni, and L. Intorre, *Ecotoxicol. Environ. Saf.*, 2009, **72**, 1170–1176.

212. J. Salminen, N. Papaiconomou, R. A. Kumar, J.-M. Lee, J. Kerr, J. Newman, and J. M. Prausnitz, *Fluid Phase Equilib.*, 2007, **261**, 421–426.

213. S. Stolte, J. Arning, U. Bottin-Weber, A. Muller, W.-R. Pitner, U. Welz-Biermann, B. Jastorff, and J. Ranke, *Green Chem.*, 2007, **9**, 760–767.

214. P. J. Carvalho, S. P. M. Ventura, M. L. S. Batista, B. Schröder, F. Gonçalves, J. Esperança, F. Mutelet, and J. A. P. Coutinho, *J. Chem. Phys.*, 2014, **140**, 064505.

215. D. S. H. Wong, J. P. Chen, J. M. Chang, and C. H. Chou, *Fluid Phase Equilib.*, 2002, **194–197**, 1089–1095.

216. P. J. Carvalho, T. Regueira, L. M. N. B. F. Santos, J. Fernandez, and J. A. P. Coutinho, *J. Chem. Eng. Data*, 2010, **55**, 645–652.

217. C. Tsonopoulos, *Fluid Phase Equilib.*, 1999, **156**, 21–33.

218. J. N. A. Canongia Lopes and A. A. H. Pádua, *J. Phys. Chem. B*, 2006, **110**, 3330–3335.

219. C. J. Adkins, Equilibrium Thermodynamics, McGraw-Hill, London, 1968.

220. R. L. Gardas and J. A. P. Coutinho, *Fluid Phase Equilib.*, 2008, **263**, 26–32.

221. R. L. Gardas and J. A. P. Coutinho, *AIChE J.*, 2009, **55**, 1274–1290.

222. A. Klamt, *Wiley Interdiscip. Rev. Comput. Mol. Sci.*, 2011, **1**, 699–709.

223. TURBOMOLE, University of Karlsruhe and Forschungszentrum Karlsruhe Gmb, 2009.

224. COSMOtherm Version C2.1 Release 01.08, F. Eckert and A. Klamt, Leverkusen, Germany, 2008.

225. W. Smith and T. R. Forester, The DL_POLY Package of Molecular Simulation Routines (V.2.17). The Council for The Central Laboratory of Research Councils, W. Smith and T. R. Forester, Daresbury Laboratory: Warrington, U.K., 2006.

226. J. N. Canongia Lopes and A. A. H. Pádua, *J. Phys. Chem. B*, 2004, **108**, 16893–16898.

227. J. N. Canongia Lopes and A. A. H. Padua, *J. Phys. Chem. B*, 2006, **110**, 19586–19592.

228. Gaussian 03, Revision C.05, M. J. Frisch, G. W. Trucks, H. B. Schlegel, G. E. Scuseria, M. A. Robb, J. R. Cheeseman, J. Montgomery, J. A., T. Vreven, K. N. Kudin, J. C. Burant, J. M. Millam, S. S. Iyengar, J. Tomasi, V. Barone, B. Mennucci, M. Cossi, G. Scalmani, N. Rega, G. A. Petersson, H. Nakatsuji, M. Hada, M. Ehara, K. Toyota, R. Fukuda, J. Hasegawa, M. Ishida, T. Nakajima, Y. Honda, O. Kitao, H. Nakai, M. Klene, X. Li, J. E. Knox, H. P. Hratchian, J. B. Cross, V. Bakken, C. Adamo, J. Jaramillo, R. Gomperts, R. E. Stratmann, O. Yazyev, A. J. Austin, R. Cammi, C. Pomelli, J. W. Ochterski, P. Y. Ayala, K. Morokuma, G. A. Voth, P. Salvador, J. J. Dannenberg, V. G. Zakrzewski, S. Dapprich, A. D. Daniels, M. C. Strain, O. Farkas, D. K. Malick, A. D. Rabuck, K. Raghavachari, J. B. Foresman, J. V. Ortiz, Q. Cui, A. G. Baboul, S. Clifford, J. Cioslowski, B. B. Stefanov, G. Liu, A. Liashenko, P. Piskorz, I. Komaromi, R. L. Martin, D. J. Fox, T. Keith, M. A. Al.Laham, C. Y. Peng, A. Nanayakkara, M. Challacombe, P. M. W. Gill, B. Johnson, W. Chen, M. W. Wong, C. Gonzalez, and J. A. Pople, Wallingford CT, 2004.

229. J. R. Harjani, R. D. Singer, M. T. Garcia, and P. J. Scammells, *Green Chem.*, 2008, **11**, 83–90.

230. W. L. Jorgensen, D. S. Maxwell, and J. Tirado-Rives, *J. Am. Chem. Soc.*, 1996, **118**, 11225–11236.

231. G. Kaminski and W. L. Jorgensen, *J. Phys. Chem.*, 1996, **100**, 18010–18013.

232. N. A. McDonald and W. L. Jorgensen, *J. Phys. Chem. B*, 1998, **102**, 8049–8059.

233. M. Praprotnik, D. Janežič, and J. Mavri, *J. Phys. Chem. A*, 2004, **108**, 11056–11062.

234. W. Smith and T. R. Forester, The DL_POLY Package of Molecular Simulation Routines (v.2.2), 2006.

235. J. N. Canongia Lopes, J. Deschamps, and A. A. H. Pádua, *J. Phys. Chem. B*, 2004, **108**, 2038–2047.

236. K. Shimizu, D. Almantariotis, M. F. Costa Gomes, A. A. H. Pádua, and J. N. Canongia Lopes, *J. Phys. Chem. B*, 2010, **114**, 3592–600.

237. H. L. Ngo, K. LeCompte, L. Hargens, and A. B. McEwen, *Thermochim. Acta*, 2000, **357-358**, 97–102.

238. M. G. Freire, L. M. N. B. F. Santos, A. M. Fernandes, J. A. P. Coutinho, and I. M. Marrucho, *Fluid Phase Equilib.*, 2007, **261**, 449–454.

239. M. Tariq, P. J. Carvalho, J. A. P. Coutinho, I. M. Marrucho, J. N. Canongia Lopes, and L. P. N. Rebelo, *Fluid Phase Equilib.*, 2011, **301**, 22–32.

240. F. S. Oliveira, M. G. Freire, P. J. Carvalho, J. A. P. Coutinho, J. N. Canongia Lopes, L. P. N. Rebelo, and I. M. Marrucho, *J. Chem. Eng. Data*, 2010, **55**, 4514–4520.

241. M. A. A. Rocha, C. M. S. S. Neves, M. G. Freire, O. Russina, A. Triolo, J. A. P. Coutinho, and L. M. N. B. F. Santos, *J. Phys. Chem. B*, 2013, **117**, 10889–10897.

242. R. L. Gardas, H. F. Costa, M. G. Freire, P. J. Carvalho, I. M. Marrucho, I. M. A. Fonseca, A. G. M. Ferreira, and J. A. P. Coutinho, *J. Chem. Eng. Data*, 2008, **53**, 805–811.

243. I. Bandrés, B. Giner, H. Artigas, C. Lafuente, and F. M. Royo, *J. Chem. Eng. Data*, 2009, **54**, 236–240.

244. I. Bandrés, B. Giner, I. Gascón, M. Castro, and C. Lafuente, *J. Phys. Chem. B*, 2008, **112**, 12461–12467.

245. I. Bandrés, B. Giner, H. Artigas, F. M. Royo, and C. Lafuente, *J. Phys. Chem. B*, 2008, **112**, 3077–3084.

246. L. G. Sánchez, J. R. Espel, F. Onink, G. W. Meindersma, and A. B. de Haan, *J. Chem. Eng. Data*, 2009, **54**, 2803–2812.

247. J. Jacquemin, P. Husson, A. A. H. Padua, and V. Majer, *Green Chem.*, 2006, **8**, 172–180.

248. J. M. Crosthwaite, M. J. Muldoon, J. K. Dixon, J. L. Anderson, and J. F. Brennecke, *J. Chem. Thermodyn.*, 2005, **37**, 559–568.

249. A. Chapeaux, L. D. Simoni, M. A. Stadtherr, and J. F. Brennecke, *J. Chem. Eng. Data*, 2007, **52**, 2462–2467.

250. L. P. N. Rebelo, V. Najdanovic-Visak, Z. P. Visak, M. Nunes da Ponte, J. Szydlowski, C. A. Cerdeiriña, J. Troncoso, L. Romaní, J. M. S. S. Esperança, H. J. R. Guedes, and H. C. de Sousa, *Green Chem.*, 2004, **6**, 369–381.

251. M. Blesic, M. H. Marques, N. V. Plechkova, K. R. Seddon, L. P. N. Rebelo, and A. Lopes, *Green Chem.*, 2007, **9**, 481–490.

252. T. M. Letcher, D. Ramjugernath, K. Tumba, M. Królikowski, and U. Domańska, *Fluid Phase Equilib.*, 2010, **294**, 89–97.

253. L. P. N. Rebelo, *Phys. Chem. Chem. Phys.*, 1999, **1**, 4277–4286.

254. H. C. De Sousa and L. P. N. Rebelo, *J. Polym. Sci. Part B Polym. Phys.*, 2000, **38**, 632–651.

255. J. N. Canongia Lopes, M. F. Costa Gomes, and A. A. H. Pádua, *J. Phys. Chem. B*, 2006, **110**, 16816–16818.

256. N. Shvedene, S. Borovskaya, V. Sviridov, E. Ismailova, and I. Pletnev, *Anal. Bioanal. Chem.*, 2005, **381**, 427–430.

257. A. Pohorille and L. R. Pratt, *J. Am. Chem. Soc.*, 1990, **112**, 5066–5074.

258. L. R. Pratt and A. Pohorille, *Proc. Natl. Acad. Sci.*, 1992, **89**, 2995–2999.

259. K. Machanová, J. Jacquemin, Z. Wagner, and M. Bendová, *Procedia Eng.*, 2012, **42**, 1229–1241.

260. R. L. Gardas, R. Ge, N. Ab Manan, D. W. Rooney, and C. Hardacre, *Fluid Phase Equilib.*, 2010, **294**, 139–147.

261. U. Domańska, A. Rękawek, and A. Marciniak, *J. Chem. Eng. Data*, 2008, **53**, 1126–1132.

262. M. A. A. Rocha, F. M. S. Ribeiro, B. Schröder, J. A. P. Coutinho, and L. M. N. B. F. Santos, *J. Chem. Thermodyn.*, 2014, **68**, 317–321.

263. M. A. A. Rocha, J. A. P. Coutinho, and L. M. N. B. F. Santos, *J. Chem. Phys.*, 2013, **139**, 104502.

264. M. A. A. Rocha, M. Bastos, J. A. P. Coutinho, and L. M. N. B. F. Santos, *J. Chem. Thermodyn.*, 2012, **53**, 140–143.

265. M. Tariq, M. G. Freire, B. Saramago, J. A. P. Coutinho, J. N. C. Lopes, and L. P. N. Rebelo, *Chem. Soc. Rev.*, 2012, **41**, 829–68.

266. P. J. Carvalho, M. G. Freire, I. M. Marrucho, A. J. Queimada, and J. A. P. Coutinho, *J. Chem. Eng. Data*, 2008, **53**, 1346–1350.

267. M. Tariq, P. A. S. Forte, M. F. C. Gomes, J. N. Canongia Lopes, and L. P. N. Rebelo, *J. Chem. Thermodyn.*, 2009, **41**, 790–798.

268. A. A. C. C. Pais, A. Sousa, M. E. Eusébio, and J. S. Redinha, *Phys. Chem. Chem. Phys.*, 2001, **3**, 4001–4009.

269. S. Cabani, P. Gianni, V. Mollica, and L. Lepori, *J. Solution Chem.*, 1981, **10**, 563–595.

270. M. A. A. Rocha, J. A. P. Coutinho, and L. M. N. B. F. Santos, *J. Phys. Chem. B*, 2012, **116**, 10922–10927.

271. Y. Watanabe and S. Katsuta, *J. Chem. Eng. Data*, 2014, **59**, 696–701.

272. N. V Ignat'ev, U. Welz-Biermann, A. Kucheryna, G. Bissky, and H. Willner, *J. Fluor. Chem.*, 2005, **126**, 1150–1159.

273. D. Almantariotis, S. Stevanovic, O. Fandiño, A. S. Pensado, A. A. H. Pádua, J.-Y. Coxam, and M. F. Costa Gomes, *J. Phys. Chem. B*, 2012, **116**, 7728–7738.

274. Q.-S. Liu, J. Tong, Z.-C. Tan, U. Welz-Biermann, and J.-Z. Yang, *J. Chem. Eng. Data*, 2010, **55**, 2586–2589.

275. S. Seki, N. Serizawa, K. Hayamizu, S. Tsuzuki, Y. Umebayashi, K. Takei, and H. Miyashiro, *J. Electrochem. Soc.*, 2012, **159**, A967–A971.

276. M. Součková, J. Klomfar, and J. Pátek, *J. Chem. Thermodyn.*, 2012, **48**, 267–275.

277. NIST Chemistry Webbook at http://webbook.nist.gov/ chemistry/, accessed April 3rd, 2014.

278. U. Domańska, M. Królikowski, A. Pobudkowska, and P. Bocheńska, *J. Chem. Thermodyn.*, 2012, **55**, 225–233.

279. S. Martinho, J. M. M. Araújo, L. P. N. Rebelo, A. B. Pereiro, and I. M. Marrucho, *J. Chem. Thermodyn.*, 2013, **64**, 71–79.

280. M. A. A. Rocha, C. F. R. A. C. Lima, L. R. Gomes, B. Schröder, J. A. P. Coutinho, I. M. Marrucho, J. M. S. S. Esperança, L. P. N. Rebelo, K. Shimizu, J. N. Canongia Lopes, and L. M. N. B. F. Santos, *J. Phys. Chem. B*, 2011, **115**, 10919–10926.

281. A. B. Pereiro, M. J. Pastoriza-Gallego, K. Shimizu, I. M. Marrucho, J. N. Canongia Lopes, M. M. Piñeiro, and L. P. N. Rebelo, *J. Phys. Chem. B*, 2013, **117**, 10826–10833.

282. O. Borodin, *J. Phys. Chem. B*, 2009, **113**, 12353–12357.

283. U. L. Bernard, E. I. Izgorodina, and D. R. MacFarlane, *J. Phys. Chem. C*, 2010, **114**, 20472–20478.

284. F. S. Oliveira, A. B. Pereiro, J. M. M. Araújo, C. E. S. Bernardes, J. N. Canongia Lopes, S. Todorovic, G. Feio, P. L. Almeida, L. P. N. Rebelo, and I. M. Marrucho, *Phys. Chem. Chem. Phys.*, 2013, **15**, 18138–18147.

285. K. Ueno, H. Tokuda, and M. Watanabe, *Phys. Chem. Chem. Phys.*, 2010, **12**, 1649–1658.

286. J. F. Wishart, *Energy Environ. Sci.*, 2009, **2**, 956–961.

287. M. G. Freire, C. L. S. Louros, L. P. N. Rebelo, and J. A. P. Coutinho, *Green Chem.*, 2011, **13**, 1536–1545.

288. M. G. Freire, J. F. B. Pereira, M. Francisco, H. Rodríguez, L. P. N. Rebelo, R. D. Rogers, and J. A. P. Coutinho, *Chem. – A Eur. J.*, 2012, **18**, 1831–1839.

289. A. W. W. A., Water quality and treatment: a handbook of community water supplies, McGraw-Hill, 4th edn., 1990.

290. J. C. Merchuk, B. A. Andrews, and J. A. Asenjo, *J. Chromatogr. B*, 1998, **711**, 285–293.

291. A. F. M. Cláudio, M. G. Freire, C. S. R. Freire, A. J. D. Silvestre, and J. A. P. Coutinho, *Sep. Purif. Technol.*, 2010, **75**, 39–47.

292. P. González-Tello, F. Camacho, G. Blázquez, and F. J. Alarcón, *J. Chem. Eng. Data*, 1996, **41**, 1333–1336.

293. T. A. Graber, H. Galleguillos, J. A. Asenjo, and B. A. Andrews, *J. Chem. Eng. Data*, 2001, **47**, 174–178.

294. M. Perumalsamy and T. Murugesan, *J. Chem. Eng. Data*, 2009, **54**, 1359–1366.

295. S. M. Snyder, K. D. Cole, and D. C. Szlag, *J. Chem. Eng. Data*, 1992, **37**, 268–274.

296. M. Czerwicka, S. Stolte, A. Müller, E. M. Siedlecka, M. Golebiowski, J. Kumirska, and P. Stepnowski, *J. Hazard. Mater.*, 2009, **171**, 478–483.

297. E. M. Siedlecka, M. Czerwicka, S. Stolte, and P. Stepnowski, *Curr. Org. Chem.*, 2011, **15**, 1974–1991.

298. C. M. S. S. Neves, M. G. Freire, and J. A. P. Coutinho, *RSC Adv.*, 2012, **2**, 10882–10890.

299. S. Stolte, J. Arning, and J. Thöming, *Chemie Ing. Tech.*, 2011, **15**, 1946 –1973.

300. C. Abrusci, J. Palomar, J. L. Pablos, F. Rodriguez, and F. Catalina, *Green Chem.*, 2011, **13**, 709–717.

301. G. W. Meindersma and A. B. de Haan, *Chem. Eng. Res. Des.*, 2008, **86**, 745–752.

302. P. Nockemann, K. Binnemans, and K. Driesen, *Chem. Phys. Lett.*, 2005, **415**, 131–136.

303. J. Kröckel and U. Kragl, *Chem. Eng. Technol.*, 2003, **26**, 1166–1168.

304. T. Schäfer, C. M. Rodrigues, C. A. M. Afonso, and J. G. Crespo, *Chem. Commun.*, 2001, 1622–1623.

305. M. E. Mahmoud and H. M. Al-Bishri, *Chem. Eng. J.*, 2011, **166**, 157–167.

306. A. Farooq, L. Reinert, J.-M. Levêque, N. Papaiconomou, N. Irfan, and L. Duclaux, *Microporous Mesoporous Mater.*, 2012, **158**, 55–63.

307. L. Reinert, K. Batouche, J.-M. Lévêque, F. Muller, J.-M. Bény, B. Kebabi, and L. Duclaux, *Chem. Eng. J.*, 2012, **209**, 13–19.

308. J. Lemus, C. M. S. S. Neves, C. F. C. Marques, M. G. Freire, J. A. P. Coutinho, and J. Palomar, *Environ. Sci. Process. Impacts*, 2013, **15**, 1752–1759.

309. M. Goyal and R. C. Bansal, Activate Carbon Adsorption, CRC Press, 2005.

310. C. Yin, M. Aroua, and W. Daud, *Sep. Purif. Technol.*, 2007, **52**, 403–415.

311. J. Lemus, M. Martin-Martinez, J. Palomar, L. Gomez-Sainero, M. A. Gilarranz, and J. J. Rodriguez, *Chem. Eng. J.*, 2012, **211-212**, 246–254.

312. Gaussian 03, Revision B.05, M. J. Frisch, G. W. Trucks, H. B. Schlegel, G. E. Scuseria, M. A. Robb, J. R. Cheeseman, J. A. Montgomery, Jr., T. Vreven, K. N. Kudin, J. C. Burant, J. M. Millam, S. S. Iyengar, J. Tomasi, V. Barone, B. Mennucci, M. Cossi, G. Scalmani, N. Rega, G. A. Petersson, H. Nakatsuji, M. Hada, M. Ehara, K. Toyota, R. Fukuda, J. Hasegawa, M. Ishida, T. Nakajima, Y. Honda, O. Kitao, H. Nakai, M. Klene, X. Li, J. E. Knox, H. P. Hratchian, J. B. Cross, V. Bakken, C. Adamo, J. Jaramillo, R. Gomperts, R. E. Stratmann, O. Yazyev, A. J. Austin, R. Cammi, C. Pomelli, J. W. Ochterski, P. Y. Ayala, K. Morokuma, G. A. Voth, P. Salvador, J. J. Dannenberg, V. G. Zakrzewski, S. Dapprich, A. D. Daniels, M. C. Strain, O. Farkas, D. K. Malick, A. D. Rabuck, K. Raghavachari, J. B. Foresman, J. V. Ortiz, Q. Cui, A. G. Baboul, S. Clifford, J. Cioslowski, B. B. Stefanov, G. Liu, A. Liashenko, P. Piskorz, I. Komaromi, R. L. Martin, D. J. Fox, T. Keith, M. A. Al-Laham, C. Y. Peng, A. Nanayakkara, M. Challacombe, P. M. W. Gill, B. Johnson, W. Chen, M. W. Wong, C. Gonzalez, and J. A. Pople, Wallingford CT, 2004.

313. J. Perdew, *Phys. Rev. B*, 1986, **33**, 8822–8824.

314. C. Sosa, J. Andzelm, B. C. Elkin, E. Wimmer, K. D. Dobbs, and D. A. Dixon, *J. Phys. Chem.*, 1992, **96**, 6630–6636.

315. COSMOtherm Version C2.1, Release 01.06, F. Eckert and A. Klamt, Leverkusen, Germany, 2006.

Universidade de Aveiro Departamento de Química
2014

CATARINA MAIA SECO SEIÇA NEVES

TRATAMENTO DE EFLUENTES AQUOSOS CONTAMINADOS COM LÍQUIDOS IÓNICOS

TREATMENT OF AQUEOUS EFFLUENTS CONTAMINATED WITH IONIC LIQUIDS

APPENDIX

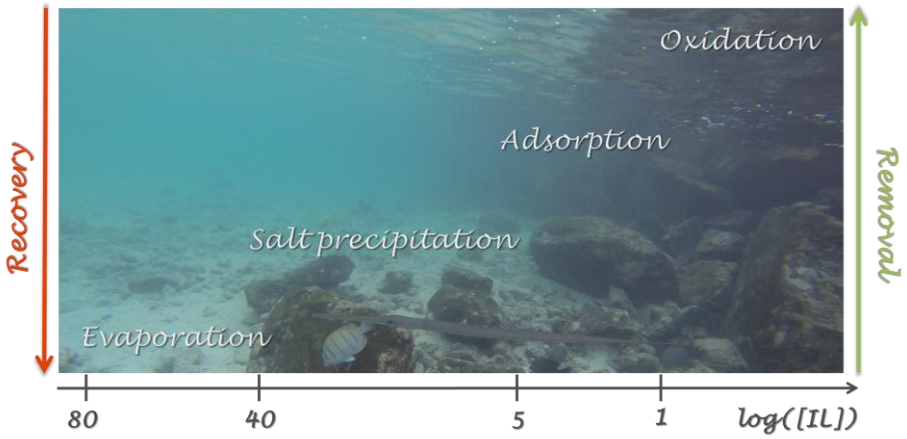

Universidade de Aveiro Departamento de Química
2014

CATARINA MAIA SECO SEIÇA NEVES

TRATAMENTO DE EFLUENTES AQUOSOS CONTAMINADOS COM LÍQUIDOS IÓNICOS

TREATMENT OF AQUEOUS EFFLUENTS CONTAMINATED WITH IONIC LIQUIDS

Tese apresentada à Universidade de Aveiro para cumprimento dos requisitos necessários à obtenção do grau de Doutor em Química, realizada sob a orientação científica do Professor Doutor. João Manuel da Costa e Araújo Pereira Coutinho, Professor Catedrático do Departamento de Química da Universidade de Aveiro, e coorientação da Doutora Mara Guadalupe Freire Martins, Investigadora Coordenadora no Departamento de Química, CICECO, da Universidade de Aveiro

Apoio financeiro do POCTI no âmbito do III Quadro Comunitário de Apoio. Cofinanciamento do POPH/FSE.

O doutorando agradece o apoio financeiro da FCT no âmbito do III Quadro Comunitário de Apoio (SFRH / BD / 70641 / 2010).

Contents

List of Figures

List of Tables

Appendix Chapter 2 – Ionic-Liquid-based Processes

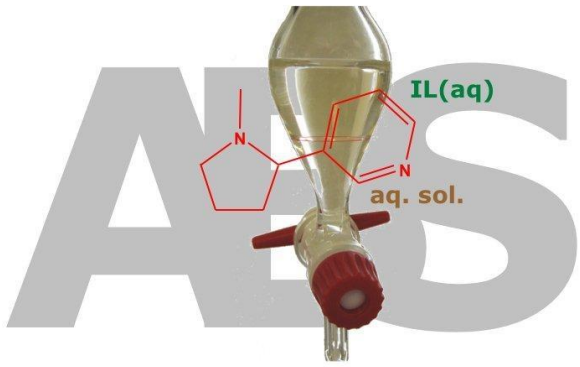

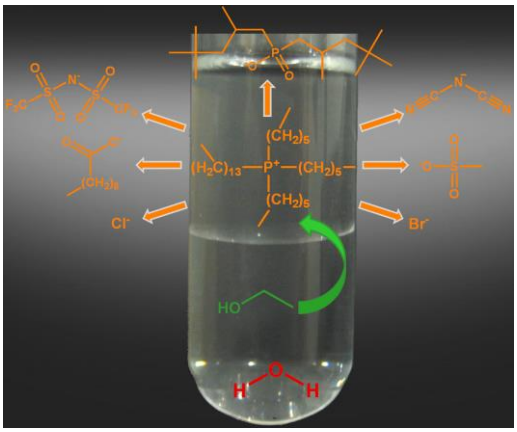

2.1. High-performance extraction of alkaloids using aqueous two-phase systems with ionic liquids

Mara G. Freire, Catarina M. S. S. Neves, Isabel M. Marrucho, José N. Canongia Lopes, Luís Paulo N. Rebelo and João A. P. Coutinho, Green Chemistry 12 (2010) 1715-1718, DOI: 10.1039/c0gc00179a

EXPERIMENTAL PROCEDURE

Nicotine, > 99 wt% pure, was purchased from Sigma-Aldrich while caffeine, > 98.5 wt% pure, was acquired at Marsing & Co. Ltd. A/S. All ionic liquids (ILs) were commercially acquired at Iolitec, with the exception of $[C_4C_1im][CF_3CO_2]$ that was purchased from Solchemar. Ionic liquids individual samples were dried under constant conditions at moderate vacuum and temperature, for a minimum of 48 h, before use. The purity of each ionic liquid was further checked by ^{1}H, ^{13}C, and ^{19}F NMR spectra and found to be superior to 99 wt% for all samples. Urea, 99 wt% pure, was supplied by Panreac and used without further purification. K_3PO_4, 98 wt% pure, and NaCl, 99.9 % wt% pure, were from Sigma and Normapur, respectively. In order to remove water, the inorganic salts were dried under vacuum for a minimum of 12 h before use. Water used was ultrapure water, double distilled, passed by a reverse osmosis system and finally treated with a Milli-Q plus 185 water purification equipment.

Synthetic human urine aqueous phases were prepared by dissolution of urea and NaCl, in pure water, at the concentrations of 1.2 $g \cdot dm^{-3}$ and 4.0 $g \cdot dm^{-3}$, respectively. The alkaloids quantification, in both phases, was carried out by UV spectroscopy using a SHIMADZU UV-1700, Pharma-Spec spectrometer, at a wavelength of 274 nm or 261 nm for caffeine and nicotine, respectively, and using calibration curves previously established. Initial concentrations of caffeine and nicotine for phase distribution at the water ternary composition were, respectively, 2.6×10^{-2} $mol \cdot dm^{-3}$ and 2.5×10^{-2} $mol \cdot dm^{-3}$. Possible interferences of both the inorganic salt and the ionic liquid with the analytical method were taken into account and blank controls were employed whenever necessary. The partition coefficients of caffeine (K_{caf}) or nicotine (K_{nic}) are defined as the ratio between

the concentration of the alkaloids in the IL- and K_3PO_4-rich phases.Partition Coefficients and Extraction Efficiencies

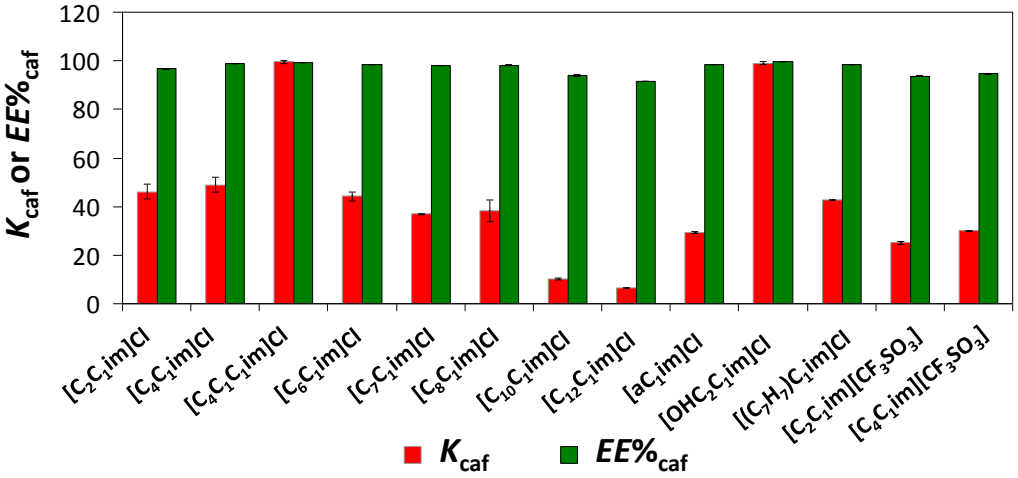

Figure S 2.1. Partition coefficients (K_{caf}) and extraction efficiencies percentages ($EE\%_{caf}$) of caffeine in chloride-based ILs/K_3PO_4 ABS at 298 K (IL at 25 wt% and K_3PO_4 at 15 wt%, except for $[(C_7H_7)C_1im]Cl$ at 40 wt% and K_3PO_4 at 15 wt%).

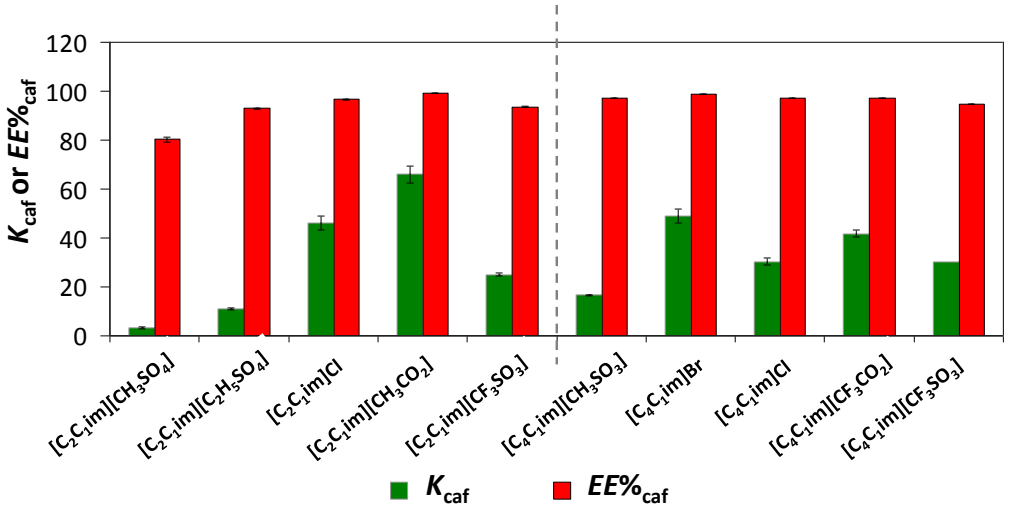

Figure S 2.2. Partition coefficients (K_{caf}) and extraction efficiencies percentages ($EE\%_{caf}$) of caffeine in $[C_2C_1im]$- and $[C_4C_1im]$-based ILs/K_3PO_4 ABS at 298 K (IL at 25 wt% and K_3PO_4).

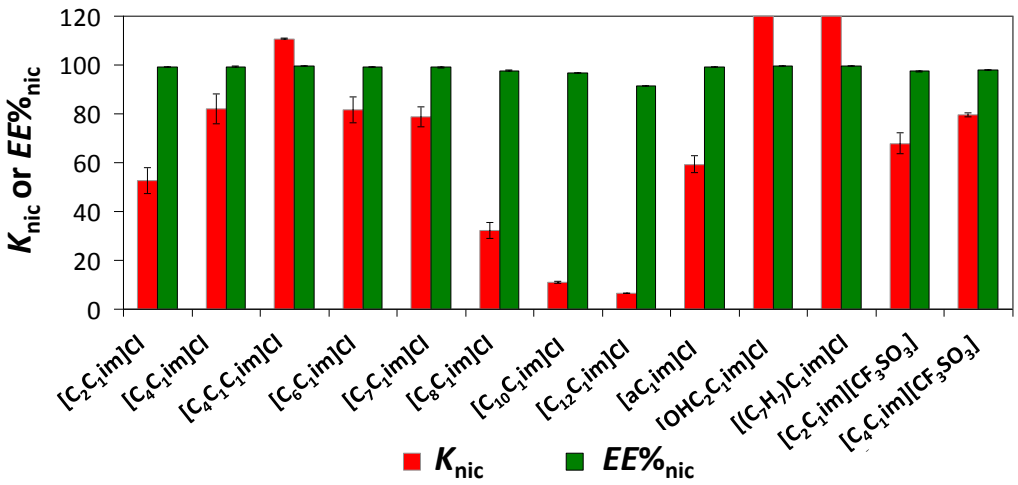

Figure S 2.3. Partition coefficients (K_{nic}) and extraction efficiencies percentages ($EE\%_{nic}$) of nicotine in chloride-based ILs/K_3PO_4 ABS at 298 K (IL at 25 wt% and K_3PO_4 at 15 wt%, except for [(C_7H_7)C_1im]Cl at 40 wt% and K_3PO_4 at 15 wt%).

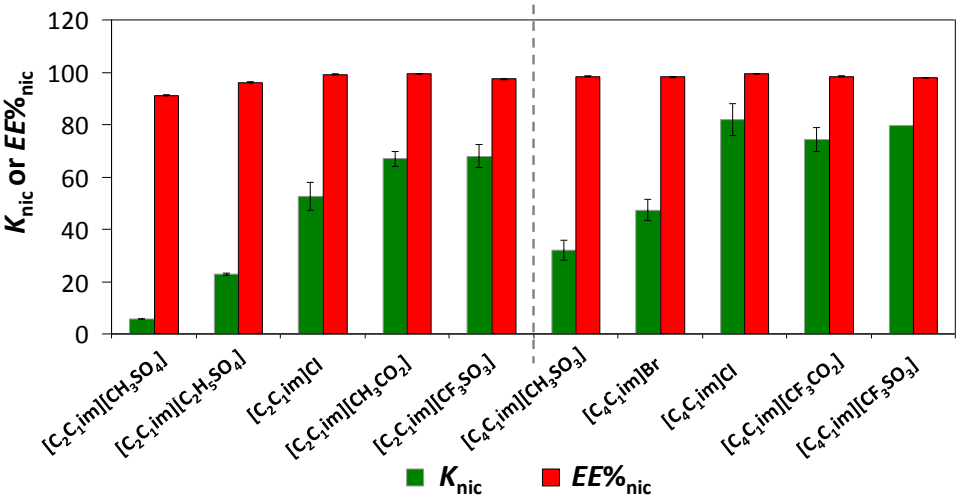

Figure S 2.4. Partition coefficients (K_{nic}) and extraction efficiencies percentages ($EE\%_{nic}$) of nicotine in [C_2C_1im]- and [C_4C_1im]-based ILs/K_3PO_4 ABS at 298 K (IL at 25 wt% and K_3PO_4).

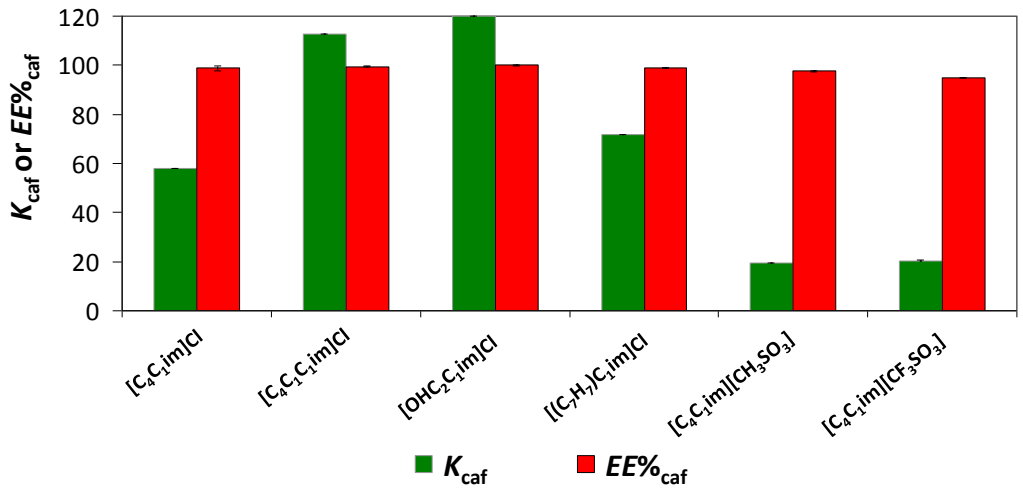

Figure S 2.5. Partition coefficients (K_{caf}) and extraction efficiencies percentages ($EE\%_{caf}$) of caffeine in human urine-based ILs/K_3PO_4 ABS at 298 K (IL at 25 wt% and K_3PO_4 at 15 wt%, except for $[(C_7H_7)C_1im]Cl$ at 40 wt% and K_3PO_4 at 15 wt%).

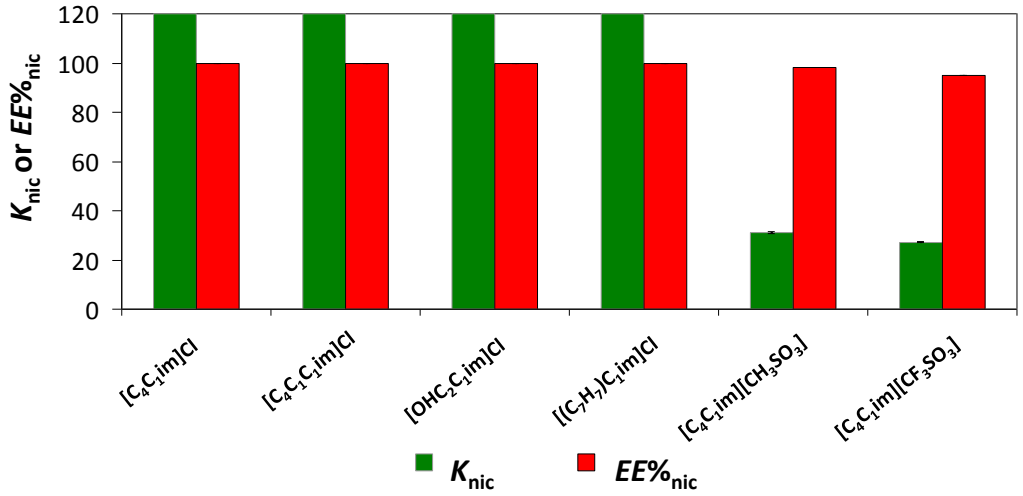

Figure S 2.6. Partition coefficients (K_{nic}) and extraction efficiencies percentages ($EE\%_{nic}$) of nicotine in human urine-based ILs/K_3PO_4 ABS at 298 K (IL at 25 wt% and K_3PO_4 at 15 wt%, except for $[(C_7H_7)C_1im]Cl$ at 40 wt% and K_3PO_4 at 15 wt%).

Table S 2.1. Weight fraction composition, partition coefficients and extraction efficiencies of caffeine in IL-based ABS and respective tie-lines (TLs) and tie-line lengths (TLLs).

IL	wt%		TL equation IL (wt%) = $a + b \cdot K_3PO_4$ (wt%)		TLL	$K_{caf} \pm \sigma^a$	$EE\%_{caf} \pm \sigma^a$
	IL	K_3PO_4	a	b			
$[C_2C_1im]Cl$	25.185	14.962	42.205	-1.138	43.386	46.1 ± 2.9	96.70 ± 0.20
	40.093	15.129	58.722	-1.231	73.811	120	100
$[C_4C_1im]Cl$	24.361	14.923	42.269	-1.200	44.493	49.0 ± 2.9	98.89 ± 0.07
	30.320	14.760	49.407	-1.293	57.788	120	100

	34.989	15.479	55.708	-1.339	67.523	120	100
	39.855	15.004	59.968	-1.341	73.856	120	100
	44.853	15.040	66.399	-1.433	80.650	120	100
$[C_4C_1C_1im]Cl$	25.127	15.080	44.154	-1.262	47.966	99.6 ± 0.6	99.41 ± 0.03
$[C_6C_1im]Cl$	24.921	14.856	46.455	-1.450	45.907	44.1 ± 1.8	98.53 ± 0.06
$[C_7C_1im]Cl$	25.066	15.166	49.496	-1.611	44.417	37.0 ± 0.2	97.96 ± 0.01
$[C_8C_1im]Cl$	25.068	15.073	50.675	-1.699	36.784	38.2 ± 4.6	98.16 ± 0.22
$[C_{10}C_1im]Cl$	25.046	15.207	53.181	-1.850	24.853	10.1 ± 0.5	94.01 ± 0.26
$[C_{12}C_1im]Cl$	25.038	15.014	51.344	-1.752	27.518	6.65 ± 0.01	91.61 ± 0.01
	24.262	15.293	42.449	-1.189	42.842	29.4 ± 0.3	98.32 ± 0.02
	30.023	14.813	47.901	-1.207	56.670	120	100
$[aC_1im]Cl$	35.148	14.956	54.115	-1.268	66.449	120	100
	40.132	14.871	60.586	-1.375	73.839	120	100
	44.817	15.193	64.543	-1.298	81.148	32.3 ± 0.3	98.47 ± 0.04
$[OHC_2C_1im]Cl$	39.963	15.049	85.826	-3.048	63.673	98.9 ± 0.6	99.69 ± 0.02
	25.123	14.925	50.512	-1.701	43.036	42.62 ± 0.06	98.26 ± 0.02
	30.105	14.962	55.816	-1.718	56.054	120	100
	34.893	15.001	60.784	-1.726	65.219	120	100
	40.057	14.930	66.055	-1.741	73.246	120	100
$[(C_7H_7)C_1im]Cl$	44.996	14.930	69.071	-1.613	79.476	120	100
	49.962	14.883	75.540	-1.719	86.458	90.0 ± 5.7	99.51 ± 0.04
	25.152	19.997	59.596	-1.723	63.229	120	100
	25.053	25.067	66.647	-1.659	75.361	120	100
	25.130	29.832	71.663	-1.560	83.829	120	100
$[C_2C_1im][CF_3SO_3]$	24.996	14.891	69.540	-2.991	61.973	25.1 ± 0.8	93.59 ± 0.18
$[C_4C_1im][CF_3SO_3]$	24.996	15.352	70.967	-2.995	70.428	30.0 ± 0.2	94.70 ± 0.04
$[C_2C_1im][CH_3SO_4]$	25.007	15.178	51.644	-1.755	31.551	3.3 ± 0.5	80.27 ± 1.05
$[C_2C_1im][C_2H_5SO_4]$	24.853	15.648	54.162	-1.873	44.687	11.1 ± 0.3	92.86 ± 0.18
$[C_2C_1im][CH_3CO_2]$	25.172	14.931	39.995	-0.993	48.132	66.0 ± 3.6	99.34 ± 0.04
$[C_4C_1im]Br$	24.822	15.085	50.345	-1.692	45.396	30.4 ± 1.3	97.18 ± 0.11
$[C_4C_1im][CH_3SO_3]$	24.917	15.090	44.622	-1.306	38.919	16.6 ± 0.2	96.98 ± 0.04
$[C_4C_1im][CF_3CO_2]$	24.785	15.475	58.626	-2.187	56.984	41.8 ± 1.6	97.09 ± 0.14

[a]associated standard deviation

Table S 2.2. Weight fraction composition, partition coefficients and extraction efficiencies of nicotine in IL-based ABS and respective tie-lines (TLs) and tie-line lengths (TLLs).

IL	wt%		TL equation IL (wt%) = $a + b \cdot K_3PO_4$ (wt%)		TLL	$K_{nic} \pm \sigma^a$	$EE\%_{nic} \pm \sigma^a$
	IL	K_3PO_4	*a*	*b*			
$[C_2C_1im]Cl$	25.292	14.778	41.527	-1.099	43.583	52.7 ± 5.3	99.18 ± 0.08
	40.093	15.129	51.916	-1.237	73.950	58.7 ± 2.7	99.31 ± 0.03
$[C_4C_1im]Cl$	25.569	14.882	43.662	-1.216	47.673	82.1 ± 6.1	99.34 ± 0.05
	29.990	16.281	51.758	-1.337	60.914	120	100
	35.005	15.271	56.611	-1.415	67.114	120	100
	39.832	14.876	60.539	-1.392	73.521	120	100
	45.014	15.279	66.739	-1.422	81.312	120	100
	49.957	15.159	71.248	-1.405	87.410	95.5 ± 1.3	99.51 ± 0.03
$[C_4C_1C_1im]Cl$	25.007	15.170	44.057	-1.256	47.953	110.7 ± 0.2	99.47 ± 0.01
$[C_6C_1im]Cl$	25.125	14.891	47.112	-1.477	46.634	81.7 ± 5.4	99.17 ± 0.05
$[C_7C_1im]Cl$	25.014	15.263	49.737	-1.620	44.798	78.8 ± 4.0	99.01 ± 0.05
$[C_8C_1im]Cl$	25.010	15.079	50.901	-1.717	36.597	32.1 ± 3.3	97.71 ± 0.23
$[C_{10}C_1im]Cl$	24.992	15.146	53.162	-1.860	23.302	11.0 ± 0.3	96.72 ± 0.09
$[C_{12}C_1im]Cl$	25.000	15.010	51.576	-1.771	27.095	6.5 ± 0.1	91.49 ± 0.10
$[aC_1im]Cl$	24.945	15.198	43.838	-1.773	44.833	59.3 ± 3.6	99.17 ± 0.05
	29.895	14.931	47.853	-1.203	56.717	120	100
	34.916	15.013	53.812	-1.259	66.201	120	100
	39.761	15.222	53.383	-1.223	74.348	120	100
	45.146	15.093	63.720	-1.231	81.772	120	100
$[OHC_2C_1im]Cl$	40.072	14.915	86.128	-3.088	63.369	120	100
$[(C_7H_7)C_1im]Cl$	25.081	14.807	50.444	-1.691	43.240	120	100
	30.100	15.043	47.689	-1.169	54.397	120	100
	35.183	15.013	60.969	-1.718	65.685	120	100
	40.873	15.017	65.921	-1.668	74.182	120	100
	45.070	14.987	69.977	-1.662	79.952	120	100
	49.923	15.001	73.733	-1.554	86.007	120	100
	25.081	14.807	50.444	-1.691	43.241	120	100
	24.991	20.053	59.757	-1.734	63.292	120	100
	25.047	25.021	66.908	-1.673	75.522	120	100
	25.222	30.159	74.701	-1.641	86.515	120	100
$[C_2C_1im][CF_3SO_3]$	24.983	15.124	70.755	-3.027	63.646	67.9 ± 4.4	97.46 ± 0.16
$[C_4C_1im][CF_3SO_3]$	25.080	14.957	67.901	-2.863	65.409	79.6 ± 0.9	97.89 ± 0.02
$[C_2C_1im][CH_3SO_4]$	24.846	14.670	49.547	-1.684	24.412	5.7 ± 0.2	91.17 ± 0.22
$[C_2C_1im][C_2H_5SO_4]$	24.185	16.381	52.733	-1.743	45.780	22.8 ± 0.5	96.12 ± 0.08

$[C_2C_1im][CH_3CO_2]$	24.933	15.571	39.046	-0.936	48.787	66.9 ± 2.9	99.28 ± 0.03
$[C_4C_1im]Br$	25.046	14.937	50.237	-1.686	45.300	47.3 ± 4.0	98.24 ± 0.15
$[C_4C_1im][CH_3SO_3]$	24.998	14.979	44.769	-1.320	38.511	32.1 ± 3.8	98.38 ± 0.19
$[C_4C_1im][CF_3CO_2]$	24.933	14.779	56.326	-2.124	53.478	74.2 ± 4.7	98.47 ± 0.10

[a]associated standard deviation

Table S 2.3. Weight fraction composition, partition coefficients and extraction efficiencies, of caffeine and nicotine, in human urine-based ILs/K3PO4 ABS at 298 K.

IL	wt%		$K_{caf} \pm \sigma^a$	$EE\%_{caf} \pm \sigma^a$	wt%		$K_{nic} \pm \sigma^a$	$EE\%_{nic} \pm \sigma^a$
	IL	K_3PO_4			IL	K_3PO_4		
$[C_4C_1im]Cl$	25.117	14.997	57.8 ± 0.1	98.80 ± 0.01	24.844	14.937	120	100
$[C_4C_1C_1im]Cl$	24.896	15.119	112.7 ± 0.5	99.45 ± 0.07	24.889	15.275	120	100
$[OHC_2C_1im]Cl$	40.224	14.891	120	100	40.235	15.046	120	100
$[(C_7H_7)C_1im]Cl$	24.952	15.096	71.8 ± 0.2	98.88 ± 0.01	24.891	15.057	120	100
$[C_4C_1im][CH_3SO_3]$	25.050	14.982	19.3 ± 0.5	97.51 ± 0.07	24.837	15.513	31.1 ± 0.3	98.27 ± 0.02
$[C_4C_1im][CF_3SO_3]$	24.959	15.078	20.2 ± 1.7	94.97 ± 0.41	24.902	15.281	27.2 ± 0.2	94.95 ± 0.03

[a]associated standard deviation

2.2. Separation of ethanol-water mixtures by liquid-liquid extraction using phosphonium-based ionic liquids

Catarina M.S.S. Neves, José F.O. Granjo, Mara G. Freire, Al Robertson, Nuno M. C. Oliveira and João A. P. Coutinho, Green Chemistry 13 (2011) 1517-1526, DOI: 10.1039/C1GC15079K

EXPERIMENTAL DATA OF THE TERNARY SYSTEMS IL + WATER + ETOH

Table S 2.4. Experimental data and critical point calculated by the Sherwood method[1] for the ternary systems composed of IL + H_2O + EtOH.

IL	Phase	Mass Fraction			Selectivity (*S*)
		w_{IL}	w_{EtOH}	w_{H2O}	
$[P_{66614}][Phosph]$		0.840	0.000	0.160	
	Top	0.356	0.449	0.195	1.74
	Bottom	0.053	0.539	0.408	
	Top	0.524	0.335	0.141	3.13
	Bottom	0.001	0.432	0.567	
	Top	0.620	0.255	0.125	4.39
	Bottom	0.001	0.317	0.682	

	Top	0.718	0.161	0.121	5.68
	Bottom	0.000	0.190	0.810	
	Critical Point	0.18	0.54	0.28	
$[P_{66614}][Deca]$		0.851	0.000	0.149	
	Top	0.392	0.419	0.189	2.00
	Bottom	0.032	0.509	0.459	
	Top	0.513	0.341	0.146	3.09
	Bottom	0.003	0.429	0.568	
	Top	0.615	0.256	0.129	4.34
	Bottom	0.000	0.315	0.685	
	Top	0.716	0.162	0.122	5.31
	Bottom	0.000	0.201	0.799	
	Critical Point	0.21	0.55	0.24	
$[P_{66614}]Cl$		0.866	0.000	0.134	
	Top	0.438	0.395	0.167	2.24
	Bottom	0.079	0.472	0.449	
	Top	0.620	0.271	0.109	5.28
	Bottom	0.000	0.319	0.681	
	Top	0.807	0.082	0.111	6.61
	Bottom	0.000	0.100	0.900	
	Top	0.723	0.175	0.102	6.97
	Bottom	0.000	0.198	0.802	
	Critical Point	0.25	0.49	0.26	
$[P_{66614}][CH_3SO_3]$		0.872	0.000	0.128	
	Top	0.590	0.257	0.153	2.29
	Bottom	0.031	0.306	0.663	
	Top	0.703	0.176	0.121	3.64
	Bottom	0.006	0.218	0.776	
	Top	0.510	0.305	0.185	5.18
	Bottom	0.088	0.381	0.531	
	Top	0.795	0.085	0.120	6.67
	Bottom	0.004	0.096	0.900	
	Critical Point	0.40	0.37	0.23	
$[P_{66614}]Br$		0.932	0.000	0.068	
	Top	0.128	0.572	0.300	0.566
	Bottom	0.448	0.426	0.126	

	Top	0.054	0.555	0.391	2.74
	Bottom	0.562	0.348	0.090	
	Top	0.645	0.280	0.075	4.73
	Bottom	0.010	0.436	0.554	
	Top	0.718	0.223	0.059	7.76
	Bottom	0.001	0.326	0.673	
	Critical Point	0.28	0.53	0.19	
$[P_{66614}][N(CN)_2]$		0.967	0.000	0.033	
	Top	0.434	0.458	0.108	1.69
	Bottom	0.114	0.634	0.252	
	Top	0.622	0.313	0.065	3.41
	Bottom	0.020	0.574	0.406	
	Top	0.712	0.238	0.050	5.48
	Bottom	0.009	0.463	0.528	
	Top	0.787	0.169	0.044	7.76
	Bottom	0.008	0.330	0.662	
	Critical Point	0.28	0.16	0.56	
$[P_{66614}][NTf_2]$		0.998	0.000	0.002	
		0.384	0.553	0.063	
		0.318	0.612	0.070	
		0.272	0.652	0.076	
		0.235	0.686	0.079	
		0.210	0.707	0.083	
		0.189	0.727	0.084	
		0.174	0.738	0.088	
		0.160	0.752	0.088	
		0.153	0.754	0.093	
		0.141	0.766	0.093	
		0.135	0.767	0.098	
		0.041	0.765	0.193	
		0.176	0.741	0.083	
		0.222	0.702	0.076	
		0.244	0.684	0.072	
		0.263	0.668	0.069	
		0.281	0.652	0.067	
		0.297	0.638	0.065	
		0.470	0.048	0.482	
	Top	0.090	0.788	0.122	2.57

	Bottom	0.848	0.144	0.008	
	Top	0.012	0.737	0.251	4.16
	Bottom	0.937	0.058	0.005	
	Top	0.001	0.605	0.394	6.12
	Bottom	0.955	0.041	0.004	
	Top	0.000	0.485	0.515	11.31
	Bottom	0.964	0.033	0.003	
	Top	0.000	0.226	0.774	21.66
	Bottom	0.983	0.015	0.002	
	Critical Point	0.73	0.26	0.01	

Table S 2.5. Absolute deviations between experimental data and NRTL correlated data of the ternary system IL + H_2O + EtOH.

IL	Phase	Experimental data			NRTL correlated data			Absolute Deviation ($\lvert w_{exp}-w_{NRTL}\rvert$)		
		w_{IL}	w_{EtOH}	w_{H2O}	w_{IL}	w_{EtOH}	w_{H2O}	w_{IL}	w_{EtOH}	w_{H2O}
[P_{66614}][Phosph]		0.840	0.000	0.160	0.842	0.000	0.158	0.002	0.000	0.002
	Top	0.356	0.449	0.195	0.363	0.437	0.200	0.007	0.012	0.005
	Bottom	0.053	0.539	0.408	0.059	0.542	0.399	0.006	0.003	0.009
	Top	0.524	0.335	0.141	0.519	0.330	0.151	0.005	0.005	0.010
	Bottom	0.001	0.432	0.567	0.007	0.427	0.567	0.006	0.005	0.000
	Top	0.621	0.255	0.125	0.614	0.259	0.128	0.007	0.004	0.003
	Bottom	0.001	0.317	0.682	0.001	0.313	0.686	0.000	0.005	0.004
	Top	0.718	0.161	0.121	0.718	0.173	0.109	0.000	0.012	0.012
	Bottom	0.000	0.190	0.810	0.000	0.186	0.814	0.000	0.004	0.004
[P_{66614}][Deca]		0.851	0.000	0.149	0.855	0.000	0.146	0.003	0.000	0.003
	Top	0.512	0.341	0.146	0.508	0.335	0.157	0.005	0.006	0.011
	Bottom	0.004	0.429	0.568	0.009	0.424	0.567	0.005	0.005	0.001
	Top	0.615	0.256	0.129	0.610	0.259	0.131	0.005	0.003	0.002
	Bottom	0.000	0.315	0.685	0.001	0.311	0.688	0.001	0.004	0.003
	Top	0.716	0.163	0.122	0.710	0.177	0.113	0.005	0.014	0.009
	Bottom	0.000	0.201	0.799	0.000	0.194	0.806	0.000	0.007	0.007
	Top	0.392	0.419	0.189	0.400	0.409	0.191	0.008	0.010	0.003
	Bottom	0.031	0.509	0.459	0.040	0.510	0.450	0.009	0.001	0.009
[P_{66614}]Cl		0.866	0.000	0.134	0.861	0.001	0.138	0.005	0.001	0.004
	Top	0.438	0.395	0.168	0.429	0.387	0.184	0.008	0.008	0.017
	Bottom	0.079	0.472	0.449	0.058	0.488	0.455	0.021	0.016	0.006
	Top	0.620	0.271	0.109	0.623	0.254	0.123	0.003	0.017	0.014
	Bottom	0.000	0.319	0.681	0.005	0.322	0.674	0.005	0.003	0.007

	Top	0.723	0.175	0.102	0.729	0.170	0.101	0.006	0.005	0.001
	Bottom	0.000	0.198	0.802	0.000	0.202	0.798	0.000	0.004	0.004
	Top	0.807	0.082	0.111	0.815	0.091	0.094	0.007	0.009	0.017
	Bottom	0.000	0.100	0.900	0.000	0.099	0.901	0.000	0.002	0.001
$[P_{66614}][CH_3SO_3]$		0.872	0.000	0.128	0.881	0.000	0.119	0.009	0.000	0.009
	Top	0.590	0.257	0.153	0.597	0.245	0.158	0.007	0.013	0.005
	Bottom	0.031	0.306	0.663	0.034	0.311	0.655	0.002	0.005	0.008
	Top	0.703	0.176	0.121	0.695	0.171	0.135	0.008	0.005	0.013
	Bottom	0.006	0.218	0.776	0.019	0.208	0.774	0.012	0.010	0.002
	Top	0.510	0.305	0.185	0.504	0.308	0.188	0.006	0.003	0.003
	Bottom	0.088	0.381	0.531	0.067	0.395	0.538	0.021	0.014	0.007
	Top	0.795	0.085	0.120	0.798	0.083	0.119	0.002	0.002	0.001
	Bottom	0.003	0.092	0.905	0.013	0.093	0.894	0.009	0.001	0.010
$[P_{66614}]Br$		0.937	0.000	0.063	0.934	0.000	0.066	0.003	0.000	0.003
	Top	0.054	0.555	0.391	0.047	0.555	0.398	0.007	0.000	0.007
	Bottom	0.562	0.348	0.090	0.551	0.346	0.103	0.012	0.002	0.013
	Top	0.645	0.280	0.075	0.649	0.273	0.078	0.004	0.007	0.003
	Bottom	0.010	0.436	0.554	0.007	0.440	0.553	0.003	0.004	0.001
	Top	0.128	0.572	0.300	0.129	0.579	0.292	0.000	0.007	0.008
	Bottom	0.449	0.426	0.126	0.451	0.418	0.132	0.002	0.008	0.006
	Top	0.718	0.223	0.059	0.718	0.220	0.062	0.000	0.003	0.003
	Bottom	0.001	0.326	0.673	0.001	0.326	0.673	0.000	0.001	0.000
$[P_{66614}][N(CN)_2]$		0.967	0.000	0.033	0.978	0.009	0.013	0.011	0.009	0.021
	Top	0.622	0.313	0.065	0.623	0.311	0.067	0.001	0.003	0.002
	Bottom	0.020	0.574	0.406	0.021	0.574	0.405	0.001	0.000	0.001
	Top	0.712	0.238	0.050	0.689	0.256	0.054	0.023	0.018	0.005
	Bottom	0.009	0.463	0.528	0.003	0.457	0.539	0.006	0.006	0.011
	Top	0.434	0.458	0.108	0.462	0.437	0.102	0.028	0.021	0.006
	Bottom	0.115	0.634	0.252	0.144	0.626	0.230	0.029	0.008	0.022
	Top	0.787	0.169	0.044	0.753	0.204	0.043	0.034	0.035	0.001
	Bottom	0.009	0.330	0.662	0.000	0.318	0.681	0.008	0.011	0.020
$[P_{66614}][NTf_2]$		0.998	0.000	0.002	0.999	0.000	0.001	0.001	0.000	0.001
	Top	0.012	0.737	0.252	0.049	0.697	0.254	0.037	0.039	0.002
	Bottom	0.937	0.058	0.005	0.903	0.090	0.007	0.034	0.032	0.002
	Top	0.090	0.789	0.122	0.152	0.735	0.114	0.062	0.054	0.008
	Bottom	0.848	0.144	0.009	0.864	0.128	0.008	0.017	0.016	0.001
	Top	0.000	0.485	0.515	0.005	0.480	0.515	0.005	0.005	0.000
	Bottom	0.964	0.033	0.003	0.930	0.065	0.005	0.035	0.032	0.002
	Top	0.001	0.605	0.394	0.015	0.593	0.392	0.014	0.012	0.002

Bottom	0.955	0.041	0.004	0.920	0.074	0.006	0.035	0.033	0.002
Top	0.000	0.226	0.774	0.000	0.222	0.778	0.000	0.004	0.004
Bottom	0.983	0.015	0.002	0.954	0.043	0.003	0.029	0.028	0.001

COMPARISON BETWEEN ALL EXPERIMENTAL TERNARY PHASE DIAGRAMS

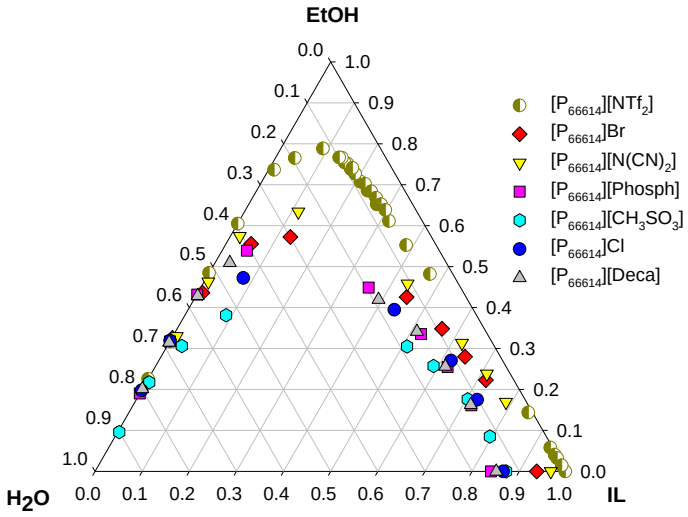

Figure S 2.7. Experimental ternary phase diagrams for all IL + EtOH + H_2O systems at 298.15 K (mass fraction units).

CONSISTENCY OF THE EXPERIMENTAL TIE-LINES

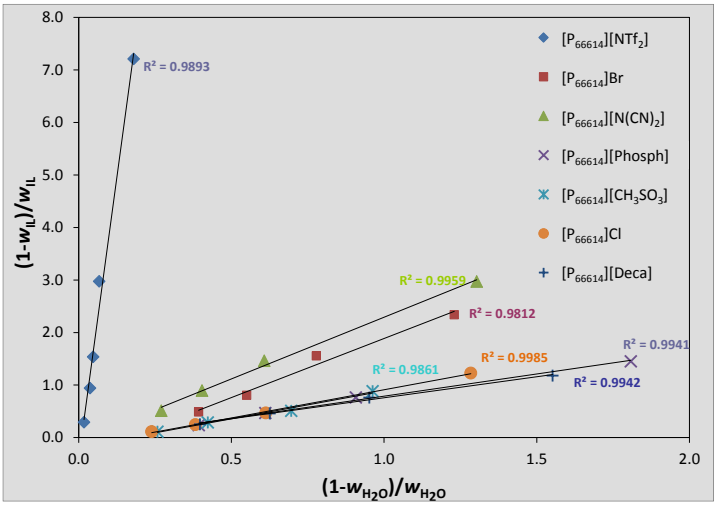

Figure S 2.8. Tie-Lines correlation using the Othmer-Tobias correlation[2] for each ternary system IL + EtOH + Water.

S AND *D* DEPENDENCE ON THE ETHANOL CONTENT

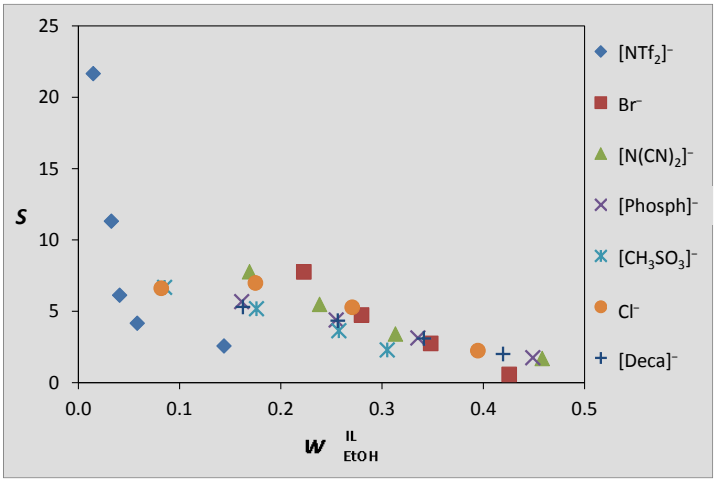

Figure S 2.9. Correlation of ethanol selectivities (*S*) as a function of the ethanol content in the IL-rich phase (w_{EtOH}^{IL}).

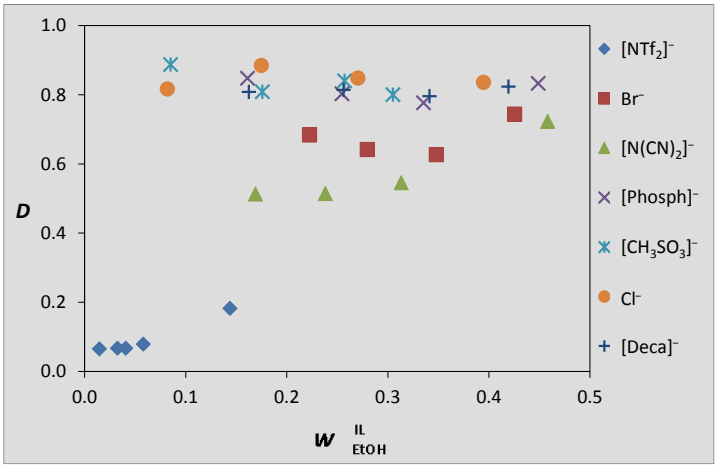

Figure S 2.10. Correlation of ethanol distribution coefficients (*D*) as a function of the ethanol content in the IL-rich phase (w_{EtOH}^{IL}).

NRTL PARAMETER ESTIMATION

The expressions for the excess Gibbs energy (g^E) and the logarithm of the activity coefficient ($\ln \gamma_i$) given by the NRTL model can be written as:[3]

$$\frac{g^E}{RT} = \sum_i^{n_c} x_i \ln \gamma_i = \sum_i^{n_c} \frac{x_i L_i}{M_i} \tag{S2.1}$$

$$\ln \gamma_i = \frac{L_i}{M_i} + \sum_j^{n_c} \frac{x_j G_{ij}}{M_j} (\tau_{ij} - \frac{L_j}{M_j}) \tag{S2.2}$$

$$L_i = \sum_k^{n_c} x_k \tau_{ki} G_{ki} \tag{S2.3}$$

$$M_i = \sum_k^{n_c} x_k G_{ki} \tag{S2.4}$$

$$G_{ij} = e^{-\alpha_{ij}\tau_{ij}} \tag{S2.5}$$

$$\tau_{ij} = \frac{(g_{ij} - g_{ii})}{RT} = \frac{\Delta g_{ij}}{RT},\ i \neq j \text{ and } \tau_{ij} = 0,\ i = j \tag{S2.6}$$

Here $i, j, k \in \{1,2,3\}$ represent the different molecular species in the mixture (1 – water, 2 – ethanol, 3 – ionic liquid), n_c is the number of components, and x_i refers to molar fractions. In the present work, the parameter estimation task was formulated as the solution of a nonlinear programming problem (NLP), using the weighted norm of the differences between the experimental mass fractions and the values predicted by the model as an objective function:[4]

$$\min_z \ \phi = \sum_i^{n_t} \sum_j^{n_c} \sum_k^{2} \omega_{ijk} e_{ijk}(\tau)^2 \tag{S2.7}$$

where $e_{ijk}(\tau) = w_{ijk}^{\exp} - w_{ijk}^{\mathrm{mod}}(\tau)$, and the superscripts *exp* and *mod* correspond to experimental and predicted mass fraction values, respectively. The summations in this equation are taken over all tie-lines (i), components (j) and phases (k), and ω_{ijk} is a weight factor associated with each error term. Using the isothermal data available for each system, the objective function ϕ was minimized by simultaneous determination of all model variables (here denoted as z), subject to constraints of iso-activity, the NRTL

activity model described by equations (S2-S6), sum of mass and molar fraction restrictions, and magnitude bounds for the model parameters τ_{ij}. Mass fractions were used in the data regression, due to the large differences in molecular weights between the ionic liquids and the molecular components.

To address the non-convexity of this nonlinear parameter estimation problem, which often leads to multiple local optimal solutions, this problem was implemented in GAMS,[5] taking advantage of the robustness of the numerical solvers available in this system. Additionally, considerable care was placed in the reformulation of the original model equations, as NLP constraints. This was done by introducing new terms and using algebraic rearrangements in the resultant equations that allowed the nonlinearity of each individual component of the model to be significantly decreased. Scaling of the resulting variables and equations was performed, also with the purpose of reducing the overall model nonlinearity. A subset of fundamental model variables was identified, and proper initialization and bounds were established for them. These values were then propagated throughout the model to initialize and bound the remaining variables, allowing both a more consistent global model initialization, and avoiding the nonconvergence of the NLP due to the inability of locating feasible solutions. This step was verified to be an essential task to guarantee the convergence of the parameter estimation. The following numerical solvers were used in this study:

CONOPT[6] – based on the General Reduced Gradient and Successive Quadratic Programming algorithms; provides a very robust initialization and location of feasible points in highly constrained problems; suitable for medium to large scale NLPs;

OQNLP[7] – a global solver based on various heuristic multistart algorithms; designated to rapidly finding various local optima of smooth constrained NLPs;

BARON[8] – a global numerical solver for continuous and discrete variables; based on a deterministic global optimization algorithm; capable of determining and refining model bounds in different regions of the solution domain.

Each of these solvers was tested with each LLE ternary system, to ensure that the set of parameters obtained corresponds to the best possible solutions using this type of formulation. The values of the residual function ϕ at the optimum were comprised between 0.7×10^{-3} (system with Br^-) and 7×10^{-3} (for the system with $[N(CN)_2]^-$). This was possible through the extensive search for alternative solutions (especially with the OQNLP solver) and by increasing the bounds allowed for the τ_{ij} parameters, which in various cases resulted in higher values for the interaction parameter τ_{13} (water – ionic liquid). This step should be interpreted with caution, since it corresponds to larger values of the respective Δg_{ij} interaction term, and would perhaps benefit from additional confirmation provided by including in the regression experimental data obtained at different temperatures.

The computer requirements for the parameter estimation task were of the order of one second of CPU, using GAMS/CONOPT on a current Intel Xeon Linux workstation. Due to different nature of the algorithms, a maximum of 30 minutes of CPU were allowed for the runs with the OQNLP solver, and 60 minutes for BARON. Within the time allowed and for all the systems considered, BARON was unable to find a guaranteed global solution, stopping often at a local solution. On the other hand, the OQNLP solver was able to identify several distinct local solutions of the problems. This number of local optima found varied from 5 (for the system with $[NTf_2]^-$) to 77 (system with Br^-), and corresponded typically to approximately 20 different local optima, in most of the cases considered. Within this set, the solutions provided by CONOPT corresponded typically to the best (or second best) local solutions known for each problem, after reasonable tuning of the initialization scheme. From an overall perspective, the experience acquired in this part of the work indicates that the critical steps in this parameter estimation task were the proper construction of the NLP (through reformulation, scaling, initialization and bounding of the original mathematical model), and the availability of a multistart optimizer, capable of largely eliminating the effects of the initial estimates on the quality of the solutions obtained.

Appendix Chapter 3 – Mutual Solubilities of Ionic Liquids and Water

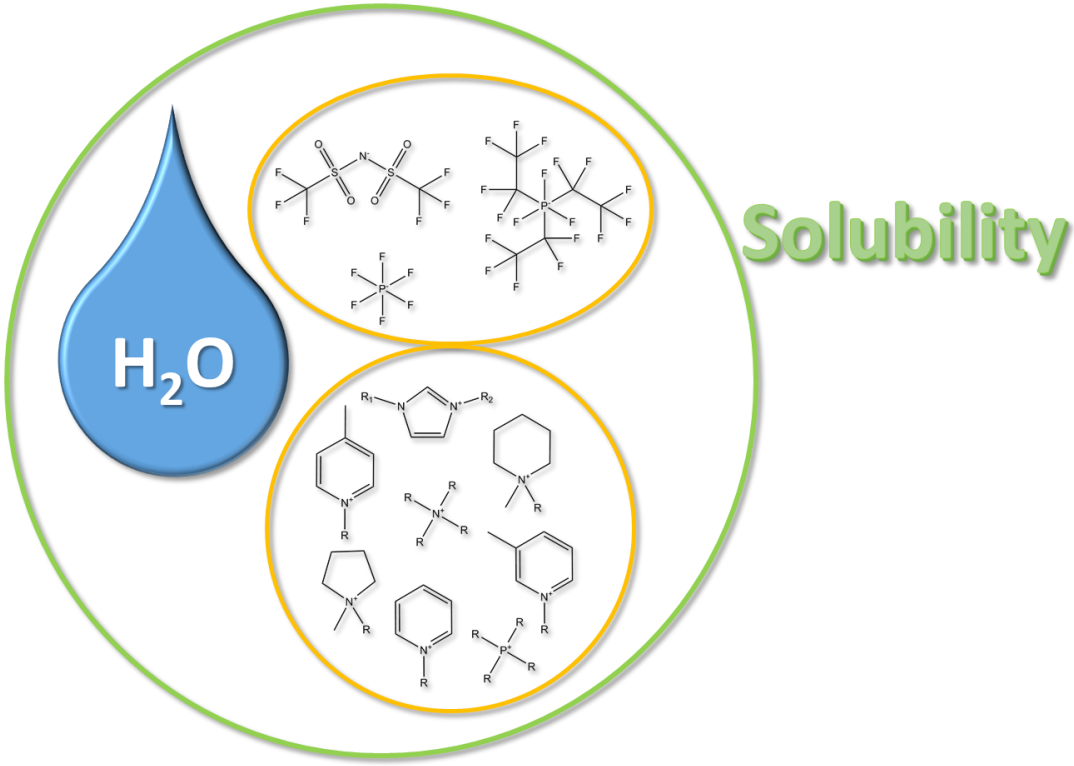

3.4. Thermophysical properties and water saturation of [PF_6]-based ionic liquids

Catarina M. S. S. Neves, Marta L. S. Batista, Ana Filipa M. Cláudio, Luís M. N. B. F. Santos, Isabel M. Marrucho, Mara G. Freire and João A. P. Coutinho, Journal of Chemical & Engineering Data 55 (2010) 5065-5073, DOI: 10.1021/je100638g

DSC THERMOGRAMS

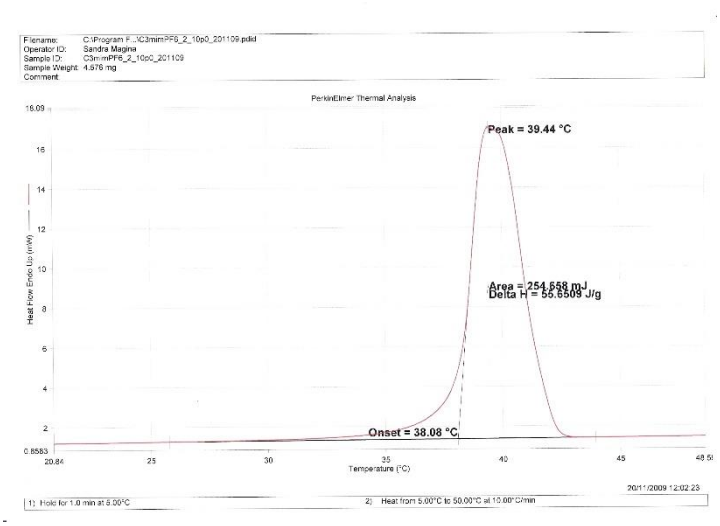

Figure S 3.1. Thermogram for [C_3C_1im][PF_6] obtained using a Diamond DSC PerkinElmer equipment.

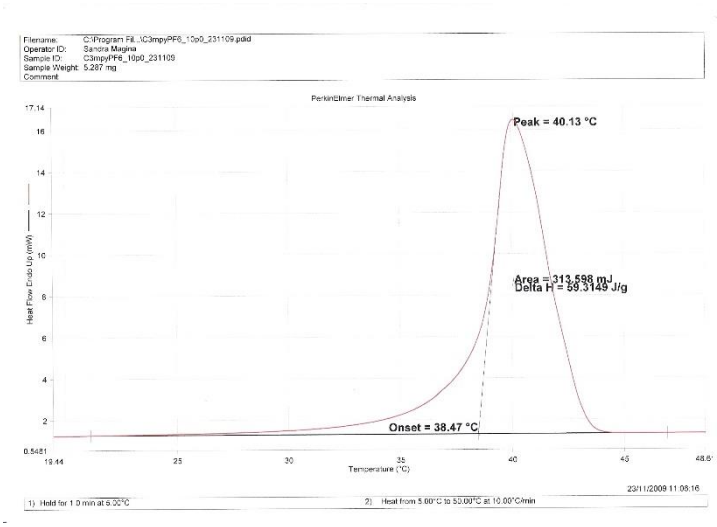

Figure S 3.2. Thermogram for [C_3-3-C_1py][PF_6] obtained using a Diamond DSC PerkinElmer equipment.

MUTUAL SOLUBILITIES MEASUREMENTS

Calibration curves for the ionic liquids solubility in water determination were achieved using a stock solution of each ionic liquid in ultra-pure water with a concentration of ≈ 0.5 $g \cdot dm^{-3}$. Proper dilutions in ultra-pure water of the stock solution guided to nine standard solutions. The concentration of each standard is given in Table S3.3, and the calibration curves are given in Figure S3.1. The absorbance of each standard solution is an average of at least 5 independent readings.

Table S 3.1. Concentration of the stock solution and respective standard solutions of each IL, as well as respective absorbance at λ = 211 nm or 266 nm.

	$[C_3C_1im][PF_6]$		$[C_3\text{-}3\text{-}C_1py][PF_6]$	
Stock Solution / $g \cdot dm^{-3}$	0.4424		0.4884	
Standard Solutions	[IL] / $g \cdot dm^{-3}$	Absorbance at λ = 211 nm	[IL] / $g \cdot dm^{-3}$	Absorbance at λ = 266 nm
1	0.0044	0.072	0.0146	0.251
2	0.0088	0.150	0.0195	0.329
3	0.0133	0.210	0.0244	0.415
4	0.0177	0.284	0.0293	0.494
5	0.0265	0.426	0.0342	0.577
6	0.0354	0.550	0.0391	0.661
7	0.0442	0.686	0.0440	0.747
8	0.0531	0.829	0.0488	0.836
9	0.0619	0.967	0.0733	1.243

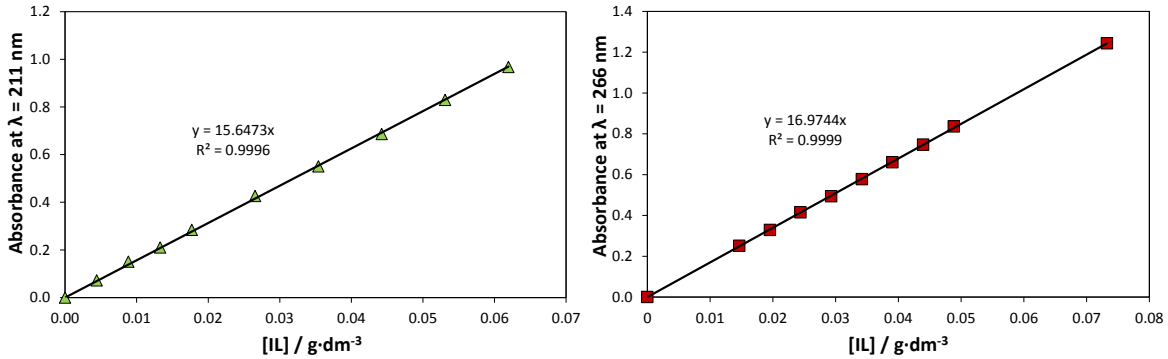

Figure S 3.3. Calibration Curves (Absorbance at λ = 211 nm or 266 nm as a function of the IL concentration) for ILs: ▲, $[C_3C_1im][PF_6]$; ■, $[C_3\text{-}3\text{-}C_1py][PF_6]$.

Table S 3.2. Experimental mole fraction solubility of water in ILs, x_w, and of ILs in water, x_{IL}, as a function of temperature and at 0.1 MPa.

	$x_w \pm \sigma$[a]		10^3 ($x_{IL} \pm \sigma$[a])	
T / K	$[C_3C_1im][PF_6]$	$[C_3\text{-}3C_1py][PF_6]$	$[C_3C_1im][PF_6]$	$[C_3\text{-}3\text{-}C_1py][PF_6]$
288.15	0.2437 ± 0.0016	---	1.158 ± 0.040	0.918 ± 0.050
293.15	0.2709 ± 0.0009	---	1.543 ± 0.008	1.223 ± 0.024
298.15	0.2925 ± 0.0009	---	1.957 ± 0.011	1.646 ± 0.029
303.15	0.3168 ± 0.0025	0.2949 ± 0.0020	2.528 ± 0.012	1.990 ± 0.002
308.15	0.3461 ± 0.0003	0.3248 ± 0.0008	2.772 ± 0.066	2.204 ± 0.028
313.15	0.3769 ± 0.0029	0.3516 ± 0.0035	2.965 ± 0.021	2.363 ± 0.020
318.15	0.4050 ± 0.0017	0.3772 ± 0.0025	3.314 ± 0.015	2.689 ± 0.027

[a]Standard deviation

Table S 3.3. Correlation parameters for the mole fraction solubility of water in ILs and ILs in water as a function of temperature using eqs 3.1 and 3.2, respectively.

IL	A	B / K	R^2 [(a)]	C [(b)]	D / K [(b)]	E [(b)]	R^2 [(a)]
$[C_3C_1im][PF_6]$	3.94 ± 0.15	-1541 ± 44	0.9990	-315 ± 405	12816 ± 18676	47 ± 60	0.9969
$[C_3\text{-}3\text{-}C_1py][PF_6]$	3.99 ± 0.44	-1579 ± 180	0.9965	-425 ± 537	17712 ± 24742	63 ± 80	0.9955

[(a)] Correlation coefficient.

[(b)] Note that three correlation constants were calculated from four experimental data points [from (303.15 to 318.15) K] to avoid discrepancies between liquid-liquid and solid-liquid equilibria.

DENSITY

Table S 3.4. Experimental density values, ρ, for pure ILs and (IL + water) systems as a function of temperature and at 0.1 MPa, where x_w is the constant mole fraction solubility of water in the IL at $T \approx 300$ K.

	ρ / kg·m^{-3}			
	$[C_3C_1im][PF_6]$	$[C_3\text{-}3\text{-}C_1py][PF_6]$	$[C_3C_1im][PF_6]$	$[C_3\text{-}3\text{-}C_1py][PF_6]$
T / K	Pure		x_w = (0.306 ± 0.004[a])	x_w = (0.249 ± 0.006[a])
303.15	---	---	1389.2	1362.5
308.15	---	---	1384.7	1358.3
313.15	---	---	1380.2	1354.0
318.15	1397.5	1365.4	1375.7	1349.8
323.15	1393.2	1361.3	1371.3	1345.6
328.15	1389.0	1357.3	1366.9	1341.4
333.15	1384.7	1353.2	1362.5	1337.2
338.15	1380.5	1349.2	1358.1	1333.1
343.15	1376.3	1345.2	1353.8	1328.9
348.15	1372.1	1341.2	1349.4	1324.8
353.15	1367.9	1337.2	1345.1	1320.7

358.15	1363.8	1333.2	1340.8	1316.6
363.15	1359.6	1329.2	1336.5	1312.5

[a]Standard deviation

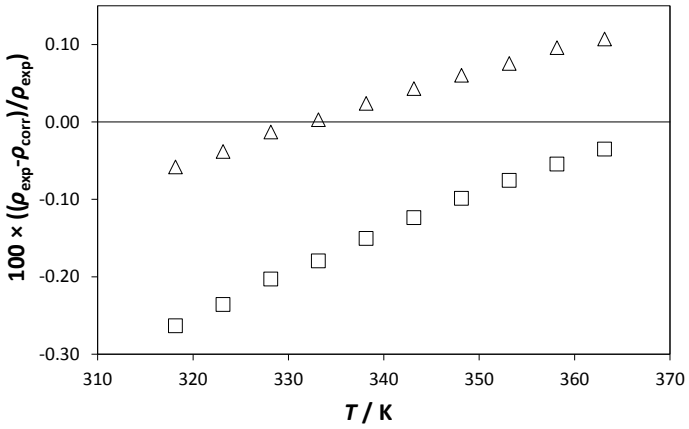

Figure S 3.4. Density deviation plot between measured data and predicted values using eq 3.6: △, $[C_3C_1im][PF_6]$; □, $[C_3\text{-}3\text{-}C_1py][PF_6]$.

VISCOSITY

Table S 3.5. Experimental viscosity values, η, for pure ILs and (IL + water) systems as a function of temperature and at 0.1 MPa, where x_w is the constant mole fraction solubility of water in the IL at $T \approx 300$ K.

	η / mPa·s			
	$[C_3C_1im][PF_6]$	$[C_3\text{-}3\text{-}C_1py][PF_6]$	$[C_3C_1im][PF_6]$	$[C_3\text{-}3\text{-}C_1py][PF_6]$
T / K	Dried		x_w = (0.306 ± 0.004 [a])	x_w = (0.249 ± 0.006 [a])
303.15	---	---	39.408	73.388
308.15	---	---	32.254	57.548
313.15	---	---	26.844	45.980
318.15	85.006	132.870	22.612	37.356
323.15	68.178	102.170	19.285	30.806
328.15	55.458	79.968	16.581	25.755
333.15	45.700	63.669	14.386	21.759
338.15	38.092	51.520	12.612	18.602
343.15	32.099	42.287	11.134	16.037
348.15	27.321	35.160	9.905	13.976
353.15	23.469	29.579	8.874	12.277
358.15	20.337	25.148	7.983	10.861
363.15	17.771	21.594	7.228	9.677

[a]Standard deviation

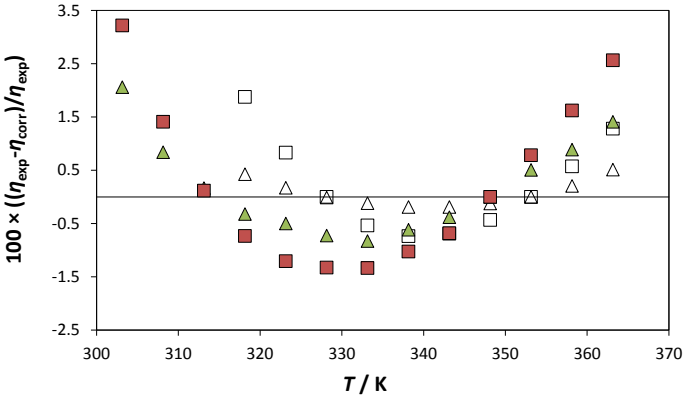

Figure S 3.5. Viscosity deviation plot between measured data and predicted values using eqs 3.8 to 3.10 for pure (empty symbols) and water-saturated (full symbols) ILs: △, ▲, [C_3C_1im][PF_6]; □, ■, [C_3-3-C_1py][PF_6].

3.5. Mutual solubility of water and structural/positional isomers of N-alkylpyridinium-based ionic liquids

Mara G. Freire, Catarina M. S. S. Neves, Karina Shimizu, Carlos E. S. Bernardes, Isabel M. Marrucho, João A. P. Coutinho, José N. Canongia Lopes and Luís Paulo N. Rebelo, Journal of Physical Chemistry B 114 (2010) 15925-15934, DOI: 10.1021/jp1093788

NMR SPECTRA

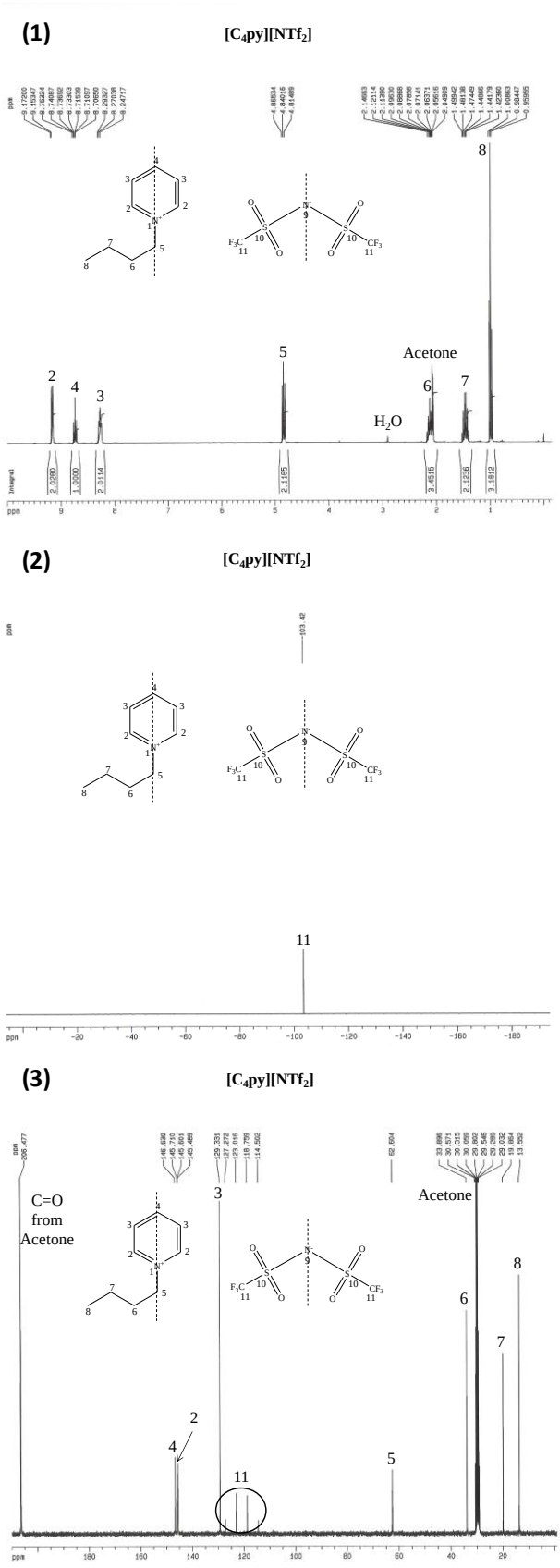

Figure S 3.6. ^{1}H (1), ^{19}F (2), ^{13}C (3) NMR spectra of [C4py][NTf2] in CD_3COCD_3.

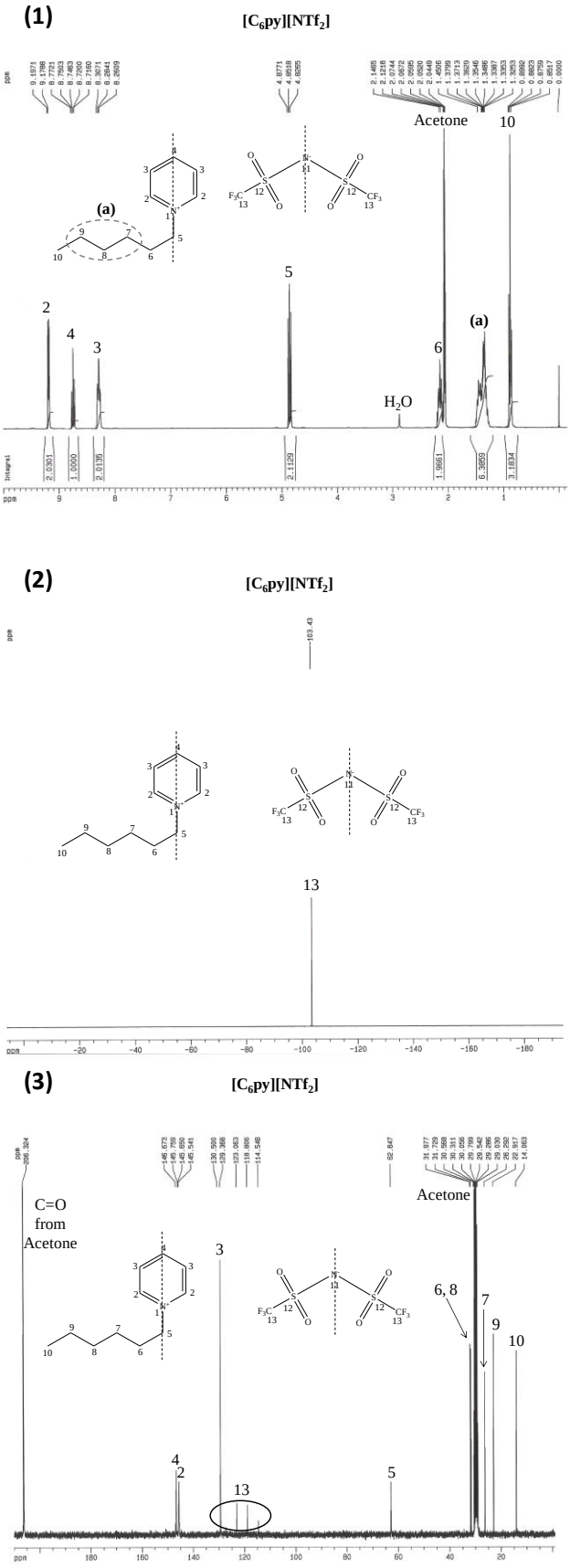

Figure S 3.7. ^{1}H (1), ^{19}F (2), ^{13}C (3) NMR spectra of $[C_6py][NTf_2]$ in CD_3COCD_3.

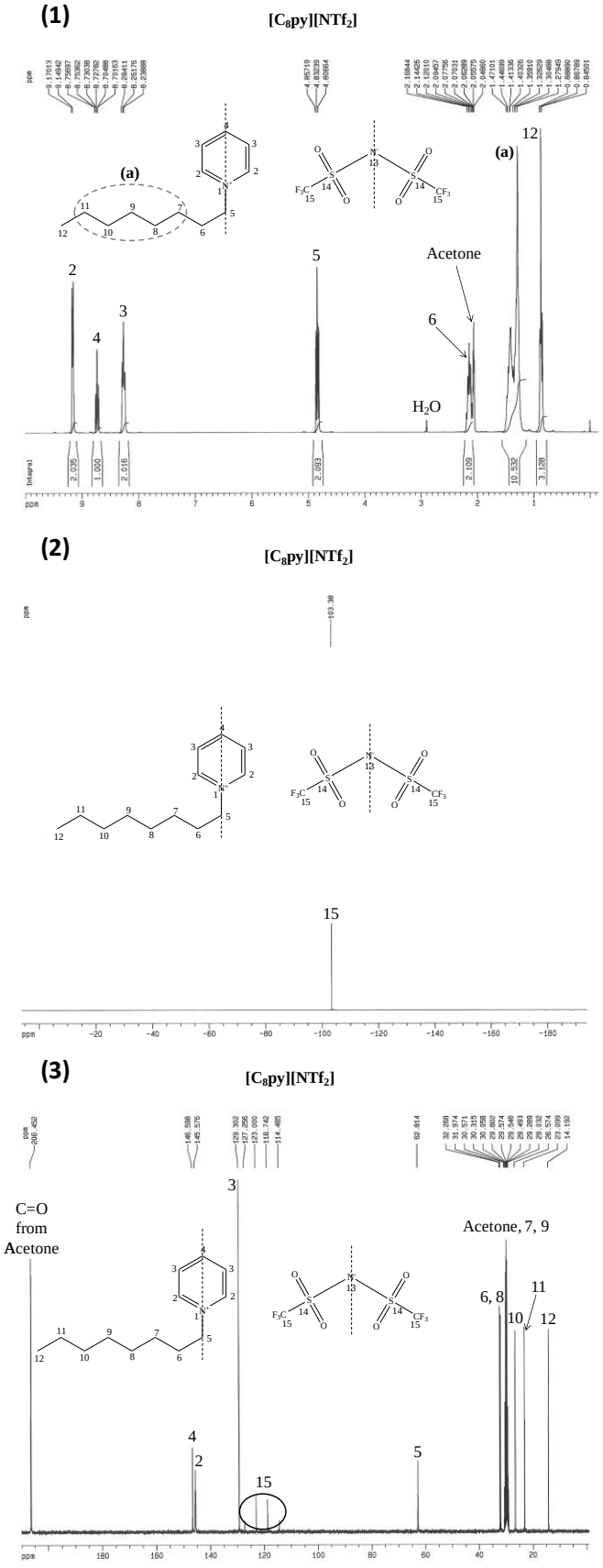

Figure S 3.8. ^{1}H (1), ^{19}F (2), ^{13}C (3) NMR spectra of $[C_8py][NTf_2]$ in CD_3COCD_3.

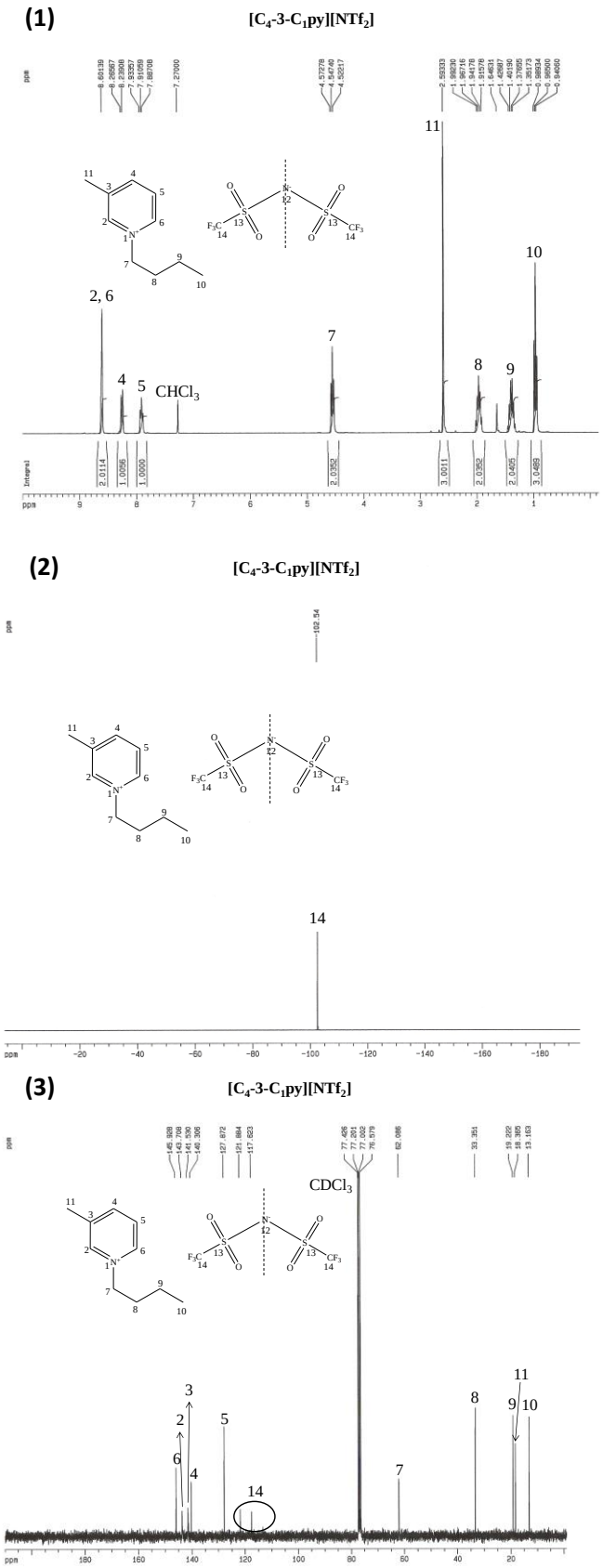

Figure S 3.9. ^{1}H (1), ^{19}F (2), ^{13}C (3) NMR spectra of $[C_4\text{-}3\text{-}C_1py][NTf_2]$ in CD_3COCD_3.

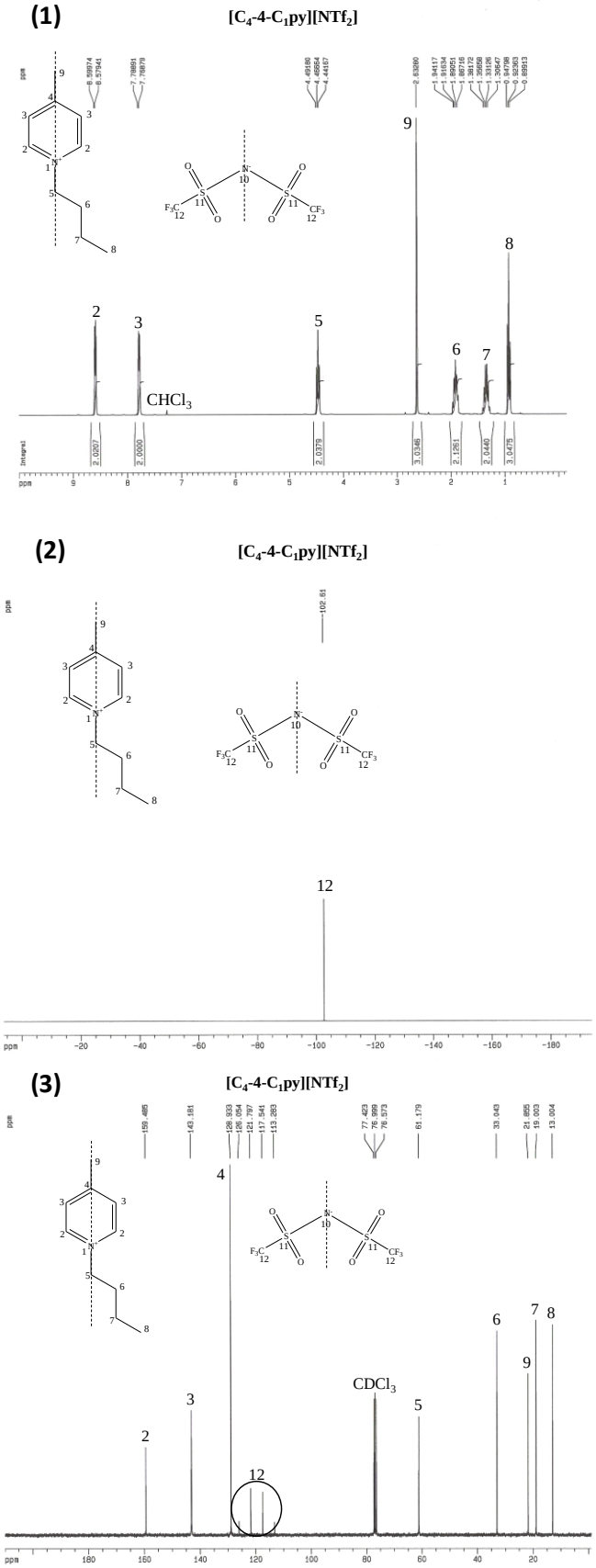

Figure S 3.10. ^{1}H (1), ^{19}F (2), ^{13}C (3) NMR spectra of $[C_4\text{-}4\text{-}C_1py][NTf_2]$ in CD_3COCD_3.

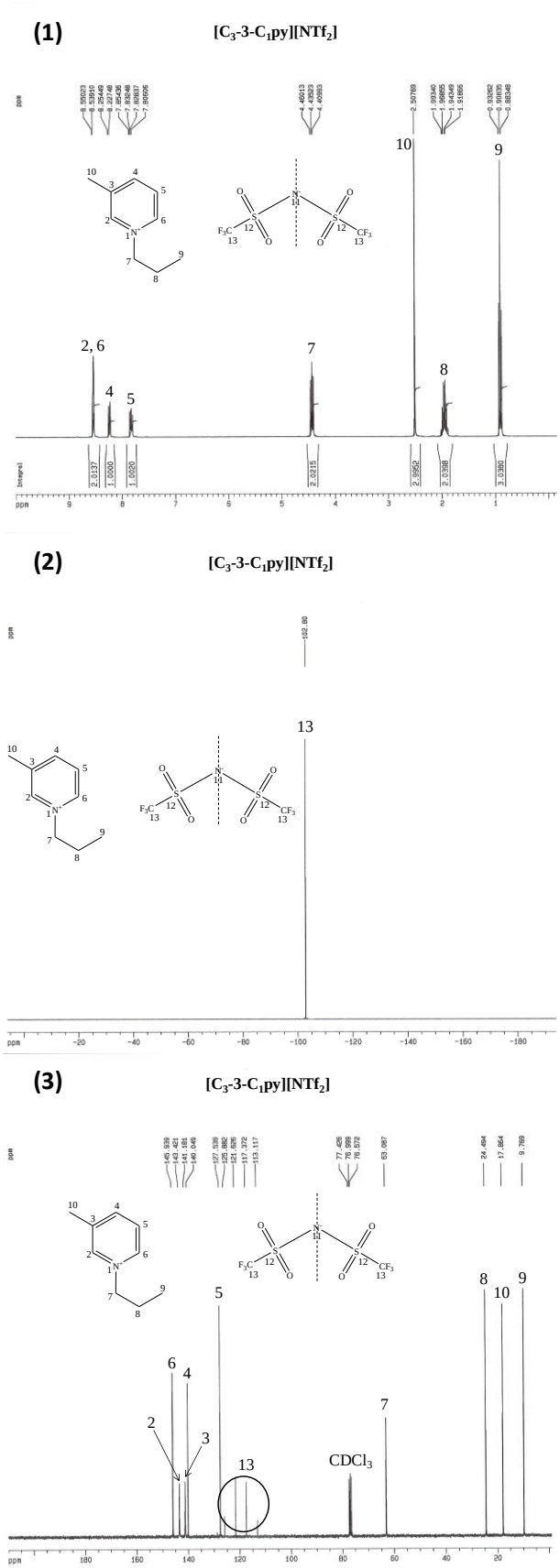

Figure S 3.11. ^{1}H (1), ^{19}F (2), ^{13}C (3) NMR spectra of $[C_3\text{-}3\text{-}C_1py][NTf_2]$ in CD_3COCD_3.

MUTUAL SOLUBILITIES MEASUREMENTS

Table S 3.6. Solubilities of water in the IL-rich phase (expressed in water mole fraction, x_w) and of IL in the water-rich phase (expressed in IL mole fraction, x_{IL}) at different temperatures, and respective deviations.

	[C4py][NTf2]	[C6py][NTf2]	[C8py][NTf2]	[C4-3-C1py][NTf2]	[C4-4-C1py][NTf2]
T/K			x_w		
288.15	0.221 ± 0.003	0.204 ± 0.002	0.175 ± 0.003	0.190 ± 0.002	0.219 ± 0.001
293.15	0.238 ± 0.001	0.216 ± 0.001	0.188 ± 0.010	0.202 ± 0.001	0.234 ± 0.003
298.15	0.252 ± 0.001	0.225 ± 0.002	0.197 ± 0.010	0.213 ± 0.001	0.247 ± 0.003
303.15	0.269 ± 0.003	0.246 ± 0.003	0.216 ± 0.060	0.232 ± 0.002	0.264 ± 0.002
308.15	0.291 ± 0.001	0.260 ± 0.001	0.234 ± 0.030	0.248 ± 0.001	0.285 ± 0.003
313.15	0.309 ± 0.003	0.277 ± 0.005	0.250 ± 0.010	0.261 ± 0.003	0.302 ± 0.002
318.15	0.327 ± 0.003	0.294 ± 0.001	0.267 ± 0.020	0.277 ± 0.001	0.319 ± 0.001
T/K			$10^4 \cdot x_{IL}$		
288.15	3.31 ± 0.02	1.85 ± 0.01	0. 309 ± 0.001	1.99 ± 0.01	2.06 ± 0.02
293.15	3.39 ± 0.03	1.96 ± 0.02	0.337 ± 0.003	2.06 ± 0.01	2.12 ± 0.03
298.15	3.55 ± 0.05	2.00 ± 0.01	0.350 ± 0.003	2.10 ± 0.04	2.21 ± 0.06
303.15	3.73 ± 0.02	2.07 ± 0.05	0.389 ± 0.04	2.18 ± 0.04	2.38 ± 0.03
308.15	3.98 ± 0.02	2.26 ± 0.08	0.420 ± 0.002	2.30 ± 0.05	2.52 ± 0.07
313.15	4.11 ± 0.01	2.43 ± 0.09	0.446 ± 0.007	2.44 ± 0.02	2.62 ± 0.08
318.15	4.53 ± 0.03	2.56 ± 0.06	0.507 ± 0.009	2.54 ± 0.02	2.82 ± 0.07

Table S 3.7. Weight fraction solubility of water in the IL-rich phase (w_w) and weigth fraction solubility of IL in the water-rich Phase (w_{IL}) at different temperatures

	[C4py][NTf2]	[C6py][NTf2]	[C8py][NTf2]	[C4-3-C1py][NTf2]	[C4-4-C1py][NTf2]
T / K			$100(w_w \pm \sigma^a)$		
288.15	1.212 ± 0.014	1.029 ± 0.007	0.804 ± 0.012	0.970 ± 0.009	1.159 ± 0.004
293.15	1.334 ± 0.004	1.107 ± 0.004	0.873 ± 0.005	1.049 ± 0.004	1.262 ± 0.013
298.15	1.435 ± 0.005	1.165 ± 0.007	0.927 ± 0.003	1.119 ± 0.006	1.353 ± 0.014
303.15	1.571 ± 0.015	1.307 ± 0.011	1.037 ± 0.022	1.248 ± 0.009	1.479 ± 0.010
308.15	1.741 ± 0.005	1.408 ± 0.003	1.153 ± 0.010	1.362 ± 0.005	1.643 ± 0.011
313.15	1.896 ± 0.011	1.528 ± 0.020	1.252 ± 0.003	1.460 ± 0.014	1.776 ± 0.010
318.15	2.056 ± 0.011	1.659 ± 0.004	1.369 ± 0.008	1.579 ± 0.001	1.919 ± 0.005
T / K			$100(w_{IL} \pm \sigma^a)$		
288.15	0.760 ± 0.004	0.454 ± 0.001	0.0810 ± 0.0026	0.473 ± 0.002	0.490 ± 0.006
293.15	0.778 ± 0.006	0.481 ± 0.005	0.0883 ± 0.0007	0.489 ± 0.003	0.505 ± 0.008
298.15	0.815 ± 0.011	0.491 ± 0.001	0.0917 ± 0.0008	0.500 ± 0.010	0.526 ± 0.015
303.15	0.855 ± 0.004	0.508 ± 0.012	0.1018 ± 0.0010	0.518 ± 0.009	0.565 ± 0.008
308.15	0.911 ± 0.004	0.554 ± 0.019	0.1102 ± 0.0005	0.546 ± 0.012	0.598 ± 0.016

313.15	0.942 ± 0.002	0.596 ± 0.022	0.1168 ± 0.0019	0.579 ± 0.004	0.623 ± 0.018
318.15	1.036 ± 0.006	0.628 ± 0.015	0.1328 ± 0.0046	0.604 ± 0.006	0.670 ± 0.018

[a]Standard Deviation

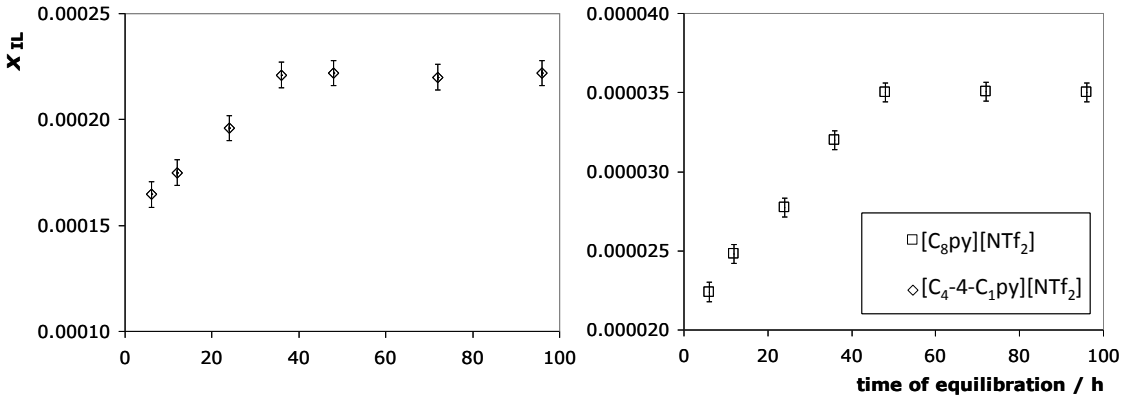

Figure S 3.12. Solubility of [C_4-4-C_1py][NTf_2] and [C_8py][NTf_2] *versus* time of equilibration at 298.15 K.

3.6. Solubility of non-aromatic hexafluorophosphate-based salts and ionic liquids in water determined by electrical conductivity

Catarina M. S. S. Neves, Ana R. Rodrigues, Kiki A. Kurnia, José M. S. S. Esperança, Mara G. Freire and João A. P. Coutinho, Fluid Phase Equilibria 358 (2013) 50-55, DOI: 10.1016/j.fluid.2013.07.061

SOLUBILITY OF HEXAFLUOROPHOSPHATE-BASED SALTS IN WATER

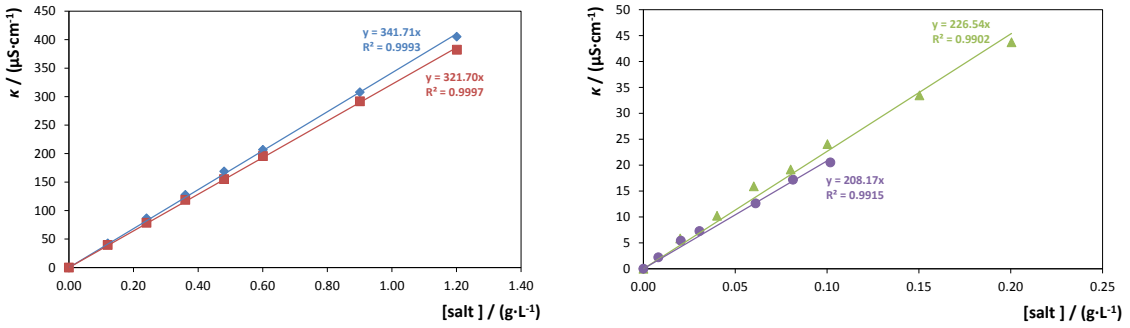

Figure S 3.13. Calibration curves for (◆) [C_3C_1pyr][PF_6], (■) [C_3C_1pip][PF_6], (▲) [N_{4444}][PF_6] and (●) [P_{4444}][PF_6].

Table S 3.8. Experimental mole fraction solubilities (x_{salt}) and respective uncertainty ($2u(x_{salt})$) of the [PF_6]-based salts in water, as function of temperature and at 0.1 MPa.

T / K	[C_4C_1im][PF_6]	[C_3C_1pyr][PF_6]	[C_3C_1pip][PF_6]	[N_{4444}][PF_6]	[P_{4444}][PF_6]
		10^3 (x_{salt} ± 2u(x_{salt})[a])		10^5 (x_{salt} ± 2u(x_{salt})[a])	
288.15	1.08 ± 0.02	1.28 ± 0.02	0.936 ± 0.004	2.24 ± 0.26	1.71 ± 0.16
293.15	1.15 ± 0.02	1.36 ± 0.02	0.985 ± 0.012	2.43 ± 0.04	1.80 ± 0.02
298.15	1.22 ± 0.02	1.57 ± 0.06	1.090 ± 0.008	2.60 ± 0.22	1.85 ± 0.06
303.15	1.41 ± 0.04	1.82 ± 0.02	1.337 ± 0.006	2.82 ± 0.20	1.94 ± 0.04
308.15	1.61 ± 0.02	2.19 ± 0.04	1.562 ± 0.016	3.07 ± 0.10	2.11 ± 0.24
313.15	1.77 ± 0.02	2.81 ± 0.02	1.787 ± 0.016	3.26 ± 0.24	2.24 ± 0.08
318.15	2.02 ± 0.02	3.10 ± 0.04	2.133 ± 0.024	3.40 ± 0.16	2.38 ± 0.14

[a] Expanded uncertainty at the 0.95 confidence level, $2u(x_{salt})$, evaluated from the standard deviation and applying a coverage factor $k = 2$.

COSMO-RS

Table S 3.9. Predicted solubility of the [PF_6]-based salts in water using COSMO-RS and the different contributions from their enthalpies of phase transition.

Salt	T/K	ΔH_{fus}/ (kJ·mol^{-1})	($\Delta H_{fus} + \Delta H_{T,2}$)/ (kJ·mol^{-1})	($\Delta H_{fus} + \Delta H_{T,1} + \Delta H_{T,2}$)/ (kJ·mol^{-1})
		lnx_{salt}	lnx_{salt}	lnx_{salt}
[C_3C_1pyr][PF_6]	288.15	-4.48	-4.72	-5.01
	293.15	-4.44	-4.66	-4.93
	298.15	-4.40	-4.60	-4.85
	303.15	-4.34	-4.53	-4.76
	308.15	-4.29	-4.46	-4.67
	313.15	-4.22	-4.39	-4.58
	318.15	-4.16	-4.30	-4.48
[C_3C_1pip][PF_6]	288.15	-4.72	-4.97	-5.69
	293.15	-4.67	-4.91	-5.57
	298.15	-4.62	-4.84	-5.45
	303.15	-4.57	-4.76	-5.32
	308.15	-4.50	-4.68	-5.19
	313.15	-4.44	-4.60	-5.05
	318.15	-4.37	-4.51	-4.92
[N_{4444}][PF_6]	288.15	-11.0	-11.4	-11.8
	293.15	-10.9	-11.3	-11.7
	298.15	-10.8	-11.2	-11.5
	303.15	-10.7	-11.0	-11.4
	308.15	-10.6	-10.9	-11.2

	313.15	-10.4	-10.7	-11.1
	318.15	-10.3	-10.6	-10.9
$[P_{4444}][PF_6]$	288.15	-10.6	-10.6	-10.9
	293.15	-10.5	-10.5	-10.8
	298.15	-10.4	-10.4	-10.7
	303.15	-10.3	-10.3	-10.6
	308.15	-10.2	-10.2	-10.5
	313.15	-10.1	-10.1	-10.3
	318.15	-9.9	-9.9	-10.2

3.7. Impact of the cation symmetry on the mutual solubilities between Water and imidazolium-based ionic liquids

Mónia A. R. Martins, Catarina M. S. S. Neves, Kiki A. Kurnia, Andreia Luís, Luís M. N. B. F. Santos, Mara G. Freire, Simão P. Pinho and João A. P. Coutinho, Fluid Phase Equilibria 375 (2014) 161-167, DOI: 10.1016/j.fluid.2014.05.013

MUTUAL SOLUBILITIES MEASUREMENTS

Table S 3.10. Experimental mole fraction solubility of water (x_w) in ILs, and respective standard deviations, as a function of temperature and at 0.10 MPa.

T/K	$[C_1C_1im][NTf_2]$	$[C_2C_2im][NTf_2]$	$[C_3C_3im][NTf_2]$	$[C_4C_4im][NTf_2]$	$[C_5C_5im][NTf_2]$
			x_w		
288.15	0.312 ± 0.002	0.241 ± 0.004	0.194 ± 0.007	0.159 ± 0.004	0.132 ± 0.002
293.15	0.335 ± 0.002	0.261 ± 0.001	0.206 ± 0.001	0.172 ± 0.001	0.148 ± 0.001
298.15	0.354 ± 0.004	0.277 ± 0.001	0.223 ± 0.001	0.184 ± 0.003	0.158 ± 0.001
303.15	0.376 ± 0.001	0.290 ± 0.001	0.240 ± 0.002	0.196 ± 0.002	0.170 ± 0.001
308.15	0.395 ± 0.001	0.305 ± 0.002	0.255 ± 0.002	0.207 ± 0.002	0.184 ± 0.002
313.15	0.424 ± 0.006	0.322 ± 0.002	0.270 ± 0.001	0.219 ± 0.006	0.197 ± 0.001
318.15	0.451 ± 0.007	0.341 ± 0.001	0.285 ± 0.003	0.233 ± 0.002	0.209 ± 0.002

Table S 3.11. Experimental mole fraction solubility of ionic liquid (x_{IL}) in water, and respective standard deviations, as a function of temperature and at 0.10 MPa.

T/K	$[C_1C_1im][NTf_2]$	$[C_2C_2im][NTf_2]$	$[C_3C_3im][NTf_2]$	$[C_4C_4im][NTf_2]$	$[C_5C_5im][NTf_2]$
	$10^3 \cdot x_{IL}$	$10^4 \cdot x_{IL}$	$10^4 \cdot x_{IL}$	$10^5 \cdot x_{IL}$	$10^5 \cdot x_{IL}$
288.15	1.38 ± 0.03	5.23 ± 0.04	1.82 ± 0.02	6.89 ± 0.02	1.94 ± 0.03
293.15	1.42 ± 0.01	5.31 ± 0.03	1.86 ± 0.01	7.03 ± 0.02	2.05 ± 0.08
298.15	1.49 ± 0.01	5.36 ± 0.01	1.92 ± 0.02	7.25 ± 0.01	2.11 ± 0.02

303.15	1.60 ± 0.02	5.79 ± 0.04	2.00 ± 0.01	7.62 ± 0.01	2.23 ± 0.01
308.15	1.69 ± 0.01	6.13 ± 0.05	2.06 ± 0.04	7.90 ± 0.07	2.35 ± 0.01
313.15	1.72 ± 0.01	6.50 ± 0.06	2.14 ± 0.02	9.00 ± 0.06	2.50 ± 0.02
318.15	2.03 ± 0.02	7.04 ± 0.08	2.25 ± 0.02	9.61 ± 0.07	2.71 ± 0.04

COSMO-RS

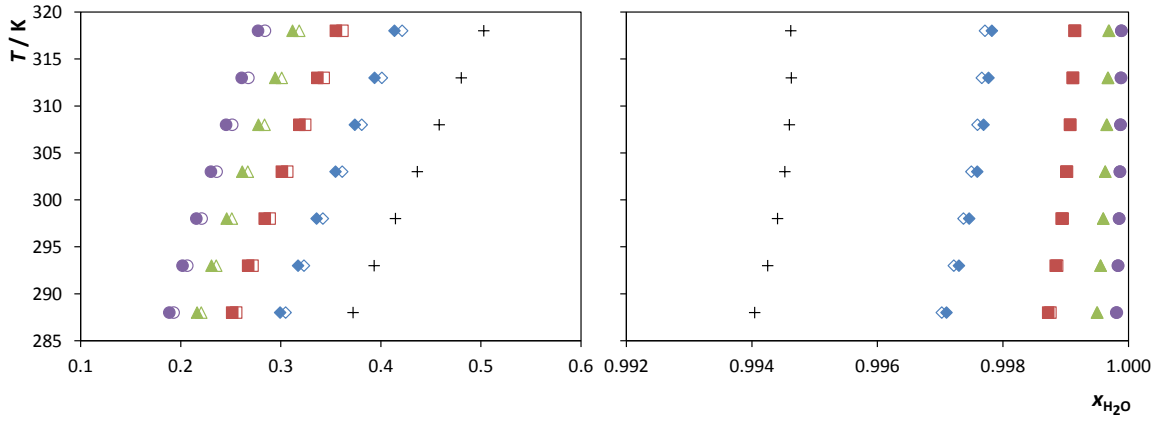

Figure S 3.14. Liquid-liquid phase diagram for water and ILs with the same number of alkyl side chain, *N*, estimate by COSMO-RS using file parameterization, BP_TZVP_C30_1301. Symbols: (+), $[C_1C_1im][NTf_2]$; (◆),$[C_2C_2im][NTf_2]$; (◇),$[C_3C_1im][NTf_2]$;(■), $[C_3C_3im][NTf_2]$; (□),$[C_5C_1im][NTf_2]$; (▲), $[C_4C_4im][NTf_2]$; (△), $[C_7C_1im][NTf_2]$; (●), $[C_5C_5im][NTf_2]$; and (○), $[C_9C_1im][NTf_2]$.

3.8. Analysis of the isomerism effect on the mutual solubilities of bis(trifluoromethylsulfonyl)imide-based ionic liquids with water

Mónia A. R. Martins, Catarina M. S. S. Neves, Kiki A. Kurnia, Luís M. N. B. F. Santos, Mara G. Freire, Simão P. Pinho, and João A. P. Coutinho, Fluid Phase Equilibria 381 (2014) 28-35, DOI: 10.1016/j.fluid.2014.08.007

MUTUAL SOLUBILITIES MEASUREMENTS

Table S 3.12. Experimental mole fraction solubility of water in ILs, x_w, and ionic iquid in water, x_{IL}, at different temperatures and at 0.10 MPa, and respective standard deviations.

T/K	$[C_1im][NTf_2]$	$[C_2im][NTf_2]$	$[C_2C_3im][NTf_2]$	$[C_4C_1C_1im][NTf_2]$
		x_w		
288.15	0.627 ± 0.009	0.604 ± 0.010	0.209 ± 0.002	0.168 ± 0.001
293.15	0.648 ± 0.003	0.612 ± 0.010	0.222 ± 0.002	0.183 ± 0.002
298.15	0.667 ± 0.005	0.628 ± 0.006	0.239 ± 0.001	0.191 ± 0.001

303.15	0.686 ± 0.001	0.641 ± 0.004	0.256 ± 0.001	0.212 ± 0.001
308.15	0.709 ± 0.001	0.659 ± 0.005	0.278 ± 0.006	0.229 ± 0.001
313.15	0.720 ± 0.003	0.673 ± 0.007	0.296 ± 0.003	0.244 ± 0.002
318.15	0.736 ± 0.010	0.682 ± 0.012	0.314 ± 0.003	0.263 ± 0.001
T/K			$10^3 x_{IL}$	
288.15	4.132 ± 0.037	2.360 ± 0.004	0.311 ± 0.001	0.203 ± 0.002
293.15	4.206 ± 0.027	2.388 ± 0.019	0.317 ± 0.001	0.206 ± 0.008
298.15	4.359 ± 0.011	2.451 ± 0.008	0.325 ± 0.001	0.209 ± 0.001
303.15	4.499 ± 0.053	2.549 ± 0.001	0.336 ± 0.002	0.217 ± 0.003
308.15	4.811 ± 0.032	2.669 ± 0.019	0.351 ± 0.002	0.237 ± 0.001
313.15	5.393 ± 0.020	2.979 ± 0.060	0.387 ± 0.002	0.246 ± 0.003
318.15	5.945 ± 0.026	3.233 ± 0.010	0.410 ± 0.014	0.270 ± 0.001

THERMODYNAMIC FUNCTIONS OF SOLUTION

Table S 3.13. Correlation parameters for the mole fraction solubility of water in the IL-rich phase and IL in the water-rich phase using eqs 3.1 and 3.2, and respective standard deviations.

IL	*A*	*B* / K	*C*	*D* / K	*E*
[C_1im][NTf_2]	1.252 ± 0.055	-494.1 ± 16.6	-554.0 ± 62.7	23802.9 ± 2826.8	82.3 ± 9.3
[C_2im][NTf_2]	0.853 ± 0.051	-392.4 ± 15.5	-503.6 ± 60.9	21623.2 ± 2746.8	74.6 ± 9.1
[C_2C_3im][NTf_2]	2.860 ± 0.084	-1277.7 ± 25.3	-382.0 ± 61.3	16139.1 ± 2764.5	56.1 ± 9.1
[$C_4C_1C_1$im][NTf_2]	2.987 ± 0.145	-1376.3 ± 43.9	-390.6 ± 68.7	16495.2 ± 3098.6	57.4 ± 10.2

COSMO-RS

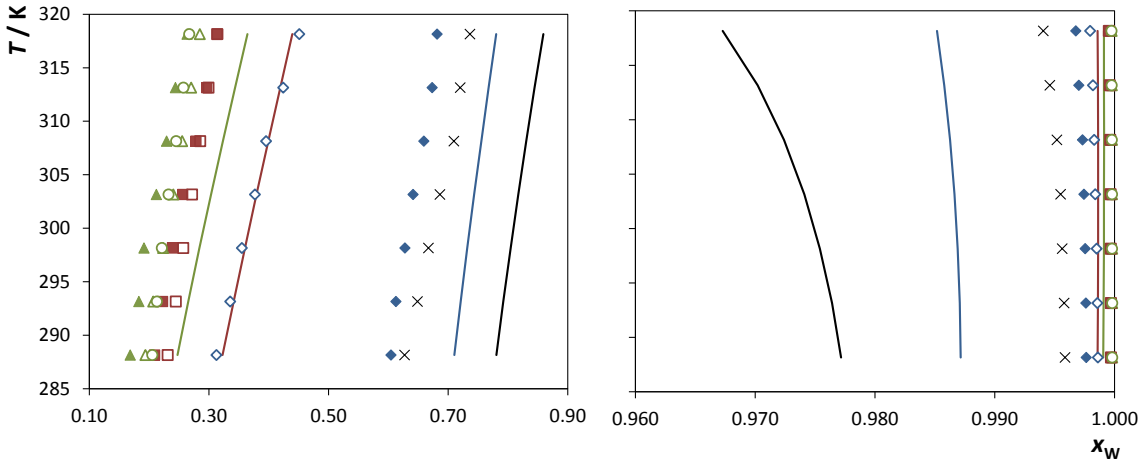

Figure S 3.15. Liquid-liquid phase diagram for water and ILs: (×), [C_1im][NTf_2]; (◆), [C_2im][NTf_2]; (◇), [C_1C_1im][NTf_2]; (■), [C_2C_3im][NTf_2]; (□), [C_4C_1im][NTf_2]; (▲), [$C_4C_1C_1$im][NTf_2]; (△), [C_3C_3im][NTf_2]; and (○), [C_5C_1im][NTf_2]. The lines at the same colours represent the COSMO-RS predictions using the file parameterization BP_TZVP_C30_1401.

3.9. The impact of ionic liquids fluorinated moieties on their thermophysical properties and aqueous phase behaviour

Catarina M. S. S. Neves, Kiki Adi Kurnia, Karina Shimizu, Isabel M. Marrucho, Luís Paulo N. Rebelo, João A. P. Coutinho, Mara G. Freire, José N. Canongia Lopes, Physical Chemistry Chemical Physics 16 (2014) 21340-21348, DOI: 10.1039/C4CP02008A

NMR SPECTRUM

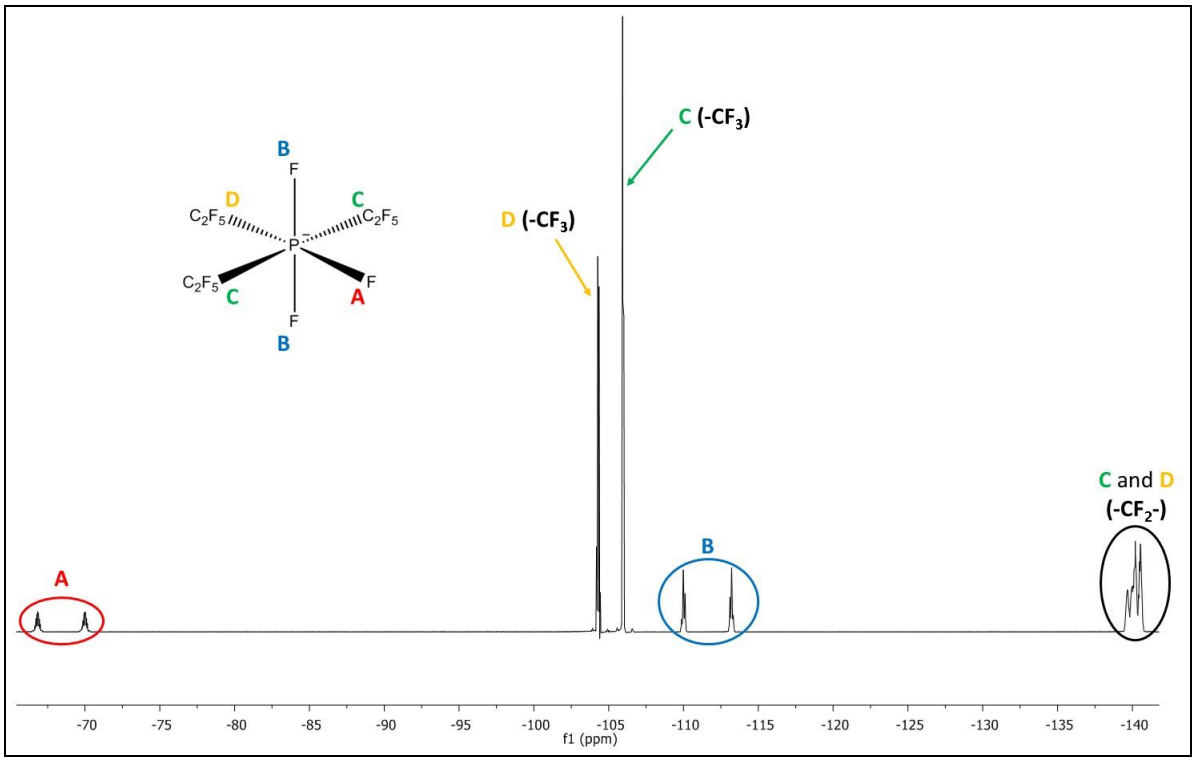

Figure S 3.16. ^{19}F NMR spectra of $[C_2C_1im][FAP]$.

DENSITY AND VISCOSITY

Table S 3.14. Experimental density, ρ, and viscosity, η, for pure ILs as function of temperature and at 0.1 MPa.

T / K	ρ / (kg·m^{-3})		η / (mPa·s)	
	$[C_2C_1im][FAP]$	$[C_2C_1im][PF_6]$	$[C_2C_1im][FAP]$	$[C_2C_1im][PF_6]$
278.15	1726.7	---	168.750	---
283.15	1720.6	---	126.710	---
288.15	1714.5	---	97.357	---

293.15	1708.1	---	76.410	---
298.15	1701.6	---	61.022	---
303.15	1695.0	---	49.617	---
308.15	1688.3	---	40.934	---
313.15	1681.6	---	34.213	---
318.15	1674.9	---	28.934	---
323.15	1668.2	---	24.722	---
328.15	1661.5	---	21.327	---
333.15	1654.8	---	18.552	---
338.15	1648.4	1437.6	16.263	26.830
343.15	1641.9	1433.3	14.355	23.296
348.15	1635.4	1429.1	12.726	20.330
353.15	1629.1	1424.8	11.371	17.920
358.15	1622.8	1420.6	10.216	15.810
363.15	1616.6	1416.4	9.223	14.075

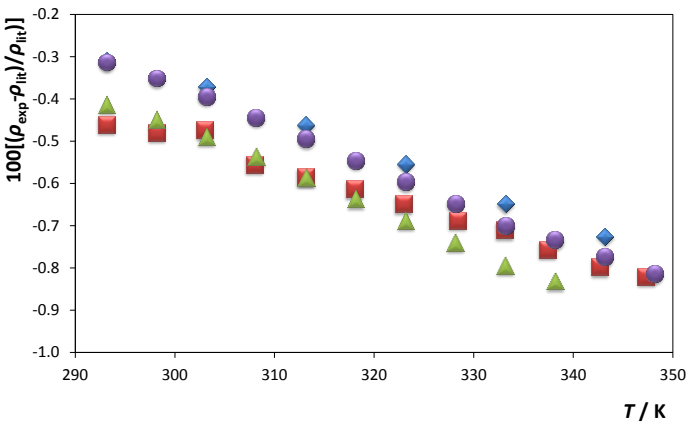

Figure S 3.17. Relative deviations between the experimental densities measured in this work (ρ_{exp}) and those reported in literature (ρ_{lit}) as a function of temperature for [C_2C_1im][FAP]: ●, Seki et al.[9]; ▲, Liu et al.[10]; ◆, Almantariotis et al.[11]; ■, Součková et al.[12].

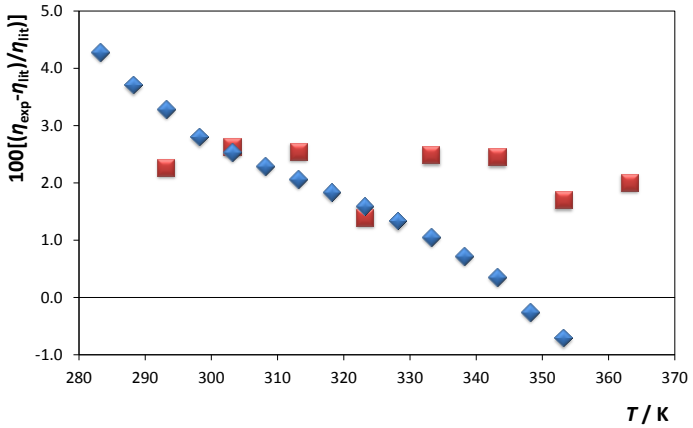

Figure S 3.18. Relative deviations between the experimental viscosities measured in this work (η_{exp}) and those reported in literature (η_{lit}) as a function of temperature for [C_2C_1im][FAP]: ◆, Seki et al.[9]; ■, Almantariotis et al.[11].

MUTUAL SOLUBILITIES MEASUREMENTS

Table S 3.15. Experimental mole fraction solubility of water in ILs, x_w, and of ILs in water, x_{IL}, as a function of temperature and at 0.1 MPa.

	[C_2C_1im][FAP]		[C_2C_1im][PF_6]	
T / K	$10^5 \times (x_{IL} \pm \sigma^a)$	$10^1 \times (x_w \pm \sigma^a)$	$10^2 \times (x_{IL} \pm \sigma^a)$	$x_w \pm \sigma^a$
288.15	0.999 ± 0.014	0.577 ± 0.008	0.167 ± 0.003	---
293.15	1.325 ± 0.034	0.614 ± 0.021	0.260 ± 0.008	---
298.15	1.624 ± 0.024	0.682 ± 0.011	0.288 ± 0.002	---
303.15	1.805 ± 0.019	0.769 ± 0.006	0.567 ± 0.005	---
308.15	1.965 ± 0.238	0.835 ± 0.018	0.848 ± 0.006	---
313.15	2.164 ± 0.041	0.923 ± 0.022	1.027 ± 0.003	---
318.15	2.483 ± 0.009	1.010 ± 0.018	1.148 ± 0.004	---
333.15	3.011 ± 0.066	1.387 ± 0.001	1.785 ± 0.082	---
338.15	3.313 ± 0.007	1.541 ± 0.012	1.973 ± 0.072	---
343.15	3.643 ± 0.036	1.633 ± 0.070	2.191 ± 0.078	0.644 ± 0.015
348.15	3.845 ± 0.004	1.756 ± 0.018	2.365 ± 0.086	0.694 ± 0.024
353.15	4.070 ± 0.010	1.831 ± 0.006	2.529 ± 0.083	0.733 ± 0.011
358.15	4.499 ± 0.021	1.947 ± 0.007	2.712 ± 0.079	0.765 ± 0.004
363.15	4.753 ± 0.058	2.073 ± 0.024	2.934 ± 0.073	0.802 ± 0.074

[a] Standard deviation

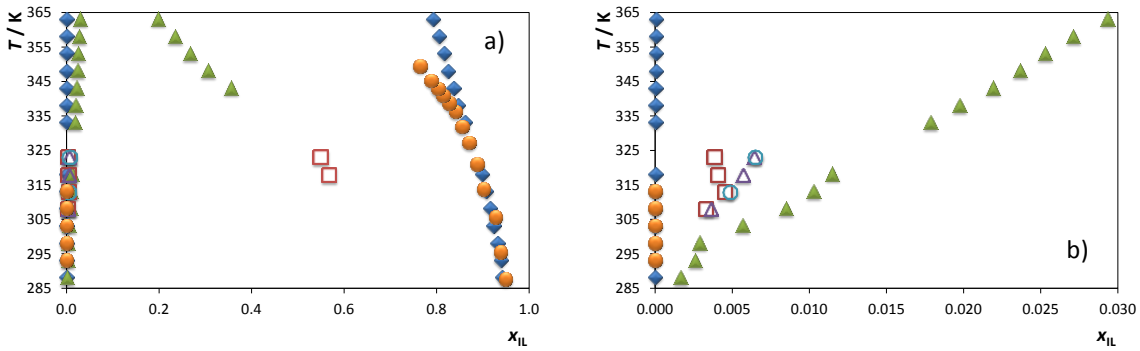

Figure S 3.19. LLE phase diagrams obtained in this work (▲, $[C_2C_1im][PF_6]$; ◆, $[C_2C_1im][FAP]$) and those reported in literature: □, Wong et al.[13] with values obtained by KF; ○, Wong et al.[13] with values obtained by UV; △, Wong et al.[13] with values obtained by TGA; ●, Domańska et al.[14] with values obtained by UV (solubility of IL in water) and dynamic (synthetic) method (solubility of water in IL).

MOLECULAR DYNAMICS SIMULATION

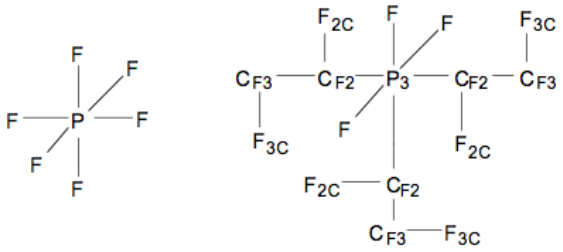

Figure S 3.20. Nomenclature adopted for the atomistic force-field modeling of the $[PF_6]^-$ (left) and $[FAP]^-$ (right) anions (equivalent atoms are not shown in the latter scheme for clarity reasons).

Table S 3.16. Force field non-bonded parameters – atomic point charges (q), Lennard-Jones diameter and interaction parameters (σ_{LJ} and ε_{LJ}) – for the $[PF_6]^-$ and $[FAP]^-$ anions adopted in this work.[15–18] The different partial charges conferred to each type of atom in the two ions are highlighted in bold. These were calculated using quantum-mechanics methods described in literature.[16–18]

$[PF_6]^-$ [15–17]			
Atom	q (a.c.u.)	σ_{LJ} (10^{-10}m)	ε_{LJ} / (kJ·mol^{-1})
P	**1.34**	3.74	0.8368
F	**-0.39**	3.12	0.2552
$[FAP]^-$ [18]			
P3	**0.62**	3.74	0.8368
CF2	**0.24**	3.50	0.27614
F2C	**-0.12**	3.12	0.25520
CF3	**0.42**	3.50	0.27614
F3C	-0.19	3.12	0.2552

Appendix Chapter 4 – Removing Ionic Liquids from Aqueous Solutions Using Aqueous Biphasic Systems

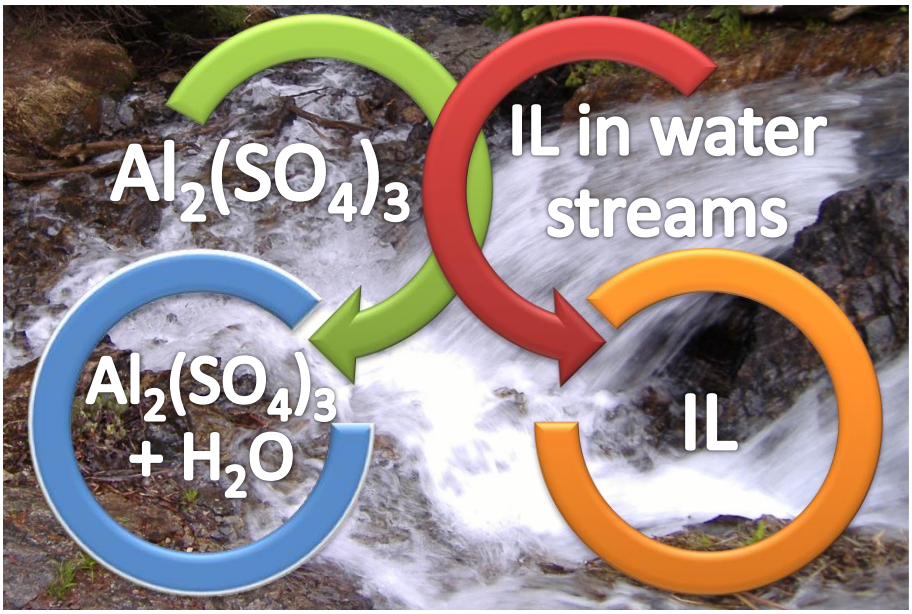

4.3. Improved recovery of ionic liquids from contaminated aqueous streams using aluminium-based salts

Catarina M. S. S. Neves, Mara G. Freire and João A. P. Coutinho, RSC Advances 2 (2012) 10882-10890, DOI: 10.1039/C2RA21535G

The experimental solubility data obtained, at 298 K and at atmospheric pressure, are presented in Tables S4.1 and S4.2. Figure S4.1 depicts the gathered results in molality units. It should be remarked that for the salt $AlK(SO_4)_2$ the concentrations reported were calculated without the contribution of the water complexed with the salt.

Table S 4.1. Experimental mass fraction data for the system composed of IL (1) + $Al_2(SO_4)_3$ (2) + H_2O (3) at 298 K.

$[C_2C_1im][CF_3SO_3]$ M_w = 260.23					
100 w_1	100 w_2	100 w_1	100 w_2	100 w_1	100 w_2
12.997	27.292	27.011	15.625	34.456	10.650
13.985	26.307	27.543	15.183	34.757	10.415
14.961	25.337	28.056	14.869	35.173	10.164
15.741	24.571	28.564	14.493	35.537	9.964
16.570	23.764	29.051	14.143	35.855	9.766
17.707	22.861	29.646	13.790	35.988	9.522
18.762	22.000	30.060	13.454	36.289	9.389
19.830	21.129	30.415	13.178	36.580	9.177
20.783	20.361	30.874	12.882	37.464	8.948
21.386	19.901	31.349	12.567	37.720	8.752
22.278	19.228	31.746	12.305	38.376	8.495
23.044	18.613	32.111	12.039	38.663	8.239
23.697	18.057	32.633	11.745	39.826	7.911
24.117	17.617	32.802	11.538	40.385	7.202
25.149	16.972	32.980	11.377	42.004	6.656
25.849	16.512	33.377	11.152	44.480	6.048
26.462	16.055	33.975	10.857		
$[C_4C_1im][CF_3SO_3]$ M_w = 288.28					
100 w_1	100 w_2	100 w_1	100 w_2	100 w_1	100 w_2
4.151	27.119	17.233	11.710	26.368	7.931
5.162	25.205	17.598	11.538	27.239	7.678
6.264	23.134	18.224	11.106	28.220	7.347

6.767	22.060	18.530	10.868	29.226	7.045
8.727	19.385	18.945	10.753	30.307	6.729
9.873	17.908	19.466	10.530	31.766	6.400
10.666	16.970	19.985	10.316	33.136	5.992
11.398	16.264	20.469	10.152	34.565	5.555
12.069	15.550	20.865	9.857	36.370	5.178
12.599	15.053	21.567	9.700	38.470	4.742
14.160	13.784	22.186	9.398	40.565	4.122
14.676	13.333	22.889	9.191	44.066	3.620
15.177	13.131	23.355	8.827	48.718	2.819
15.872	12.621	24.076	8.621	51.022	2.065
16.346	12.230	24.809	8.430	57.809	1.074
16.672	12.114	25.555	8.194		

$[C_4C_1im][Tos]$ M_w = 310.42

100 w_1	100 w_2	100 w_1	100 w_2	100 w_1	100 w_2
7.659	27.371	16.398	20.827	35.211	10.339
8.613	26.487	17.750	19.966	37.797	9.288
9.448	25.775	18.819	19.343	39.529	8.942
10.347	25.038	20.745	18.143	42.944	7.621
11.217	24.364	22.789	16.923	45.492	6.956
12.192	23.633	24.732	15.859	48.439	6.224
13.127	22.995	27.420	14.272	51.902	5.310
14.167	22.275	29.885	12.959		
15.204	21.608	32.373	11.735		

$[C_4C_1im][N(CN)_2]$ M_w = 205.26

100 w_1	100 w_2	100 w_1	100 w_2	100 w_1	100 w_2
8.893	26.678	21.133	16.414	35.688	7.255
11.229	24.349	22.458	15.449	37.576	6.234
12.870	22.789	23.644	14.584	39.024	5.807
13.926	21.837	24.318	14.159	40.387	5.179
15.222	20.784	25.877	13.069	41.762	4.611
16.141	20.063	27.194	12.199	43.816	3.989
16.842	19.531	28.687	11.195	45.372	3.289
17.502	19.034	29.765	10.577	47.133	2.543
18.244	18.487	31.021	9.862	49.885	1.851
19.318	17.686	33.106	8.621	58.498	0.800
20.140	17.111	34.005	8.216		

$[C_8py][N(CN)_2]$ M_w = 258.36

100 w_1	100 w_2	100 w_1	100 w_2	100 w_1	100 w_2

1.430	35.132	12.491	12.294	20.066	8.014
2.116	30.754	12.777	12.150	20.542	7.801
2.608	28.773	13.124	11.995	21.190	7.636
3.071	26.845	13.413	11.741	21.704	7.433
3.469	25.118	13.717	11.482	22.204	7.222
3.929	24.058	14.028	11.217	22.821	7.000
4.712	22.543	14.227	11.117	23.577	6.744
5.510	20.994	14.387	10.974	24.323	6.483
5.811	19.245	14.550	10.839	25.007	6.200
7.167	17.499	14.799	10.745	25.953	5.949
8.021	16.258	14.965	10.609	26.741	5.603
8.579	15.619	15.159	10.470	27.991	5.351
9.137	15.072	15.411	10.361	29.329	5.040
9.515	14.714	15.605	10.218	30.624	4.655
9.816	14.397	15.876	10.106	32.098	4.245
10.147	14.091	16.239	10.035	34.384	3.886
10.416	13.852	16.714	9.761	37.033	3.423
10.736	13.661	17.180	9.402	40.237	2.934
11.032	13.392	17.506	9.243	45.576	2.385
11.326	13.134	17.848	9.089	49.903	1.855
11.578	12.985	18.313	8.992	59.041	1.000
11.828	12.844	19.028	8.655		
12.072	12.646	19.635	8.210		
$[(C_7H_7)C_1im][C_2H_5SO_4]$ M_w = 298.36					
100 w_1	100 w_2	100 w_1	100 w_2	100 w_1	100 w_2
10.211	31.136	30.872	14.733	30.872	14.733
12.491	29.191	31.694	14.183	31.694	14.183
13.403	27.885	32.268	13.743	32.268	13.743
15.218	26.299	33.052	13.228	33.052	13.228
17.315	24.811	33.922	12.730	33.922	12.730
18.807	23.490	34.556	12.303	34.556	12.303
20.350	22.323	35.371	11.865	35.371	11.865
21.674	21.304	35.676	11.568	35.676	11.568
22.614	20.381	36.504	11.167	36.504	11.167
24.219	19.344	37.062	10.844	37.062	10.844
25.128	18.620	37.561	10.542	37.561	10.542
26.252	17.853	38.080	10.229	38.080	10.229
27.457	17.115	38.619	9.942	38.619	9.942
28.487	16.412	39.209	9.672	39.209	9.672

29.221	15.849	39.791	9.376	39.791	9.376
29.763	15.348	40.360	9.096		

$[P_{i(444)1}][Tos]$ M_w = 385.52

100 w_1	100 w_2	100 w_1	100 w_2	100 w_1	100 w_2
6.968	19.962	11.100	16.959	18.869	13.064
7.075	19.880	11.342	16.754	19.319	12.935
7.188	19.790	11.501	16.713	19.807	12.776
7.351	19.618	11.749	16.545	20.590	12.261
7.533	19.424	11.913	16.520	21.113	12.097
7.667	19.328	12.204	16.305	21.651	11.925
7.810	19.225	12.397	16.245	22.581	11.360
8.013	18.999	12.705	16.032	23.227	11.122
8.164	18.892	12.906	15.970	23.926	10.854
8.321	18.769	13.238	15.748	24.584	10.614
8.487	18.650	13.460	15.697	25.307	10.322
8.650	18.491	13.827	15.436	26.060	10.045
8.838	18.344	14.061	15.362	27.360	9.312
9.028	18.177	14.316	15.282	28.252	9.040
9.199	18.055	14.559	15.201	29.179	8.705
9.381	17.917	14.954	14.942	30.242	8.352
9.500	17.890	15.212	14.853	32.040	8.047
9.690	17.737	15.487	14.749	33.353	7.583
9.895	17.577	15.915	14.457	34.777	7.094
10.029	17.547	16.207	14.356	36.186	6.634
10.234	17.391	16.512	14.264	38.604	6.231
10.358	17.356	16.820	14.164	41.588	5.788
10.571	17.200	17.382	13.795	44.969	5.303
10.718	17.187	17.762	13.674	49.247	4.675
10.959	17.003	18.160	13.538	54.358	3.894

$[P_{4444}]Br$ M_w = 339.34

100 w_1	100 w_2	100 w_1	100 w_2	100 w_1	100 w_2
4.190	21.128	9.087	15.820	15.425	11.634
4.379	20.908	9.273	15.633	15.948	11.205
4.552	20.640	9.394	15.578	16.318	11.019
4.721	20.419	9.596	15.367	16.692	10.857
4.888	20.147	9.726	15.314	17.105	10.679
5.013	20.010	9.938	15.097	17.990	10.235
5.136	19.862	10.078	15.032	18.723	9.663
5.274	19.694	10.295	14.812	19.803	9.111

5.453	19.465	10.444	14.759	20.319	8.885
5.611	19.288	10.600	14.696	20.930	8.628
5.776	19.099	11.300	14.113	23.349	7.690
5.950	18.921	11.475	14.021	24.120	7.339
6.113	18.747	11.639	13.965	24.936	6.956
6.293	18.547	11.929	13.695	25.743	6.636
6.540	18.184	12.128	13.604	27.239	6.299
6.752	17.955	12.467	13.293	28.329	5.788
6.977	17.745	12.704	13.197	29.943	5.443
7.203	17.508	12.912	13.101	32.009	4.952
7.408	17.351	13.261	12.778	34.363	4.431
7.675	17.053	13.486	12.674	37.818	3.917
7.810	16.919	13.740	12.565	46.099	3.370
8.042	16.733	14.148	12.232	52.891	2.920
8.299	16.527	14.432	12.107	23.349	7.690
8.457	16.372	14.740	11.973	24.120	7.339
8.732	16.160	11.300	14.113		
8.904	15.985	11.475	14.021		

$[P_{4444}]Cl$ M_w = 294.89

100 w_1	100 w_2	100 w_1	100 w_2	100 w_1	100 w_2
4.829	26.091	9.462	20.463	19.113	12.385
5.033	25.786	9.818	20.089	19.805	11.959
5.226	25.503	10.198	19.700	20.535	11.573
5.410	25.246	10.530	19.388	21.320	11.168
5.586	25.016	10.948	18.983	22.028	10.757
5.786	24.743	11.321	18.653	22.866	10.252
6.079	24.308	11.742	18.254	23.793	9.696
6.292	24.042	12.165	17.882	24.460	9.478
6.549	23.709	12.655	17.451	25.142	9.200
6.789	23.416	13.047	17.132	26.653	8.642
7.011	23.151	13.491	16.786	27.850	7.969
7.283	22.823	14.040	16.291	28.731	7.707
7.539	22.526	14.650	15.730	29.809	7.406
7.815	22.213	15.186	15.296	30.945	7.036
8.063	21.954	15.741	14.874	32.596	6.803
8.303	21.695	16.364	14.382	33.846	6.398
8.574	21.403	17.015	13.883	36.683	6.171
8.894	21.028	17.528	13.587	39.580	5.731
9.190	20.719	18.289	13.006	41.527	5.178

$[P_{4441}][CH_3SO_4]$ M_w = 358.52					
100 w_1	100 w_2	100 w_1	100 w_2	100 w_1	100 w_2
7.253	22.156	16.210	14.507	26.822	8.406
8.475	20.764	17.251	13.872	28.281	7.543
9.010	20.136	19.481	12.616	29.473	7.005
10.616	18.751	20.295	12.054	30.426	6.748
11.226	18.252	21.115	11.548	31.807	6.168
11.904	17.641	22.125	10.820	33.864	5.682
12.643	17.074	22.834	10.526	36.390	4.975
13.240	16.723	23.926	9.819	39.395	4.193
14.166	15.977	24.590	9.574	50.781	3.265
15.269	15.097	25.836	8.819	56.178	2.762

Table S 4.2. Experimental mass fraction data for the system composed of IL (1) + $AlK(SO_4)_2$ (2) + H_2O (3) at 298 K.

$[C_4C_1im][CF_3SO_3]$ M_w = 288.28					
100 w_1	100 w_2	100 w_1	100 w_2	100 w_1	100 w_2
28.905	4.312	37.099	3.018	42.396	2.287
29.415	4.219	37.411	2.964	42.723	2.247
29.673	4.121	37.923	2.903	42.959	2.212
29.892	4.088	38.256	2.850	43.333	2.170
30.915	3.954	38.553	2.807	43.651	2.133
31.427	3.857	39.024	2.743	43.815	2.115
32.003	3.759	39.327	2.698	44.303	2.053
32.568	3.669	39.574	2.671	44.534	2.024
33.145	3.585	39.872	2.625	45.107	1.961
33.694	3.502	40.335	2.553	45.618	1.902
34.260	3.412	40.856	2.499	46.095	1.851
34.823	3.331	41.097	2.458	46.450	1.821
35.737	3.203	41.441	2.409	54.621	1.010
35.991	3.163	41.812	2.365	61.240	0.612
36.696	3.073	42.046	2.329	65.196	0.424
$[C_8py][N(CN)_2]$ M_w = 258.36					
100 w_1	100 w_2	100 w_1	100 w_2	100 w_1	100 w_2
22.417	4.613	30.612	3.349	35.460	2.649
22.861	4.513	31.045	3.282	36.387	2.291
23.444	4.389	31.466	3.213	38.301	2.075
23.990	4.297	31.815	3.165	40.321	1.865
24.660	4.192	32.092	3.113	42.313	1.678

25.713	4.022	32.543	3.051	43.970	1.527
26.170	3.941	33.052	2.984	45.465	1.408
27.023	3.831	33.541	2.922	46.850	1.304
27.560	3.752	33.750	2.875	48.893	1.151
28.050	3.672	34.266	2.811	61.431	0.501
28.392	3.610	34.673	2.759	64.680	0.390
29.675	3.486	34.780	2.732	67.666	0.293
29.967	3.425	35.014	2.695		

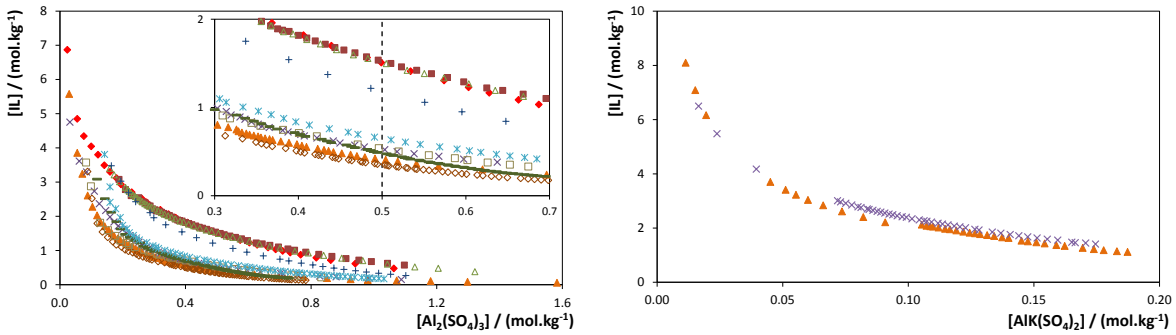

Figure S 4.1. Ternary phase diagrams for the systems composed of IL + aluminium-based salt + water at 298 K and atmospheric pressure (molality units): ■, $[C_2C_1im][CF_3SO_3]$; ×, $[C_4C_1im][CF_3SO_3]$; ●, $[C_4C_1im][SCN]$; +, $[C_4C_1im][Tos]$; ◆, $[C_4C_1im][N(CN)_2]$;▲, $[C_8py][N(CN)_2]$; △, $[(C_7H_7)C_1im][C_2H_5SO_4]$; ▬, $[P_{i(444)1}][Tos]$; ◇, $[P_{4444}]Br$; ✳, $[P_{4444}]Cl$; □, $[P_{4441}][CH_3SO_4]$.

Table S 4.3. Critical point of each system composed of IL + $Al_2(SO_4)_3$ + H_2O at 298 K and respective values obtained from the fitting.

IL	*f*	*g*	R^2	Critical Point / wt%	
				[*IL*]	[*Salt*]
$[C_2C_1im][CF_3SO_3]$	1.327	9.722	0.9926	14.32	28.72
$[C_4C_1im][CF_3SO_3]$	0.716	56.085	0.8568	1.49	57.15
$[C_4C_1im][Tos]$	1.268	-1.893	0.9895	17.88	20.79
$[C_4C_1im][N(CN)_2]$	2.034	-23.422	0.9292	19.72	16.68
$[C_8py][N(CN)_2]$	1.044	35.283	0.9747	3.13	38.55
$[(C_7H_7)C_1im][C_2H_5SO_4]$	1.273	5.979	0.9970	16.91	27.50
$[P_{i(444)1}][Tos]$	1.924	-13.816	0.9816	14.86	14.78
$[P_{4444}]Br$	1.846	8.992	0.9997	7.72	23.25
$[P_{4444}]Cl$	0.656	30.910	0.8203	35.03	6.29
$[P_{4441}][CH_3SO_4]$	1.714	-1.610	0.9193	12.05	19.04

Table S 4.4. Experimental density (ρ) and viscosity (η) data of the coexisting phases in diverse ABS composed of 40 wt% of IL + 15 wt% of $Al_2(SO_4)_3$ + 45 wt% of H_2O in the temperature range between 298.15 K and 328.15 K.

IL	Phase	*T*	*P*	*H*
		K	g·cm^{-3}	mPa·s
			$Al_2(SO_4)_3$	
$[C_4C_1im][CF_3SO_3]$	IL – rich phase	298.15	1.2374	3.7387
		308.15	1.2296	2.8957
		318.15	1.2215	2.3083
		328.15	1.2132	1.8999
	Salt – rich phase	298.15	1.2899	12.128
		308.15	1.2842	8.5076
		318.15	1.2780	6.1348
		328.15	1.2710	4.5322
$[C_8py][N(CN)_2]$	IL – rich phase	298.15	1.0105	11.372
		308.15	1.0040	8.1779
		318.15	0.9935	5.9367
		328.15	0.9812	4.5779
	Salt – rich phase	298.15	1.2630	8.8931
		308.15	1.2576	6.4328
		318.15	1.2517	4.7492
		328.15	1.2450	3.5907
$[(C_7H_7)C_1im][EtSO_4]$	IL – rich phase	298.15	1.1642	6.9866
		308.15	1.1573	5.0923
		318.15	1.1502	3.8604
		328.15	1.1430	3.0241
	Salt – rich phase	298.15	1.3061	15.242
		308.15	1.3006	10.478
		318.15	1.2944	7.4514
		328.15	1.2876	5.4609
$[C_4C_1im][N(CN)_2]$	IL – rich phase	298.15	1.0415	4.5958
	Salt – rich phase	298.15	1.3135	17.177
		308.15	1.3076	11.664
		318.15	1.3010	8.2411
$[C_2C_1im][CF_3SO_3]$	IL – rich phase	298.15	1.2394	3.7823
		308.15	1.2314	2.9436
		318.15	1.2233	2.361
		328.15	1.2151	1.9244
	Salt – rich phase	298.15	1.2911	12.214

		308.15	1.2855	8.5628
		318.15	1.2793	6.177
		328.15	1.2723	4.5755
$[C_4C_1im][Tos]$	IL – rich phase	298.15	1.1355	9.3852
		308.15	1.1284	6.5792
		318.15	1.1211	4.8017
		328.15	1.1137	3.6367
	Salt – rich phase	298.15	1.2969	15.568
		308.15	1.2912	10.582
		318.15	1.2848	7.4506
		328.15	1.2777	5.3999
$[P_{4444}]Br$	IL – rich phase	298.15	1.0591	19.382
		308.15	1.0515	12.462
		318.15	1.0439	8.5298
		328.15	1.0362	6.1428
	Salt – rich phase	298.15	1.2696	8.1799
		308.15	1.2643	5.9425
		318.15	1.2587	4.4584
		328.15	1.2524	3.4339
$[P_{4444}]Cl$	IL – rich phase	298.15	0.9999	12.795
		308.15	0.9929	8.4367
		318.15	0.9857	5.9034
		328.15	0.9784	4.3341
	Salt – rich phase	298.15	1.2928	13.02
		308.15	1.2876	9.1173
		318.15	1.2819	6.5977
		328.15	1.2757	4.8988
$[P_{i(444)1}][Tos]$	IL – rich phase	298.15	1.0709	14.363
		308.15	1.0638	9.5221
		318.15	1.0566	6.6981
		328.15	1.0493	4.9375
	Salt – rich phase	298.15	1.2802	10.527
		308.15	1.2750	7.5126
		318.15	1.2692	5.5288
		328.15	1.2628	4.1661
$[P_{4441}][CH_3SO_4]$	IL – rich phase	298.15	1.0495	10.385
		308.15	1.0420	7.0628
		318.15	1.0346	5.0561
		328.15	1.0271	3.7836

Salt – rich phase	298.15	1.3045	14.579
	308.15	1.2991	10.117
	318.15	1.2933	7.2546
	328.15	1.2866	5.3356

The consistency of the tie-line compositions was ascertained by the empirical correlations given by Othmer–Tobias[2] (eq S4.1) and Bancroft[192] (eq S4.2).

$$\left(\frac{1-[IL]_{\text{IL}}}{[IL]_{\text{IL}}}\right) = k_1\left(\frac{1-[Salt]_{\text{Salt}}}{[Salt]_{\text{Salt}}}\right)^{n} \quad \text{(S4.1)}$$

$$\left(\frac{[H_2O]_{\text{Salt}}}{[Salt]_{\text{Salt}}}\right) = k_2\left(\frac{[H_2O]_{\text{IL}}}{[IL]_{\text{IL}}}\right)^{r} \quad \text{(S4.2)}$$

where "IL" and "Salt" designate the ionic liquid rich-phase and the salt rich-phase, respectively; [*IL*], [*Salt*] and [H_2O] represent, respectively, the weight fraction of ionic liquid, salt and water. The k_1, n, k_2 and r are fitting parameters. A linear dependency of the plots $\log\left(\frac{1-[IL]_{\text{IL}}}{[IL]_{\text{IL}}}\right)$ against $\log\left(\frac{1-[Salt]_{\text{Salt}}}{[Salt]_{\text{Salt}}}\right)$ and $\log\left(\frac{[H_2O]_{\text{Salt}}}{[Salt]_{\text{Salt}}}\right)$ against $\log\left(\frac{[H_2O]_{\text{IL}}}{[IL]_{\text{IL}}}\right)$ indicate an acceptable consistency of the results.

Table S 4.5. Values of the fitting parameters of eqs S4.1 and S4.2 for the systems composed of IL + $Al_2(SO_4)_3$ + H_2O at 298 K, and respective correlation coefficients (R^2).

IL	*Othmer – Tobias*, eq S4.1			*Bancroft*, eq S4.2		
	n	k_1	R^2	r	k_2	R^2
$[C_2C_1im][CF_3SO_3]$	1.3625	0.3385	0.9940	1.5451	0.3340	0.9920
$[C_4C_1im][CF_3SO_3]$	0.8348	0.1397	0.8129	0.9241	0.1305	0.8256
$[C_4C_1im][Tos]$	1.2994	0.6254	0.9911	1.2449	0.5726	0.9909
$[C_4C_1im][N(CN)_2]$	2.1597	0.3040	0.9175	0.4155	1.6808	0.9176
$[C_8py][N(CN)_2]$	0.1945	0.4004	0.9326	4.8194	89.5332	0.9298
$[(C_7H_7)C_1im][C_2H_5SO_4]$	1.2920	0.4474	0.9962	0.7072	1.8015	0.9970
$[P_{i(444)1}][Tos]$	1.9492	0.2628	0.9743	0.5051	2.0566	0.9740
$[P_{4444}]Br$	1.9628	0.1052	0.9985	2.0474	0.0969	0.9988
$[P_{4444}]Cl$	0.6422	0.5771	0.8135	0.6643	0.5414	0.8179

$[P_{4441}][CH_3SO_4]$	1.7494	0.2420	0.9020	0.4868	2.1296	0.9039

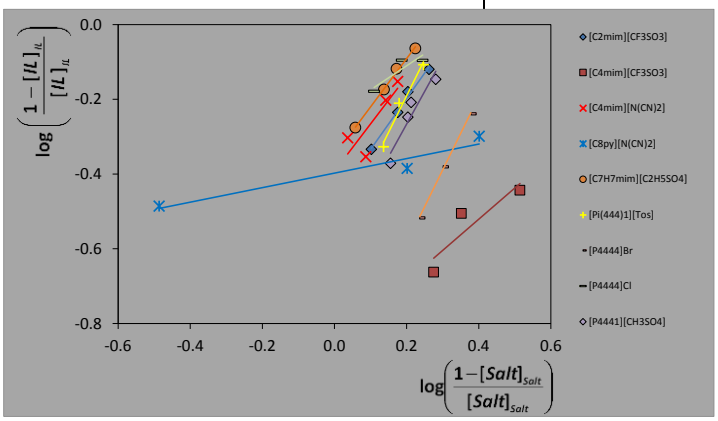

Figure S 4.2. Tie-lines correlation using the Othmer-Tobias correlation for each system composed of IL + $Al_2(SO_4)_3$ + H_2O.

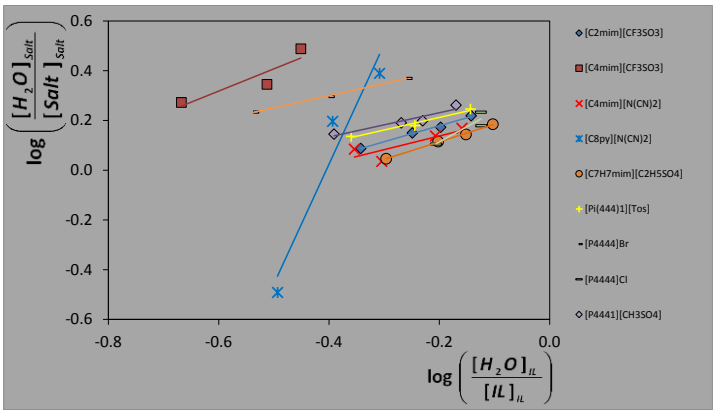

Figure S 4.3. Tie-lines correlation using the Bancroft correlation for each system composed of IL + $Al_2(SO_4)_3$ + H_2O.

References

1. J. D. Seader and E. J. Henley, Separation Process Principles, John Wiley & Sons, New York, 1998.

2. D. Othmer and P. Tobias, *Ind. Eng. Chem.*, 1942, **34**, 693–696.

3. J. P. O'Connell and J. M. Haile, Thermodynamics: Fundamentals for Applications, Cambridge University Press, New York, 2005.

4. J. M. Sørensen, T. Magnussen, P. Rasmussen, and A. Fredenslund, *Fluid Phase Equilib.*, 1979, **3**, 47–82.

5. A. Brooke, D. Ketndrick, A. Meeraus, and R. Raman, GAMS - A User's Guide, GAMS Development Corporation, Washington DC, 2005.

6. A. S. Drud, *ORSA J. Comput.*, 1992, **6**, 207–216.

7. 2010.

8. M. Tawarmalani and N. V Sahinidis, Convexification and Global Optimization in Continuous and Mixed-Integer Nonlinear Programming, Kluwer Academic Publishers, Dordrecht, 2002.

9. S. Seki, N. Serizawa, K. Hayamizu, S. Tsuzuki, Y. Umebayashi, K. Takei, and H. Miyashiro, *J. Electrochem. Soc.*, 2012, **159**, A967–A971.

10. Q.-S. Liu, J. Tong, Z.-C. Tan, U. Welz-Biermann, and J.-Z. Yang, *J. Chem. Eng. Data*, 2010, **55**, 2586–2589.

11. D. Almantariotis, S. Stevanovic, O. Fandiño, A. S. Pensado, A. A. H. Pádua, J.-Y. Coxam, and M. F. Costa Gomes, *J. Phys. Chem. B*, 2012, **116**, 7728–7738.

12. M. Součková, J. Klomfar, and J. Pátek, *J. Chem. Thermodyn.*, 2012, **48**, 267–275.

13. D. S. H. Wong, J. P. Chen, J. M. Chang, and C. H. Chou, *Fluid Phase Equilib.*, 2002, **194–197**, 1089–1095.

14. U. Domańska, M. Królikowski, A. Pobudkowska, and P. Bocheńska, *J. Chem. Thermodyn.*, 2012, **55**, 225–233.

15. G. A. Kaminski and W. L. Jorgensen, *J. Chem. Soc. Perkin Trans. 2*, 1999, 2365–2375.

16. J. N. Canongia Lopes, J. Deschamps, and A. A. H. Pádua, *J. Phys. Chem. B*, 2004, **108**, 2038–2047.

17. J. N. Canongia Lopes and A. A. H. Pádua, *J. Phys. Chem. B*, 2004, **108**, 16893–16898.

18. K. Shimizu, D. Almantariotis, M. F. Costa Gomes, A. A. H. Pádua, and J. N. Canongia Lopes, *J. Phys. Chem. B*, 2010, **114**, 3592–600.

19. P. González-Tello, F. Camacho, G. Blázquez, and F. J. Alarcón, *J. Chem. Eng. Data*, 1996, **41**, 1333–1336.